



Universitat de Girona

# ON THE USE OF ENERGY DECOMPOSITION ANALYSES TO UNRAVEL THE ORIGIN OF THE RELATIVE STABILITIES OF ISOMERS

**Majid El Hamdi Lahfid**

**Dipòsit legal: Gi. 1531-2013**  
<http://hdl.handle.net/10803/124220>

**ADVERTIMENT.** L'accés als continguts d'aquesta tesi doctoral i la seva utilització ha de respectar els drets de la persona autora. Pot ser utilitzada per a consulta o estudi personal, així com en activitats o materials d'investigació i docència en els termes establerts a l'art. 32 del Text Refós de la Llei de Propietat Intel·lectual (RDL 1/1996). Per altres utilitzacions es requereix l'autorització prèvia i expressa de la persona autora. En qualsevol cas, en la utilització dels seus continguts caldrà indicar de forma clara el nom i cognoms de la persona autora i el títol de la tesi doctoral. No s'autoritza la seva reproducció o altres formes d'explotació efectuades amb finalitats de lucre ni la seva comunicació pública des d'un lloc aliè al servei TDX. Tampoc s'autoritza la presentació del seu contingut en una finestra o marc aliè a TDX (framing). Aquesta reserva de drets afecta tant als continguts de la tesi com als seus resums i índexs.

**ADVERTENCIA.** El acceso a los contenidos de esta tesis doctoral y su utilización debe respetar los derechos de la persona autora. Puede ser utilizada para consulta o estudio personal, así como en actividades o materiales de investigación y docencia en los términos establecidos en el art. 32 del Texto Refundido de la Ley de Propiedad Intelectual (RDL 1/1996). Para otros usos se requiere la autorización previa y expresa de la persona autora. En cualquier caso, en la utilización de sus contenidos se deberá indicar de forma clara el nombre y apellidos de la persona autora y el título de la tesis doctoral. No se autoriza su reproducción u otras formas de explotación efectuadas con fines lucrativos ni su comunicación pública desde un sitio ajeno al servicio TDR. Tampoco se autoriza la presentación de su contenido en una ventana o marco ajeno a TDR (framing). Esta reserva de derechos afecta tanto al contenido de la tesis como a sus resúmenes e índices.

**WARNING.** Access to the contents of this doctoral thesis and its use must respect the rights of the author. It can be used for reference or private study, as well as research and learning activities or materials in the terms established by the 32nd article of the Spanish Consolidated Copyright Act (RDL 1/1996). Express and previous authorization of the author is required for any other uses. In any case, when using its content, full name of the author and title of the thesis must be clearly indicated. Reproduction or other forms of for profit use or public communication from outside TDX service is not allowed. Presentation of its content in a window or frame external to TDX (framing) is not authorized either. These rights affect both the content of the thesis and its abstracts and indexes.







Doctoral thesis:

On the use of energy decomposition analyses to unravel the origin of the  
relative stabilities of isomers

Majid El Hamdi Lahfid  
2013

Programa de Doctorat en Ciències Experimentals i Sostenibilitat

Directed by:  
Prof. Miquel Solà i Puig  
Dr. Jordi Poater i Teixidor

This memory has been presented to obtain the degree of international doctor by the  
Universitat de Girona



El professor Miquel Solà i Puig, catedràtic d'Universitat a l'àrea de Química Física de la Universitat de Girona i el doctor Jordi Poater i Teixidor, investigador Ramón y Cajal a l'Institut de Química Computacional i Catàlisi de la Universitat de Girona,

CERTIFIQUEM:

Que aquest treball titulat “On the use of energy decomposition analyses to unravel the origin of the relative stabilities of isomers”, que presenta en Majid El Hamdi Lahfid per a l'obtenció del títol de Doctor, ha estat realitzat sota la nostra direcció i que compleix els requeriments per a poder optar a la Menció Internacional.

Signatura

Prof. Miquel Solà i Puig

Dr. Jordi Poater i Teixidor

Girona,



A la meva família: la meva mare, el meu pare,  
els meus germans, les meves germanes,  
la meva àvia, els meus oncles,  
les meves ties

A tots vosaltres



# Agraïments

M'agradaria donar les gràcies a Déu que em va donar la gràcia i el privilegi de seguir aquesta tesi i completar-la amb èxit malgrat els molts desafiaments que he hagut d'afrontar.

En primer lloc he d'agrair especialment al Dr. Miquel Solà. Li agraeixo moltíssim la paciència, l'entusiasme i l'interès que sempre ha mostrat. Sempre aprenc un munt de coses i per qualsevol problema que pugui sorgir sempre té una bona solució. Moltes gràcies per tota l'ajuda Miquel!!! Gràcies tant des d'un punt de vista acadèmic com personal, perquè avui puc optar al grau de doctor en Química, títol amb el qual tant de temps he estat somniant.

Seguint amb la supervisió de la tesi, en aquest punt també he d'agrair al Prof. Jordi Poater, l'altre co-director de la meua tesi, no sé què faria sense l'ajuda d'en Jordi, el gran avanç en la realització d'aquesta tesi ha estat gràcies a ell. Valoro molt la paciència que tens, les ganes de treballar, també l'interès i el suport. Moltes gràcies Jordi per les teves explicacions, per la qualitat científica. Gràcies tant des d'un punt de vista acadèmic com personal.

També agraeixo al Ministerio de Educación i Ciencia la concessió d'una beca predoctoral per la Formació de Personal Investigador (FPI) que ha permès finançar la realització d'aquesta tesi.

Ara em toca agrair a tots aquells membres de l'IQC, passats i presents, amb els quals he compartit un munt de coses durant aquest temps. Primer de tot, gràcies als companys de despatx, sinó amics, que m'han hagut d'aguantar en el dia a dia: Eloy, Lluís, Marc, Sílvia, Yevhen, Eduard, Marcel, Verònica, Carles, Pedro, Anna, Quansong, Laia, Sergi, Luz, Cristina, David, Albert, Rafa i Mikael Johansson. També a tota la nova generació d'iqccians: Joaquim Antolin, Mauricio, Abril, Juan Pablo, Erik, Ouissam,...

També agraeixo de cor a la Carme de l'IQCC per tota l'ajuda des de la meua arribada a Girona, per les xerrades que feiem al seu despatx. Un gran agraïment també a en Dani que ha reparat el meu ordinador diverses vegades i m'ha facilitat l'accés a les màquines de l'IQCC.

També vull agrair als molts col.laboradors externs que han contribuït als resultats presentats en aquest manuscrit, i que sovint em van donar la benvinguda als seus equips el que em va permetre aprendre moltes noves tècniques.

Finalment, vull donar les gràcies a tots els membres de l'IQCC que han aconseguit que aquests anys de tesi hagin estat molt agradables.

No em puc oblidar de la resta d'excompanys experimentals i els actuals, amb els que també hem compartit molts moments durant les celebracions o sopars: Rafael, Montse, Marc Font, Jordi, Magdalena,....

Sortint del món químic...hi ha un munt de gent que m'ha acompanyat durant aquests anys de la meva vida i els quals m'han donat suport. Sobretot he d'agrair a la meva mare, qui sempre m'ha donat una empenta i ànims per tal que arribés el dia d'avui i obtenir aquestes dues lletres. Finalment, moltíssimes gràcies als meus germans, les meves germanes, la meva àvia, ties, i oncles pel seu suport incondicional sempre.

I per acabar, moltíssimes gràcies el meu cosí Abdellatif i també company meu d'estudis durant molts anys. Hem compartit molts moments majoritàriament de diligència i perseverança (estudis, participar en els concursos, buscant beques o treball, ....). Així mateix, no m'he oblidat de les teves ajudes durant els moments difícils. Has estat l'amic lleial i el gran germà compassiu. Moltes gràcies per tota l'ajuda que m'has proporcionat!!

Moltes gràcies a tots els que han contribuït al meu èxit.

***El Hamdi Lahfid, Majid***

## Table of Contents

<b>Summary</b> .....	15
<b>Resum</b> .....	17
<b>Resumen</b> .....	19
<b>Full List of Publications</b> .....	23
<b>List of Acronyms</b> .....	27
<b>List of Figures</b> .....	29
<b>List of Tables</b> .....	31
<b>List of Schemes</b> .....	33
<b>Chapter 1: General Introduction</b> .....	37
<b>1. Introduction</b> .....	39
<b>1.1 The chemical bond definition</b> .....	40
<b>1.2 Types of Chemical Bonds</b> .....	41
1.2.1 Strong chemical bond .....	41
1.2.1.1 The covalent bond .....	41
1.2.1.2 Donor-acceptor bonds .....	43
1.2.1.3 The one-electron bond.....	44
1.2.1.4 The three-electron bond .....	44
1.2.1.5 The three-center, two-electron chemical bond .....	46
1.2.1.6 The resonance chemical .....	47
1.2.2 The ionic bond .....	49
1.2.3 Covalent polar bond.....	50
1.2.4 The metallic bond .....	51
<b>1.3 Weak chemical bonds</b> .....	52
1.3.1 Hydrogen bonds.....	53
1.3.1.1 List of criteria .....	54
1.3.1.2 Some extra characteristics of hydrogen bonds .....	55
1.3.2 Van der Waals intermolecular interactions .....	56

<b>1.4 Isomerization</b>	59
1.4.1 Structural isomers	59
1.4.2 Geometric isomers	61
1.4.3 Conformational isomers	61
1.4.4 Optical isomers	63
<b>1.5 Aromaticity</b>	64
1.5.1 Description of aromaticity	70
1.5.2 Energetic Aromaticity: ASE	73
1.5.3 Structural Aromaticity: HOMA	74
1.5.4 Magnetic Aromaticity: NICS	74
1.5.5 Aromaticity from ESI	76
<b>2. Methodology</b>	77
<b>2.1 The basis of quantum chemistry</b>	79
2.1.1 The birth of the wavefunction	79
A-The Born-Oppenheimer Approximation	79
B- Approximations of the wavefunction	80
2.1.2 Hartree-Fock theory	81
<b>2.2 RHF ("Restricted HF") - UHF ("Unrestricted HF") formalisms</b>	82
<b>2.3 Hole of Coulomb and Fermi</b>	82
<b>2.4 Dynamic and static correlations</b>	83
<b>2.5 Treatment of correlation</b>	84
<b>2.6 The perturbative approach of the wave function</b>	85
2.6.1 Møller-Plesset Method	85
2.6.2 "Coupled Cluster" Method	86
2.6.3 The method of Configuration Interaction (CI)	87
<b>2.7 Multireference methods: CASSCF and MCSCF</b>	88
2.7.1 The density functional	89
2.7.2 Hohenberg and Kohn theorems	89
2.7.3 The Thomas-Fermi model	90
2.7.4 Kohn-Sham model	90
2.7.5 Purely local functional (LDA)	92
2.7.6 The generalized gradient approximation (GGA)	92
<b>2.8 Hybrid Functionals</b>	92

<b>2.9 Bond Energy Decomposition</b> .....	93
<b>Chapter 2: Objectives</b> .....	95
<b>Chapter 3:</b> .....	101
An Analysis of the Isomerization Energies of 1,2-/1,3-Diazacyclobutadiene, Pyrazole/Imidazole, and Pyridazine/Pyrimidine with the Turn-Upside Down Approach .....	101
<b>Chapter 4:</b> .....	113
X <sub>2</sub> Y <sub>2</sub> Isomers: Tuning Structure And Relative Stability Through Electronegativity Differences (X = H, Li, Na, F, Cl, Br, I; Y = O, S, Se, Te) .....	113
<b>Chapter 5:</b> .....	123
A comparison between Alkalimetal and Group 11 Transition Metal Halide and Hydride Tetramers: Molecular Structure and Bonding .....	123
<b>Chapter 6:</b> .....	135
An Analysis of the Relative Stabilities of Ortho, Meta, and Para MCIY(XC <sub>4</sub> H <sub>4</sub> )(PH <sub>3</sub> ) <sub>2</sub> Heterometallabenzenes (M = Rh, Ir; X = N, P; Y = Cl and M = Ru, Os; X = N, P; Y = CO) ...	135
<b>Chapter 7: Results and Discussion</b> .....	149
<b>Chapter 8: Conclusions</b> .....	179
<b>References</b> .....	183
<b>Annex</b> .....	197
A.1 Supplementary Information Chapter 3 .....	199
A.2 Supplementary Information Chapter 4 .....	201
A.3 Supplementary Information Chapter 5 .....	211
A.4 Supplementary Information Chapter 6 .....	223



## Summary

The formulation of quantum mechanics in the beginning of the 20<sup>th</sup> century represented the most important step towards the knowledge and understanding of the general laws describing the motion of the matter at the microscopic level. Furthermore, with the passage of time the improvement in the methods and approximations used in the resolution of the Schrödinger equation led theoretical and computational chemistry in the position to play a crucial role in chemistry. Now, many concepts of quantum and theoretical chemistry are used to solve complex problems in chemistry and large areas of sciences. One of the greatest achievements of quantum theory was the ability to describe the chemical bond. This understanding of the chemical bond was one of the most important achievements of modern chemical language. In fact, the calculation of chemical bond properties enables us to extract relevant information as the structure, geometry, stability, and reactivity of substances. Over the past decades, the stability of the isomers and the nature of the chemical bond have attracted considerable attention since many of these species intervene in industrial, biochemical, and atmospheric processes. The understanding of the relative stabilities of these species has not been fully achieved yet and, moreover, some thermochemical data is still missing.

In general, it is found that density functional theory (DFT) performs reasonably well, unlike many other theoretical methods that fail to correctly reproduce the molecular structure, either giving too short or too long bond distances. For this purpose, we decided to use the DFT calculations performed with the Amsterdam Density Functional (ADF) program that allows the use of energy decomposition analyses. These analyses are very useful to unravel the origin of the relative stabilities of isomers.

The thesis is divided into eight chapters including four related publications. The first study in Chapter 3 discusses the isomerization energies of 1,2-/1,3-diazacyclobutadiene, pyrazole/imidazole, and pyridazine/pyrimidine with the turn-upside-down approach. This research project aimed to provide a better comprehension on the origin of the NN bond destabilization. In this study, it was found that, in the three cases, the higher stability of the 1,3-isomers is not due to lower Pauli repulsions but because of the more favorable  $\sigma$ -orbital interactions involved in the formation of two C–N bonds in comparison with the generation of C–C and N–N bonds in the 1,2-isomers.

Furthermore, in Chapter 4, we have studied the  $XYXX$  and  $X_2YY$  isomers of the  $X_2Y_2$  species ( $X = \text{H, Li, Na, F, Cl, Br, I}$ ;  $Y = \text{O, S, Se, Te}$ ) using DFT at the ZORA-BP86/QZ4P level. Our computations show that, over the entire range of our model systems, the  $XYXX$  isomers are more stable than the  $X_2YY$  forms except for  $X = \text{F}$  and  $Y = \text{S}$  and  $\text{Te}$ , for which the  $\text{F}_2\text{SS}$  and  $\text{F}_2\text{TeTe}$  isomers are slightly more stable. Our results also point out that the  $Y\text{--}Y$  bond length can be tuned quite generally through the  $X\text{--}Y$  electronegativity difference. The mechanism behind this electronic tuning is the population or depopulation of the  $\pi^*$  in the  $YY$  fragment.

Moreover, in Chapter 5 a comparison between alkalimetal ( $M = \text{Li, Na, K, and Rb}$ ) and group 11 transition metal ( $M = \text{Cu, Ag, and Au}$ )  $(MX)_4$  tetramers with  $X = \text{H, F, Cl, Br, and I}$  has been carried out by means of the Amsterdam Density Functional software using DFT at the BP86/QZ4P level of theory and including relativistic effects through the ZORA approximation. We have obtained that, in the case of alkalimetals, the cubic isomer of  $T_d$  geometry is more stable than the ring structure with  $D_{4h}$  symmetry, whereas in the case of group 11 transition metal tetramers, the isomer with  $D_{4h}$  symmetry (or  $D_{2d}$  symmetry) is more stable than the  $T_d$  form. To better understand the results obtained we have made energy decomposition analyses of the tetramerization energies. The results show that in alkalimetal halide and hydride tetramers, the cubic geometry is the most stable because the larger Pauli repulsion energies are compensated by the attractive electrostatic and orbital interaction terms. In the case of group 11 transition metal tetramers, the  $D_{4h}/D_{2d}$  geometry is more stable than the  $T_d$  one due to the reduction of electrostatic stabilization and the dominant effect of the Pauli repulsion.

Finally, the last chapter of this thesis (Chapter 6) is based on an analysis of the relative stabilities of ortho, meta, and para  $MClY(XC_4H_4)(PH_3)_2$  heterometallabenzenes ( $M = \text{Rh, Ir}$ ;  $X = \text{N, P}$ ;  $Y = \text{Cl}$  and  $M = \text{Ru, Os}$ ;  $X = \text{N, P}$ ;  $Y = \text{CO}$ ). The results show that the meta isomer is the most stable for  $X = \text{N}$  and  $M = \text{Ir, Rh}$ , the ortho is the lowest-lying isomer for  $X = \text{P}$  irrespective of the metal, and for  $X = \text{N}$  and  $M = \text{Ru, Os}$ , the ortho and meta isomers are almost degenerate. The electronic structure and bonding situation have been investigated with energy decomposition analyses of the interaction energy between various fragments to discuss the origin of the differences observed.

## Resum

La formulació de la mecànica quàntica a principis del segle XX va representar el pas més important en el coneixement i comprensió de les lleis generals del moviment de la matèria a nivell microscòpic. A més, amb el pas del temps la millora en els mètodes i aproximacions usats per resoldre l'equació de Schrödinger han portat a la química teòrica i computacional a una posició d'exercir un paper crucial en la química. Ara, molts dels conceptes de la química quàntica són usats per resoldre problemes complexos de la química i altres àrees de les ciències. Un dels grans èxits de la teoria quàntica és la capacitat de descriure l'enllaç químic. Aquesta comprensió de l'enllaç química va ser un dels èxits més importants del llenguatge químic modern. De fet, el càlcul de les propietats químiques dels enllaços ens permet obtenir informació química rellevant com l'estructura, la geometria, l'estabilitat i la reactivitat de les substàncies. Durant les últimes dècades, l'estabilitat dels isòmers i la naturalesa de l'enllaç químic han atret una atenció considerable ja que moltes d'aquestes espècies intervenen en reaccions industrials, bioquímiques i en processos atmosfèrics. No s'ha aconseguit comprendre de forma completa l'estabilitat relativa d'aquestes espècies i algunes dades termoquímiques encara manquen.

En general, es troba que la teoria funcional de la densitat (DFT) funciona raonablement bé a diferència d'altres mètodes teòrics que no reproduïxen correctament l'estructura molecular, ja sigui donant distàncies d'enllaç massa curtes o llargues. Per aquest motiu, vam decidir utilitzar DFT i realitzar els càlculs amb el programa Amsterdam Density Functional (ADF) usant l'anàlisi de descomposició d'energia. Aquests anàlisis són molt útils per desentranyar l'origen de les estabilitats relatives d'isòmers.

La tesi es divideix en vuit capítols, incloent quatre publicacions relacionades. El primer estudi en el Capítol 3 discuteix les energies d'isomerització dels sistemes 1,2-/1,3-diazaciclobutadiè, pirazol/imidazol i piridacina/pirimidina amb l'enfocament "turn-upside-down". Aquest projecte de recerca va tenir com a objectiu proporcionar una millor comprensió sobre l'origen de la desestabilització de l'enllaç NN. Es va trobar que en els tres casos la major estabilitat dels isòmers 1,3- no és deguda a menors repulsions de Pauli, sinó a interaccions  $\sigma$ -orbitals més favorables presents en la formació de dos enllaços CN en comparació amb la generació d'enllaços CC i NN en els isòmers 1,2-.

D'altra banda, en el Capítol 4 s'ha estudiat l'estabilitat relativa dels isòmers  $XYXX$  i  $X_2YY$  de les espècies  $X_2Y_2$  ( $X = H, Li, Na, F, Cl, Br, I$ ;  $Y = O, S, Se, Te$ ) utilitzant DFT a nivell ZORA-BP86/QZ4P. Els nostres càlculs mostren que, en tota la gamma dels nostres sistemes model, els isòmers  $XYXX$  són més estables que les formes  $X_2YY$  excepte per  $X = F$  i  $Y = S$  i  $Te$ , pels quals els isòmers  $F_2SS$  i  $F_2TeTe$  són una mica més estables. Els nostres resultats també assenyalen que la longitud d'enllaç  $YY$  es pot ajustar a través de la diferència d'electronegativitat  $XY$ . El mecanisme darrere d'aquesta afinació electrònica és la població o despoblació de l'orbital  $\pi^*$  en el fragment  $YY$ .

D'altra banda, el Capítol 5 inclou una comparació entre els tetràmers  $(MX)_4$  dels metalls alcalins ( $M = Li, Na, K, Rb$ ) i metalls de transició del grup 11 ( $M = Cu, Ag, i Au$ ) amb  $X = H, F, Cl, Br$  i  $I$ , que s'ha dut a terme mitjançant ADF utilitzant DFT amb el nivell de teoria BP86/QZ4P i incloent efectes relativistes a través de l'aproximació ZORA. Hem obtingut que, en el cas dels metalls alcalins, l'isòmer cúbic de geometria  $T_d$  és més estable que l'estructura d'anell amb simetria  $D_{4h}$ , mentre que en el cas del grup 11 l'isòmer amb simetria  $D_{4h}$  (o simetria  $D_{2d}$ ) és més estable que la forma  $T_d$ . Per comprendre millor els resultats obtinguts hem realitzat anàlisis de descomposició d'energia de les energies de tetramerització. Els resultats mostren que en tetràmers d'halogenurs i hidrurs de metall alcalí, la geometria cúbica és la més estable a causa que les importants energies de repulsió de Pauli són compensades per les interaccions electrostàtiques i orbitalàries que són atractives. En el cas dels tetràmers del grup 11 dels metalls de transició, la geometria  $D_{4h}/D_{2d}$  és més estable que la  $T_d$  a causa de la reducció de l'estabilització electrostàtica i l'efecte dominant de la repulsió de Pauli.

Finalment, l'últim capítol d'aquesta tesi (Capítol 6) es basa en una anàlisi de les estabilitats relatives dels heterometalabenzens orto, meta i para  $MClY(XC_4H_4)(PH_3)_2$  ( $M = Rh, Ir, X = N, P$ ;  $Y = Cl$  i  $M = Ru, Os$ ;  $X = N, P, Y = CO$ ). El resultat mostra que l'isòmer meta és el més estable per  $X = N$  i  $M = Ir, Rh$ , l'orto és l'isòmer de més baixa energia per a  $X = P$ , independentment del metall, i per a  $X = N$  i  $M = Ru, Os$ , els isòmers orto i meta són gairebé degenerats. L'estructura electrònica i la naturalesa de l'enllaç s'han investigat amb anàlisis de descomposició de l'energia d'interacció entre els diversos fragments per determinar l'origen de les diferències observades.

## Resumen

La formulación de la mecánica cuántica a principios del siglo XX representó el paso más importante en el conocimiento y comprensión de las leyes generales que describen el movimiento de la materia a nivel microscópico. Además, con el paso del tiempo la mejora en los métodos y aproximaciones usados para resolver la ecuación de Schrödinger han llevado a la química teórica y computacional a una posición de desempeñar un papel crucial en la química. Ahora, muchos de los conceptos de la química cuántica son usados para resolver problemas complejos de la química y otras áreas de las ciencias. Uno de los grandes logros de la teoría cuántica es la capacidad de describir el enlace químico. Y esta comprensión del enlace químico fue uno de los logros más importantes del lenguaje químico moderno. De hecho, el cálculo de las propiedades químicas de los enlaces nos permite obtener información química relevante como la estructura, la geometría, la estabilidad y la reactividad de las sustancias. Durante las últimas décadas, la estabilidad de los isómeros y la naturaleza del enlace químico han atraído una atención considerable puesto que muchas de estas especies intervienen en reacciones industriales, bioquímicas y en procesos atmosféricos. No se ha conseguido aun comprender de forma completa la estabilidad relativa de estas especies y todavía desconocemos algunos datos termoquímicos.

En general, se encuentra que la teoría del funcional de la densidad (DFT) funciona razonablemente bien a diferencia de otros métodos teóricos que no reproducen correctamente la estructura molecular, ya sea dando distancias de enlace demasiado cortas o largas. Por este motivo, decidimos utilizar DFT y realizar los cálculos con el programa Amsterdam Density Functional (ADF) usando el análisis de descomposición de energía. Estos análisis son muy útiles para desentrañar el origen de las estabilidades relativas de isómeros.

La tesis se divide en ocho capítulos, incluyendo cuatro publicación relacionada. El primer estudio en el Capítulo 3 discute las energías de isomerización de los sistemas 1,2-/1,3-diazaciclobutadieno, pirazol/imidazol y piridacina/pirimidina con el enfoque “turn-upside-down”. Este proyecto de investigación tuvo como objetivo proporcionar una mejor comprensión sobre el origen de la desestabilización del enlace NN. En este estudio, se encontró que, en los tres casos, la mayor estabilidad de los isómeros 1,3- no es debida a las menores repulsiones de Pauli sino a las interacciones  $\sigma$ -orbitales más favorables que participan en la formación de dos enlaces CN en comparación con la generación de enlaces CC y NN en los isómeros 1,2-.

Por otra parte, en el Capítulo 4 se ha estudiado la estabilidad relativa de los isómeros  $XYXX$  y  $X_2YY$  de las especies  $X_2Y_2$  ( $X = H, Li, Na, F, Cl, Br, I$ ;  $Y = O, S, Se, Te$ ) utilizando DFT al nivel ZORA-BP86/QZ4P. Nuestros cálculos muestran que, en toda la gama de nuestros sistemas modelo, los isómeros  $XYXX$  son más estables que las formas  $X_2YY$  excepto para  $X = F$  e  $Y = S$  y  $Te$ , para los que los isómeros  $F_2SS$  y  $F_2TeTe$  son un poco más estables. Nuestros resultados también señalan que la longitud de enlace  $YY$  se puede ajustar a través de la diferencia de electronegatividad  $XY$ . El mecanismo detrás de esta afinación electrónica es la población o despoblación del orbital  $\pi^*$  en el fragmento  $YY$ .

Por otra parte, el Capítulo 5 incluye una comparación entre los tetrámeros  $(MX)_4$  de los metales alcalinos ( $M = Li, Na, K, Rb$ ) y metales de transición del grupo 11 ( $M = Cu, Ag, y Au$ ) con  $X = H, F, Cl, Br$  y  $I$ , que se ha llevado a cabo mediante ADF utilizando DFT con el nivel de teoría BP86/QZ4P e incluyendo efectos relativistas a través de la aproximación ZORA. Hemos obtenido que, en el caso de los metales alcalinos, el isómero cúbico de geometría  $T_d$  es más estable que la estructura de anillo con simetría  $D_{4h}$ , mientras que en el caso del grupo 11 el isómero con simetría  $D_{4h}$  (o simetría  $D_{2d}$ ) es más estable que la forma  $T_d$ . Para comprender mejor los resultados obtenidos hemos realizado análisis de descomposición de energía de las energías de tetramerización. Los resultados muestran que en tetrámeros de halogenuros e hidruros de metal alcalino, la geometría cúbica es la más estable debido a que las importantes energías de repulsión de Pauli son compensadas por las interacciones electrostáticas y orbitarias que son atractivas. En el caso de los tetrámeros del grupo 11 de los metales de transición, la geometría  $D_{4h}/D_{2d}$  es más estable que el  $T_d$  debido a la reducción de la estabilización electrostática y el efecto dominante de la repulsión de Pauli.

Finalmente, el último capítulo de esta tesis (Capítulo 6) se basa en un análisis de las estabilidades relativas de los heterometalabencenos orto, meta y para  $MClY(XC_4H_4)(PH_3)_2$  ( $M = Rh, Ir, X = N, P$ ;  $Y = Cl$  y  $M = Ru, Os$ ;  $X = N, P$ ;  $Y = CO$ ). El resultado muestra que el isómero meta es el más estable para  $X = N$  y  $M = Ir, Rh$ , el orto es el isómero de más baja energía para  $X = P$ , independientemente del metal, y para  $X = N$  y  $M = Ru, Os$ , los isómeros orto y meta son casi degenerados. La estructura electrónica y la naturaleza del enlace se han investigado con análisis de descomposición de la energía de interacción entre los diversos fragmentos para determinar el origen de las diferencias observadas.

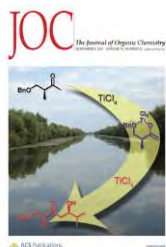




## Full List of Publications

The thesis is based on the following publications:

### Chapter 3:

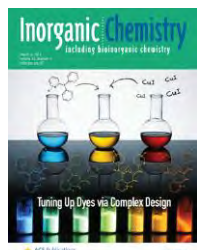


Majid El-Hamdi, William Tiznado, Jordi Poater, Miquel Solà, “An Analysis of the Isomerization Energies of 1,2-/1,3- Diazacyclobutadiene, Pyrazole/Imidazole, and Pyridazine/Pyrimidine with the Turn-Upside-Down Approach”, *J. Org. Chem.* **2011**, 76, 8913–8921.

Impact Factor: 4.564

Time published: September 27, 2011

### Chapter 4:

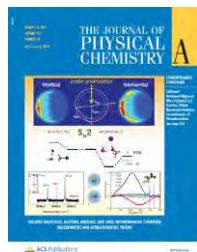


Majid El-Hamdi, Jordi Poater, F. Matthias Bickelhaupt, Miquel Solà, “ $X_2Y_2$  Isomers: Tuning Structure and Relative Stability through Electronegativity Differences ( $X = H, Li, Na, F, Cl, Br, I; Y = O, S, Se, Te$ )”, *Inorg. Chem.* **2013**, 52, 2458–2465.

Impact Factor: 4.593

Time published: February 19, 2013

### Chapter 5:

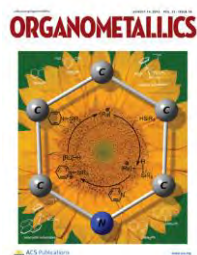


Majid El-Hamdi, Miquel Solà, Gernot Frenking, Jordi Poater, “A Comparison between Alkalimetal and Group 11 Transition Metal Halide and Hydride Tetramers: Molecular Structure and Bonding”, *J. Phys. Chem. A.*, **2013**, 117, 8026–8034.

Impact Factor: 2.771

Time published: July 23, 2013

### Chapter 6:



Majid El-Hamdi, Ouissam El Bakouri El Farri, Pedro Salvador, Ben Ali Abdelouahid, Mohamed Soussi El Begrani, Jordi Poater, Miquel Solà, “An Analysis of the Relative Stabilities of Ortho, Meta, and Para  $MClY(XC_4H_4)(PH_3)_2$  Heterometallabenzenes ( $M = Rh, Ir; X = N, P; Y = Cl$  and  $M = Ru, Os; X = N, P; Y = CO$ )”, *Organometallics*, **2013**, accepted, DOI: 10.1021/om400629w..

Impact Factor: 4.145

Time published: August 28, 2013







## List of Acronyms

Abbreviation	Description
ACID	Anisotropy of the current-induced density
ARCS	Aromatic ring current shielding
ASE	Aromatic stabilization energy
BAC	Bond alternation coefficient
BLW	Block-localized wave function
BP86	Perdew86 correlation and Becke88 exchange GGA functional
B3LYP	Becke, three-parameter, Lee-Yang-Parr
CASSCF	Complete Active Space Self Consistent Field
cc-pvDZ-PP	Correlated consistent valence double zeta + polarization including pseudopotentials basis set
CCSD	Coupled Cluster Singles and Doubles
CD	Circular dichroism
CI	Configurations interaction
D	Debye
DFT	Density Functional Theory
DNA	Deoxyribonucleic Acid
ELF	Electron localization function
ESI	Electron Sharing Indices
eV	Electron-volt
FLU	Aromatic fluctuation index
GGA	Generalized gradient approximation
GIAO	Gauge-Independent Atomic Orbital
HF	Hartree-Fock
HOMO	Highest occupied molecular orbital
HOMA	Harmonic Oscillator Model of Aromaticity
HPLC	High-performance liquid chromatography
IGLO	Individual gauge for localized orbitals
IUPAC	International Union of Pure and Applied Chemistry
LCAO	Linear combination of atomic orbitals

LDA            Local density approximation

---

<b>Abbreviation</b>	<b>Description</b>
LMO	Localized molecular orbital
LUMO	Lowest unoccupied molecular orbital
MCI	Multicenter index
MCSCF	Multiconfiguration self consistent field
MNDO	Modified Neglect of Diatomic Overlap
MO	Molecular orbital
MP2	Second-order Moller-Plesset Perturbation Theory
NBO	Natural bond orbital
NICS	Nucleus independent chemical shifts
NMR	Nuclear Magnetic Resonance
PDI	Para-delocalizaion index
pK <sub>a</sub>	Acid dissociation constant
QZ4P	core triple zeta, valence quadruple zeta, with 4 polarization functions
RE	Resonance energy
RHF	Restricted Hartree-Fock
ROHF	Restricted Open-Shell Hartree-Fock
TZ2P	core double zeta, valence triple zeta, doubly polarized basis
UHF	Unrestricted Hartree-Fock
VB	Valence bond
ZORA	zeroth order regular approximation for relativistic corrections
$\mu_e$	Electric dipole moment
3c-2e	Three-Center, two electrons

---

## List of Figures

Figure 1.1. Potential fluctuation $\hat{V}_F$ of beryllium ( $Z = 4$ ) for the two electrons 1s obtained by o. sinanoglu .....	84
Figure 7.1. Geometries (in Å, deg) of the studied diaza compounds computed at BP86/TZ2P. experimental values are given in parentheses. key: (a) from ref. <sup>[486]</sup> ; (b) from ref. <sup>[487]</sup> ; (c) from ref <sup>[488]</sup> ; (d) from ref. <sup>[489]</sup> .....	152
Figure 7.2. Molecular orbital diagram for the interaction of $Y_2\cdot\cdot$ with two $X\cdot$ to yield isomer XYYX. ....	160
Figure 7.3. Molecular orbital diagram for the interaction of $Y_2\cdot\cdot$ with two $X\cdot$ to yield isomer $X_2YY$ . ....	161
Figure 7.4. Some resonance structures for FSSF and $F_2SS$ isomers. ....	163
Figure 7.5. Structure of alkalimetal tetramers $M_4X_4$ with $X = H, F, Cl, Br, I$ and $M = Li$ in both $T_d$ and $D_{4h}$ symmetries. ....	166
Figure 7.6. Structure of group 11 transition metal tetramers $M_4X_4$ with $X = H, F, Cl, Br, I$ and $M = Cu$ . ....	170



## List of Tables

Table 1.1: Examples of different H-bonds .....	55
Table 1.2: Some important aromaticity criteria and key developments.....	70
Table 7.1. Geometrical parameters of XSSX, X <sub>2</sub> SS, XOOX and X <sub>2</sub> OO isomers (bond lengths in Å and angles in degrees) .....	159
Table 7.2. Relative energy of the isomerization between XSSX and X <sub>2</sub> SS (in kcal.mol <sup>-1</sup> ).....	160
Table 7.3. Energy decomposition analysis for XSSX and X <sub>2</sub> SS isomers (in kcal.mol <sup>-1</sup> ), together with the average population of the two somo orbitals of SS (in electrons), and energy of the somo orbital for X (in eV).....	162
Table 7.4. Energy decomposition analysis (in kcal.mol <sup>-1</sup> ) of the tetramerization of M <sub>4</sub> X <sub>4</sub> systems with M = Li, Na, K and Rb. <sup>a</sup> .....	168
Table 7.5. Energy decomposition analysis (in kcal.mol <sup>-1</sup> ) of the tetramerization of M <sub>4</sub> X <sub>4</sub> systems with M = Cu, Ag, and Au. <sup>a</sup> .....	171
Table 7.6. Analysis of the bonding (in kcal/mol) between triplet azaethenediyl A(x-IrN) <sub>N</sub> and triplet IrCl <sub>2</sub> (Ph <sub>3</sub> ) <sub>2</sub> (C <sub>3</sub> H <sub>3</sub> ) B(X-IrN) <sub>Ir</sub> fragments in o-IrN, m-IrN, and deformed m-IrN (m-IrN <sub>a</sub> and m-IrN <sub>b</sub> ). <sup>a</sup> .....	174
Table 7.7. Analysis of the bonding (in kcal/mol) between triplet azaethenediyl A(x-IrN) <sub>N</sub> and triplet IrCl <sub>2</sub> (Ph <sub>3</sub> ) <sub>2</sub> (C <sub>3</sub> H <sub>3</sub> ) B(x-IrN) <sub>Ir</sub> fragments in M-IrN and P-IrN, and deformed P-IrN (P-IrN <sub>a</sub> and P-IrN <sub>b</sub> ). <sup>a</sup> .....	176



## List of Schemes

Scheme 1.1: Lewis electronic presentation for some of the atoms .....	41
Scheme 1.2: Example of a double or triple bond between two atoms .....	42
Scheme 1.3: Lewis representation of the water molecule .....	42
Scheme 1.4: Lewis representation of ammonia molecule .....	42
Scheme 1.5: Conventional formal charge in trimethylamine oxide, ammonium ion .....	43
Scheme 1.6: Representation of the molecule of boron trifluoride $\text{BF}_3$ .....	43
Scheme 1.7: Representation of the donor-acceptor bond of borazane $\text{NH}_3\text{BF}_3$ .....	44
Scheme 1.8: The two different ways of introducing the 3-e- into the two existing orbitals .....	45
Scheme 1.9: Dimer geometry example. ....	45
Scheme 1.10: The attack of the two-proton on the double bond of $\text{B}_2\text{H}_4^{2-}$ .....	46
Scheme 1.11: The structure of $\text{B}_2\text{H}_6$ molecule.....	46
Scheme 1.12: The Pseudo- $\text{SP}^3$ hybridization of borane.....	46
Scheme 1.13: banana bond.....	47
Scheme 1.14: Kekule forms of benzene molecule .....	47
Scheme 1.15: Delocalization of the $\pi$ bonds in benzene molecule .....	48
Scheme 1.16: The six p orbitals of benzene overlap to form three bonding orbitals, (a), (b), and (c). the three orbitals superimposed are shown in (d) .....	48
Scheme 1.17: Formation of a lif molecule. (a) electronic structure and size of the isolated lithium and fluorine atoms. (b) electron transfer from li to f creating an ionic bond between $\text{Li}^+$ and $\text{F}^-$ ions. ....	50

Scheme 1.18: The average dipolar moment of a H <sub>2</sub> O molecule .....	51
Scheme 1.19: The interaction between charged species of ionic and metallic crystals .....	52
Scheme 1.20: H-bonds in different geometrical structures .....	54
Scheme 1.21: dipole-dipole interaction.....	57
Scheme 1.22: Interaction between polar and apolar species.....	57
Scheme 1.23: From left to right, top to bottom: quinoxaline, quinazoline, phthalazine, benzo[c]cinnoline, phenazine, 1,10 phenanthroline, and triphenyl-amine. standards: 2,6-dimethylquinoline, 2-phenylpyridine, 4,7-phenanthroline, 7,8-benzoquinoline, and acridine....	60
Scheme 1.24: From left to right, top to bottom: (a) 1,2/1,3-azacyclobutadiene; (b) pyrazole/imidazole and (c) pyridazine/pyrimidine. ....	61
Scheme 1.25: Geometric structure of trans and cis isomers of azobenzene .....	61
Scheme 1.26: The staggered and eclipsed conformation for ethane .....	62
Scheme 1.27: Conformational analysis of cyclohexane.....	63
Scheme 1.28: Different aromatic molecules .....	68
Scheme 1.29: Geometric structure of some metal clusters .....	69
Scheme 2.1 The formation of (a) 1,2- and 1,3-diazacyclobutadiene, (b) pyrazole/imidazole, (c) pyridazine/pyrimidine structural isomers from two triplet biradical fragments with the turn-upside-down approach.....	98
Scheme 2.2 An schematic representation of the three isomers of the MClY(XC <sub>4</sub> H <sub>4</sub> )(PH <sub>3</sub> ) <sub>2</sub> heterometallabenzenes considered. ....	100
Scheme 7.1. The formation of (a) 1,2- and 1,3-diazacyclobutadiene, (b) pyrazole/imidazole, (c) pyridazine/pyrimidine structural isomers from two triplet biradical fragments with the turn-upside-down approach.....	154
Scheme 7.2. The two possible X <sub>2</sub> Y <sub>2</sub> structural isomers.....	158

Scheme 7.3. Isomeric forms ( $T_d$ , ladder, and  $D_{4h}$ ) of the tetramer  $(MX)_4$  clusters ..... 165

Scheme 7.4. Fragments considered in the eda for the formation of the ortho, meta, and para isomers of  $MClY(XC_4H_4)(PH_3)_2$  complexes ( $M = Ir, Rh, X = N, P$  AND  $Y = Cl$  and  $M = Os, Ru, X = N, P$  and  $Y = CO$ ). ..... 173



## **Chapter 1: General Introduction**

---

In this part I shall attempt to present a general introduction about the nature of chemical bonds and different isomer types. Moreover, I make a detail explanation of the concept and different descriptors of aromaticity. Finally, general and recent methods on the basis of quantum chemistry are discussed.

---



## 1. Introduction

Many concepts related to the nature of chemical bond and molecular structure were formulated by chemists by induction from enormous body of chemical facts. The chemical bond is one of the most important and fruitful concepts of modern chemical language and acts as a central idea of our knowledge concerning the structure, geometry, stability, and reactivity of substances. The study of the chemical bond and molecular structure was originally carried out by chemists using methods of investigation that were significantly chemical in nature, related to the chemical composition of the substances, the reactivity thereof, the existence of compounds having identical composition but different properties, and so on. A set of ideas were gradually emerging about molecular structure, which were originated initially based on the primary chemical intuition.

In 1852, Frankland<sup>[1]</sup> proposed the concept of the valence stating that each element forms compounds by reacting with an accurate number of what we now call equivalents of other elements. After Kekulé<sup>[2]</sup> and Kolbe<sup>[3]</sup> extended the concept of valence to carbon and said that the carbon generally has valence 4. In the following year, Kekulé<sup>[4]</sup> suggested that carbon atoms can unite with an indefinite number of other carbon atoms into long chains. At the same year, Cooper, a Scottish<sup>[5, 6]</sup> chemist, independently discussed the quadrivalence of carbon and the capability of carbon atoms to form chains and he was the first one to draw a line between symbols to represent the chemical bond. In 1861, Butlerov<sup>[7]</sup> formulated the theory of the valence and wrote the first structural formulas for molecules, which show how each atom is attached to other atoms in the molecule of the substance. In the next step, van't Hoff<sup>[8]</sup> and le Bel<sup>[9]</sup> assigned structures in three dimensional spaces to the molecules and guided to bring classical organic stereochemistry into its final form using the tetrahedral orientation of the four valence bonds of the carbon atom. After that, Werner<sup>[10]</sup> was led to his advancement of the theory of the stereochemistry of complex inorganic substances. During this 19<sup>th</sup> century, the valence bond was represented by a line drawn between the symbols of two chemical elements and the nature of the bond was totally unknown. The discovery of the electron represented a big advance since it was the first step towards the development of an electronic theory of the chemical bond.

The discovery of the electron was a great support to Lewis, who in his 1916 paper,<sup>[11]</sup> managed to form the basis of the modern electronic theory of the valence. He discussed not only the

formation of ions by the completion of stable shells of electrons, but also the formation of the chemical bond which today would be called covalent bond by the sharing two electrons from different atoms. This idea was also treated separately at about the same time by W. Kossel.<sup>[12]</sup> Lewis showed the importance of the phenomena of the pairing of unshared as well as of shared electrons in the chemical structures. He pointed out that atoms in molecules try to reach their most stable electronic configuration to increase the stability of the molecules formed. These ideas were developed by many researchers. Langmuir, in 1919,<sup>[13]</sup> applied new ideas, he suggested that the special stability and inertness of the N<sub>2</sub> molecule might be accounted for by the following assumptions: (a) each N nucleus retains its two most tightly bound electrons, (b) eight of the remaining ten electrons form a group of eight or “octet”, (c) the last two electrons form a pair which is detained in this octet and helps to stabilize the whole structure. As we have seen before, the atoms are bonded together by sharing electrons so as the aim to complete their outer shell. Moreover, they can interact in various ways to form aggregates. In the following sections we will illustrate the different types of chemical bonds.

There is no single and unique classification of the chemical bonds; it is practical to consider three general extreme types of chemical bonds: electrostatic bonds, covalent bonds, and metallic bonds. Whereas the bonds of each type have well-defined properties, it has been possible to deduce from the properties of substances a number of general principles about the nature of the bonds depending on the nature of the two atoms connected by it. During the 19<sup>th</sup> century the discussion whether the transition from one extreme bond type to another take place continuously or discontinuously was a subject of great controversy between the scientists. In 1916, Lewis said that the bond has a certain amount of ionic or polar character, and he supported the idea that the transition would be continuous. In polar bonds, the shared electron pair is attracted more strongly by one than by the other of two unlike bonded atoms. Moreover, Sidgwick<sup>[14]</sup> and London<sup>[15]</sup> provided the opinion that the transition between two extreme bond types might occur also continuously, but there is an indispensable difference between the two types of bonds.

### **1.1 The chemical bond definition**

Linus Pauling<sup>[16]</sup> defined the chemical bond between two atoms or groups of atoms in the case that the forces acting between them are such as to lead to the formation of an aggregate with sufficient stability to make it convenient for the chemist to consider it as an independent molecular species. Moreover, A. Coulson<sup>[17]</sup> said that the description of an intimate chemical

bond must be basically due to electrostatic interactions. It is the behavior and distribution of electrons around the nucleus that gives the essential character of an atom and must be the same for the molecules. Therefore, in one sense, the description of the bond in any molecule is simply the description of the electron distribution.

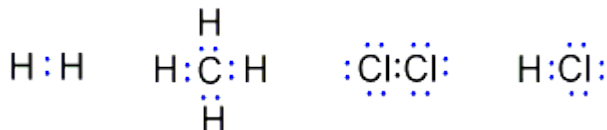
## 1.2 Types of chemical bonds

It is advantageous to categorize firstly the chemical bonds between strong bonds and weak bonds. The energy of these bonds is taken as a measure of their "strength". Then we can involve specific mechanisms that characterize the various chemical bonds encountered in nature.

### 1.2.1 Strong chemical bond

#### 1.2.1.1 The covalent bond

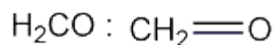
In the representation of Lewis of the covalent bond, the electrons from the valence shell involved in building the bond between atoms are represented by points. Then it is considered that the atoms of the second period of the periodic table (C, N, O, and F) are stable with eight electrons in their valence shell (octet rule). These 8 electrons in each atom are formed by the valence electrons belonging to the atom considered plus the electrons shared by the atoms to which this atom is bounded:



Scheme 1.1: Lewis electronic presentation for some of the atoms

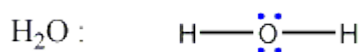
The symbol of the element represents the nucleus of the atom in these Lewis electronic formulas. A pair of electrons in between two atoms is regarded as a bond. Sharing electrons allow atoms to reach the octet. Thus, for instance, the carbon atom in methane molecule, with its two inner electrons and its outer shell of eight shared electrons, has presupposed the stable ten-electron (eight valence electron) configuration of neon, and that each of the other atoms in the structures shown has accomplished a noble-gas configuration.

Forming a double or triple bond between two atoms implies four and six shared electrons, as in the following examples:



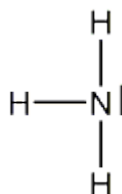
Scheme 1.2: Example of a double or triple bond between two atoms

It should be noted that the Lewis representation gives no indication of the actual spatial form of molecules; as in the following example of the water:



Scheme 1.3: Lewis representation of the water molecule

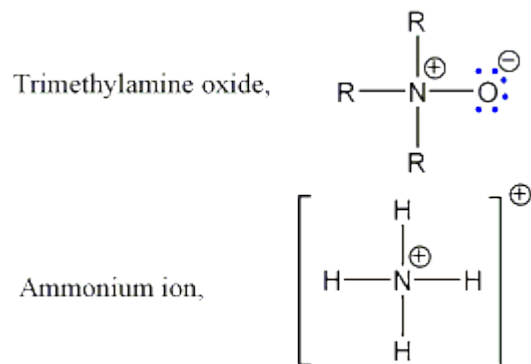
We know in fact that the molecule is bent with an angle of  $105^\circ$ . On the other hand, ammonia is represented by:



Scheme 1.4: Lewis representation of ammonia molecule

It has a pyramidal shape, the angle between two N-H bonds is  $107^\circ$ . The  $\text{NH}_4^+$  ion has a tetrahedral shape, such as  $\text{CH}_4$ , but with N in the center.

If it is supposed that the electrons of a shared pair are divided between the two atoms which they connect, then it is found on counting electrons by using this formula that the nitrogen and oxygen atoms in ammonia and water have a charge of zero. These charges calculated using the Lewis electronic structure and dividing shared electrons equally between the bonded atoms were first discussed by I. Langmuir,<sup>[18]</sup> and we shall often symbolize them by signs near the symbols of the atoms, as in the following examples:



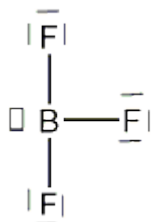
Scheme 1.5: Conventional formal charge in Trimethylamine oxide, ammonium ion

These formal charges can be considered as conventional in significance. Therefore, the unit positive charge of the complex in the ammonium ion is not to be considered as residing exclusively on the nitrogen atom.

In trimethylamine oxide, the bond between nitrogen and oxygen may be considered a sort of double bond, consisting of one single covalent bond and one ionic bond of unit strength. This type of bond has been called by Lowry<sup>[19, 20]</sup> as a semipolar double bond.

### 1.2.1.2 Donor-acceptor bonds

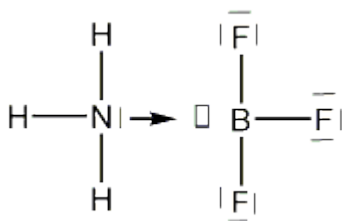
Sidgwick<sup>[21]</sup> proposed the name of coordinate or dative covalent bond to the bond in which one of the two atoms bring the shared electron pair. This bond is recognized by an especial symbol,  $\rightarrow$ , to point out the transfer of electric charge from one atom to another. For instance, the molecule of boron trifluoride  $\text{BF}_3$  can be represented as:



Scheme 1.6: Representation of the molecule of boron trifluoride  $\text{BF}_3$

The boron atom B has three valence electrons. Counting the three electrons coming from the fluoride atoms, B is surrounded by six electrons in total. So, there are 2 electrons left in order to satisfy the octet rule. These two missing electrons are shown in the figure above by an empty "box". The lone pair of  $\text{NH}_3$ , for example, can interact with boron in  $\text{BF}_3$  molecule forming

borazane  $\text{NH}_3\text{BF}_3$ . Scheme 1.7 is a representation of the donor-acceptor bond, where the nitrogen is the donor and the boron is the acceptor.



Scheme 1.7: Representation of the donor-acceptor bond of borazane  $\text{NH}_3\text{BF}_3$

### 1.2.1.3 The one-electron bond

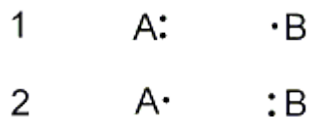
Certain molecules have bonds between the atoms that involve one electron or three electrons (instead of a shared pair).

The simplest of all chemical bonds which involves one electron shared by two atoms is the hydrogen molecule-ion  $\text{H}_2^+$ . The structure was discussed theoretically by considering the motion of the electron in the field of the atomic nuclei regarded to be fixed in a definite configuration.<sup>[22]</sup> Very precise calculations<sup>[23-25]</sup> have led to the value for the energy of formation  $\text{H}_2^+$  from a hydrogen atom and a hydrogen ion ( $D_0=60.95 \pm 0.10$  kcal/mole). It can be anticipated that molecules containing one-electron bonds will be less stable than those which are formed by an electron-pair-bond. Furthermore, the two atoms that form one-electrons bonds should be identical or very similar. This is a required condition for a stable one-electron bond to be formed between two atoms.

### 1.2.1.4 The three-electron bond

G.N. Lewis in his 1916 paper<sup>[11]</sup> (The Atom and the Molecule) showed the existence of few stable molecules and complex ions for which the total number of electrons is odd. He mentioned that such molecules, as nitric oxide or nitrogen dioxide, could use its unpaired electron to form a bond with another similar molecule. The “three-electron bond”<sup>[26]</sup> was a good explanation for the stability of molecules with an odd number of electrons as a result of the power of certain pairs of atoms to form this new type of bond.

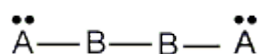
Let us consider two nuclei A and B, each of them with one stable bonding orbital. There are basically just two different ways of introducing the three electron into the two existing orbitals, 1 and 2:



Scheme 1.8: The two different ways of introducing the 3-e- into the two existing orbitals

Because of the exclusion principle, only two electrons of different spin can occupy the same orbital. The third electron must occupy the other orbital. The energy calculations carrying out for each case (1 and 2) leads to a similar result. Repulsive forces were observed between atoms A and B or at best a very weak attraction is found. However, if the atoms A and B are identical or are quite similar, the two structures (1 and 2) have almost the same energy, and then resonance will take place between them, which will stabilize the molecule and lead to the formation of a stable bond. This formed bond may be called the three-electron bond and represented as  $A\cdots B$ . It is found experimentally and theoretically that one-half of the three-electron bonds have character of an electron-pair. The helium molecule-ion  $He_2^+$ , consisting of two nuclei, is the simplest molecule in which the three-electron bond can occur. The theoretical result<sup>[27-29]</sup> of this molecule has shown that the bond is relatively strong, with a bond energy of about 55 kcal/mol and with an equilibrium internuclear distance of ca. 1.09 Å. This result was supported by experimental values (spectroscopic data) in which the energy of excited states of the helium molecule were about 58 kcal/mol and the internuclear distance was 1.080 Å.

The interaction between two molecules (each of them containing a stable three-electron bond) leads to the formation of a dimer that has the geometry indicated in Scheme 1.9.

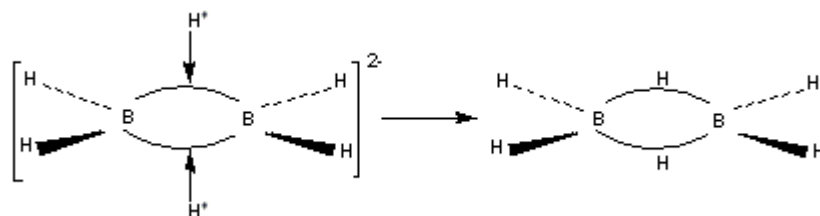


Scheme 1.9: Dimer geometry example.

In some cases, the heat of formation of the dimer is positive and in others is negative. For instance, the enthalpy of formation of  $N_2O_2$  from nitric oxide is 3.7 kcal/mol, therefore the heat of the reaction  $2NO \rightarrow N_2O_2$  is positive,<sup>[28]</sup> and the substance does not form a stable dimer in the gas phase. On the other hand, the nitrogen dioxide does form its dimer, dinitrogen tetraoxide.

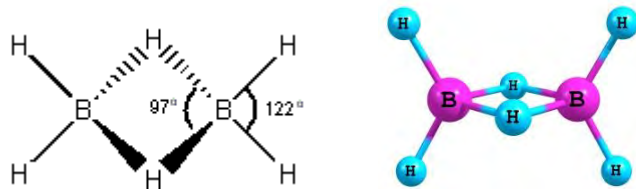
### 1.2.1.5 The Three-Center, Two-Electron Chemical Bond

In the early 1930's, Erich Hückel was the first who recognized the possibility of having an electron pair delocalized over more than two nuclei.<sup>[30-32]</sup> For example, the allyl cation ( $C_3H_5^+$ ) contains a three-center two-electron (3c-2e)  $\pi$  bond. The simplest 3c-2e bond is found in  $H_3^+$ , which was first observed in 1912 by Thomson<sup>[33]</sup>, although in this case is a 3c-2e  $\sigma$  bond.<sup>[34]</sup> This concept was not used in chemistry until 1945 when Pitzer<sup>[35]</sup> introduced the 3c-2e bond to clarify the structure of  $B_2H_6$  in terms of a two-proton attack on the double bond of " $B_2H_4^{2-}$ ".



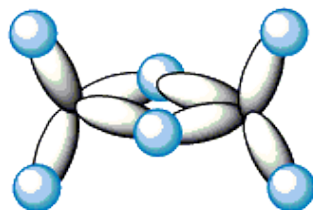
Scheme 1.10: The attack of the two-proton on the double bond of  $B_2H_4^{2-}$

The 3c-2e bond type of  $B_2H_6$  involves bridge H-atoms. The B-H-B bond is forced to be bent with an acute B-H-B angle of  $84^\circ$ .<sup>[36]</sup>

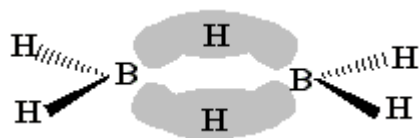


Scheme 1.11: The structure of  $B_2H_6$  molecule

Let us now theorize how such a bonding situation is possible and what produces the bridge. The B-H-B bond is a 3c-2e bond. The three center BHB orbital containing two electrons is the result of the combination of one 1s-orbital of the H atom and two pseudo- $sp^3$  orbitals of the boron atoms forming a banana bond as show in the Scheme 1.13.



Scheme 1.12: The pseudo- $sp^3$  hybridization of borane



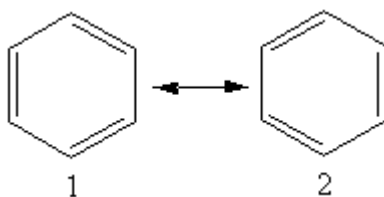
Scheme 1.13: Banana bond

### 1.2.1.6 The resonance chemical

The concept of resonance was introduced by Pauling in 1928.<sup>[16]</sup> The Lewis structures can adequately describe many compounds but still are insufficient in many other cases. Only the quantum theory of the chemical bond could fully explain the structure of these compounds, which have one or more bonding orbitals that are not restricted to two atoms, but that are settled down over three or more atoms, and the molecule is taken to be a weighted average of different Lewis structures (resonant structures). Such bonding is said to be delocalized.<sup>[29]</sup> Thus, each  $\Psi$  can be described as:

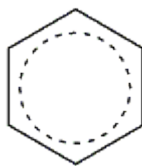
$$\Psi = C_1\psi_1 + C_2\psi_2 + \dots \quad (1.1)$$

The molecular orbital method can be used to obtain the solution of the wave equations such as that of Eq. (1.1).<sup>[28]</sup> The case of benzene is particularly interesting, this molecule is planar and hexagonal, but the carbon is tetravalent. Then, the Lewis representation (when placing the  $\pi$  bond) leads to the following two forms (Kekulé forms):



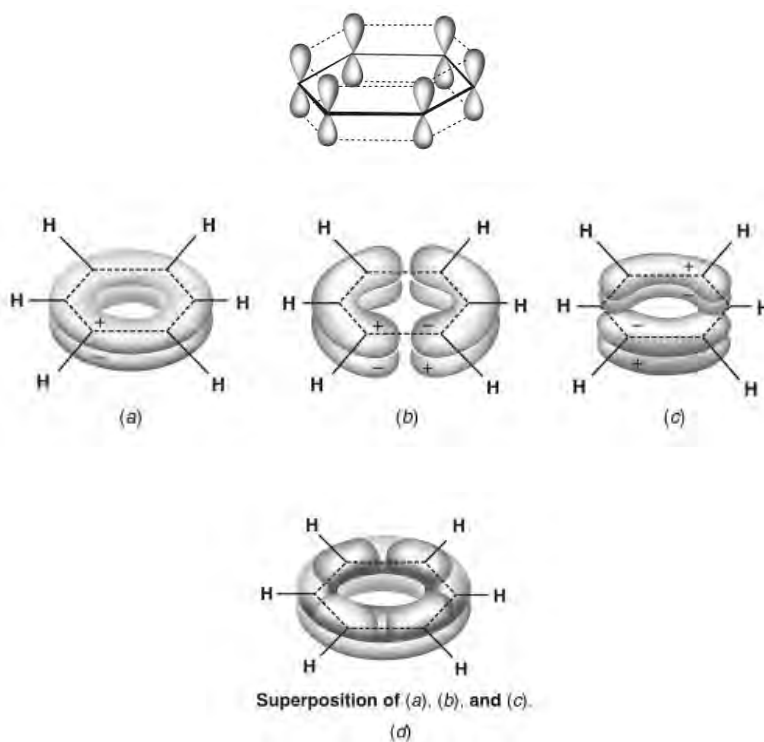
Scheme 1.14: Kekulé forms of benzene molecule

Theoretically it is found that the energy value obtained by seeing that 1 and 2 participate likewise is lower than that for 1 or 2 alone.<sup>[37]</sup> The explanation given by the quantum theory is that the electrons form  $\pi$  bonds that are actually "delocalized". This means that  $\pi$  electrons are free to move along the carbon hexagonal ring, with an average of one electron  $\pi$  for each C-C bond, which lead to represent the benzene molecule as follows:



Scheme 1.15: Delocalization of the  $\pi$  bonds in benzene molecule

According to this picture, each C-C bond is about halfway between a single and a double bond. The difference in energy between the actual molecule and the Lewis structure of the lowest energy is called the “resonance energy”. If we look at benzene, we see that each atom is connected to three other atoms. Using the molecular-orbital method, it is found that every carbon has three same  $sp^2$  hybridization and that the  $2p_z$  orbitals (considering the plane of the molecule to be the  $xy$  plane) line up. Each of these  $2p_z$  orbitals overlap equally with the two adjacent  $2p_z$  orbitals, which produces 6 new molecular orbitals, three of which are bonding and occupy approximately the same space.<sup>[38-42]</sup> These orbitals have the plane of the ring as a node and so are in two parts, one above and one below the plane (See Scheme 1.16).

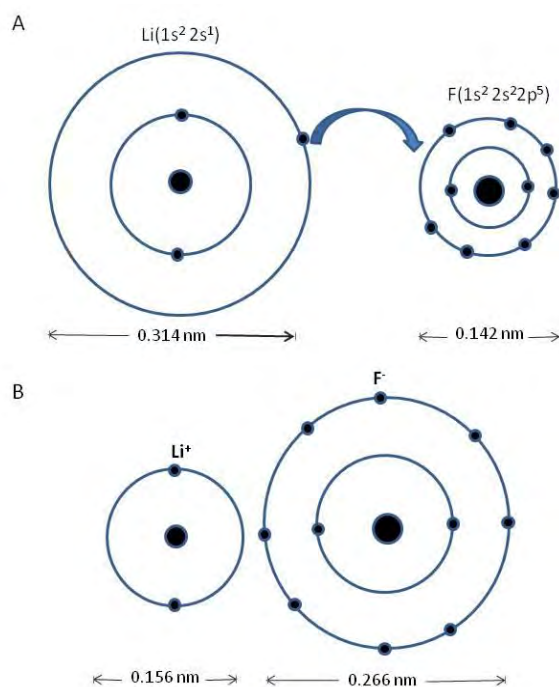


Scheme 1.16: The six  $p$  orbitals of benzene overlap to form three bonding orbitals, (a), (b), and (c). The three orbitals superimposed are shown in (d)<sup>[43]</sup>

The six electrons are distributed in these three orbitals and are called the aromatic sextet.

### 1.2.2 The ionic bond

In general, the ionic bonds are formed between a cation and an anion. This means that one of the atoms involved has to easily lose electrons (low ionization energy) and the other must have high electron affinity. The interaction is carried out between ions of opposite signs, which means that the bonding is not directed in space and has no preferred direction. Such interactions are set up between each two atoms or groups of atoms and leads to strong attraction and to the formation of a chemical bond; we say that the bond is ionic and results from the Coulomb attraction of the electric charges of oppositely charged ions. Close to pure ionic bonds can be found only in solids formed from elements of the opposite columns of the periodic table, such as alkali halides (LiF, NaCl) or alkaline earth (CaCl<sub>2</sub>). The atoms of metallic elements lose their outer electrons easily, whereas those of nonmetallic elements tend to incorporate additional electrons. Consider the formation of the molecule LiF from initially separated neutral lithium and fluorine atoms. Li is extremely reactive because of the great ability to yield its 2s valence electron with a relatively low ionization energy of 5.4 eV to create the Li<sup>+</sup> cation. The same is observed for F which exhibits a strong electron affinity because the incorporation of an electron into its incomplete 2p shell is energetically favorable with an energy reduction of 3.7 eV.<sup>[44]</sup> The final electrostatic interaction between Li<sup>+</sup> and F<sup>-</sup> is highly stabilizing and the formation of the bond between Li<sup>+</sup> and F<sup>-</sup> is exothermic by 184.1 kcal/mol (homolytic dissociation of LiF requires 137.5 kcal/mol).<sup>[45]</sup>



Scheme 1.17: Formation of a LiF molecule. (A) Electronic structure and size of the isolated lithium and fluorine atoms. (B) Electron transfer from Li to F creating an ionic bond between  $Li^+$  and  $F^-$  ions.<sup>[46]</sup>

On the other hand, the type of bonding in complexes such as  $[Fe(H_2O)_6]^{++}$ ,  $[Ni(H_2O)_6]^{++}$  and many others is considered electrostatic, and may be called ion-dipole bonds. In this theory, the complex formation involves interaction between the central ion and the surrounding molecules or anions called ligands, which led to the electrostatic attraction of the excess charge of the central metal ion and the permanent electronic dipole of the ligands.

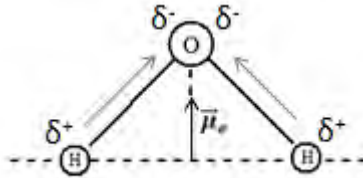
### 1.2.3 Covalent polar bond

The covalent or ionic bonds are limit cases. Nevertheless, there is an intermediate situation which is called ionic-covalent bond, and such bonding is partially covalent and partially ionic. It depends on the electronegativity of the atoms involved. The concept of electronegativity was developed by Pauling<sup>[47]</sup> for giving a measure of the unequal sharing of electrons in a chemical bond. Various methods have been developed<sup>[48-53]</sup> as alternative to Pauling's scale for estimating the electronegativity values of the elements.

The  $H_2O$  molecule is the typical example for this type of covalent polar bonding. The electrons of the O-H bond in  $H_2O$  molecule are attracted to the O atom because of its high

electronegativity. This bond is polarized; it appears a small positive charge  $\delta^+$  upon H atom and a small negative charge  $\delta^-$  on O. So, when a covalent bond is formed between two different atoms, it is still partially ionic.

Dyke et al.<sup>[54]</sup> experimentally measured the dipole moment (1.855 D) of an isolated water molecule. The shape of water molecule is bent, so the partial charge of the polar bonds between the hydrogen atoms and the oxygen atom do not cancel out one another.



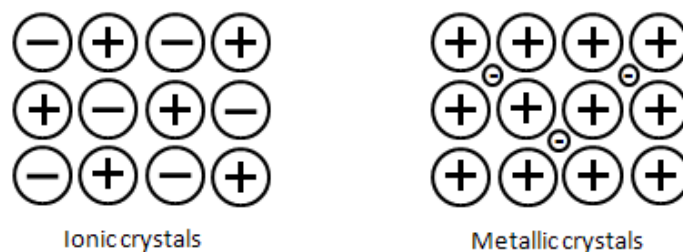
Scheme 1.18: The average dipolar moment of a H<sub>2</sub>O molecule

Then, the water molecule has a permanent electric dipole moment,  $\vec{\mu}_e$ , that is responsible of the particular properties of the water as a solvent.

#### 1.2.4 The metallic bond

The elements in the lower left region of the periodic table that are considered metals have characteristic properties such as thermal and electric conductivity, metallic luster, malleability, ductibility...

In 1916, Lorentz<sup>[55]</sup> developed a theory of metals, he thought the metal as a crystalline arrangement of several spheres which hold together by electrostatic forces and free electrons moving in the interstices. Consequently, this free electron motion offers explanation to various metallic properties such as the electronic conductivity. In an ionic structure, the Coulomb forces allow the ions of opposite charge to hold together. Every ion tends to be surrounded as uniformly as possible by oppositely charged counter-ions, so forming electrically neutral structures (see Scheme 1.19). The crystal structure is formed as a result of the attempt of spherical atoms to approximate each other as close as possible with the aim to form a package of maximum density.



Scheme 1.19: The interaction between charged species of ionic and metallic crystals

In 1927, Pauli<sup>[56]</sup> developed the fundamental concept of the modern electronic theory of metals, which considers that it exists in a metal a continuous or partially continuous set of energy levels for the  $N$  free electrons. These electrons occupy the  $N/2$  most stable levels in pairs at the absolute zero of temperature. The spin of each pair of electrons has to be opposed to satisfy the Pauli exclusion principle. Some of these pairs are broken at higher temperature and the number of unpaired electrons grow with increasing temperature.

According to the bond theory of solids,<sup>[57-59]</sup> the discrete electronic energy states of the isolated atoms combine to generate energy levels in the solid corresponding to the allowed energies for electrons in the crystal. Its classification as a metal, semiconductor, or insulator, depends upon the distribution of electrons in the allowed energy bands and the gaps between the bands. Correlations have been proposed between band gaps and the properties of the crystals.<sup>[60,61]</sup>

### 1.3 Weak chemical bonds

The weak chemical bonds derive mainly from electrostatic interactions between molecules or part of these molecules. No electron transfer is usually involved in such weak chemical bonds. These interactions result from the forces that occur between charges, dipoles, quadripoles, or multipoles of polar molecules or a mix of them. There are three major kinds of weak chemical interactions, namely, dipole-dipole, charge-dipole, and dipole-induced dipole interactions. The first type is maintained between two or more molecules with permanent dipole moments and the strength of the interaction is very related to the orientation and distances between the molecules. The interaction between an ion and a dipole is generally stronger than the dipole-dipole interaction. The dipole-induced dipole interaction occurs when a dipole is near to a non-polar molecule and polarizes it. The dipole of the polar molecule attracts and repels the electrons of the other molecule and induces a temporal dipole, which interacts with the permanent dipole.

In addition to the aforementioned weak interactions, another type of important weak interactions are the hydrogen bond and van der Waals interactions. These will be largely explained in the next sections.

### 1.3.1 Hydrogen bonds

During the last decades many books have been published on hydrogen bonding as well as on hydrogen bonds within the larger aspects of molecular interactions<sup>[62]</sup> and molecular clusters.<sup>[63]</sup> These properties are geometrical, energetic, thermodynamic, and functional in nature. Such hydrogen bonds play a fundamental importance in molecular association both in biology and chemistry.

In 2011, IUPAC<sup>[64]</sup> recommended a novel definition for the hydrogen bond that takes into account the theoretical and experimental knowledge acquired over the past century. The definition was as follows:

*“The hydrogen bond is an attractive interaction between a hydrogen atom from a molecule or a molecular fragment X–H in which X is more electronegative than H, and an atom or a group of atoms in the same or a different molecule, in which there is evidence of bond formation”.*

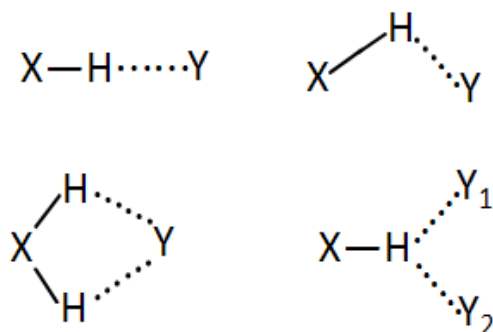
A model hydrogen bond may be drawn as X–H···Y–Z, where the three dots denote the bond. X–H represents the hydrogen bond donor. The acceptor may be an atom or an anion Y, or a fragment or a molecule Y–Z, where Y is bonded to Z. In some cases, X and Y are the same. In more specific cases, where X and Y are the same and X–H and Y–H distances are the same as well, we get symmetric hydrogen bonds. In any phenomenon, the acceptor is an electron rich region such as, but not limited to, a lone pair of Y or  $\pi$ -bonded pair of Y–Z.

Finally, it is worth mentioning that in 1968 Tuck reviewed the structures and properties of  $\text{HX}_2^-$  and  $\text{HXY}^-$  anions that have strong hydrogen bonds.<sup>[65]</sup> Since then there have been detected in a variety of systems the hydrogen bonding and not only in anions, but between neutral molecules and cations.

### 1.3.1.1 List of criteria

For a hydrogen bond  $X-H\cdots Y-Z$ :

- (1) The forces engaged in the formation of a hydrogen bond include those of an electrostatic origin, those arising from charge transfer between the donor and acceptor leading to partial covalent bond formation between H and Y, and those originating from dispersion.
- (2) The atoms X and H are covalently bonded to one another and the X–H bond is polarized, the  $H\cdots Y$  bond strength increasing with the increase in electronegativity of X.
- (3) The X–H $\cdots$ Y angle is usually linear ( $180^\circ$ ) and the closer the angle is to  $180^\circ$ , the stronger is the hydrogen bond and the shorter is the  $H\cdots Y$  distance.



Scheme 1.20: H-bonds in different geometrical structures

- (4) The length of the X–H bond usually increases on hydrogen bond formation leading to a red shift in the infrared X–H stretching frequency and an increase in the infrared absorption cross-section for the X–H stretching vibration. The greater the lengthening of the X–H bond in X–H $\cdots$ Y, the stronger is the  $H\cdots Y$  bond. Simultaneously, new vibrational modes associated with the formation of the  $H\cdots Y$  bond are generated.
- (5) The X–H $\cdots$ Y–Z hydrogen bond leads to characteristic NMR signatures that typically include pronounced proton deshielding for H in X–H, through hydrogen bond spin–spin couplings between X and Y, and nuclear Overhauser enhancements.
- (6) The Gibbs energy of formation for the hydrogen bond should be greater than the thermal energy of the system for the hydrogen bond to be detected experimentally.

In a configuration such as  $X-H\cdots Y$ , the two atoms  $X$  and  $Y$  approach more closely to each other to achieve the lowest energy of the system, and the  $H$  atom is accepted as a bridging or bonding agent between them. Then,  $X$  should be sufficiently electronegative to enhance the acid character of  $H$  and  $Y$  should have a region of high electron density (like a lone pair) which can interact strongly with the acidic hydrogen. In general, hydrogen bonds are not stronger than other intermolecular forces between polar groups or molecules, but their directional power is more pronounced despite the interaction can take place in different ways and geometries (see Scheme 1.20). Usually  $X$  and  $Y$  are any of the following elements:  $F$ ,  $O$ ,  $Cl$ ,  $N$ ,  $Br$ , and  $I$ .

In 1980, Emsley<sup>[66]</sup> made a case that certain hydrogen bonds were stronger and quantitatively different from normal hydrogen bonds. On other hand, the existence of weak hydrogen bonds is well-established.<sup>[67-70]</sup> Indeed, we can classify the hydrogen bonds as very strong, strong, and weak. Table 1.1 presents some examples of different types of hydrogen bond.

Table 1.1: Examples of different H-bonds

	Very strong	Strong	Weak
Bond energy (kcal/mol)	15-40	4-15	<4
Examples	$[F\cdots H\cdots F]^-$	$O-H\cdots O=C$	$C-H\cdots O$
	$[N\cdots H\cdots N]^+$	$N-H\cdots O=C$	$O-H\cdots \pi$
	$P-OH\cdots O=P$	$O-H\cdots O-H$	$Os-H\cdots O$

There is nowadays a surge in network designing and noncovalent synthesis that makes use of relatively strong hydrogen bond interactions such as  $O-H\cdots O$ ,  $O-H\cdots N$ ,  $N-H\cdots O$ , etc. In this sense, the seminal works of Dunitz, Gavezzotti, Bishop, Boese, Desiraju, Mazik, and Madhavi made a substantial step forward in the knowledge of these weak interactions and their utility in crystal engineering.<sup>[71-78]</sup>

### 1.3.1.2 Some extra characteristics of hydrogen bonds

Other characteristics of the hydrogen bonds are the following:

(1) The  $pK_a$  of  $X-H$  and  $pK_b$  of  $Y-Z$  in a given solvent correlate strongly with the energy of the hydrogen bond formed between them.

(2) Hydrogen bonds are implicated in proton-transfer reactions ( $X-H\cdots Y \rightarrow X\cdots H-Y$ ) and may be considered the partially activated precursors to such reactions.

(3) Networks of hydrogen bonds can display the phenomenon of co-operativity, leading to deviations from pair-wise additivity in hydrogen bond properties.

(4) Hydrogen bonds show directional preferences and influence packing modes in crystal structures.

(5) Estimates of charge transfer in hydrogen bonds indicate that the interaction energy correlates well with the extent of charge transfer between the donor and the acceptor.

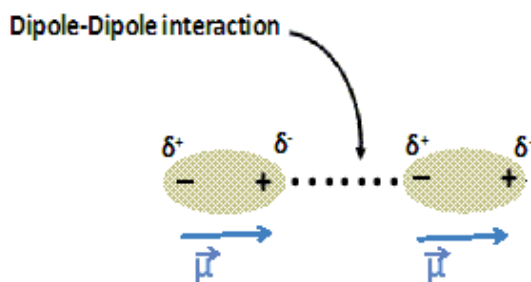
(6) Analysis of the electron density topology of hydrogen-bonded systems usually shows a bond path connecting H and Y and a (3,-1) bond critical point between H and Y.

### 1.3.2 Van der Waals intermolecular interactions

Historically, the idea that the materia can be made of atoms and molecules is the result of the kinetic theory of gases and considerations of stoichiometry in chemical reactions. The existence of condensed phases is, in fact, evidence of the existence of attractive forces between molecules. In contrast, the incompressibility properties are the result of strong repulsion at small distances between the components of the system studied. Van der Waals was the first to incorporate these ideas into the description of the gas, which in contrast to the "ideal gas", took the name of models of "real gas". In 1873, he proposed an equation in which the volumes occupied by the molecules reduce the mean free path of the latter, taking into account that strong repulsions are present at short distances. Another factor is included in the model as the gas pressure decreases compared to that of ideal gases due to the effects of attractive forces between molecules because of long-range intermolecular forces. It has long been recognized that these forces were electrostatic in origin. Therefore, the van der Waals interaction impacts the precise determination of interatomic potential curves,<sup>[79]</sup> and has a major impact on the binding and properties of many molecules.<sup>[80-84]</sup>

There are three types of van der Waals interactions:

A- The interaction of van der Waals-Keesom<sup>[85]</sup> present in polar molecules that establish a dipole-dipole interaction (Scheme 1.21):



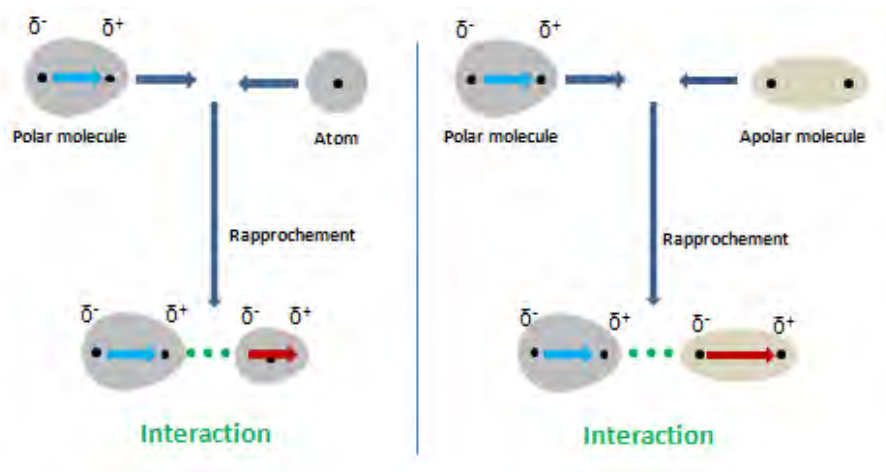
Scheme 1.21: Dipole-dipole interaction

The potential energy of this interaction is given by:

$$E_k = -C_k \frac{\mu^4}{TR^6} \quad (1.2)$$

With:  $C_k$  constant;  $\mu$ : dipolar moment;  $T$ : absolute temperature;  $R$ : distance.

B- The interaction of van der Waals-Debye<sup>[86]</sup> corresponding to the attraction between a polar and an apolar molecule. The induced dipole in the apolar molecule exists because the electronic cloud is deformed by the electrical influence of the polar molecule.



Scheme 1.22: Interaction between polar and apolar species

The potential energy in this case is written as:

$$E_D = -C_D \frac{\alpha\mu^2}{R^6} \quad (1.3)$$

With:  $C_D$  constant;  $\mu$ : dipolar moment;  $\alpha$ : polarizability of the non-polar molecule wherein an electric dipole is induced;  $R$ : distance.

C- The van der Waals-London<sup>[87]</sup> interaction, also known as dispersion London forces, exerted between two apolar molecules.

$$E_L = -C_L \frac{\alpha^2}{R^6} \quad (1.4)$$

With:  $C_L$  constant;  $\alpha$ : polarizability;  $R$ : distance

The latter interaction is the most basic of the three because it always exists, even between atoms or non-polar molecules, as shown by London through a quantum computation. Although the molecules or atoms are not polar, the dipole induced always exists due to the polarizability of the atoms (or molecules), that is to say the distortion of the distribution of the electrical charge. This polarizability is that the electron cloud is deformed by electric influence. Thus, when two molecules are sufficiently close, mutually influence their charge distributions, and distorted, creating small dipole or quadrupole snapshots that will attract low. It is difficult to represent in a simple way the existence of this continuous induction of electric dipole or quadrupole. Quantum computations show that it results in an average attraction.

The three types of intermolecular interactions are attractive and have the same decreasing with  $1/R^6$  ( $R$  is the intermolecular distance). They can therefore be included in the same potential.<sup>[88]</sup>

Thus, for two molecules  $i$  and  $j$ , the free energy of van der Waals interaction is written:

$$U(r) = -\frac{C_{ij}}{R^6} \quad (1.5)$$

Where the constant  $C_{ij}$  (van der Waals interaction between the molecules  $i$  and  $j$  is the sum of three contributions due to Keesom, Debye, and London interactions, respectively).

The van der Waals interactions are the basis of a large number of more or less complex phenomena present in chemistry, biology and solid state physics. As a result, they receive especial attention both experimentally and theoretically. Experimentally, they are, for example, observed and designated as responsible for the cohesion of many liquid crystals and molecular

ensembles, but also they are present in the polymerization phenomena,<sup>[89]</sup> and provide cohesion graphitic materials,<sup>[90]</sup> and other lamellar systems. It has also been recently shown their importance in adhesion phenomena<sup>[91]</sup> and physisorption. In addition, it is worth recalling the role played by these interactions in biology, and more specifically in DNA.

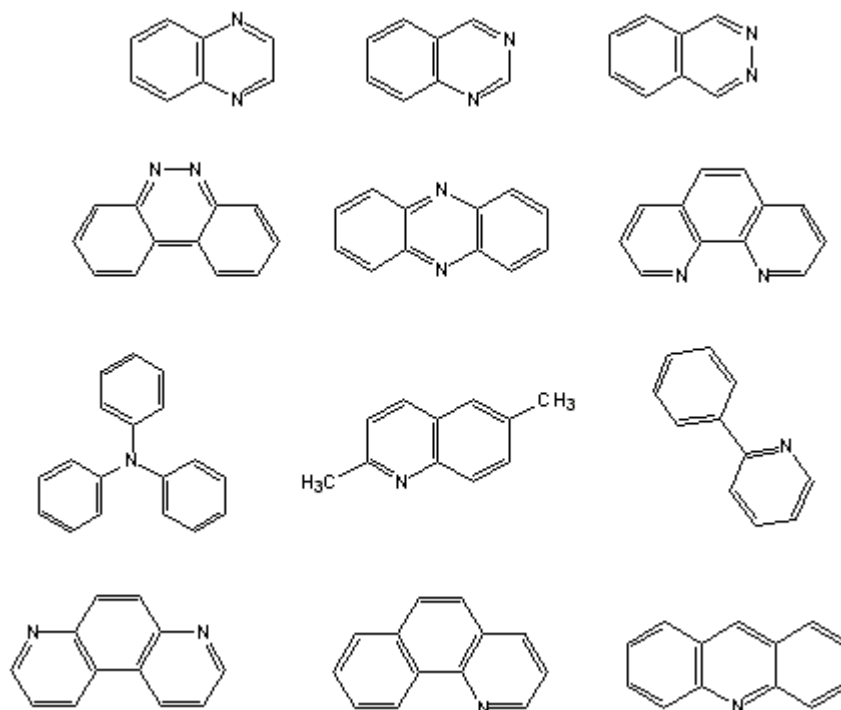
Moreover, it had been seen that these forces play a central role in the "host-receptor" interactions in reactions involving proteins<sup>[92]</sup> and also in the simple complex formation in a given chemical reaction. Finally, another benefit of the study of these forces is the problem they pose theoretically for their inclusion in the ab initio methods of quantum chemistry but also in the specific context of the theory of density functional (DFT ).<sup>[93-94]</sup>

## **1.4 Isomerization**

Molecules that are different but share the same molecular formula are called isomers. They differ from each other by the different arrangement of the atoms in space. There are four main types of isomers: structural, geometric, conformational, and optical isomers. The isomerization energy is the energy difference between two isomers, i.e., the energetic cost corresponding to the transformation of a molecule into another, both having the same number and type of atoms but rearranged in different manner.

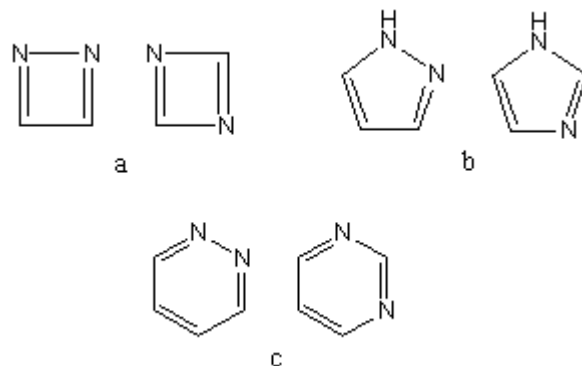
### **1.4.1 Structural isomers**

Any of two or more compounds with identical chemical formulas, such as those in Scheme 1.23, that differ structurally in the sequence in which the atoms are linked are structural isomers. In many cases, structural isomers can be constructed from the same fragments but just connecting the two fragments in different ways.



Scheme 1.23: From left to right, top to bottom: quinoxaline, quinazoline, phthalazine, benzo[c]cinnoline, phenazine, 1,10 phenanthroline, and triphenyl-amine. Standards: 2,6-dimethylquinoline, 2-phenylpyridine, 4,7-phenanthroline, 7,8-benzoquinoline, and acridine.

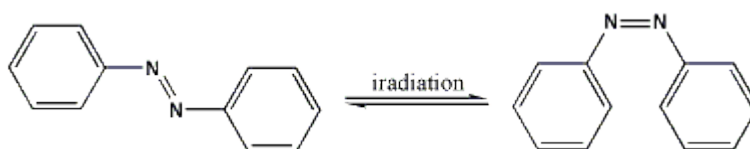
A particular case of structural isomers corresponds to the 1,2- and 1,3-diazanes. In general, 1,2-compounds with two adjacent nitrogen atoms are less stable than the corresponding 1,3-isomers (Scheme 1.24). Standard enthalpies of formation indicate that pyrimidine and imidazole are more stable than pyridazine and pyrazole by about 20<sup>[95,96]</sup> and 10<sup>[97-99]</sup> kcal/mol, respectively. Lone-pair repulsion in NN bonds is the usual explanation for the lower stabilities of the NN isomers.<sup>[100,101]</sup> However, lone-pair protonation and diprotonation of pyridazine and pyrimidine barely change its energy difference,<sup>[102]</sup> which is at odds with the usual explanation through lone-pair repulsions. Over the last few years, Lipkind et al.<sup>[103]</sup> measured the vaporization enthalpies and liquid vapor pressures of the derivative compounds of pyrazine, pyrimidine, and pyridazine by correlation-gas chromatography and they concluded that 1,2-diazines exhibit an additional intermolecular stabilizing interaction of approximately 1.4 kcal/mol, which is not present in other diazine isomers.



Scheme 1.24: From left to right, top to bottom: (a) 1,2/1,3-Azacyclobutadiene; (b) Pyrazole/Imidazole and (c) Pyridazine/Pyrimidine

### 1.4.2 Geometric isomers

The geometric isomers have the same structural formula but differ in the arrangement of groups at a single atom, at double bonds, or in rings. The azobenzene molecule is an example of geometric isomers (Scheme 1.25). It exists in the form of two isomers, *trans* (or E) and *cis* (or Z). Both were isolated for the first time by Hartley through successive extractions.<sup>[104]</sup> Hartley showed that the *trans* isomer is thermodynamically more stable than the *cis* form as the energy difference between the two forms is about 12 kcal/mol.<sup>[105]</sup>



Scheme 1.25: Geometric structure of *trans* and *cis* isomers of azobenzene

The azobenzene molecule and most of its derivatives may reversibly isomerize *trans*→*cis* and *cis*→*trans* by light irradiation; this is known as photochemical isomerization or photoisomerization.

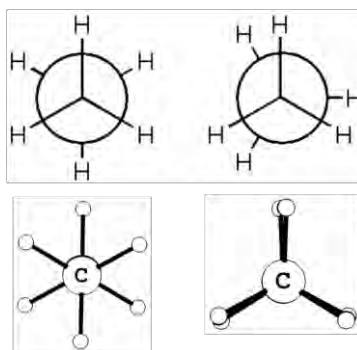
### 1.4.3 Conformational isomers

Within this variety there are similarities in structure (have the same chemical formula) and they have the same sequence of atom connections. These stereoisomerism molecules can be interconverted by rotation around a single bond, followed by rotation of the entire structure, so

they are conformational isomers.<sup>[106]</sup> Furthermore, there exists a rotational energy barrier that requires to be overcome to convert one conformer into another. The barrier to rotation, or rotational barrier, is the activation energy desired to interconvert rotamers. Conformational isomerism arises over relatively unhindered rotation about a chemical bond. It can be changed without breaking bonds.

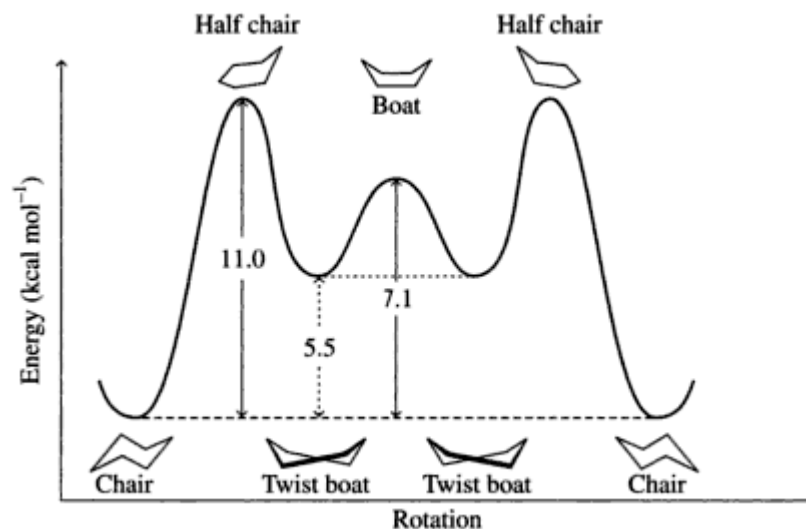
In fact, there are four major types of conformational isomerism:

- Linear alkane conformations: Alkane conformers grow from rotation around  $sp^3$  hybridized carbon carbon sigma bonds. Two of these conformations are recognized as energy minimum (staggered conformation) and energy maximum (eclipsed conformation) forms. In the example of staggered ethane in Newman projection (scheme 1.26), a hydrogen atom on one carbon atom has a  $60^\circ$  torsional angle with respect to the nearest hydrogen atom on the other carbon so that steric hindrance is minimized. In the eclipsed conformation the torsional angle is minimized.



Scheme 1.26: The staggered and eclipsed conformation for ethane

- Ring conformation: The cyclohexane conformation is one of the example molecules that tends to assume certain non-planar conformations. Therefore the cyclohexane ring tends to assume certain non-planar (warped) conformations, which have all angles closer to  $109^\circ$  and therefore a lower strain energy than the flat hexagonal shape. The most important shapes are called chair, half-chair, boat, and twist-boat.<sup>[107]</sup> The molecule can easily switch between these conformations, and only two of them (chair and twist-boat) can be isolated in pure form. The chair conformation is the most stable, followed by the twist boat, while the boat and half-chair conformations correspond to transition states.<sup>[108]</sup>



Scheme 1.27: Conformational analysis of cyclohexane<sup>[109]</sup>

- Atropisomerism: These are stereoisomers resulting from hindered rotation around single bonds where the steric strain barrier to rotation is high enough to allow for the isolation of the conformers.<sup>[110]</sup> Atropisomers are a significant class of compounds because they exhibit axial chirality. They differ from other chiral compounds in that they can be equilibrated thermally while in the other forms of chirality isomerization is generally only possible chemically.
- Folding of molecules or foldamers: The most animated domain of interest in the folding of molecules is the process of protein folding. The foldamer systems are organized into four categories: peptidomimetics, single-stranded abiotics, nucleotidomimetics, and multistranded abiotics, which their stability depend on various effects (solvent, temperature, pressure,..).<sup>[111]</sup>

#### 1.4.4 Optical isomers

Two mirror images of a chiral molecule are called enantiomers or optical isomers. They can be distinguished by how they rotate with plane-polarized light. A mixture of equal parts of an optically active isomer and its enantiomer is termed racemic. Many studies have been reported where compounds that differ in chirality display varying biological properties.<sup>[112]</sup>

## 1.5 Aromaticity

Aromaticity is a key concept in a variety of areas and has a major importance in experimental and theoretical organic chemistry research.<sup>[113]</sup> This concept makes up the rational basis to understand the structure, stability, and reactivity of many molecules. Aromaticity has a long history dating back to the early 19<sup>th</sup> century. In 1825, Michael Faraday extracted a compound from an oily mixture collected in tanks used to store coal gas at high pressures. Faraday establishes that the compound has uncommonly small hydrogen-to-carbon ratio 1:1 and he named the compound “bicarburet of hydrogen”.<sup>[114]</sup> Ten years later, Eilardh Mitscherlich synthesized the same compound by heating benzoic acid, isolated from gum benzoin, with lime and he also found the empirical formula of CH. Ever after the new compound was derived from gum benzoin, he named it as benzin,<sup>[115]</sup> which became benzene when translated to English. He also found that the molecular formula of this compound was C<sub>6</sub>H<sub>6</sub>. Later, it was discovered that although benzene is an unsaturated compound, it chemically differs from the corresponding unsaturated aliphatic compounds. Benzene displayed higher stability and included higher percentage of carbon. It does not offer the reactivity associated with typical unsaturated compounds such as alkenes and alkynes. Later, it was found that many other compounds that are isolated from coal (e.g. phenol, aniline, benzoic acid, salicylic acid, and anthranilic acid) also had similar properties. The molecular formula of these compounds indicated the presence of multiple unsaturated bonds but these compounds were not reactive enough in comparison to alkenes. They were collectively grouped as aromatic compounds based on their distinct odor, or aroma, and benzene became the prototype of this class of substances.

The structure and stability of benzene were a chronic problem during most of the 19<sup>th</sup> century. In 1865, Kekulé suggested that benzene forms a ring structure made by six carbon atoms with alternating single and double bonds.<sup>[116-119]</sup> Because there are two paths in which these compounds can be produced, Kekulé suggested that the benzene was a mixture of two compounds in equilibrium. Kekulé elucidated the structure of benzene but he could not explain its extra stability. In subsequent decades, many scientists tried<sup>[120-134]</sup> to explain the stability and the especial chemical behavior of benzene from its structure and bonding.

The aromatic sextet theory, proposed by Robinson in 1925, was the first to relate the aromaticity with the number of electrons. This theory says that six electrons, with each carbon atom sharing one, form a “closed loop” which gives rise to the aromatic properties.<sup>[135]</sup> Following, valence

bond theory was applied to the benzene problem, and the uncommon stability of benzene was attributed to the resonating structures,<sup>[136-138]</sup> stating that benzene is a resonance hybrid of five hypothetical resonant structures, where the Kekulé structures contribute about 80% and the Dewar structures by 20%. The resonance theory, however, could not explain the fact that even though cyclobutadiene and cyclooctatetraene have electronic conjugation, they do not have extra stability.

The molecular orbital diagram of benzene shows three bonding and three anti-bonding molecular orbital (MO) hugging all six carbon atoms. From this information it was suggested that benzene is unusually stable due to delocalization of three pairs of electrons. In 1931, Hückel attempted to solve the benzene problem<sup>[30-31,139]</sup> with the idea of  $\pi$  orbitals and  $\sigma$ - $\pi$  separation. The  $\sigma$ - $\pi$  separation technique in a benzene structure of  $D_{6h}$  symmetry, gave six  $\pi$  electrons completely delocalized over the hexagonal  $\sigma$  frame. The delocalized  $\pi$  system was found to have a closed-shell and higher stability than the sum of three isolated  $\pi$  bonds. Extra applications by Hückel authorized him to generalize his observations and to formulate the  $4n+2$  rule for the entire class of aromatic compounds. This rule can be strictly applied only to monocyclic conjugated species. Subsequent, many developments, namely azulene's synthesis and structure representation,<sup>[140-142]</sup> synthesis of tropylium,<sup>[143]</sup> and cyclopropenium aromatic cation<sup>[144]</sup> and so on, confirmed Hückel's  $(4n+2)\pi$  rule. In 1964, on purely theoretical grounds, Heilbronner speculated that large cyclic molecules with  $4n\pi$  electrons, rather than  $(4n+2)\pi$ -electrons, would be an aromatic system if their constructed annulene have one end half a twist, that is, Möbius topology.<sup>[145]</sup> In 1965, Breslow inserted the "antiaromatic" term from his quantum mechanical calculations.<sup>[146-149]</sup> He proposed that systems with  $4n\pi$  electron should have an antiaromatic character and, consequently, would be destabilized. The forecast was studied for the case of cyclopropenyl anion, the simplest system having  $4n\pi$  electrons ( $n=1$ ).<sup>[148,150]</sup> Thereafter till date, both these  $(4n+2)$  and  $4n\pi$  rules are amongst the most important criteria for the ranking of a molecule, as aromatic or antiaromatic, respectively.

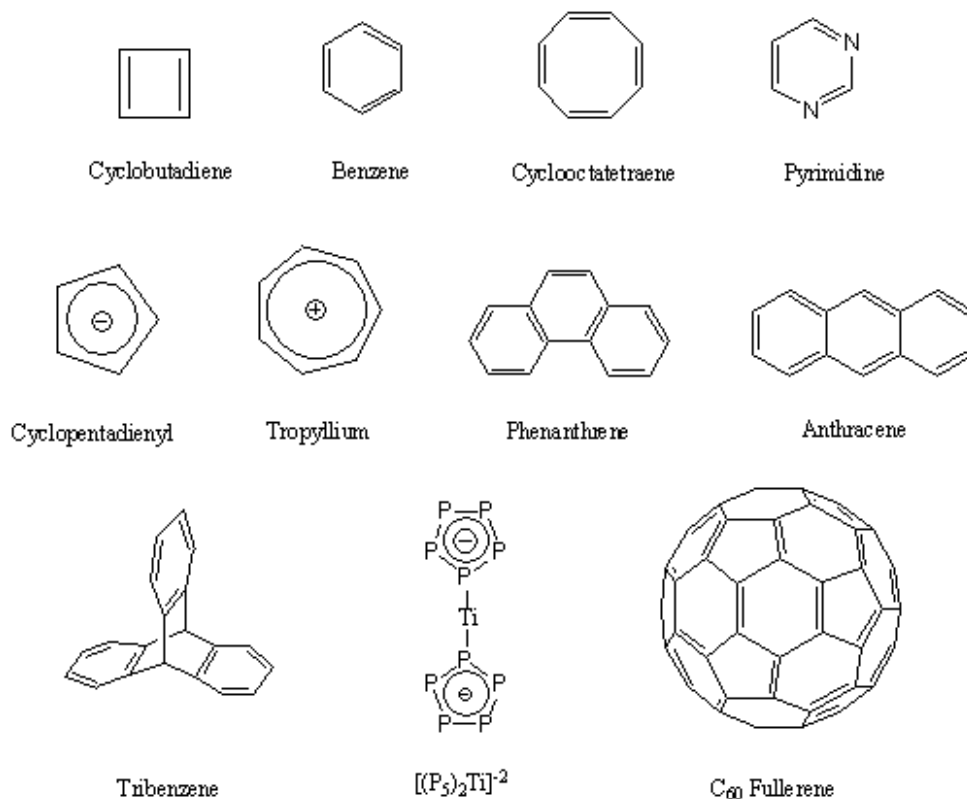
During the epoch of post-Hückel theory, various criteria have been set forward to rationalize and quantify aromaticity. These criteria can be divided into five categories: energetic, structural or geometrical, magnetic, electronic, and reactivity-based measures. Most of the indicators of aromaticity measure a certain manifestation of electronic cyclic delocalization. Among them, the most vastly accepted categories<sup>[151-154]</sup> can be grouped into energetic criterion (aromatic

stabilization energy,<sup>[155-157]</sup> HOMO- LUMO energy gap, the absolute and relative hardness<sup>[158-161]</sup>, structural criterion (bond length equalization,<sup>[162]</sup> planarity, geometric indices of aromaticity like the Harmonic Oscillator Model of Aromaticity (HOMA)<sup>[163,164]</sup>), chemical reactivity criterion (electrophilic substitution rather than addition<sup>[165,166]</sup>), and magnetic criterion (exalted magnetic susceptibilities,<sup>[167]</sup> anisotropies,<sup>[168-170]</sup> displaced chemical shift,<sup>[171,172]</sup> plotted maps of the ring current density (CD plots),<sup>[173-177]</sup> nucleus-independent chemical shifts (NICS),<sup>[178-180]</sup> aromatic ring current shielding (ARCS),<sup>[181]</sup> ring current intensities,<sup>[182-185]</sup> and anisotropy of the current-induced density (ACID).<sup>[186]</sup> More recently, several measures of aromaticity based on electron delocalization properties have been defined. For example, Santos et al. provided a topological analysis of the  $\sigma$ - and  $\pi$ -contributions to electron localization function (ELF) to study aromaticity,<sup>[187,188]</sup> while Solà and co-workers proposed the para-delocalization index (PDI)<sup>[159]</sup> and the aromatic fluctuation index (FLU), this latter describing the fluctuation of electronic charge between adjacent atoms in a given ring.<sup>[189]</sup> Already in 2000, Giambiagi and coworkers employed multicenter bond indices as a measure of aromaticity.<sup>[190-192]</sup> These indices evaluate the extension of  $\pi$ -electron delocalization in the ring, which is anticipated to be especially large for aromatic systems. More recently, Bultinck et al.<sup>[193-199]</sup> and Mandado et al.<sup>[200-204]</sup> have used multicenter delocalization indices computed from Mulliken-type calculations to study the local and total aromaticity of polycyclic aromatic hydrocarbons,<sup>[193-195;197-201;203]</sup> heterocycles,<sup>[202]</sup> homoaromaticity,<sup>[196-199]</sup> and the aromaticity of concerted reaction mechanisms along the reaction path.<sup>[204]</sup> However, because of its multiple manifestations, there is, till date, no generally accepted single and unique quantitative measure of aromaticity. There is no direct way to measure the aromaticity in a molecule experimentally. For example, the aromatic stabilization energy (ASE) depends on the choice of reference. In benzene, which is a prototype aromatic molecule, the experimental investigation was done only by indirect methods, namely through the study of heat of hydrogenation and the nuclear magnetic resonance (NMR) chemical shifts. Although different definitions and indices of aromaticity have their own blemish, quantitatively there has never been a real controversy on the fact that aromatic compounds are described by special stability and this additional stabilization is due to the cyclic electron delocalization.<sup>[151]</sup> In other words, aromaticity is basically an excess property, that is, a deviation from an additive scheme and it is not a directly measurable experimental quantity.

In 2005, Schleyer et al.<sup>[152,153]</sup> proposed a qualitative definition of aromaticity as:

*“Aromaticity is a manifestation of electron delocalization in closed circuits, either in two or three dimensions. This results in energy lowering, often quite substantial, and a variety of unusual chemical and physical properties. These include a tendency toward bond length equalization, unusual reactivity, and characteristic spectroscopic features. Since aromaticity is related to the induced ring currents, magnetic properties are particularly important for its detection and evaluation.”*

Despite many controversial arguments concerning the definition and physical origin of aromaticity,<sup>[113;151-154]</sup> the concept of aromaticity has passed the boundary of benzenoid hydrocarbons to include heterosystems<sup>[205-210]</sup> like pyridine, thiophene, cations such as tropylium<sup>[144]</sup> and cyclopropenium,<sup>[145]</sup> anions like cyclopentadienyl,<sup>[211]</sup> organometallic systems as ferrocene,<sup>[212,213]</sup> or purely carbon-free systems<sup>[214-217]</sup> such as  $P_5^-$  in  $[(P_5)_2Ti]^{2-}$ . The three-dimensional aromaticity of boron-based clusters<sup>[218]</sup> and of fullerenes,<sup>[219-223]</sup> the homoaromaticity of cationic systems,<sup>[224-226]</sup> the aromaticity of triplet state annulenes,<sup>[227]</sup> and pericyclic transition states<sup>[228]</sup> has enlarged the boundaries concept of aromaticity. The extension of the aromaticity concept (Scheme 1.28) has also made it obvious that it must be measured with a variety of indices. Hence, aromaticity is not assured just on the basis of  $\pi$  electrons of planar rings. Moreover, there are an increasing number of methods of assessing different aspects of cyclic electron delocalization.

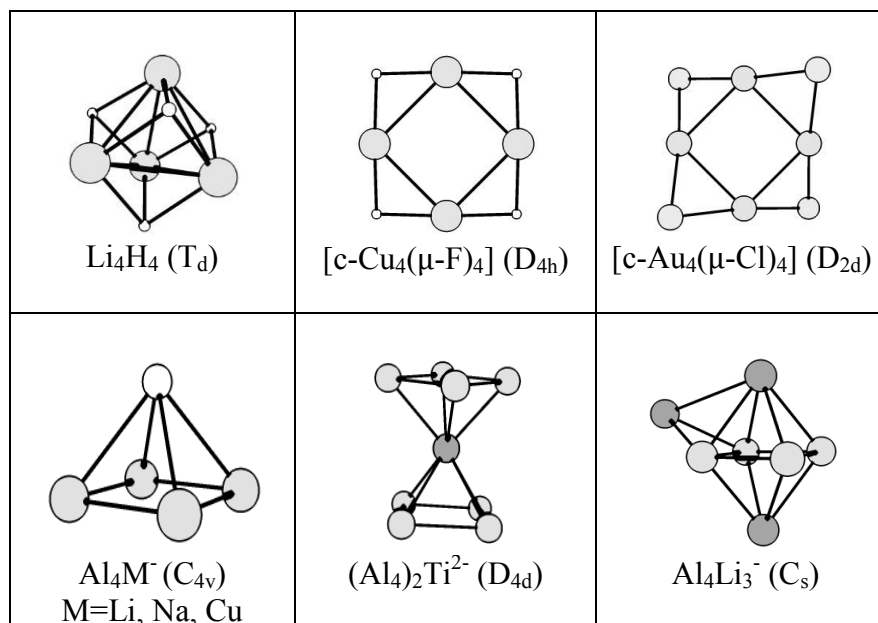


Scheme 1.28: Different aromatic molecules

Very recently, Li et al. determined aromaticity in purely metallic  $MAl_4^-$  and  $Al_4^{2-}$  ( $M = Li, Na$  and  $Cu$ ) clusters using experimental and theoretical techniques.<sup>[229]</sup> These bimetallic anionic clusters were produced in the gas phase and their electronic energy spectra were recorded using photoelectron spectroscopy. Ab initio calculations indicated that these  $MAl_4^-$  clusters possess a  $C_{4v}$  pyramidal structure, where an  $M^+$  cation is interacting with an  $Al_4^{2-}$  unit, showing cyclic planar structure with two delocalized  $\pi$ -electrons, confirming the  $(4n+2)\pi$  counting rule of aromaticity. This discovery introduced the aromaticity concept into the territories of metal systems and opened up a new area, which suggests that even metal cluster can show aromatic character. Thereafter, the aromaticity of  $Al_4^{2-}$  dianion has been verified using many different techniques.<sup>[187;230-241]</sup>

Since then, aromaticity has been found in a large number of new gaseous all-metal or metalloid clusters:  $NaGa_4^-$  and  $NaIn_4^-$ ,<sup>[242]</sup>  $Au_5Zn^+$ ,<sup>[243-244]</sup>  $Al_2(CO)_2$ ,<sup>[245]</sup>  $X_5^-$  ( $X = N, P, As, Sb, Bi$ ),<sup>[234,246-259]</sup>  $X_4^{2-}$  ( $X = B, Al, Ga, In, Ti$ ),<sup>[234,242,255,229,259-260]</sup> sandwich structures of  $[Al_4TiAl_4]^{2-}$  and  $Na[Al_4TiAl_4]^{2-}$ ,<sup>[255]</sup>  $X_3^-$  and  $NaX_3$  ( $X = Al, Ga$ ),<sup>[258]</sup>  $Hg_6^{4-}$ ,<sup>[261]</sup>  $XAl_3^-$  ( $X = C, Si, Ge, Sn, Pb$ ),<sup>[262]</sup>  $XGa_3^-$  ( $X = Si, Ge$ ),<sup>[263]</sup>  $X_4^{2-}$  and  $NaX_4^-$  ( $X = N, P, As, Sb, Bi$ ).<sup>[264]</sup>  $C_2N_2^-$ ,  $M(C_2N_2)$  ( $M = Li, Na$ ,

K),  $[N(C_2N_2)]^+$  (N = Be, Mg, Ca),<sup>[265]</sup>  $Al_2P_2^{2-}$ ,  $[M(Al_2P_2)]^-$ , M= Li, Na, K, Cu, N( $Al_2P_2$ ); N= Be, Mg, Ca, Zn,<sup>[266]</sup>  $Cu_6Sc^+$  and  $Cu_5Sc$ ,<sup>[267]</sup>  $B_2XY$ , X = N, P and Y = O, S, Se,<sup>[268]</sup>  $Al_2MN$ , M= C, Si, Ge; N= S, Ge,<sup>[268]</sup>  $Si_2BX$  (X= Li, K, O, S),<sup>[269]</sup>  $Sb_5^-$  and  $Sb_5M$  (M =Li, Na and K),<sup>[270]</sup>  $O_4^{2+}$ ,  $Si_4^{2+}$ ,  $Se_4^{2+}$ ,<sup>[271]</sup>  $Re_3Cl_9$ ,  $Re_3Br_9$  and their dianions,<sup>[272]</sup>  $Cu_4Na^-$  and  $Au_4Na^-$ ,<sup>[273]</sup>  $BiGa_3$ ,<sup>[274]</sup>  $Au_6Y^-$ ,<sup>[275]</sup>  $Be_3^{2-}$  and  $Mg_3^{2-}$ ,<sup>[276]</sup>  $Be_8^-$ ,<sup>[277]</sup>  $Na_6$  and  $K_6$ ,<sup>[278]</sup>  $Cu_7Sc$ ,<sup>[279]</sup>  $N_6^-$ ,<sup>[280]</sup>  $P_4M^q$ , (M= S, Se, q=0; M= Si, Ge, q= -2),<sup>[281]</sup>  $N_5^-$ ,  $SN_4$ ,  $S_2N_3^-$ , and  $S_3N_2^{2+}$ .<sup>[282]</sup>



Scheme 1.29: Geometric structure of some metal clusters

Significantly, the discovery of all-metal aromatic systems has added a new feature in the concept of aromaticity, namely multifold aromaticity (simultaneous presence of several types of aromaticity, for instance,  $\pi$  and  $\sigma$  aromaticity like in  $Al_4^{2-}$ ). The multifold aromaticity of the  $Al_4^{2-}$  dianion has been founded with a variety of theoretical methods: bifurcation analysis of the electron localization function (ELF),<sup>[187]</sup> nucleus-independent chemical shifts (NICS),<sup>[236]</sup> valence bond (VB) estimate of  $\pi$  and  $\sigma$  aromaticity,<sup>[238]</sup> resonance energy (RE) assessment,<sup>[239]</sup> maps of ring current,<sup>[242,244,283-284]</sup> and ARCS.<sup>[234]</sup> Very recently, for  $Cu_4^{2-}$  cluster, the cyclical delocalization due to d electrons instead of the habitual p orbitals has provided the first quantitative evidence for the existence of “d-orbital aromaticity” or “ $\delta$ -aromaticity”.<sup>[285]</sup> Later, the possibility of three-dimensional aromatic clusters including d-orbitals was also discussed in the pseudo-octahedral coinage metal cages of  $M_6Li_2$  (M=Cu, Ag, Au), as well as the tetrahedral coinage metal cages of  $M_4Li_4$  (M=Cu, Ag).<sup>[286]</sup>

In the recent past, Nigam has explored the possibility of aromaticity in various tetramer clusters comprising of homo- and heteroatomic elements.<sup>[287-289]</sup> The choice of tetramer clusters was established by the fact that these are the smallest clusters, which can have either planar or nonplanar atomic structure in the ground state. In particular, the interest was to find out neutral clusters that provide an aromatic character and are more stable than the charged clusters.

### 1.5.1 Description of aromaticity

As previously said, the most common aromaticity descriptors are those based on structural parameters, energetic criteria, magnetic properties, reactivity indices, or electron delocalization measures. Actually, this has been realized in many systems and based on this various measures of aromaticity have been defined. Despite its multiple manifestations, one may think that all aromaticity indices lead to the same conclusions. However, Katrizky et al. demonstrated by means of a statistical analysis that the magnetic-aromaticity is orthogonal to other measures, such as the energetic aromaticity or geometrical aromaticity.<sup>[290]</sup> In this sense, many authors consider aromaticity as a multidimensional property.

The most important advances in the field of aromaticity indices are summarized in Table 1.2, where they are classified in function of the measured property. Next we outline the aromaticity indices that have been used in this thesis.

Table 1.2: Some Important Aromaticity Criteria and Key Developments

	main contributor(s)	contribution	Type a
1925	Armit/Robinson <sup>[135]</sup>	aromatic sextet; inscribed circle notation	
1931	Hückel <sup>[30-32]</sup>	theory of cyclic $(4n + 2) \pi$ electron systems	
1933	Pauling <sup>[16,29,291]</sup>	valence bond method and resonance	E
1936	Kistiakowski <sup>[292]</sup>	experimental resonance energy of benzene	E
1936	Pauling and others <sup>[138,293-297]</sup>	ring current theory	M
1937	London <sup>[298]</sup>	quantum mechanical treatment of the ring current, London diamagnetism	M
1937	London <sup>[299-305]</sup>	GIAO method	
1953	Meyer and others <sup>[306]</sup>	the difference in the proton magnetic shielding between benzene and noncyclic olefins	

		observed	
1956	Pople <sup>[170,307]</sup>	Induced ring current effects on NMR chemical shifts: deshielding of benzene protons	M
1969	Dewar <sup>[308-311]</sup>	Dewar resonance energy	E
1967	Sondheimer <sup>[312-313]</sup>	define molecules with an induced diamagnetic ring current as diatropic	M
1967	Julg and François <sup>[314]</sup>	Julg structural index	S
1968	Dauben <sup>[315-316]</sup>	diamagnetic susceptibility exaltation	M
1970	Flygare <sup>[169,317-320]</sup>	microwave spectroscopy, aromatic systems showed enhanced magnetic anisotropies	M
1971	Hess and Schaad <sup>[321-326]</sup>	Hess-Schaad resonance energy	E
1972	Clar <sup>[327]</sup>	Clar “aromatic sextet”	
1972	Krygowski <sup>[162-164,328]</sup>	harmonic oscillator model of aromaticity (HOMA)	S
1974	Fringuelli <sup>[329]</sup>	Fringuelli structural index	S
1975	Gutman, Milun, Trinajstić, Aihara <sup>[330-332]</sup>	topological resonance energy	E
1980	Kutzelnigg <sup>[333-336]</sup>	IGLO calculation of magnetic properties: chemical shifts, magnetic susceptibilities and magnetic susceptibility anisotropies	M
1981	Lazzeretti and Zanasi <sup>[337-338]</sup>	ab initio current density plots	M
1983	Jug <sup>[339]</sup>	Jug structural index	S
1985	Pozharskii <sup>[340]</sup>	Pozharskii structural index	S
1985	Bird <sup>[341-346]</sup>	Bird structural index	S
1987	Mizoguchi <sup>[347]</sup>	magnetic susceptibilities of Hückel and Möbius annulenes show an opposite tendency	M
1988	Zhou Parr, Garst <sup>[101,348-351]</sup>	hardness (low reactivity) as aromaticity index	R
1990-	Schleyer <sup>[352-355]</sup>	extensively using Li <sup>+</sup> NMR to study aromaticity	M
1994-	Schleyer and Jiao <sup>[353,356-364]</sup>	extensively using magnetic exaltation criterion to study aromaticity	M

1994	Saunders et al. <sup>[221,365-367]</sup>	experimental endohedral <sup>3</sup> He NMR to measure aromaticity in fullerenes and their derivatives	M
1994	Bühl and Hirsch <sup>[221,368]</sup>	computed endohedral <sup>3</sup> He NMR to measure aromaticity in fullerenes and their derivatives	M
1995	Krygowski <sup>[369]</sup>	bond alternation coefficient (BAC) structural index	S
1996	Schleyer <sup>[178]</sup>	nucleus-independent chemical shifts (NICS)	M
<hr/>			
1996	Fowler and Steiner <sup>[370]</sup>	extensive application of current density plots to study aromaticity	M
1997	Schleyer <sup>[179-180]</sup>	dissected NICS, localized molecular orbital (LMO) IGLO	M
1997	Bohmann, Weinhold, Farrar <sup>[371]</sup>	NBO-GIAO dissected canonical molecular orbital (CMO) and LMO NICS	M
1998	Bean, Sadlej-Sosnowska <sup>[372-373]</sup>	application of natural bond orbital analysis to delocalization and aromaticity	
1998	Balawender, Komorowski, De Proft, Geerlings <sup>[374]</sup>	derivatives of molecular valence as a measure of aromaticity	
1998	Chesnut <sup>[375]</sup>	measure differences in ring proton shieldings between the fully unsaturated species and its monoene counterpart recommended as aromaticity	
1999	Mo <sup>[376-378]</sup>	block-localized wave function (BLW) method based on modern ab initio valence bond theory to approach the absolute resonance energy	E
1999	Sundholm <sup>[181,234,379-383]</sup>	aromatic ring-current shielding (ARCS)	M
2000	Giambiagi <sup>[192]</sup>	multicenter bond indices	E
2000	Chesnut, <sup>[384]</sup> Silvi <sup>[385-386]</sup>	using the electron localization function (ELF)	E
2000	Patchkovskii and Thiel <sup>[387]</sup>	computing NICS using MNDO method	M
2001	Herges <sup>[186]</sup>	ACID (anisotropy of the current induced density)	M

2001	Fowler and Steiner <sup>[175-176]</sup>	ipsocentric partition of total ( $\rho + \delta$ ) current density into orbital contributions	M
------	-----------------------------------------	-----------------------------------------------------------------------------------------------	---

Table 1.2. (continued)

	main contributor(s)	contribution	Type <sup>a</sup>
2002	Schleyer <sup>[388]</sup>	isomerization stabilization energy (ISE),	E
2002	Sakai <sup>[389-390]</sup>	CiLC (CI/LMO/CASSCF) analysis; Index of deviation from the aromaticity (IDA)	
2003	Solà and Poater <sup>[159-160]</sup>	para-delocalization index (PDI)	E
2003	Matta, Hernández-Trujillo <sup>[391]</sup>	aromaticity index based on the delocalization of the Fermi hole density	E
2003	Corminboeuf, Heine, Weber, Seifert, Reviakine, Schleyer <sup>[392-394]</sup>	GIAO-CMO NICS and NICS <sub>zz</sub> tensors	M
2004	Merino, Heine, Seifert <sup>[395]</sup>	induced magnetic field as aromaticity index	M
2004	Santos, Tiznado, Contreras, Fuentealba <sup>[187-188]</sup>	topological analysis of the $\sigma$ - and $\pi$ -contribution to electron localization function (ELF) to quantify aromaticity	E
2005	Solà and Matito <sup>[189]</sup>	aromatic fluctuation index (FLU) (describing the fluctuation of electronic charge between adjacent atoms in a given ring)	E
2005	Sundholm <sup>[235,396-398]</sup>	integrated induced currents	M

<sup>a</sup> Structural (S), energetic (E), magnetic (M), reactivity (R).

### 1.5.2 Energetic Aromaticity: ASE

In 1933, Pauling and Wheland analyzed the differences between the actual  $\pi$ -electron energy of benzene and the  $\pi$ -electron energy of analogous hypothetical species with localized  $\pi$ -electrons. This study guided to the introduction of the concept of resonance energy (RE) in terms of valence bond theory.<sup>[16]</sup> Therefore, the energetic-based indicators of aromaticity make use of the fact that conjugated cyclic  $\pi$ -electrons compounds are more stable than their chain analogues which have no cyclic  $\pi$ -electron delocalization. The most common involved energetic measure of aromaticity is the aromatic stabilization energy (ASE), calculated as the reaction energy of an

homodesmotic reaction.<sup>[399]</sup> The main disadvantage of these methods is the difficulty to isolate the aromatic stabilization from other important effects that stabilize or destabilize a molecule.

### 1.5.3 Structural Aromaticity: HOMA

The structural aromaticity descriptors are based on the idea that the tendency toward bond length equalization and the symmetry of the ring are important manifestations of aromaticity. Among the most common structural-based measures, the harmonic oscillator model of aromaticity (HOMA)<sup>[164]</sup> index defined by Kruszewski and Krygowski has proven to be one of the most effective structural indicators of aromaticity:

$$HOMA = 1 - \frac{\alpha}{n} \sum_{i=1}^n (R_{opt} - R_i)^2 \quad (1.6)$$

Where  $n$  is the number of bonds considered and  $\alpha$  is an empirical constant (for C-C, C-N, C-O and N-N bonds  $\alpha = 257.7, 93.5, 157.4,$  and  $130.3,$  respectively) fixed to give HOMA=0 for a model nonaromatic system and HOMA=1 for a system with all bonds equal to an optimal value  $R_{opt}$ , assumed to be achieved for fully aromatic systems.  $R_i$  stands for the running bond length. The HOMA value can be decomposed into the energetic (EN) and geometric (GEO) contributions according to the next relation.<sup>[328]</sup>

$$HOMA = 1 - EN - GEO = 1 - \alpha(R_{opt} - \bar{R})^2 - \frac{\alpha}{n} \sum_i (\bar{R} - R_i)^2 \quad (1.6)$$

The GEO contribution measures the decrease or increase in bond length alternation while the EN term takes into account the lengthening/shortening of the mean bond lengths of the ring.

### 1.5.4 Magnetic Aromaticity: NICS

Magnetic indices of aromaticity are based on the  $\pi$ -electron ring current that is induced when the system is exposed to external magnetic fields. Originally, the magnetic susceptibility exaltation and anisotropy of magnetic susceptibility received substantial support but, undoubtedly, nowadays the most widely used magnetic-based indicator of aromaticity is the nucleus-independent chemical shift (NICS), proposed by Schleyer and co-workers.<sup>[152,178]</sup> NICS is defined as the negative value of the absolute shielding computed at a ring center or at some other interesting point of the system, for instance 1 Å above the ring center. Rings with large negative NICS values are considered aromatic. The more negative the NICS values, the more aromatic the rings are.

NICS has many advantages among other indicators of aromaticity. First, it is a very accessible and easy to compute descriptor; second, it can be used to discuss both the local and global aromaticity of molecules, and, third, it does not use reference values, so it can be easily applied to any molecule. However, it is not free from criticism. Lazzeretti<sup>[183,185]</sup> and Aihara<sup>[400]</sup> have pointed out in several works that NICS's validity to indicate diamagnetic ring currents is limited by the potential spurious contributions from the in-plane tensor components that, at least in classical organic aromatic compounds, are not related to aromaticity. This is partially avoided by using NICS(1),<sup>[179]</sup> that is considered to better reflect the  $\pi$ -electrons effects, or with its corresponding out-of-plane tensor components (NICS(1))<sub>zz</sub>) or even better with the  $\pi$  contribution to this component computed at the ring center or at 1 Å above (NICS(0)) <sub>$\pi$ zz</sub> and NICS(1)) <sub>$\pi$ zz</sub>, respectively). In 1997, the first dissected NICS were introduced by Schleyer et al.<sup>[180]</sup> and were applied to study the aromaticity of some inorganic rings. NICS <sub>$\pi$</sub>  values can be calculated through the decomposition of NICS indices into their canonical molecular orbital (CMO) components<sup>[392]</sup> using the NBO 5.0 program.<sup>[401]</sup> NICS(1) <sub>$\pi$</sub>  and NICS(1)) <sub>$\pi$ zz</sub> were reported to be the best measures of aromaticity among the different NICS-related definitions in organic molecules.<sup>[394,402]</sup> Other problems that can be found are related to ring size dependence of NICS values<sup>[210]</sup> or, recently, Castro and coworkers have shown that NICS values strongly depend on the inclusion of relativistic effects in molecules containing heavy elements.<sup>[403]</sup>

Every aromaticity index introduced up to now presents its advantages and drawbacks. Some descriptors, such as HOMA, are computationally inexpensive but, for instance, may fail on predicting the aromatic character of the Diels-Alder reaction transition state.<sup>[404]</sup> Other descriptors, such as NICS, have been extensively used to predict the aromaticity of a large series of systems. As previously mentioned, some drawbacks have been also reported.<sup>[405-406]</sup> Therefore, some aromaticity descriptors fail on giving the expected answer from most elementary chemical problems. For this reason, the performance of aromaticity indices and their adequacy for each chemical situation must be a prime aim for aromaticity researchers. In our group, a set of several aromaticity tests using a number of examples for which most chemists would agree about the expected aromaticity trends in a given series of compounds was proposed.<sup>[407-409]</sup> The tests were chosen to fulfill two requirements. First, the size of the systems involved must be relatively small to facilitate a fast application and, second, controversial cases must be avoided. Then, we analyze the advantages and drawbacks of a group of widely used aromaticity descriptors.

### 1.5.5 Aromaticity from ESI

Our group has a large experience on the field of characterizing the electronic structure of molecules by means of electron localization and delocalization measures.<sup>[160,189,404,410-419]</sup> In 2003, this knowledge was directed to propose a new measure of aromaticity, the so-called para-delocalization index (PDI) that measures the electron sharing between C atoms in the *para* position for a given six-membered ring (6-MR).<sup>[160]</sup> The idea of PDI derives from the work of Fulton<sup>[420]</sup> and Bader<sup>[421]</sup> who found a higher electron delocalization between *para* carbons than between *meta* despite the longer distance between the carbon atoms of the former. Before introducing PDI, let us consider that the ring structure consists of  $n$  atoms, represented by the following string  $\mathcal{A} = \{A_1, A_2, \dots, A_n\}$ , whose elements are ordered according to the connectivity of the atoms in the ring. Thus, PDI is defined as the average of para delocalization indices:

$$PDI(\mathcal{A}) = \frac{\delta(A_1, A_4) + \delta(A_2, A_5) + \delta(A_3, A_6)}{3} \quad (1.7)$$

The main shortcoming of PDI is that it is limited to 6-MRs. Two years later, with the aim of extending the applicability to any given size of a ring, Matito et al. constructed a new measure called aromatic fluctuation index (FLU) based on the comparison of the electron sharing between bonded pairs of atoms in a ring:<sup>[189]</sup>

$$FLU(\mathcal{A}) = \frac{1}{n} \sum_{i=1}^n \left[ \left( \frac{V(A_i)}{V(A_{i-1})} \right)^\alpha \left( \frac{\delta(A_i, A_{i-1}) - \delta_{ref}(A_i, A_{i-1})}{\delta_{ref}(A_i, A_{i-1})} \right) \right]^2 \quad (1.8)$$

where  $A_0 \equiv A_n$  and  $V(A)$  is the atomic valence.  $\delta_{ref}(A_i, A_{i-1})$  is taken from an aromatic molecule, for instance, for C-C bonds the molecule chosen as a reference is benzene. Finally,  $\alpha$  is a simple function to ensure the first term in Eq. 1.8 is always greater or equal to 1,

$$\alpha = \begin{cases} 1 & V(B) \leq V(A) \\ -1 & V(B) < V(A) \end{cases} \quad (1.9)$$

FLU is close to zero in aromatic species, and greater than zero for non-aromatic or antiaromatic species. However, FLU strongly depends on reference values and this prevents its use to study the aromaticity of inorganic systems.

From the work of Giambiagi,<sup>[191-192]</sup> the interest in multicenter indices as aromaticity descriptors has grown exponentially. The  $I_{ring}$  index was defined by Giambiagi as:

$$I_{ring}(\mathcal{A}) = \sum_{i_1, i_2, \dots, i_n}^{occ} S_{i_1 i_2}(A_1) S_{i_2 i_3}(A_2) \dots S_{i_n i_1}(A_n) \quad (1.10)$$

Where  $S_{ij}(A)$  is the overlap of molecular orbitals  $i$  and  $j$  in the basin of atom  $A$ .  $I_{ring}$  will provide large values for aromatic molecules. It is worth noticing here that the normalized version of  $I_{ring}$  has recently been defined by Cioslowski, Matito, and Solà as:<sup>[422]</sup>

$$I_{NG}(\mathcal{A}) = \frac{\pi^2}{4NN\pi} I_{ring}(\mathcal{A})^{\frac{1}{N}} \quad (1.11)$$

Where  $N$  is the total number of atoms in the ring and  $N_\pi$  the total number of  $\pi$  electrons. In 2005, Bultinck and coworkers proposed an extension of the  $I_{ring}$  index of Giambiagi.<sup>[195]</sup> This index, which is called multicenter index of aromaticity (MCI), has been successfully applied to a broad number of situations, from simple organic compounds to complex all-metal clusters with multiple aromaticities.<sup>[197-198,204,423-427]</sup>

$$MCI(\mathcal{A}) = \sum_{\mathcal{P}(\mathcal{A})} I_{ring}(\mathcal{A}) = \sum_{\mathcal{P}(\mathcal{A})} \sum_{i_1, i_2, \dots, i_n}^{occ} S_{i_1 i_2}(A_1) S_{i_2 i_3}(A_2) \dots S_{i_n i_1}(A_n) \quad (1.12)$$

Where  $\mathcal{P}(\mathcal{A})$  stands for  $n!$  permutations of elements in the string  $\mathcal{A}$ . However, this index is associated with a remarkable computational cost that limits its use to rings up to nine members. This drawback has been partially solved with the so-called pseudo- $\pi$  method, although the results obtained are less accurate.<sup>[194]</sup> For planar species,  $S_{\sigma\pi}(A) = 0$  and MCI can be exactly split into the  $\sigma$ - and  $\pi$ -contributions in order to obtain  $MCI_\sigma$  and  $MCI_\pi$ . This feature is especially interesting to evaluate multifold aromaticity in all-metal clusters. Finally, there is a normalized version of the MCI index, the so-called  $I_{NB}$  given by:<sup>[422]</sup>

$$I_{NB}(\mathcal{A}) = \frac{C}{4NN\pi} [2N \cdot MCI(\mathcal{A})]^{\frac{1}{N}} \quad (1.13)$$

Where  $C \approx 1.5155$

## 2. Methodology

The success of electromagnetism in physics in the 19<sup>th</sup> century allowed Berzelius<sup>[260]</sup> to propose a model of the atom to explain the different atomic affinities and molecular cohesion. This discovery was a major success for the design of the chemical bond, but he was criticized by

chemists who demonstrated experimentally the substitution of functional groups during reaction. In 1857, Kekulé showed the tetravalence of carbon and the ability of carbon atoms to bond to each other, which emerges the notion of atomic valence of an element.<sup>[428,4]</sup> Thereafter, Mendeleev<sup>[429]</sup> proposes the classification based on the notion of valence. It was not until the end of this century that the notion of indivisibility of the atom was finally abandoned with the discovery of the electron by Thomson.<sup>[430]</sup> This discovery forced the chemists to review the concepts previously established.

In 1907, Thomson<sup>[431]</sup> proposed an atomic model, where negative charged particles (electrons) turned -in centric rings- around a positive sphere of charge. In this model the valence was explained by the fact that each ring have limitations in the total number of electrons. After 4 years, Rutherford<sup>[432]</sup> experimentally demonstrated the presence of a positive nucleus in the atom, and he invented the planetary model of the atom. Deriving from this electrostatic vision of the chemical bond, various models were proposed in the early 20<sup>th</sup> century. The most famous one is the “Lewis pre-quantum model” that is nowadays essential in chemistry.

In 1913, Bohr<sup>[433, 434]</sup> proposed a semi-classical model, took the results obtained by Rutherford and attached some ideas based on the quantum theory of Planck and Einstein (quantization of energy). Classical electrostatics indicated that an electron orbiting the nucleus should radiate and lose its energy by radiation falling on the nucleus. But this does not occur, since the atoms are stable. This led Bohr to suggest that there are some orbits where the electron does not emit radiation. This happens every time the moment of the quantity of motion of the electron is an integer multiple of  $h/2\pi$  (where h is Planck's constant). Allowed orbits are numbered with 1, 2... n.

Afterwards, the progress of quantum mechanics gave rise to two notions of bonding that have evolved in parallel: the notion of resonance<sup>[435]</sup> based on the Valence Bond (VB) theory,<sup>[436]</sup> and the notion of molecular orbitals based on the molecular orbital (MO) theory.<sup>[437]</sup> So far, these two visions of the bond conception are widely used and integrated into the modern formalism of quantum chemistry.

In the twenties, Erwin Schrödinger (Nobel Prize in Physics in 1933) created the mathematical formula that defines the movement of a set of electrons and atoms in the form of a wavefunction. This equation is the basis of quantum chemistry. Unfortunately, it is exactly soluble only for

atomic or molecular systems having only one electron. For systems with more electrons we must be content with an approximate solution. The objective of the non-relativistic quantum chemistry is to obtain a solution for the equation of Schrödinger that is as close as possible to the solution of real physical system.

## 2.1 The basis of quantum chemistry

### 2.1.1 The birth of the wavefunction

In chemistry, we can describe a stationary state of an isolated system (atom or molecule) of  $M$  nuclei and  $N$  electrons by a wavefunction  $\Psi$  (continuous and derivable at any point). This latter function represents the wavefunction of the time-independent Schrödinger equation:

$$H\Psi = E\Psi \quad (2.1)$$

Where  $H$  is the Hamiltonian operator that acts on the wavefunction  $\Psi$ , and  $E$  is the total energy of the system.  $\Psi$  depends on both nuclear ( $R_1, R_2, \dots, R_M$ ) and electronic ( $X_1, X_2, \dots, X_N$ ) coordinates. Electron  $i$  is represented by space coordinates  $r_i$  and spin  $\sigma_i$  as  $X_i = (r_i, \sigma_i)$ . The solution of this equation requires several approximations.

#### A-The Born-Oppenheimer Approximation

Indeed, as a first approximation and because the movement of the nuclei is much slower than that of the electrons, at each moment the electrons "see" that the nuclei do not move and keep fixed, so the electronic and nuclear motions can be decoupled. This is what the Born-Oppenheimer approximation<sup>[22]</sup> does. Then, the wavefunction  $\Psi$  can be written as the product of an electronic function  $\Psi(X_1, X_2, \dots, X_N; R_1, R_2, \dots, R_M)$  describing the motion of the electrons in the field of fixed nuclei and by a nuclear function  $\Psi_{\text{nuclei}}$  describing the translational movements, vibrations and rotation of the nuclei. On the other hand, relativistic effects are often neglected, which implies the absence of spin variables in the Hamiltonian  $H$ . This approximation is well justified for the first transition metal series (Sc, Ti, ..., Cu), as the the spin-orbit coupling (fine structure) and spin-spin coupling (hyperfine structure) are very small compared to the other terms in the Hamiltonian. Finally, we can write the classical form of the electronic Hamiltonian in atomic units for a system of  $N$  electrons and  $M$  nuclei as:

$$H_{el} = T_e + V_{en} + V_{ee} = -\frac{1}{2}\sum_{i=1}^N \nabla_i^2 - \sum_{i=1}^N \sum_{\alpha=1}^M \frac{Z_\alpha}{|r_i - r_\alpha|} + \sum_{i=1}^N \sum_{j>i}^N \frac{1}{|r_i - r_j|} \quad (2.2)$$

$T_e$ : The kinetic energy operator of the electrons

$V_{en}$ : The potential energy operator for the interaction between electrons and nuclei

$V_{ee}$ : The potential energy operator for the interaction between electrons

One can immediately note that  $H_{el}$  does not contain any "chemical" contribution and does not a priori account for the existence of the chemical bond. Some attempts to integrate the chemical bonding at the Hamiltonian were proposed, such as the chemical Hamiltonian of Mayer.<sup>[438]</sup> This Hamiltonian was developed on the basis of atomic functions following the formalism of second quantization.

$\Psi$  is an eigenfunction of the electronic Schrödinger equation in which each eigenvalue is an energetic electronic state  $E$  of the system. The lowest energy is the ground state. All higher energies are called excited states.

$$H_{el}\psi(1,2, \dots, N) = E\psi(1,2, \dots, N) \quad (2.3)$$

## B- Approximations of the wavefunction

$|\psi|^2$  represents the density of probability to find simultaneously electron 1 in  $X_1$ , electron 2 in  $X_2, \dots$ , electron  $N$  in  $X_N$ . The fermionic nature of electrons and the probabilistic interpretation of the wavefunction require the compliance of the Pauli exclusion principle<sup>[439]</sup> that two identical fermions cannot occupy the same quantum state simultaneously. This imposes the antisymmetry of the wavefunction. This can be achieved by writing the  $\Psi$  as a Slater determinant for any number of fermions. For an  $N$ -electron system, the Slater determinant is defined as:

$$\psi(1, 2, \dots, N) = \begin{vmatrix} \phi_1(X_1) & \dots & \phi_N(X_1) \\ \phi_1(X_2) & \dots & \phi_N(X_2) \\ \vdots & \ddots & \vdots \\ \phi_1(X_N) & \dots & \phi_N(X_N) \end{vmatrix} \quad (2.4)$$

$\phi_i(X_i)$  is the spin-orbital  $i$  and it is the product of an orbital  $\phi_i^e(r_i)$  by a function of spin  $s(\sigma_i)$  as:

$$\phi_i(X_i) = \phi_i^e(r_i)s(\sigma_i) \quad (2.5)$$

The spin-orbitals are orthogonal to each other and can serve as a basis for irreducible representations of the symmetry group of the system. In general the Slater determinant of the wavefunction reflects the correlation between electrons of the same spin, but that between opposed spins is not included. We see that the exact function can be very far from a description by a single determinant as it should ideally be described by a linear combination of determinants in order to account for all atomic or molecular configurations.

### 2.1.2 Hartree-Fock theory

In 1930, Hartree-Fock (HF)<sup>[440,441]</sup> proposed a new method of approximation for the resolution of the Schrödinger equation following the algorithm named "Self-Consistent Field (SCF)". The Hartree-Fock method energy is a first approximation of the exact energy of the ground state. The atomic orbitals in HF method are partitioned into valence and core. The HF formalism involves the use of one-electron Fock operator  $\hat{F}(i)$ , which represents the average influence of the electrostatic field generated by the entire electron cloud on the electron under consideration. The HF wavefunction obtained is the Slater determinant that yields the lowest possible energy according to the variational principle used. These spin-orbitals (MOs occupied) are the eigenfunctions of the Fock operator:

$$\hat{F}(i) = \hat{H}^c(i) + \sum_{j=1}^N [\hat{J}_j(i) - \hat{K}_j(i)] \quad (2.6)$$

With:  $\hat{H}^c(i)$  core operator (contains all one-electronic operators);  $\hat{J}_j(i)$  coulomb operator;  $\hat{K}_j(i)$  exchange operator

$$\hat{H}^c(i) = -\frac{1}{2}\nabla_i^2 - \sum_{\alpha=1}^M \frac{Z_{\alpha}}{|r_i - r_{\alpha}|} \quad (2.7)$$

$$\langle \phi_a(1) | \hat{J}_b(1) | \phi_a(1) \rangle = \int_{X_1} \int_{X_2} \phi_a^*(1) \phi_a(1) \frac{1}{|r_2 - r_1|} \phi_b^*(2) \phi_b(2) dX_1 dX_2 \quad (2.8)$$

$$\langle \phi_a(1) | \hat{K}_b(1) | \phi_a(1) \rangle = \int_{X_1} \int_{X_2} \phi_a^*(1) \phi_b(1) \frac{1}{|r_2 - r_1|} \phi_b^*(2) \phi_a(2) dX_1 dX_2 \quad (2.9)$$

Pseudo-eigenvalue equations can be written as:

$$\hat{F}(1)\phi_i(1) = \varepsilon_i\phi_i(1) \quad \text{With } i = 1, 2, \dots, N \quad (2.10)$$

$\varepsilon_i$  represents the energy of molecular orbital  $i$ . Then, the HF energy of system can be written as:

$$E^{HF} = \sum_{i=1}^{occ} H_{ij}^c + \sum_{i=1}^{occ} \sum_{i>j}^{occ} (J_{ij} - K_{ij}) \quad (2.11)$$

In 1951, Roothaan<sup>[442]</sup> introduced the molecular orbitals constructed as a linear combination of bases of atomic functions  $\chi(i)$  in the formalism of LCAO (linear combination of atomic orbitals) such as:

$$\phi_i(i) = \sum_{\mu=1}^Q C_{i\mu} \chi_{\mu}(i) \quad (2.12)$$

Writing the HF equations in the formalism of Roothaan leads to:

$$\sum_{\mu=1}^Q C_{\mu i} [F_{\eta\mu} - \varepsilon_i S_{\eta\mu}] = 0 \quad \text{with } i = 1, 2, \dots, N \quad (2.13)$$

with  $F_{\eta\mu}$  being an element of the Fock matrix, and  $S_{\eta\mu}$  is an element of the overlap matrix.

## 2.2 RHF ("Restricted HF") - UHF ("Unrestricted HF") formalisms

In practice, we use the restricted HF (RHF) formalism for closed-shell systems<sup>[443]</sup> and the unrestricted HF (UHF) or restricted open-shell (ROHF)<sup>[444]</sup> for a system with an odd number of electrons. Besides the well-known shortcomings of the RHF or ROHF wavefunction at the dissociative limit (too large ionic contributions), the RHF and UHF descriptions are usually close in the equilibrium geometry of closed-shell molecules. The UHF wavefunction is not an eigenfunction of the operator  $S^2$  and can have a spin contamination that can be obtained from the following equation:

$$S^2 \psi^{UHF} = \left[ S_{exact}^2 + N^{\beta} - \sum_{i=1}^N \sum_{j=1}^N |S_{ij}^{\alpha\beta}| \right] \psi^{UHF} \quad (2.14)$$

$$S_{exact}^2 = \left( \frac{N_{\alpha} - N_{\beta}}{2} \right) \left( \frac{N_{\alpha} - N_{\beta}}{2} + 1 \right) \quad (2.15)$$

where  $N_{\alpha}$  and  $N_{\beta}$  are the number of electrons of spin  $\alpha$  and  $\beta$ , respectively.

## 2.3 Hole of Coulomb and Fermi

The Pauli repulsion prohibits two electrons of the same spin to be simultaneously in the same position  $r$ , thereby creating a Fermi hole ( $\pi^{\alpha\alpha}(r, r) = 0$ ). On the other hand, the probability of finding two electrons of opposite spin at the same point in space is also 0 as the repulsion becomes infinite, and this leads to the formation of a Coulomb hole. The HF function takes into

consideration the Fermi hole, but ignores the Coulomb hole so that two electrons of opposite spin can coexist simultaneously in the same position  $r$ . This leads to a non-physical extra Coulomb repulsion in the HF wavefunction. Interestingly, through integration of the Fermi hole one can get information on electronic delocalization and the nature of the chemical bond.<sup>[445]</sup>

## 2.4 Dynamic and static correlations

As defined by Löwdin<sup>[446]</sup> the correlation energy is obtained as:

$$E_{corr} = E_{exact}^{NR} - E_{HF} \quad (2.16)$$

where  $E_{HF}$  is the Hartree-Fock energy and  $E_{exact}^{NR}$  is the exact nonrelativistic energy. Although the standard HF model considers electrons as independent, Pauli's principle introduces a correlation between the electrons of the same spin. To approximate the exact energy and the exact wavefunction, it is necessary to estimate the correlation for all electronic couples. The correlation is usually divided into two contributions: the dynamic and the static correlation.

The dynamic correlation is defined as the interaction of electrons at short distances. It is the consequence of the existence of the Coulomb hole. The inability of the HF function to describe the Coulomb hole was particularly well illustrated by Sinanoglu in 1961 through the fluctuation potential  $\hat{V}_F$ . It is defined by the difference between the exact bielectronic potential and the one-electron Fock operator:

$$\hat{V}_F = \sum_{i=1} \sum_{j>i} \frac{1}{|r_i - r_j|} - \sum_{i=1} \hat{F}(i) \quad (2.17)$$

Figure 2.1, shows the evolution of potential fluctuation (solid line bold), the exact Coulomb potential (solid line) and Fock potential (dotted line) for the two electrons in the 1s orbital of Beryllium depending on the distance to the nucleus. The electron reference is set at a distance  $R$  of the nucleus. The exact Coulomb potential is infinite in  $R$ . The graph clearly shows that the potential has a finite Fock potential value in  $R$ . Through the development of  $\hat{V}_F$ , Sinanoglu describes the difference in behavior between the two potentials and gives an illustration of the Coulomb hole (minimum  $\hat{V}_F$ ), that as can be seen, it is not centered on the electron reference.

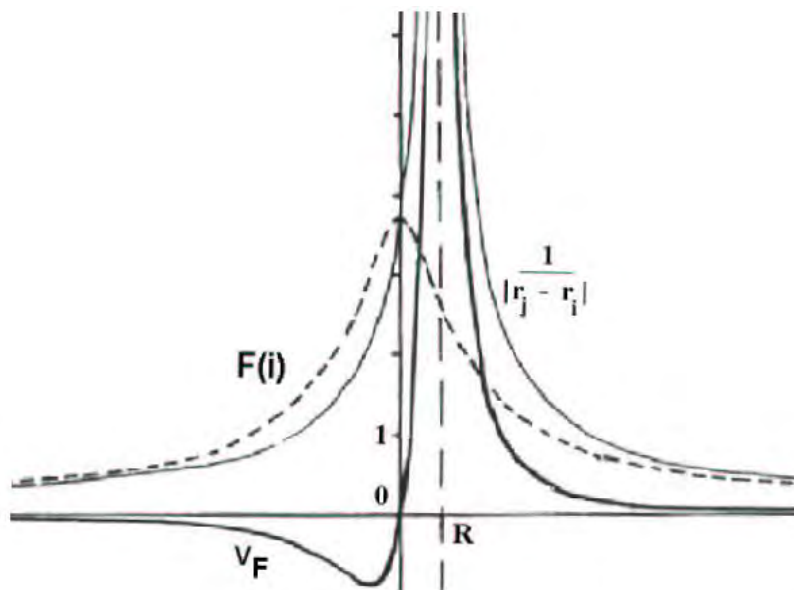


Figure 1.1. Potential fluctuation  $\widehat{V}_F$  of Beryllium ( $Z = 4$ ) for the two electrons 1s obtained by O. Sinanoglu.<sup>[447]</sup>

To set the static correlation, we must consider the fact that the wavefunction is generally better represented by a linear combination of determinants (configurations). In cases where several determinants are almost degenerate in energy, their weights (coefficients) in the wavefunction may become important and clearly contribute to a lowering of the electronic energy. Taking into account these factors, in some cases it is fundamental for a correct description of the electron density to consider more than one single Slater determinant. A good example is  $H_2$  where the function RHF terms includes 50% of covalent and 50% of ionic terms. However, at the dissociative limit, the ionic contributions ( $H^+ + H^-$ ) generate a non-physical destabilization of the system. This is the direct result of not taking into account the static correlation, the correct wavefunction being correctly described in the dissociative limit by a sum of two determinants of equal weight.

## 2.5 Treatment of correlation

In 1929, Hylleraas introduced the correlation for the two electrons of helium<sup>[448]</sup> using two variational parameters ( $\xi$  and  $b$ ) in the wavefunction:

$$\psi(1,2) = N \exp\left(\frac{-\xi \cdot r_1}{a_0}\right) \exp\left(\frac{-\xi \cdot r_2}{a_0}\right) [1 + b(|r_2 - r_1|)] \quad (2.18)$$

This relationship allowed him to exceed the HF. In 1933, James and Coolidge<sup>[449]</sup> proposed a very similar function for the H<sub>2</sub> molecule and calculated a value for the dissociation energy very close to the experimental value. In 1959, Pekeris<sup>[450]</sup> used a function for helium (1078 terms) and managed with the first computers to get closer than 2.10<sup>-9</sup> Hartree to the relativistic limit. This approach, although very efficient for atoms, proved to be difficult to transfer to any polyelectronic system. Nowadays, the methods of calculating the correlation are divided into two classes, those using the HF method as the base, these are the methods post-Hartree-Fock,<sup>[441]</sup> and that of the density functional based on the theorem of Hohenberg and Kohn.<sup>[451]</sup> The post-Hartree-Fock Methods can be classified into three categories:

1. The perturbative approach methods,
2. The variational method of Configurations interaction (CI),
3. The multideterminantal approaches MCSCF and CASSCF.

The two first consider the dynamical correlation mainly by expanding the space of configurations from a single determinant function. The third approach is entitled to an estimate of the static and dynamic correlation.

## 2.6 The perturbative approach of the wave function

### 2.6.1 Møller-Plesset Method

In 1934, Møller and Plesset (MP)<sup>[452-453]</sup> proposed a method that is in line with the methods of many-body perturbation theory.<sup>[440]</sup> The principle is to consider the Hamiltonian of a molecular system  $\hat{H}$  as the sum of an initial unperturbed Hamiltonian and a perturbation  $\lambda\hat{W}$  corresponding to the correlation ( $0 \leq \lambda \leq 1$ ) as:

$$\hat{H} = \hat{H}_o + \lambda\hat{W} \quad (2.19)$$

$$\text{With: } \hat{H}_o = \sum_{i=1}^N \hat{\mathcal{F}}(i) \text{ and } \hat{W} = \sum_i \sum_{i < j} \frac{1}{|x_i - x_j|} - (\hat{j} - \hat{\mathcal{K}}) \quad (2.20)$$

Where  $\hat{\mathcal{F}}(i)$  is the Fock operator.

The energy E of the perturbed system is developed according to the formalism of Taylor around  $\lambda=0$  in a series called Rayleigh-Schrödinger (RS) as:

$$E^{MP_n} = \sum_{k=0}^n E^{(k)} \text{ with } E^{(k)} = \frac{1}{k!} \frac{\partial^k E}{\partial \lambda^k} \quad (2.21)$$

Similarly, the perturbed wave function is written:

$$\psi^{MP_n} = \sum_{k=0}^n \psi^{(k)} \text{ with } \psi^{(k)} = \frac{1}{k!} \frac{\partial^k \psi}{\partial \lambda^k} \quad (2.22)$$

$E^{MP_n}$  is the MP energy in the order  $n$  and  $\psi^{MP_n}$  is the MP function in the order  $n$ . The expressions of the different energy levels can be written as:

$$E^{(0)} = \langle \psi^{HF} | H_0 | \psi^{HF} \rangle = \sum_{i=1}^{occ} \varepsilon(i) \quad (2.23)$$

$$E^{MP_1} = E^{HF} = E^{(0)} + \langle \psi^{HF} | \widehat{W} | \psi^{HF} \rangle = E^{(0)} + E^{(1)} \quad (2.24)$$

$$E^{MP_2} = E^{MP_1} + E^{(2)} \text{ with } E^{(2)} = \sum_{i,j} \sum_{a,b} \frac{(ij||ab)^2}{\varepsilon_i + \varepsilon_j - \varepsilon_a - \varepsilon_b} \quad (2.25)$$

$(ij||ab)$  are the integrals involving bielectronic occupied  $(i, j)$  and virtual  $(a, b)$  orbitals, and  $\varepsilon_i$  is the energy of the orbital  $i$ . The most common calculations are at the MP2 level and use di-excited configurations. The perturbation methods are size consistent, which is a necessary condition for the correct calculation of the energies of interaction. However,  $MP_n$  calculations may be of poor quality if the static correlation is strong. On the other hand, the divergent behavior of the Rayleigh-Schrödinger is relatively common. In practice, the standard formalisms closed-shell ( $MP_n$ ) and open-shell ( $UMP_n$ ) are commonly used in quantum chemistry software, although this formalism  $UMP_n$  frequently presents a spin contamination problem at the UHF function.

## 2.6.2 "Coupled Cluster" Method

Currently, the "Coupled Cluster" method<sup>[440,454-458]</sup> is the most successful post-HF method from the point of view of the inclusion of dynamic correlation. For such, we define the exponential operator  $e^T$  that acts on the reference function  $\psi^{HF}$  as follows:

$$e^T \psi^{HF} = \psi^{CC} \text{ With } e^T = \sum_{k \geq 0} \frac{1}{k!} T^k \quad (2.26)$$

$T$  is defined as the sum of the excitation operators  $T_i$  such that:

$$T_1 = \sum_i^{occ} \sum_a^{virt} t_i^a a^\dagger \dots i \quad (2.27)$$

$$T_2 = \sum_{i < j}^{occ} \sum_{a < b}^{virt} t_{ij}^{ab} a^\dagger b^\dagger \dots ji \quad (2.28)$$

And:  $T = T_1 + T_2 + \dots$

$a^\dagger$  and  $b^\dagger$  are the creation operators,  $i$  and  $j$  annihilation operators and  $t_{ij}^{ab}$  are the amplitudes. Due to coupling between  $T_i$  and  $T_j$  ( $i \neq j$ ), for example, the truncation to order 2 takes into account the double excitations. In practice, the calculations with double excitations ( $T = T_2$ , denoted CCD) or single and double excitations ( $T = T_1 + T_2$ , denoted CCSD) are the most commonly used. Then, the CCSD energy is written as:

$$E_{CCSD} = E_{HF} + \langle \psi^{HF} | \hat{H} e^{T_2} | \psi^{HF} \rangle \quad (2.29)$$

Perturbational corrections to the CCSD energy is possible by taking into account higher order excitations. Thus, the popular method CCSD(T) is written:

$$E_{CCSD(T)} = E_{CCSD} + E_T^4 + E_{ST}^5 \quad (2.30)$$

$E_T^4$  is the energy contribution of triple excitations to order 4 and  $E_T^5$  is the contribution of single to order 5. The CCSD(T) method is very expensive in computing time, but it is one of the most effective techniques for the calculation of dynamic correlation.

### 2.6.3 The method of Configuration Interaction (CI)

In this method, the wavefunction is described by a linear combination of Slater determinants (generated by the HF configuration), which form a complete basis:

$$\psi^{CI} = C_0 \psi_{HF} + \sum_s C_s \psi_s + \sum_d C_d \psi_d + \sum_t C_t \psi_t + \dots \quad (2.31)$$

The first term corresponds to the HF determinant weighted with coefficient  $C_0$ , the second ( $\psi_s$ ) corresponds to the simply excited configurations, the third ( $\psi_d$ ) is doubly excited configurations, etc... The coefficients of the expansion are optimized variationally. For  $N$ -spin occupied orbitals and  $n$  electrons, the number of virtual spin-orbitals is equal to  $(n - N)$ . The number of excited configurations is equal to:

$$\frac{n!}{N!(n-N)!} \quad (2.32)$$

If a calculation takes into account all these configurations, it is called full CI ("Full CI"), but this treatment is unworkable in practice. Generally we truncate at the mono-excited using only  $N(n-N)$  configurations (CIS), or to the di-excited (CISD),<sup>[459]</sup> or to tri-excited (CISDT) or even quadri-excited (QCISD).<sup>[460]</sup> Full CI calculation is equivalent to a "Coupled Cluster" where all non-truncated excitations operators are taken into account. This type of calculation then leads to the exact nonrelativistic energy of the system. However, a *CISD* calculation already makes a large portion of the correlation energy. The truncated CI method suffers from a serious lack of extensivity, making it ineffective for the study of dissociative processes. Because of this important issue, the formalism multi-determinant MRCI is widely used as it usually contains a good portion of all the dynamic and static correlation. However, this method is very expensive and it is only applicable to small systems.

## 2.7 Multireference methods: CASSCF and MCSCF

The multideterminant (or multireference) MCSCF<sup>[461]</sup> (multiconfiguration self-consistent field)<sup>[462]</sup> converges to an electronic solution close to the exact solution because the structure of the  $\psi^{MCSCF}$  function (linear combination of Slater determinants) allows the inclusion of the static correlation often important for excited states or molecules near to the dissociation. For example, the function  $\psi^{MCSCF}$  for the H<sub>2</sub> molecule (H<sub>a</sub>H<sub>B</sub>) writes:

$$\psi_{H_2}^{MCSCF} = \|\psi_A \bar{\psi}_A\| + C_d \|\psi_B \bar{\psi}_B\| \quad (2.33)$$

$$\text{Where: } \psi_A = a + cb \quad \text{and} \quad \psi_B = ca + b \quad (2.34)$$

$a$  and  $b$  are the atomic orbitals centered respectively on the hydrogens H<sub>a</sub> and H<sub>b</sub>. The coefficient  $c$  (weight of atomic orbitals) is optimized simultaneously to  $C_d$  coefficient (weight determinants). In practice, we use a truncated version of the method MCSCF namely CASSCF.<sup>[463]</sup> In this case, the treatment is limited to certain orbitals (often occupied valence orbitals) that become part of the active space. All configurations generated with the orbitals of the active space are taken into account. This multideterminant approach is useful in situations of strong degeneracy; it is *a priori* capable of estimating the static correlation and describes, for example, very correctly the dissociation of H<sub>2</sub>. The MRCI method mentioned above allows very exact calculations of the correlation energy because it uses the reference MCSCF wavefunction for making a configuration interaction calculation.

### 2.7.1 The density functional

The electron density  $\rho(r)$  is defined as the average distribution in space of an electron as:

$$\rho(r) = N \int \cdots \int \psi^*(x_1, x_2, \dots, x_N) \psi(x_1, x_2, \dots, x_N) d\sigma dx_2 \cdots dx_N \quad \text{with} \quad \int \rho(r) dr = N \quad (2.35)$$

This density is observable and determined experimentally (by X-ray diffraction). The model of the density functional (DFT) is undoubtedly one that gives the best compromise between quality and CPU time at the present moment. The idea that the electron density can contain all the information of an atomic or molecular system was used for the first time through the Thomas-Fermi model but was developed further. It was not until 1964, with the formulation of the two theorems of Hohenberg and Kohn,<sup>[464]</sup> which showed that the energy of any system is an atomic or molecular density functional  $E[\rho]$ , that the DFT approach<sup>[451]</sup> was fully developed.

### 2.7.2 Hohenberg and Kohn theorems

The first theorem of Hohenberg and Kohn formulated in 1964<sup>[464]</sup> shows that the knowledge of an external potential  $V$  (Coulomb potential due to nuclei) implies the uniqueness of  $\rho$  and  $\psi$  for an atomic or molecular system.

$H_1$  and  $H_2$  are two different Hamiltonians of the same system associated with two specific functions  $\psi_1$  and  $\psi_2$  for the different ground states. These two hamiltonians differ only in the external potential  $V_1 \neq V_2$ . Then, consider  $\rho_1$  and  $\rho_2$  as two distinct electron densities associated respectively to  $\psi_1$  and  $\psi_2$ .

$$H_1 = \hat{T}_e + \hat{V}_{ee} + V_1 \quad (2.36)$$

$$H_2 = \hat{T}_e + \hat{V}_{ee} + V_2 \quad (2.37)$$

According to the variational theorem ( $\psi_1$  and  $\psi_2$  are orthonormal):

$$E_1^o = \langle \psi_1 | H_1 | \psi_1 \rangle \quad (2.38)$$

$$E_1^o < \langle \psi_2 | H_1 | \psi_2 \rangle \quad (2.39)$$

$$E_1^o < E_2^o + \langle \psi_2 | H_1 - H_2 | \psi_2 \rangle \quad (2.40)$$

$$E_1^o < E_2^o + \int (V_1 - V_2) \rho_2 dr_2 \quad (2.41)$$

Similarly we have:  $E_2^o < E_1^o + \int (V_2 - V_1) \rho_1 dr_1$ . The above relationships are possible if and only if  $\rho_1 = \rho_2$ , which is contrary to the assumptions. This implies that the electron density is unique for a given system. A biunivocal correspondence is ensured between the electron density and the external potential. The second theorem shows that the energy of the ground state is obtained by minimizing a density functional  $E[\rho]$  such that:

$$E[\rho] = \hat{T}_e[\rho] + \hat{V}_{ee}[\rho] + \hat{V}[\rho] \quad (2.42)$$

Today, the major problem in DFT methods is the lack of knowledge of the exact functional. In recent years, multiple functionals have been proposed but their effectiveness to treat different problems varied greatly.

### 2.7.3 The Thomas-Fermi model

This was a precursor model of the modern DFT developed in the 1930s,<sup>[465-466]</sup> and was based on the homogeneous electron gas [ $\rho(r)=\text{ctant}$ ]. The energy functional is of the following form (in atomic units):

$$E[\rho] = C_f \int \int \rho^{\frac{5}{3}} dr + \int \int \frac{\rho(r_1)\rho(r_2)}{|r_1-r_2|} dr_1 dr_2 - Z \int \frac{\rho(r)}{r} dr \quad (2.43)$$

A further improvement came from the Thomas-Fermi-von Weizsäcker functional<sup>[467]</sup> that has the expression:

$$E[\rho] = C_w \int |\nabla\sqrt{\rho}|^2 dr + C_f \int \rho^{\frac{5}{3}} dr + \frac{\rho(r_1)\rho(r_2)}{|r_1-r_2|} dr_1 dr_2 - Z \int \frac{\rho(r)}{r} dr \quad (2.44)$$

with  $C_f = \frac{3}{10} (3\pi^2)^{\frac{2}{3}} \approx 2.871 \text{ a.u.}$  and  $C_w = 0.5 \text{ a.u.}$

### 2.7.4 Kohn-Sham Model

From the theorems of Hohenberg and Kohn, Kohn and Sham<sup>[468]</sup> have sought a fictitious system in which the electrons are independent ( $V_{ee}=0$ ) but where  $\rho$  is identical to the real system in which the electrons are correlated. The fictitious system (KS) is described by the function  $\psi^{KS}$  that is a determinant of spin-orbitals. Inspired by the philosophy of SCF, we can write a set of coupled equations (equations KS) converging by self-consistency to the real system from the fictitious system.

The real functional system  $E[\rho]$  can be written as:

$$E[\rho] = T_s[\rho] + T_{ne}[\rho] + E_{xc}[\rho] \quad (2.45)$$

With: 
$$T_s[\rho] = -\frac{1}{2} \sum_{i=1}^N \int \phi^*(X_i) \nabla^2 \phi^*(X_i) dX_i \quad (2.46)$$

$$J[\rho] = \iint \frac{\rho(r_1)\rho(r_2)}{|r_1-r_2|} dr_1 dr_2 \quad (2.47)$$

$$V_{ne}[\rho] = \int \rho(r) v(r) dr \text{ and } v(r) = -\sum_{\alpha=1}^M \frac{Z}{r_\alpha} \quad (2.48)$$

$T_s[\rho]$  : Kinetic energy of the fictitious system.

$J[\rho]$  : Classical Coulomb interaction between electrons.

$V_{ne}[\rho]$  : Core-electron Coulomb interaction.

$E^{xc}[\rho]$  is the exchange-correlation energy which contains the difference between the kinetic energy of the real system ( $T[\rho]$ ) and that of the fictitious system ( $T_s[\rho]$ ) and the difference between Coulomb repulsion term of the real system ( $V_{ee}[\rho]$ ) and  $J[\rho]$ . Its exact form is not known and this is the central problem of DFT methods. As a result, the external potential is expressed as:

$$v^{KS}(r) = v(r) + \frac{\delta J[\rho]}{\delta \rho(r)} + \frac{\delta E_{xc}[\rho]}{\delta \rho(r)} \quad (2.49)$$

$$v^{KS}(r) = v(r) + v_h + v_{xc} \quad (2.50)$$

where  $v_h$  is the Hartree potential and  $v_{xc}$  is the exchange-correlation potential.  $v_{xc}$  is a local external potential describing any correlation between the electrons in order that the fictitious KS system reaches the same electron density than the real system:

$$\rho(r) = \sum_{i=1}^{occ} |\phi_i(r)|^2 \quad (2.51)$$

Then the Kohn-Sham equations are written as:

$$K[\rho] \phi_i(r) = \varepsilon(i) \phi_i(r) \text{ for } i = 1, 2, \dots, N \quad (2.52)$$

with: 
$$K[\rho] = -\frac{1}{2} \nabla^2(r_i) + v^{KS}(r_i) \quad (2.53)$$

The whole problem is to find the most accurate possible exchange-correlation potential, which is still today a great challenge. However, the inclusion of electron correlation is intrinsic to the KS

method and this represents (together with the low CPU time required) the major advantage of this approach in comparison with post-HF methods.

### 2.7.5 Purely local functional (LDA)

The local density approximation (LDA) is directly related to the model of the electron homogeneous gas. We can separate the exchange-correlation functional with a term of exchange and another of correlation:  $E_{xc}[\rho] = E_x[\rho] + E_c[\rho]$ . Then the functional is written as follows:  $E[\rho] = \int \rho(r)\varepsilon(\rho) dr$ , with  $\varepsilon(\rho)$  being the energy density. The most widely used LDA functional is that of Slater<sup>[469]</sup> for the exchange and that for correlation of Vosko.<sup>[470]</sup> This type of approach is correct for regions where the density is almost homogeneous (between cores), but in regions near the core, the system is poorly described. Nevertheless, they can provide excellent geometric results,<sup>[451]</sup> although they overestimate the interaction and ionization energies.

### 2.7.6 The generalized gradient approximation (GGA)

To take into account the inhomogeneity of the density in the nuclei and far from nuclei, a correction using the gradient  $|\nabla\rho|$  and sometimes the Laplacian of the density  $\nabla^2\rho$  (meta-GGA) is used. The most commonly correction used is that due to Becke (B),<sup>[471]</sup> Gill (G96)<sup>[472]</sup> or Perdew, Burke, and Ernzerhof (PBEX)<sup>[473]</sup> for the exchange and those of Perdew (P86),<sup>[474]</sup> Perdew-Wang (PW91)<sup>[475]</sup> and Lee-Yang-Parr (LYP)<sup>[476]</sup> for the correlation. These corrections generally improve the binding energies, but are often insufficient.

## 2.8 Hybrid functionals

In cases where  $\rho$  is very inhomogeneous, there is a need to consider the exact exchange (Hartree-Fock)  $E_x^{HF}$ . This is the idea of the hybrid functionals. Becke proposed to replace part of the local Slater exchange by exchange coupled with an exact gradient correction as in his three parameters hybrid functional (B3):

$$E_{xc} = E_{xc}^{LDA} + a_0(E_x^{HF} - E_x^{LDA}) + a_1\Delta_x + a_2\Delta_c \quad (2.54)$$

$$\text{With: } E_x^{HF} = -\frac{1}{2} \int \int \sum_{i\sigma}^{occ} \sum_{j\sigma'}^{occ} \frac{\phi_{i\sigma}^*(r)\phi_{j\sigma'}^*(r')\phi_{j\sigma'}^*(r)\phi_{i\sigma}^*(r')}{|r-r'|} drdr' \quad (2.55)$$

$$\text{And: } \Delta_x = E_x^{GGA} - E_x^{LDA} ; \Delta_c = E_c^{GGA} - E_c^{LDA} \quad (2.56)$$

$E_{xc}$  is a purely local term. However, the non-locality of the term  $E_x^{HF}$  is only partially offset by the quasi-locality of the correlation energy. The hybrid functional must possess a gradient correction to the exchange energy in order to limit the non-locality introduced by the term  $E_{xc}$ . For example, the functional PBE0<sup>[477]</sup> includes 25% of exact exchange (and 75% PBEX) and uses the simplified functional PW91 for correlation. The functional B3LYP<sup>[471,476,478-479]</sup> uses three coefficients  $a_0, a_1, a_2$  (according to eq. 2.54) whose values are:  $a_0=0.20, a_1=0.72, a_2=0.81$ . These coefficients were calibrated on a very reliable database to correctly reproduce the dissociation energies, ionization potentials, and proton affinities. Pragmatically, hybrid functionals allow reproduction of observables closer to experimental values than GGA functionals, but conceptually, the loss of locality remains unsatisfactory. For this reason, some researches are directed towards other ways, especially towards the development of meta-GGA functional.

## 2.9 Bond Energy Decomposition

The bonding energy corresponding to the formation of a given compound from two fragments is made up of two major components (eq 2.57):

$$\Delta E = \Delta E_{prep} + \Delta E_{int} \quad (2.57)$$

In this formula, the preparation energy  $\Delta E_{prep}$  is the amount of energy required to deform the separated fragments in their interacting state from their equilibrium structure to the geometry that they acquire in the molecule. The interaction energy  $\Delta E_{int}$  corresponds to the actual energy change when the prepared fragments are combined to form the overall molecule. It is analyzed in the framework of the Kohn–Sham MO model using a Morokuma-type decomposition of the bonding energy into electrostatic interaction, exchange (or Pauli) repulsion, and orbital interactions (eq 2.58).<sup>[480-484]</sup>

$$\Delta E_{int} = \Delta V_{elstat} + \Delta E_{Pauli} + \Delta E_{oi} \quad (2.58)$$

The term  $\Delta V_{elstat}$  corresponds to the classical electrostatic interaction between the unperturbed charge distributions of the prepared (i.e., deformed) fragments and is usually attractive. The Pauli repulsion  $\Delta E_{Pauli}$  comprises the destabilizing interactions between occupied orbitals. It arises as the energy change associated with going from the superposition of the unperturbed

electron densities of the two fragments to the wave function  $\psi^0 = NA[\psi_{fragment1}^{\alpha\alpha}, \psi_{fragment2}^{\beta\beta}]$ , that properly obeys the Pauli principle through explicit antisymmetrization (A operator) and renormalization (N constant) of the product of fragment wavefunctions. It comprises the four-electron destabilizing interactions between occupied MOs and is responsible for the steric repulsion. The orbital interaction  $\Delta E_{oi}$  is the change in energy from  $\psi^0$  to the final, fully converged wavefunction  $\psi_{SCF}$  of the system. The orbital interactions account for charge transfer (i.e., donor–acceptor interactions between occupied orbitals on one fragment with unoccupied orbitals of the other, including the HOMO–LUMO interactions) and polarization (empty–occupied orbital mixing on one fragment due to the presence of another fragment). The  $\Delta E_{oi}$  term can be divided into contributions of orbitals having different symmetry (eq 2.59) using the extended transition state (ETS) scheme developed by Ziegler and Rauk.<sup>[483-484]</sup>

$$\Delta E_{oi} = \sum_{\Gamma} \Delta E_{\Gamma} \quad (2.59)$$

In case of planar systems with a clear  $\sigma/\pi$  separation, this symmetry partitioning proved to be very useful.

## **Chapter 2: Objectives**

---

The main goal of the present thesis is to unravel the origin of the relative stabilities of a series of structural isomers by using energy decomposition analyses.

---

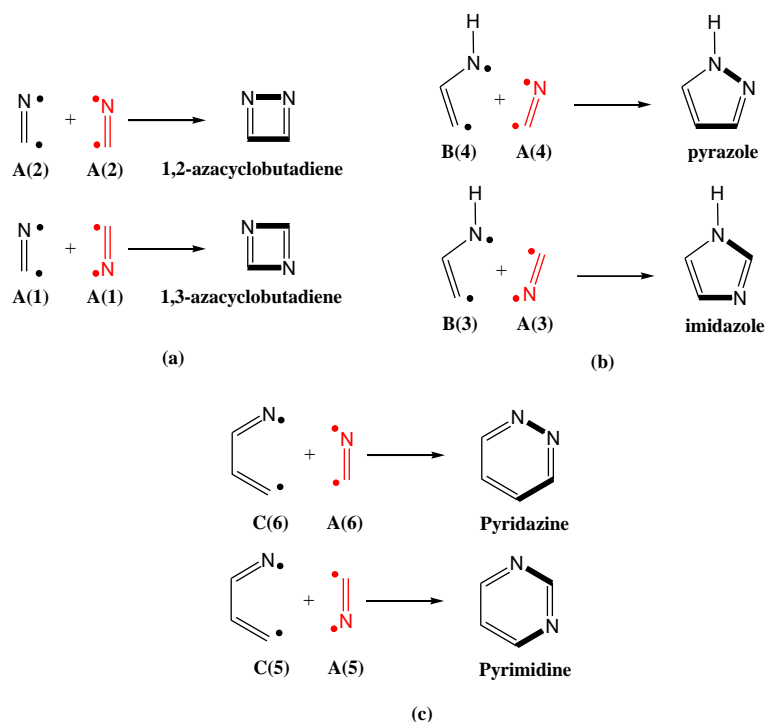


In the Introduction chapter, we have underlined the nature of chemical bonds and we have discussed the different isomers types. The results section in this thesis is divided into four different parts. The first one (Chapter 3) is devoted to the analysis of the isomerization energies of 1,2-/1,3-diazacyclobutadiene, pyrazole/imidazole, and pyridazine/pyrimidine with the so-called turn-upside-down approach (TUDA). In the second part (Chapter 4), we have studied the relative stability of  $X_2Y_2$  isomers ( $X = H, Li, Na, F, Cl, Br, I; Y = O, S, Se, Te$ ) using energy decomposition analyses. In the third part (Chapter 5), we have made a comparison between two different isomers of alkalimetal and group 11 transition metal halide and hydride tetramers. Finally, the last project (Chapter 6) was devoted to study the relative stabilities of the ortho, meta, and para  $MClY(XC_4H_4)(PH_3)_2$  heterometallabenzenes ( $M = Ir, Rh; X = N, P; Y = Cl$  and  $M = Os, Ru; X = N, P; Y = CO$ ).

### Project 1

1,2-diazabenzene and -cyclobutadiene and pyrazole with two adjacent nitrogen atoms are less stable than the corresponding 1,3-isomers. Standard enthalpies of formation indicate that pyrimidine and imidazole are more stable than pyridazine and pyrazole by about  $20^{[95-96]}$  and  $10^{[97-99]}$  kcal/mol, respectively. On the other hand, previous MNDO calculations also favored the 1,3- with respect to the 1,2-diazacyclobutadiene by 32.6 kcal/mol.<sup>[485]</sup> Lone-pair repulsion in NN bonds is the usual explanation for the lower stabilities of the NN isomers.<sup>[100-101]</sup> However, lone-pair protonation and diprotonation of pyridazine and pyrimidine barely change its energy difference.<sup>[102]</sup> Therefore, it seems that lone-pair repulsion cannot be the only cause that explains the higher stability of 1,3-isomers. Although the strength of the  $N=N$   $\pi$ -bond is somewhat lower than that of the  $C=C$  and  $C=N$  bonds, the difference of about 6 kcal/mol<sup>[102]</sup> is not enough to explain the relative energies of 1,2- and 1,3-diaza and azole compounds either. Therefore, the reason for the lower stability of 1,2-diazabenzene and -cyclobutadiene and pyrazole in comparison to their 1,3-counterparts has to be attributed in part to the  $\sigma$ -skeleton,<sup>[102]</sup> and it is not fully understood yet. The goal of this work is:

To carry out a detailed analysis of the isomerization energy of these 1,2- and 1,3-isomers with the so-called turn-upside-down approach (see Scheme 2.1) with the aim of providing a better comprehension on the origin of the NN bond destabilization.



**Scheme 2.1** The formation of (a) 1,2- and 1,3-diazacyclobutadiene, (b) pyrazole/imidazole, (c) pyridazine/pyrimidine structural isomers from two triplet biradical fragments with the turn-upside-down approach.

## Project 2

The second project is devoted to the study of the  $XYYYX$  and  $X_2YY$  isomers of the  $X_2Y_2$  species ( $X = \text{H, Li, Na, F, Cl, Br, I}$ ;  $Y = \text{O, S, Se, Te}$ ) using density functional theory at the ZORA-BP86/QZ4P level with three main objectives:

- 1) Obtain a set of consistent structural and thermochemical data for simple dicalchogenides (geometries, relative stabilities), all at the same level of theory.
- 2) To better understand the physics and the nature of the  $X\text{--}Y$  bond through quantitative bond energy decomposition analyses.
- 3) To further generalize the valuable tuning principle according to which the central  $Y\text{--}Y$  link in  $XYYYX$  can be tuned from single bond to double bond by varying the electronegativity difference across the  $X\text{--}Y$  bond.

### Project 3

The tetramer  $(XM)_4$  ( $X = F, Cl, Br, I$ , and  $M = Li, Na, K, Rb$ ) occurs among others as a cube ( $T_d$  symmetry), ladder, and ring ( $D_{4h}$  symmetry). Earlier theoretical studies showed that the cube is, in general, the most stable one. On the other hand,  $[c-M_4(\mu_2-L)_4]$  ( $M = Cu, Ag, Au$ , and  $L = H, CH_3, SiH_3, GeH_3, NH_2, PH_2, OH, F, Cl, Br, I$ ) four-membered clusters adopt square-planar structures involving bridging stabilizing ligands  $L$ . All these  $[c-M_4(\mu_2-L)_4]$  clusters are characterized by perfect planarity and equalization of all metal-metal bonds in the metallic rings, with the only exception being the  $[c-Cu_4(\mu_2-Br)_4]$  and  $[c-Cu_4(\mu_2-I)_4]$  clusters, which adopt a planar rhombic diamond-like core structure. All these group 11 metal(I) halides adopt ring  $D_{4h}$  or out-of-plane distorted butterfly-shape  $D_{2d}$  structures. These isomers were found much lower in energy than the cubic  $T_d$  form. So, from the results above, it is seen how for  $(MX)_4$  clusters, alkalimetal atoms ( $M = Li, Na, K, Rb$ ) tend to adopt a cubic  $T_d$  conformation as the most stable, whereas group 11 transition state metals ( $M = Cu, Ag, Au$ ) tend to prefer a ring  $D_{4h}/D_{2h}$  one, despite the metals in the two cases have the same  $ns^1$  valence configuration. The comprehension of the reasons for the difference observed represents a challenge and the results obtained can be relevant for the discussion of the nature of chemical bonding in inorganic clusters. For this reason, we have undertaken a detailed investigation of alkalimetal ( $M = Li, Na, K$ , and  $Rb$ ) and group 11 transition metal ( $M = Cu, Ag$ , and  $Au$ )  $(MX)_4$  tetramers with  $X = H, F, Cl, Br$ , and  $I$ , using density functional theory at the BP86/QZ4P level with the following threefold purpose:

- 1) To obtain a set of consistent structural and thermochemical data for the series of tetramers analyzed, all obtained at the same level of theory.
- 2) To compare the planar and cubic arrangements for all  $(MX)_4$  analyzed.
- 3) To achieve a better understanding of the reasons for the different geometry adopted by these clusters depending on the metal considered using quantitative bond energy decomposition analyses (EDA).

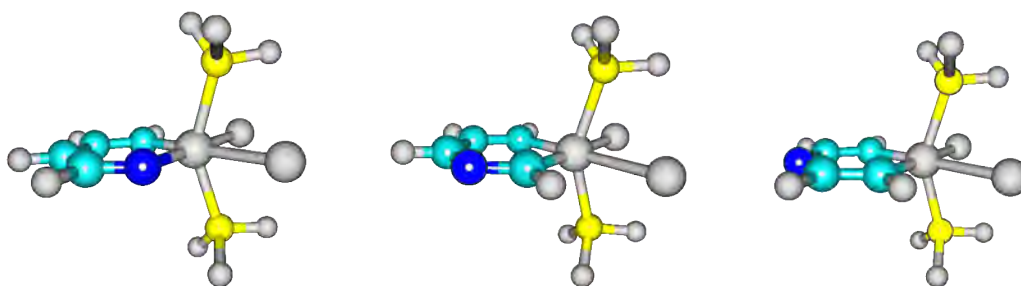
### Project 4

The chemistry of transition-metal-containing aromatic metallacycles is nowadays attracting significant attention. Among these metallacycles, the so-called metallabenzenes. These last one exhibit properties usually associated with aromatic systems, such as deshielded proton

resonances in the  $^1\text{H-NMR}$  spectrum, bond length equalization, and ring planarity. As to reactivity, metallabenzenes suffer the typical aromatic electrophilic substitutions.

In almost all heterometallacycles synthesized to date the heteroatom is directly bonded to the metal atom. To our knowledge the only exception is an osmapyridyne in which the N atom is in meta position with respect to the metal. However, depending on the degree of C 2p and metal d orbital mixing, one can consider that metallabenzenes are 6, 8 or  $10\pi$ -electron species. The different electron counting is due to the disputable participation of the metal d orbitals in  $\pi$ -bonding. While, it seems that there is some conflicting in point of views between authors which still enables to explain the reactivity and stability of this kind of compound.

Hence, we decided to study the relative stabilities of the ortho, meta, and para  $\text{MClY}(\text{XC}_4\text{H}_4)(\text{PH}_3)_2$  heterometallabenzenes ( $\text{M} = \text{Ir, Rh; X} = \text{N, P; Y} = \text{Cl}$  and  $\text{M} = \text{Os, Ru; X} = \text{N, P; Y} = \text{CO}$ ).



**Scheme 2.2** An schematic representation of the three isomers of the  $\text{MClY}(\text{XC}_4\text{H}_4)(\text{PH}_3)_2$  heterometallabenzenes considered.

The objectives of this part of the thesis is threefold:

- 1) To find the most stable heterometallabenzene isomer in each case.
- 2) To discuss the aromaticity in these compounds.
- 3) To analyze the chemical bonding in order to unravel the reasons for the different isomer stabilities. The analysis of the isomerization energy of these isomers will be carried out with an energy decomposition analysis and the so-called turn-upside-down approach.

### Chapter 3:

## An Analysis of the Isomerization Energies of 1,2-/1,3-Diazacyclobutadiene, Pyrazole/Imidazole, and Pyridazine/Pyrimidine with the Turn-Upside Down Approach



M. El-Hamdi, W. Tiznado, J. Poater, M.Solà. "An Analysis of the Isomerization Energies of 1,2-/1,3-Diazacyclobutadiene, Pyrazole/Imidazole, and Pyridazine/Pyrimidine with the Turn-Upside-Down Approach". *Journal of Organic Chemistry*. Vol. 76, núm. 21 (2011) : 8913–8921. DOI 10.1021/jo201639k

<http://dx.doi.org/10.1021/jo201639k>

<http://pubs.acs.org/doi/abs/10.1021/jo201639k>

Received: August 9, 2011

Published: September 27, 2011

## Abstract

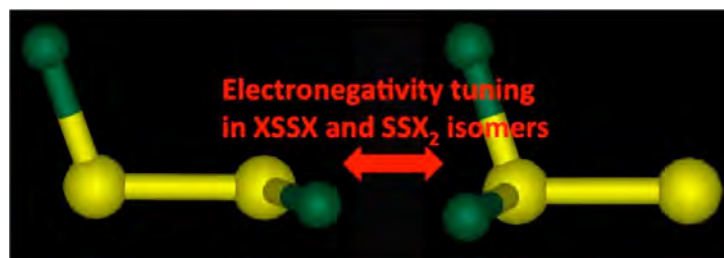


The isomerization energies of 1,2- and 1,3-diazacyclobutadiene, pyrazole and imidazole, and pyridazine and pyrimidine are 10.6, 9.4, and 20.9 kcal/mol, respectively, at the BP86/TZ2P level of theory. These energies are analyzed using a Morokuma-like energy decomposition analysis in conjunction with what we have called turn-upside-down approach. Our results indicate that, in the three cases, the higher stability of the 1,3-isomers is not due to lower Pauli repulsions but because of the more favorable  $\sigma$ -orbital interactions involved in the formation of two C–N bonds in comparison with the generation of C–C and N–N bonds in the 1,2-isomers.



## Chapter 4:

### **$X_2Y_2$ Isomers: Tuning Structure and Relative Stability through Electronegativity Differences ( $X = H, Li, Na, F, Cl, Br, I$ ; $Y = O, S, Se, Te$ )**



M. El-Hamdi, J.Poater, F.M. Bickelhaupt, M. Solà. "X<sub>2</sub>Y<sub>2</sub> Isomers: Tuning Structure and Relative Stability through Electronegativity Differences (X = H, Li, Na, F, Cl, Br, I; Y = O, S, Se, Te)". *Inorganic Chemistry*. Vol. 52, núm. 5 (2013) : 2458–2465. DOI 10.1021/ic3023503

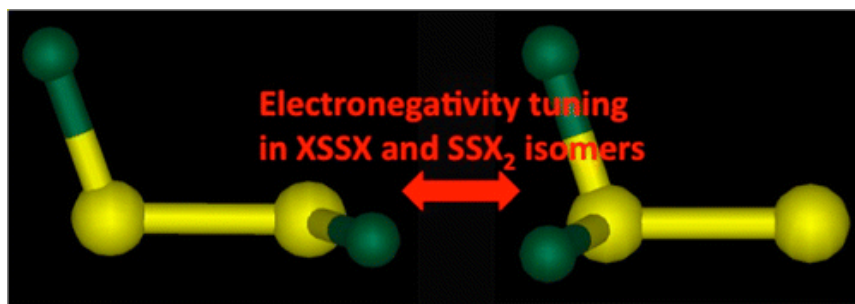
<http://dx.doi.org/10.1021/ic3023503>

<http://pubs.acs.org/doi/abs/10.1021/ic3023503>

Received: October 28, 2012

Published: February 19, 2013

### Abstract

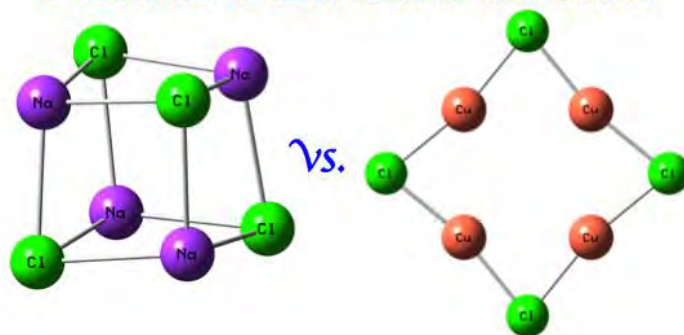


We have studied the XYXX and X<sub>2</sub>YY isomers of the X<sub>2</sub>Y<sub>2</sub> species (X = H, Li, Na, F, Cl, Br, I; Y = O, S, Se, Te) using density functional theory at the ZORA-BP86/QZ4P level. Our computations show that, over the entire range of our model systems, the XYXX isomers are more stable than the X<sub>2</sub>YY forms except for X = F and Y = S and Te, for which the F<sub>2</sub>SS and F<sub>2</sub>TeTe isomers are slightly more stable. Our results also point out that the Y–Y bond length can be tuned quite generally through the X–Y electronegativity difference. The mechanism behind this electronic tuning is the population or depopulation of the π\* in the YY fragment.

## Chapter 5:

### A Comparison between Alkalimetal and Group 11 Transition Metal Halide and Hydride Tetramers: Molecular Structure and Bonding

*from  $T_d$  alkalimetal to  $D_{4h}$  group 11  
transition metal halide tetramers*



M. El-Hamdi, M. Solà, G. Frenking, J. Poater. "Comparison between Alkalimetal and Group 11 Transition Metal Halide and Hydride Tetramers: Molecular Structure and Bonding". Vol. 117, núm. 33 (2013) : 8026–8034. DOI 10.1021/jp4051403

<http://dx.doi.org/10.1021/jp4051403>

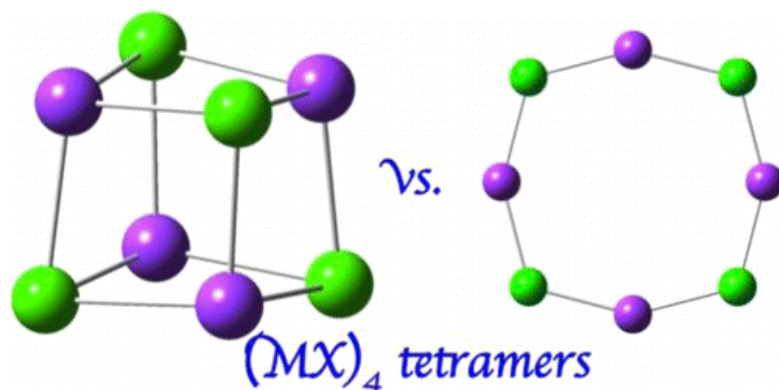
<http://pubs.acs.org/doi/abs/10.1021/jp4051403>

Received: May 24, 2013

Revised: July 23, 2013

Published: July 23, 2013

## Abstract

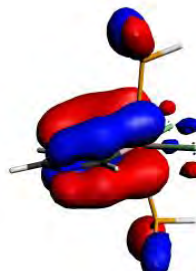
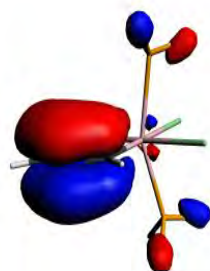


A comparison between alkalimetal ( $M = \text{Li, Na, K, and Rb}$ ) and group 11 transition metal ( $M = \text{Cu, Ag, and Au}$ )  $(MX)_4$  tetramers with  $X = \text{H, F, Cl, Br, and I}$  has been carried out by means of the Amsterdam Density Functional software using density functional theory at the BP86/QZ4P level of theory and including relativistic effects through the ZORA approximation. We have obtained that, in the case of alkalimetals, the cubic isomer of  $T_d$  geometry is more stable than the ring structure with  $D_{4h}$  symmetry, whereas in the case of group 11 transition metal tetramers, the isomer with  $D_{4h}$  symmetry (or  $D_{2d}$  symmetry) is more stable than the  $T_d$  form. To better understand the results obtained we have made energy decomposition analyses of the tetramerization energies. The results show that in alkalimetal halide and hydride tetramers, the cubic geometry is the most stable because the larger Pauli repulsion energies are compensated by the attractive electrostatic and orbital interaction terms. In the case of group 11 transition metal tetramers, the  $D_{4h}/D_{2d}$  geometry is more stable than the  $T_d$  one due to the reduction of electrostatic stabilization and the dominant effect of the Pauli repulsion.



## Chapter 6:

**An Analysis of the Relative Stabilities of Ortho, Meta, and Para  
MCIY(XC<sub>4</sub>H<sub>4</sub>)(PH<sub>3</sub>)<sub>2</sub> Heterometallabenzenes (M = Rh, Ir; X = N, P; Y = Cl  
and M = Ru, Os; X = N, P; Y = CO)**



Majid El-Hamdi, Ouissam El Bakouri El Farri, Pedro Salvador, Ben Ali Abdelouahid, Mohamed Soussi El Begrani, Jordi Poater, Miquel Solà. "An Analysis of the Relative Stabilities of Ortho, Meta, and Para  $MClY(XC_4H_4)(PH_3)_2$  Heterometallabenzenes ( $M = Rh, Ir; X = N, P; Y = Cl$  and  $M = Ru, Os; X = N, P; Y = CO$ )". *Organometallics*. Vol. 32, núm. 17 (2013) : 4892–4903. DOI 10.1021/om400629w

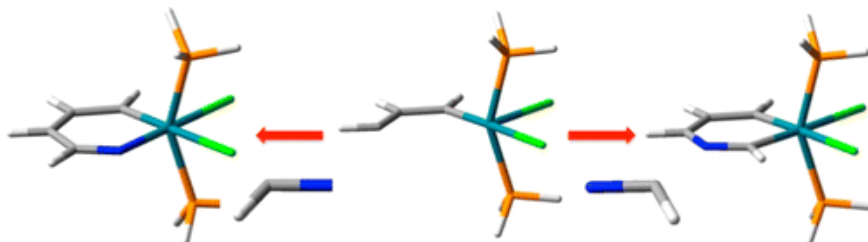
<http://dx.doi.org/10.1021/om400629w>

<http://pubs.acs.org/doi/abs/10.1021/om400629w>

Received: July 1, 2013

Published: August 28, 2013

## Abstract



Density functional theory calculations of the relative stabilities of the ortho, meta, and para  $MClY(XC_4H_4)(PH_3)_2$  heterometallabenzenes ( $M = Rh, Ir; X = N, P; Y = Cl$  and  $M = Ru, Os; X = N, P; Y = CO$ ) have been carried out. The ortho isomer is the most stable for  $X = P$ , irrespective of the metal  $M$ . For  $X = N$  and  $M = Ir, Rh$  the meta is the lowest-lying isomer, whereas for  $M = Ru, Os$  the ortho and meta isomers are almost degenerate. The electronic structure and chemical bonding have been investigated with energy decomposition analyses of the interaction energy between various fragments, to discuss the origin of the differences observed. The values of the multicenter index of aromaticity and nucleus-independent chemical shifts indicate that the heterometallabenzenes studied should be classified as aromatic or slightly aromatic.

## **Chapter 7: Results and Discussion**

---

A general outlook of the work presented in Chapters 3-6 is provided here. The most important results will be briefly summarized and extra information not included in the papers but relevant for purposes of comparison is also added and discussed. This chapter tries to connect the previously proposed objectives and the results obtained.

---



The results obtained previously and presented as separate papers will be now discussed in a more simplified way. First of all, we must mention that the four projects present a common link, which is the analysis of different isomers. For such purpose, we focus on how to justify and understand the isomerization energies encountered. In all cases, these isomerization energies are analyzed by means of an energy decomposition analysis, in order to understand whether the differences come from either repulsive Pauli or attractive electrostatic or orbital interactions. Furthermore, for most of the studied isomers, it has been possible to apply what we refer as the “turn-upside-down approach”. This methodology can be used when two isomers can be constructed from two equivalent fragments, by just modifying the way they connect to each other. For instance, this is what happens for the first project (Chapter 3), in which 1,2-diazacyclobutadiene and 1,3-diazacyclobutadiene can be constructed from the same two fragments, by just applying a turn-upside-down to one of them. And the same happens for pyrazole/imidazole or pyridazine/pyrimidine. Later, the same methodology has been applied to the fourth project (Chapter 6) in order to justify the differences observed in the isomerization energies between ortho-, meta- and para-heterometallabenzenes analyzed.

Even though the methodology applied along the thesis is common, i.e., based on the energy decomposition analysis, the set of systems studied is quite diverse. Thus, from the diaza-substituted compounds in Chapter 3, we move to the halogenated peroxides and disulfides in Chapter 4, or the alkalimetal and group 11 transition metal halide and hydride tetramers in Chapter 5, to finish with the heterometallabenzenes in Chapter 6. For the energy decomposition analysis applied, we have needed the fragments to be either diradical or triradical in most of the cases, which have implied the calculation on open-shell systems, that are always more complicated. Furthermore, in this direction, even though it could be recommended the use of multireference methods, DFT has proven to work properly for such open-shells systems. For instance, it was previously proven the good performance of DFT vs. CASPT2 for the calculation of the singlet-triplet energy gap in the case of para-, meta- and ortho-benzyne.<sup>[419]</sup>

### **7.1 The isomerization energy of 1,2- and 1,3-diazacyclobutadiene, pyrazole and imidazole, and pyridazine and pyrimidine**

1,2-diazabenzene, pyrazole, and 1,2-diazacyclobutadiene with two adjacent nitrogen atoms are less stable than the corresponding 1,3-isomers. Lone-pair repulsion in NN bonds is the habitual explanation for the lower stabilities of the NN isomers. However, lone-pair protonation and diprotonation of pyridazine and pyrimidine barely change its energy difference.<sup>[102]</sup> Therefore, it

seems that lone-pair repulsion cannot be the only cause that explains the higher stability of 1,3-isomers. Although the strength of the N=N  $\pi$ -bond is somewhat lower than that of the C=C and C=N bonds, the difference of about 6 kcal/mol<sup>[102]</sup> is not enough to explain the relative energies of 1,2- and 1,3-diaza and azole compounds either. Therefore, the reason for the lower stability of 1,2-diazabenzene, pyrazole, and 1,2-diazacyclobutadiene in comparison to their 1,3-counterparts is not fully understood yet.

In this work, it was found that the isomerization energies of 1,2- and 1,3-diazacyclobutadiene, pyrazole and imidazole, and pyridazine and pyrimidine are 10.6, 9.4, and 20.9 kcal/mol, respectively, at the BP86/TZ2P level of theory. The BP86/TZ2P and CCSD(T)/aug-ccpVTZ//BP86/TZ2P methods differ by less than half of a kcal/mol. The geometries obtained of the closed-shell singlet ground state of 1,2- and 1,3-diazacyclobutadiene, pyrazole and imidazole, and pyridazine and pyrimidine are depicted in Figure 7.1.

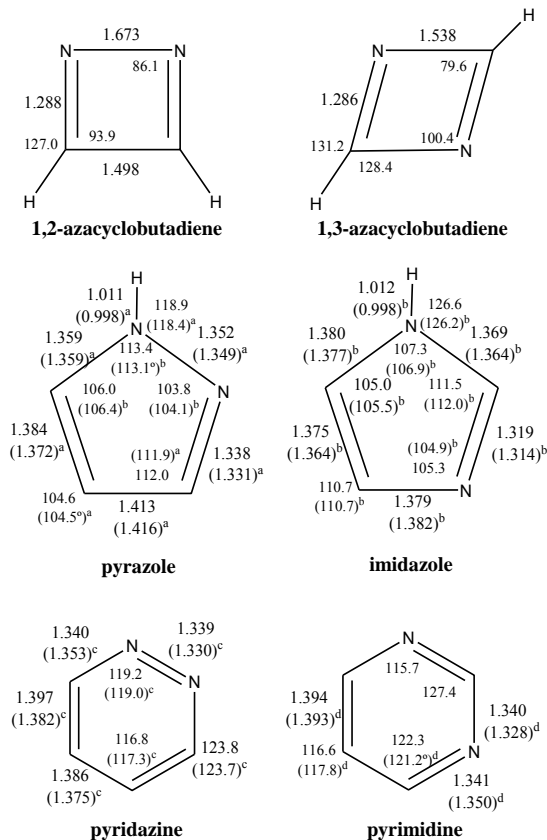


Figure 7.1. Geometries (in Å, deg) of the studied diaza compounds computed at BP86/TZ2P. Experimental values are given in parentheses. Key: (a) from ref. <sup>[486]</sup>; (b) from ref. <sup>[487]</sup>; (c) from ref <sup>[488]</sup>; (d) From ref. <sup>[489]</sup>.

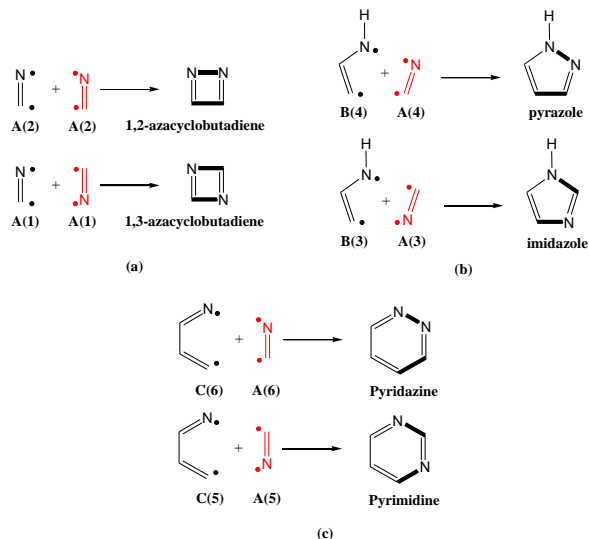
Their molecular structures are very close to the experimental values obtained from microwave spectroscopy. Differences in bond lengths being less than one hundredth of an angstrom and in angles of one tenth of a degree. The molecular structure of 1,2-diazacyclobutadiene indicates that the  $\pi$ -electrons are localized in the C=N bonds. The N–N bond in the 1,2-diazacyclobutadiene is almost broken (1.673 Å). Interestingly, in pyrazole the  $\angle$ HNN angle (118.9°) is smaller than the  $\angle$ HNC angle (126.6°) in imidazole due to the partial intramolecular hydrogen bond (H-bond) interaction between the H atom of the NH group and the lone pair of N in pyrazole. It is worth noting that NN and CN bonds in pyridazine and pyrimidine (diazines isomers) are about 0.05 Å shorter than the CC bonds, despite the fact that the latter are stronger. This has been already discussed in detail by Bickelhaupt et al.<sup>[490]</sup> in the study of the bonding mechanism in the CN dimers, and, basically, it is the consequence of the SOMO orbital on the N fragment involved in the formation of the  $\sigma$  C–N and N–N bonds being more contracted than that on the C fragment. Thus, CN and especially NN bond lengths have to shorten to reach good SOMO–SOMO overlap at the cost of higher Pauli repulsions. All angles are around the expected 120°.

### 7.1.1 Aromaticity Descriptors:

The antiaromaticity of the singlet ground state of 1,2- and 1,3-diazacyclobutadiene is supported by the positive values of the NICS indicator of aromaticity (1,2-diaza-cyclobutadiene: NICS(1) = 11.2 ppm and NICS(1)<sub>zz</sub> = 4.3 ppm; 1,3-diazacyclo-butadiene: NICS(1) = 12.0 ppm and NICS(1)<sub>zz</sub> = 43.1 ppm), the large aromatic fluctuation index (1,2-diazacyclobutadiene: FLU = 0.179; 1,3 diazacyclobutadiene: FLU = 0.148), and the negative value of the electronic delocalization multicenter index (1,2-diazacyclobutadiene: MCI = –0.001; 1,3-diazacyclobutadiene: MCI = –0.013). This situation is similar to that found in cyclobutadiene. Moreover, most of the methods used to estimate the aromaticity of the pyrazole and imidazole rings point out that the two rings have similar aromaticity. Most of these indices indicate that the pyrazole ring is marginally more aromatic than the imidazole one. Only multicenter electronic indices and some resonance energies find imidazole slightly more aromatic than pyrazole. Finally, most aromaticity indices analyzed indicate a similar aromaticity of pyridazine and pyrimidine, although in most of the cases pyridazine with the NN bond is considered slightly more aromatic.

## 7.1.2 Analysis of the isomerization energy of these 1,2- and 1,3-isomers with the so-called turn-upside-down approach

This section is divided into three subsections, each of them devoted to one of the three pairs of cyclic azaisomers analyzed in this work.



Scheme 7.1. The formation of (a) 1,2- and 1,3-diazacyclobutadiene, (b) pyrazole/imidazole, (c) pyridazine/pyrimidine structural isomers from two triplet biradical fragments with the turn-upside-down approach.

### A- 1,2- and 1,3-Diazacyclobutadiene

To comprehend the origin of the higher stability of 1,3-diazacyclobutadiene (1) in comparison with its 1,2-diazacyclobutadiene (2) isomer, we have analyzed the formation of 1 and 2 from two identical azaethendiyl fragments A in their triplet states (Scheme 7.1). Construction of 1 or 2 from A involves the formation of two new  $\sigma$ -electron pairs plus the rearrangement of the  $\pi$ -system that becomes partially delocalized.

The results of the analysis of the bonding for 1,3-diazacyclobutadiene, 1,2-diazacyclobutadiene, and two deformed 1,2-diazacyclobutadiene structures (2a and 2b) gives 1 as the most stable isomer by 10.6 kcal/mol. The higher stability of 1 cannot be ascribed to the deformation energy of the fragments ( $\Delta E_{\text{def}}$ ) that is in fact somewhat more destabilizing for fragment A(1) than A(2). The main difference comes from the interaction energy ( $\Delta E_{\text{int}}$ ) that is 12.5 kcal/mol more stabilizing in 1. The EDA results of these two  $\Delta E_{\text{int}}$  energies show that the difference is not due to Pauli repulsions ( $\Delta E_{\text{Pauli}}$ ) that stabilize 2 with respect to 1 by as much as 81.1 kcal/mol but to a combination of better electrostatic ( $\Delta V_{\text{elstat}}$ ) and orbital interaction ( $\Delta E_{\text{oi}}$ ) components.

Subsequently, higher vicinal NN lone-pair repulsion is compensated by the low Pauli repulsion of the CC bond and, therefore, cannot be used as the only explanation for the lower stability of the 1,2-diazacyclobutadiene isomer. The more stabilizing  $\Delta V_{\text{elstat}}$  term in the 1,3-diazacyclobutadiene form is easily understood by taking into account that in this isomer the dipole moments of the azaethendiyl fragments are better oriented to favor the electrostatic interactions. The  $\Delta E_{\text{oi}}$  can be further decomposed into  $\sigma$  and  $\pi$  components ( $\Delta E_{\sigma}$  and  $\Delta E_{\pi}$ ). Both favor the 1,3-diazacyclobutadiene isomer, although the main contribution (58.6 kcal/mol) comes from the  $\sigma$ -system. The lower  $\pi$ -interaction energy in 1,2-diazacyclobutadiene can be ascribed in part to the larger N–N bond length that makes  $\pi$ -delocalization somewhat less efficient. Thus, what is more remarkable is the large difference in the  $\Delta E_{\sigma}$  component. This is the situation at the optimized geometries of 1 and 2. It may happen, however, that the lower Pauli in 2 is due to the long N–N bond. In this case, the Pauli repulsion due to the NN lone-pair repulsion would have a decisive role in the final geometry and total energy of 1,2-diazacyclobutadiene. To dissect this point we have made an EDA of a deformed 1,2-diazacyclobutadiene (2a) generated from A(1) fragments but with connecting N–N and C–C bond distances equal to the corresponding C–N bond lengths in 1. In this way, 1 and 2a are exactly the same compound but just with an A(1) fragment turned upside down in 2a. Not surprisingly, the energy difference between the two isomers now increases to 28.4 kcal/mol. Interestingly, although the Pauli repulsion increases significantly from 2 to 2a, even in 2a the Pauli repulsion is somewhat smaller (12.0 kcal/mol) than in 1. So, definitely, the higher Pauli repulsion due to NN lone-pair repulsion in NN is compensated by the low Pauli repulsion of the C–C bond and is not the responsible of the lower stability of 1,2-diazacyclobutadiene. Not unexpectedly, the  $\Delta V_{\text{elstat}}$  and  $\Delta E_{\text{oi}}$  terms become more stabilizing in 2a as compared to 2 due to the shorter N–N distance. The change in the  $\Delta E_{\text{oi}}$  term is almost entirely due to the  $\Delta E_{\sigma}$  component,  $\Delta E_{\pi}$  remaining almost unchanged. As a whole, the more favorable  $\Delta V_{\text{elstat}}$  and  $\Delta E_{\text{oi}}$  terms are compensated by a larger Pauli repulsion that makes 2a less stable than 2 as could be anticipated from the fact that the latter corresponds to the optimized geometry of 1,2-diazacyclobutadiene. Finally, we move from 2a to 2b, the latter being a deformed 1,2-diazacyclobutadiene generated from A(1) fragments but with connecting N–N and C–C bond distances equal to the corresponding bond lengths in 2. Unsurprisingly, when going from 2a to 2b there is an important reduction of the Pauli repulsion term due to the longer N–N bond and a reduction of the  $\Delta V_{\text{elstat}}$  and  $\Delta E_{\text{oi}}$  terms, the latter coming almost exclusively from the  $\Delta E_{\sigma}$  component. As a whole, 2b is 4.3 kcal/mol more stable than 2a.

## B- 1,2- and 1,3-Azoles

To get insight into the origin of the higher stability of imidazole (3) in comparison with pyrazole (4), we have analyzed their formation from azaethynyl A and 1-azapropenyl B fragments, both in their triplet states. The fragments A and B that can be obtained from 3 and 4 are slightly different and, therefore, 3 and 4 can be generated using fragments derived from 3, the so-called A(3) and B(3) fragments, or originated from 4 (A(4) + B(4)); see Scheme 7.1).

The deformation energy of the fragments ( $\Delta E_{\text{def}}$ ) is somewhat less destabilizing for fragments A(4) + B(4) than A(3) + B(3), and therefore, this component does not explain the larger stability of 3. The 9.4 kcal/mol of energy difference between 3 and 4 comes mainly from the interaction energy ( $\Delta E_{\text{int}}$ ) that is 10.5 kcal/mol lower in 3. More stabilizing  $\Delta E_{\text{int}}$  energy for 3 is the result of better electrostatic (9.0 kcal/mol) and orbital interaction (29.6 kcal/mol) components. Again, the more stabilizing  $\Delta V_{\text{elstat}}$  term in 3 can be understood by taking into account that in this isomer the dipole moments of the fragments are placed in a better orientation to favor the electrostatic interactions. The absolute value of the energy associated to the  $\Delta V_{\text{elstat}}$  term is higher than in the diazacyclobutadiene isomers since larger fragments usually produce higher Pauli repulsions and electrostatic interactions. In addition, the dipole moment of the 1-azapropenyl fragment is somewhat larger than that of the azaethynyl fragment (1.626 and 2.450 D for A(4) and B(4), respectively). In the decomposition of  $\Delta E_{\text{oi}}$  into  $\sigma$  and  $\pi$  components ( $\Delta E_{\sigma}$  and  $\Delta E_{\pi}$ ),  $\Delta E_{\sigma}$  represents the main contribution (30.3 kcal/mol) to the higher stability of the imidazole isomer and comes from the larger energy release in the formation of two C–N bonds as compared to the constitution of C–C and N–N bonds. Following the same procedure, we have constructed a deformed pyrazole ring (4a) from A(3) + B(3) fragments but with connecting N–N and C–C bond distances equal to the corresponding C–N bond lengths in 3. In this way, 3 and 4a are exactly the same compound but just with an A(3) fragment turned upside down in 4a. As compared to 4, 4a is 9.7 kcal/mol less stable and the difference comes basically from a small increase in the Pauli repulsion that is not compensated by the concomitant increase in electrostatic interactions. The most important conclusion from this analysis is that the Pauli repulsion is more important in imidazole than pyrazole and cannot be used to explain the higher stability of the former. In the last step, we move from 4a to 4b, the latter being a deformed pyrazole ring generated from A(3) + B(3) fragments but with connecting N–N and C–C bond distances equal to the corresponding bond lengths in 4. Somewhat unexpectedly, 4b is slightly

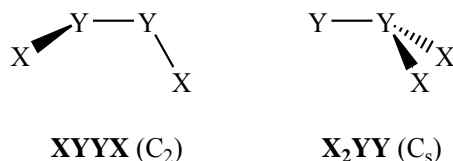
less stable than 4a, and this is due to the larger root-mean-square deviations (rmsd) found for the five angles of 4 in 4b ( $\text{rmsd} = (\sum_{i=1}^5 (\theta_i^{4a/b} - \theta_i^4)^2 / 5)^{1/2} = 7.0^\circ$ ) as compared to 4a ( $\text{rmsd} = 5.9^\circ$ ). Again, the main changes correspond to the Pauli repulsions and electrostatic interactions that come closer to the values in 4 from A(4) + B(4) fragments.

### C- 1,2- and 1,3-Diazines

The reason for the higher stability of pyrimidine can be discussed from the results of the EDA of pyrimidine (5) and pyridazine (6) generated from azaethendiyl A and 1-azabutendiyl C fragments, both in their triplet states. As before, the fragments A and C that can be obtained from 5 and 6 are slightly different and, therefore, 5 and 6 can be generated using fragments derived from 5 (A(5) and C(5)) fragments, or originated from 6 (A(6) + C(6)). The comparison between the EDA of pyrimidine and pyridazine leads to similar conclusions as in the previously studied isomers. First, deformation energy does almost not contribute to the isomerization energy; second, Pauli repulsion favors the isomer with the NN bond because the larger Pauli repulsion in the formation of the N–N bond is compensated by a low Pauli repulsion of the C–C bond; third, electrostatic interactions favor the compound with new formed C–N bonds; and finally, orbital interactions are more stabilizing in the formation of two new  $\sigma$  C–N bonds than in the generation of  $\sigma$  C–C and N–N bonds. Interestingly, the  $\Delta E_\pi$  component in compounds 5 and 6 is the largest among the different isomers analyzed in this study, as expected from the larger aromaticity of these compounds. It is worth noting that the  $\Delta E_\sigma$  component increases gradually from the diazacyclobutadienes to the diazines as a result of increased SOMO overlaps due to better orientations together with the increased polarization in larger fragments. When the deformed pyridazine 6a is formed with frozen A(5) and C(5) fragments but with connecting N–N and C–C bond distances as the corresponding C–N bond lengths in 5, it is found that, as compared to 6, the Pauli repulsion increases but still is lower than that of 5 and the stabilization due to electrostatic interactions and orbital interactions is reduced. Overall, the energy difference between 6a and 5 is 28.3 kcal/mol. It is worth noting that in 6a the  $\Delta E_\pi$  component is slightly more stabilizing than in 5, in line with the fact that most aromaticity descriptors find pyridazine somewhat more aromatic than pyrimidine. Finally, the deformed pyridazine 6b, which is pyridazine with frozen A(5) and C(5) fragments but with connecting N–N and C–C bond distances as the optimized bond lengths in 6, represents an intermediate situation between 6 and 6a.

## 7.2. $X_2Y_2$ Isomers: Tuning Structure and Relative Stability through Electronegativity Differences ( $X = H, Li, Na, F, Cl, Br, I$ ; $Y = O, S, Se, Te$ )

Although all  $X_2Y_2$  systems exist in the  $XYYX$  form ( $C_2$  symmetry; see Scheme 7.2), an isomeric hypervalent structure  $X_2YY$  ( $C_s$  symmetry) is also conceivable.



Scheme 7.2. The two possible  $X_2Y_2$  structural isomers.

Calculations indicate that the conversion of  $X_2SS$  toward  $XSSX$  becomes more exothermic<sup>[491]</sup> and goes with a lower barrier<sup>[492]</sup> when substituents  $X$  become less electronegative. Therefore, it is obvious that the electronegativity of  $X$  has a large impact on the molecular structure of  $XYYX$  species (in particular, the  $Y-Y$  bond length) and its relative stability as compared to the  $X_2YY$  isomer.

In the present study, we have undertaken a detailed investigation of  $XYYX$  and  $X_2YY$  compounds for  $Y = O, S, Se,$  and  $Te$  (with special emphasis to the  $Y = S$  case) and  $X = H, Li, Na, F, Cl, Br,$  and  $I$  using the generalized gradient approximation (GGA) of density functional theory (DFT) at the BP86/QZ4P level. An energy decomposition analysis (EDA) has been carried out considering the process  $YY\bullet\bullet + 2X\bullet \rightarrow X_2YY/XYYX$  that implies three fragments and corresponds to the interaction of  $Y_2$  diradical fragment with the two  $X$  radicals.

Our results will be presented in two blocks, first, the results for the  $XSSX$  and  $X_2SS$  isomers concerning their structure and stability will be presented ( $X = H, Li, Na, F, Cl, Br,$  and  $I$ ). In the second part, the equivalent results for the  $XYYX$  and  $X_2YY$  ( $Y = O, Se,$  and  $Te$ ) isomers will be discussed.

### 7.2.1. $XSSX$ and $X_2SS$ Isomers.

The most relevant geometrical parameters referred to the equilibrium structures of both  $XSSX$  and  $X_2SS$  are contained in Table 7.1.

Table 7.1. Geometrical parameters of XSSX, X<sub>2</sub>SS, XOOX and X<sub>2</sub>OO isomers (bond lengths in Å and angles in degrees)

X	r <sub>Y-Y</sub>	r <sub>X-Y</sub>	∠YYX	∠XYYX	r <sub>Y-Y</sub>	r <sub>X-Y</sub>	∠YYX	∠XYYX
	X <sub>2</sub> SS				XSSX			
F	1.875	1.655	108.2	98.8	1.896	1.676	110.2	88.1
Cl	1.891	2.166	110.2	107.2	1.938	2.115	111.0	87.7
Br	1.896	2.355	110.8	109.5	1.940	2.289	111.6	87.6
I	1.908	2.597	111.9	112.4	1.961	2.497	111.8	86.6
H	1.977	1.383	108.9	94.6	2.071	1.358	98.7	90.8
Li	2.204	2.225	60.3	117.9	2.204	2.225	60.3	117.9
Na	2.230	2.572	64.3	135.7	2.230	2.572	64.3	135.7
	X <sub>2</sub> OO				XOOX			
F	1.175	1.683	110.4	108.9	1.200	1.608	111.2	89.3
Cl	1.208	2.100	114.6	117.0	1.282	1.881	113.9	85.3
Br	1.219	2.245	115.9	119.0	1.283	2.034	115.0	84.2
I	1.235	2.446	118.5	119.3	1.334	2.149	115.2	79.9
H	1.536	0.978	100.6	109.2	1.469	0.975	99.9	112.8
Li	1.585	1.734	62.8	179.7	1.585	1.734	62.8	179.7
Na	1.601	2.092	67.5	179.9	1.601	2.092	67.5	179.0

<sup>a</sup> Calculated r<sub>S-S</sub> for S<sub>2</sub> is 1.912 Å and r<sub>O-O</sub> for O<sub>2</sub> is 1.221 Å.

For X = H, F, Cl, Br, and I, we get the two expected symmetry conformations: C<sub>2</sub> for XSSX and C<sub>s</sub> for X<sub>2</sub>SS. On the other hand, for X = Li and Na, we have a unique isomer, with a rhombic tetrahedron shape. The S–S bond length gets longer with the decrease of the electronegativity of X along the series F < Cl < Br < I < H < Li < Na, being longer in XSSX than in X<sub>2</sub>SS.

Molecular S<sub>2</sub> in its triplet ground state presents a S–S bond length of 1.912 Å at the BP86/QZ4P level of theory, longer than the S–S bond in FSSF (1.896 Å) and in X<sub>2</sub>SS (in the range of 1.875–1.908 Å for X = F, Cl, Br, and I), thus indicating that, in these compounds, the S–S bond has a higher double bond character than in the S<sub>2</sub> molecule. For the series X = H, F, Cl, Br, and I, the X–S bond length increases with the size of X, but in this case, X<sub>2</sub>SS presents longer X–S, except for X = F. The ∠SSX angle opens up slightly for larger X in both XSSX and X<sub>2</sub>SS species. The ∠XSSX dihedral angle in the XSSX isomer is close to 90° in all cases. For all systems, the calculated BP86/QZ4P parameters are close to the experimental ones, with differences for the X–S and S–S bond lengths of only a few hundredths of an Ångstrom or a few degrees for angles.

With respect to the relative energies given in Table 7.2, in all cases except for  $X = \text{F}$ , the isomer  $\text{XSSX}$  is more stable than  $\text{X}_2\text{SS}$ , and the energy difference increases with the electronegativity of  $X$  from  $\text{Cl}$  ( $-9.8 \text{ kcal mol}^{-1}$ ) to  $\text{H}$  ( $-24.0 \text{ kcal mol}^{-1}$ ). For  $X = \text{F}$ , both isomers are almost isoenergetic,  $\text{F}_2\text{SS}$  being only  $0.3 \text{ kcal mol}^{-1}$  more stable than  $\text{FSSF}$ . Most theoretical methods find  $\text{FSSF}$  and  $\text{F}_2\text{SS}$  close in energy, although some of them give  $\text{F}_2\text{SS}$  more stable than  $\text{FSSF}$ , whereas others yield the opposite.<sup>[491,493]</sup>

Table 7.2. Relative energy of the isomerization between  $\text{XSSX}$  and  $\text{X}_2\text{SS}$  (in  $\text{kcal.mol}^{-1}$ )

X	$\Delta E_{\text{rel}}$
F	0.3
Cl	-9.8
Br	-10.3
I	-12.0
H	-24.0
Li	-
Na	-

Now we proceed to analyze the corresponding MOs to get a better comprehension of the corresponding stabilities and structures of both isomers. Figure 7.2 depicts the MO diagram for the  $\text{XYYX}$  system.

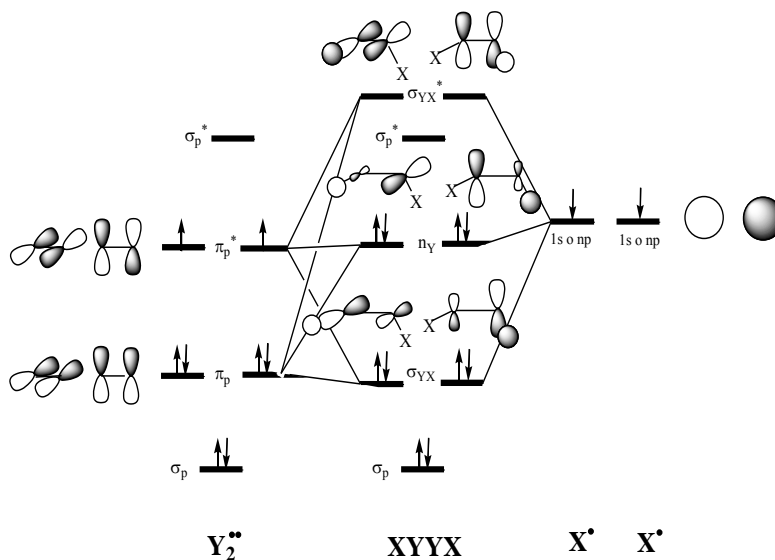


Figure 7.2. Molecular orbital diagram for the interaction of  $\text{Y}_2^{\bullet\bullet}$  with two  $\text{X}^{\bullet}$  to yield isomer  $\text{XYYX}$ .

The diagram of  $Y_2$  is that corresponding to a standard diatomic molecule, with  $\sigma_p$  and  $\sigma_p^*$  orbitals formed by  $np_z$  atomic orbitals of  $Y = S$  (but the same is found for  $Y = O, Se,$  and  $Te$ ), and  $\pi_p$  and  $\pi_p^*$  formed by  $np_x$  and  $np_y$  ones. The  $Y_2^{\bullet\bullet}$  fragment has a triplet state with two unpaired electrons in  $\pi_p^*$  single occupied molecular orbitals (SOMO). The SOMOs of  $X^\bullet$  interact with the  $\pi_p^*$  and  $\pi_p$  orbitals of  $Y_2^{\bullet\bullet}$  and lead to the formation of six orbitals that are doubly degenerated (two bonding  $\sigma_{YX}$ , two antibonding  $\sigma_{YX}^*$ , and two nonbonding  $n_Y$ ) and occupied with eight electrons. This comes down to forming two  $X$ – $Y$  electron-pair bonds involving the two perpendicular  $\pi_p^*$  SOMOs of  $YY$ , which explains the dihedral  $\angle XSSX$  close to  $90^\circ$ . It is obvious that, when  $X^\bullet$  becomes less electronegative,  $\pi_p^*$  orbitals have a more important role in the bonding, explaining the lengthening of the  $S$ – $S$  distance with the decrease of electronegativity. The relatively long  $X$ – $S$  bonds can be ascribed to the destabilizing interactions of the  $X$  groups with the closed shell  $S$ – $S$  bonding  $\pi_p$  orbitals. On the other hand, for the  $X_2YY$  isomer, Figure 7.3 depicts the corresponding MO diagram.

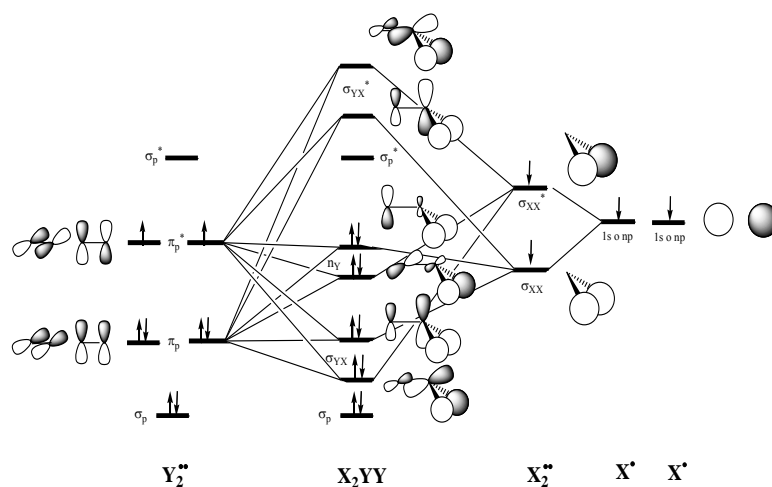


Figure 7.3. Molecular orbital diagram for the interaction of  $Y_2^{\bullet\bullet}$  with two  $X^\bullet$  to yield isomer  $X_2YY$ .

Starting from infinitely separated  $X^\bullet$  fragments, one can approach the two  $X^\bullet$  fragments and generate the positive ( $\sigma_{XX}$ ) and negative ( $\sigma_{XX}^*$ ) combination of the SOMOs of  $X^\bullet$  that interact with the  $\pi_p^*$  and  $\pi_p$  orbitals of  $Y_2^{\bullet\bullet}$  and drive to the formation of six nondegenerate orbitals (two bonding  $\sigma_{YX}$ , two antibonding  $\sigma_{YX}^*$ , and two nonbonding  $n_Y$ ) with eight electrons. The contribution of the  $\pi_p^*$  orbitals in the occupied orbitals is somewhat smaller in this  $X_2SS$  isomer if one takes into account that, for all  $X$ , the  $S$ – $S$  bond is shorter than that in the  $XSSX$  species. The effect of the electronegativity of  $X^\bullet$  on  $S$ – $S$  bonds is the same as that for the  $XSSX$  isomer. The  $X$ – $S$  bond in  $X_2SS$  is longer than that in  $XSSX$  (except for  $X = F$ ), which can be ascribed to

a stronger steric repulsion between X• groups when they bind to the same sulfur atom. Therefore, from the MO diagrams above, we can justify the longer S–S bond lengths in XSSX than in X<sub>2</sub>SS because of the larger participation of the antibonding  $\pi_p^*$  orbitals in the former, especially for the heavier X substituents. It is likely that the fact that  $\pi_p^*$  orbitals participate more in XSSX than in X<sub>2</sub>SS is because X–S can become stronger in XSSX as there is less steric X···X repulsion.

For X = Li and Na, we get the opposite case to X = F. Now 2s and 3s orbitals for Li and Na, respectively, are really high in energy; thus the corresponding electrons go to the  $\pi_p^*$  orbital of S–S, which causes the long S–S bond lengths and a system that can be simplified as an ionic X<sup>+</sup>S<sub>2</sub><sup>2-</sup>X<sup>+</sup>. The charge on X• (X = halogen) is more negative for X<sub>2</sub>SS than XSSX with the exception of X = F. The geometry of these X<sup>+</sup>S<sub>2</sub><sup>2-</sup>X<sup>+</sup> (X = Li and Na) does not correspond to the usual C<sub>2</sub> or C<sub>s</sub> isomers, but to a rhombic tetrahedral structure.

With the aim of a better comprehension of the nature of the X–S bond in both isomers, an energy decomposition analysis has been carried out (see Table 7.3). As mentioned above, we have considered the process SS•• + 2X• → X<sub>2</sub>S<sub>2</sub>/XSSX.

Table 7.3. Energy decomposition analysis for XSSX and X<sub>2</sub>SS isomers (in kcal.mol<sup>-1</sup>), together with the average population of the two SOMO orbitals of SS (in electrons), and energy of the SOMO orbital for X (in eV).

isomer	$\Delta E_{\text{Pauli}}$	$\Delta V_{\text{elstat}}$	$\Delta E_{\text{oi}}$	$\Delta E_{\text{int}}$	$\Delta E_{\text{prep}}$	$\Delta E$	P( $\pi^*(\text{SS})$ )	E(X <sub>SOMO</sub> )
FSSF	570.96	-233.96	-509.62	-172.63	0.09	-172.54	0.71	-11.217
F <sub>2</sub> SS	620.04	-253.10	-540.26	-173.32	0.46	-172.86	0.69	-11.217
ClSSCl	406.44	-182.83	-330.66	-107.04	0.21	-106.83	0.96	-8.701
Cl <sub>2</sub> SS	350.63	-159.37	-288.49	-97.22	0.15	-97.07	0.88	-8.701
BrSSBr	336.83	-160.04	-265.41	-88.62	0.26	-88.36	1.00	-7.996
Br <sub>2</sub> SS	278.86	-133.88	-223.12	-78.14	0.08	-78.06	0.91	-7.996
ISSI	297.29	-145.91	-223.80	-72.42	0.74	-71.68	1.14	-7.248
I <sub>2</sub> SS	225.45	-111.73	-173.41	-59.69	0.00	-59.69	1.00	-7.248
HSSH	326.64	-150.82	-318.34	-142.53	6.41	-136.12	1.39	-6.626
H <sub>2</sub> SS	301.89	-144.16	-271.07	-113.34	1.26	-112.08	1.27	-6.626
LiSSLi/Li <sub>2</sub> SS	241.68	-155.38	-228.99	-142.69	17.82	-124.87	1.82	-2.955
NaSSNa/Na <sub>2</sub> SS	165.89	-109.61	-161.50	-105.23	20.35	-84.88	1.88	-2.841

Results in Table 7.3 show that the  $\Delta E_{\text{prep}}$  term is, in all cases, very small except for X = Li and Na. In these latter cases, the S–S bond length in the disulfide is large for the reasons explained above and  $\Delta E_{\text{prep}}$  is about 20 kcal.mol<sup>-1</sup>. With the exception of X = F, the interaction energy and the bonding energy are more stabilizing for the isomers XSSX than X<sub>2</sub>SS, and the difference increases when the electronegativity of X decreases. Along X = F to I, the X–S bond becomes

less polar and thus less stable for both  $X_2SS$  and  $XSSX$ . However, in the former, the X–S bond weakens more quickly because it is also more and more hampered by the increasingly bulky X. Thus, while for  $X = F$ , the isomers are within some  $1 \text{ kcal.mol}^{-1}$  of equal energy, the gap between  $X_2SS$  above  $XSSX$  increases as X becomes more electronegative. A seemingly irregular behavior is observed for  $X = H$ , in which case  $H_2SS$  is significantly higher in energy than  $HSSH$ . In this case, we deal with the consequence of the very short hydrogen–element (here: H–S) bond distance, which, in turn, translates in a short, destabilizing H–H contact in the  $H_2SS$  isomer. Because of the shorter X–S bond length, isomers  $XSSX$  present larger values (in absolute value) of  $\Delta V_{\text{elstat}}$ ,  $\Delta E_{\text{Pauli}}$ , and  $\Delta E_{\text{oi}}$  than  $X_2SS$ , with the exception of  $X = F$ . Longer X–S distances cause smaller Pauli repulsion, as well as smaller electrostatic and orbital interactions (in absolute value). If we now compare the attractive terms  $\Delta V_{\text{elstat}}$  and  $\Delta E_{\text{oi}}$  for  $XSSX$  and  $X_2SS$  isomers, we see that  $\Delta\Delta V_{\text{elstat}}$  and  $\Delta\Delta E_{\text{oi}}$  differences between  $XSSX$  and  $X_2SS$  isomers favor the  $XSSX$ , except for  $X = F$ .

In this latter case, the enhanced charge transfer and polarization promoted by the higher electronegativity of F increases the contribution of double ionic resonance structure b that is more stabilizing in  $F_2SS$  than  $FSSF$  (see Figure 7.4). As a consequence, the two isomers become almost isoenergetic.

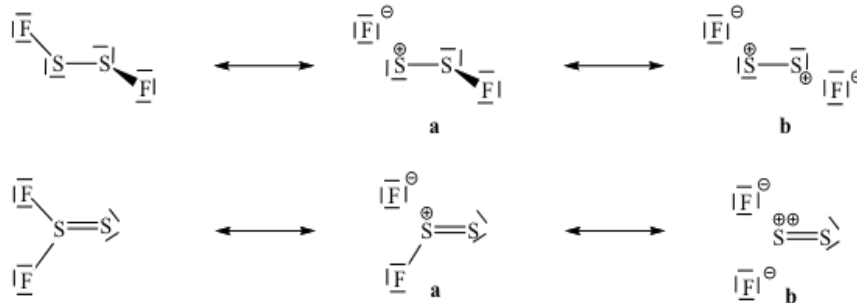


Figure 7.4. Some resonance structures for  $FSSF$  and  $F_2SS$  isomers.

### 7.2.2. $XYXX$ and $X_2YY$ Isomers ( $Y = O, Se, \text{ and } Te$ ).

The most relevant geometrical parameters referred to the equilibrium structures of both  $XOOX$  and  $X_2OO$  are presented in Table 7.1. The O–O bond length gets longer with the decrease of the electronegativity of X along the series  $F < Cl < Br < I < H < Li < Na$ . As for the  $X_2S_2$  isomers, this O–O bond distance is longer in  $XOOX$  than in  $X_2OO$  with the exception of  $X = H$ . Molecular  $O_2$  in its triplet ground state presents a O–O bond length of  $1.221 \text{ \AA}$  at the BP86/QZ4P level of theory, longer than the O–O bond in  $FOOF$  and in  $X_2OO$  ( $X = F, Cl, \text{ and } Br$ ). The double bond character of the  $O_2$  molecule is clearly, however, kept in  $X_2O_2$  for the more

electronegative X substituents. On the other hand, for the more electropositive X groups, the charge transfer from the SOMO of  $X\cdot$  to the  $\pi_p^*$  orbitals is favored by the stabilization of these  $\pi_p^*$  orbitals in  $O_2$ . This effect is clearly seen in the long O–O bond present in both HOOH and  $H_2OO$  species, not far from the bond distance in LiOOLi and NaOONa that corresponds to a single O–O bond. As found for the  $X_2S_2$  isomers, the O–X bond in  $X_2OO$  is longer than that in XOOX, now even for the case of  $X = F$ . The  $\angle OOX$  angle opens up for larger X in both XOOX and  $X_2OO$  species. The  $\angle XOOX$  dihedral angle in the XOOX isomer is close to  $90^\circ$  in all cases and somewhat decreases for larger X. This dihedral angle becomes close to  $180^\circ$  for  $X = Li$  and Na. In these two cases, we get again a unique conformation, but now with a rhombic planar shape.

With respect to the relative energies, in all cases the isomer XOOX is more stable than  $X_2OO$ , and the energy difference increases with the decrease in the electronegativity of X from F ( $-12.0 \text{ kcal.mol}^{-1}$ ) to H ( $-46.9 \text{ kcal.mol}^{-1}$ ). The energy differences in the  $X_2O_2$  isomers are in absolute value larger than those corresponding to the  $X_2S_2$  isomers. The smaller electronegativity difference between F and O makes the contribution of double ionic resonance structure less decisive for the relative energy of the FOOF and  $F_2OO$  isomers.

The higher electronegativity of the  $O_2\bullet\bullet$  group, which is translated into lower  $\pi_p^*$  orbitals, reduces the transfer of charge from the  $O_2\bullet\bullet$  fragment to  $2X\cdot$  for  $X = \text{halogen}$  when compared to the analogous  $X_2S_2$  species. The results of the energy decomposition analysis carried out for these isomers do not differ significantly from the analysis given for  $X_2S_2$  isomers, except in the following two aspects: first, the large deformation energy of HOOH and  $H_2OO$  isomers that is due to the long O–O bond length found in these systems, as discussed above, and second, the fact that the attractive  $\Delta V_{\text{elstat}}$  and  $\Delta E_{\text{oi}}$  terms are in absolute value larger for FOOF than  $F_2OO$ . This translates into a more stable FOOF than  $F_2OO$ , at variance to what is observed for the FSSF species. As said before, for X more electronegative than Y, the larger the electronegativity difference, the more stable the  $X_2YY$  system is. In FOOF, the electronegativity difference is not enough to make  $F_2OO$  more stable than FOOF.

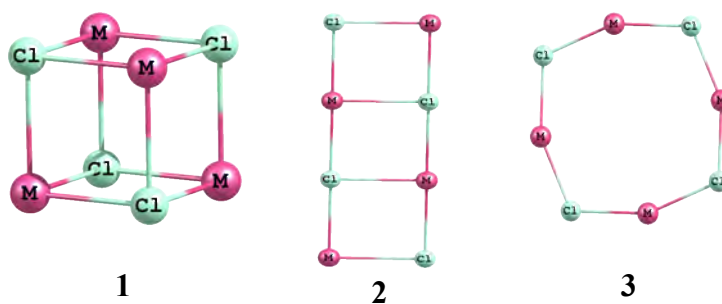
If we would like to find  $X_2Y_2$  species with the  $X_2YY$  isomer more stable than the XYYX form, we should try less electronegative chalcogen atoms. According to both Pauling<sup>[47]</sup> and Allen<sup>[494]</sup> electronegativity scales,  $\chi(S) \geq \chi(\text{Se}) > \chi(\text{Te})$ . For this reason, we analyze the  $X_2\text{Se}_2$  and  $X_2\text{Te}_2$  isomers. The results show that the trends in Y–Y and X–Y bond distances are the same as those found for  $X_2S_2$  and  $X_2O_2$ . Thus, with no exception, Y–Y distances are longer in XYYX systems

and Y–X bond lengths are shorter in XYYX species, FYYF being the only exception to the Y–X bond distance. However, for Y = Se and Te, the F–Y bonds lengths in FYYF and F<sub>2</sub>YY species differ by only a few hundredths or even a few thousandths of an Ångstrom.

Relative energies between the C<sub>2</sub> and C<sub>s</sub> isomers for X<sub>2</sub>S<sub>2</sub> and X<sub>2</sub>Se<sub>2</sub> for each X differ by less than 1 kcal.mol<sup>-1</sup>. This is not completely unexpected since the two atoms have almost the same electronegativity. However, in this case, the FSeSeF isomer is marginally more stable than the F<sub>2</sub>SeSe form. On the other hand, and because of the lower electronegativity, X<sub>2</sub>Te<sub>2</sub> presents the lowest energy differences between forms XTeTeX and X<sub>2</sub>TeTe. Interestingly, F<sub>2</sub>TeTe is found about 2 kcal.mol<sup>-1</sup> more stable than FTeTeF. We can conclude that, for X<sub>2</sub>Y<sub>2</sub> (Y = O, S, Se, and Te), the XYYX isomer is more stable than X<sub>2</sub>YY except for difluorides of S, Se, and Te, for which the X<sub>2</sub>YY system can coexist with the XYYX isomer. Since the electronegativities of Te and Po are quite similar,<sup>[47,494]</sup> we expect similar trends for X<sub>2</sub>Po<sub>2</sub> as those observed for X<sub>2</sub>Te<sub>2</sub>.

### 7.3 A Comparison between Alkalimetal and Group 11 Transition Metal Halide and Hydride Tetramers: Molecular Structure and Bonding

Metallic clusters can exist in several isomeric forms that may be in the thermal equilibrium with each other. The tetramer (XM)<sub>4</sub> (X = F, Cl, Br, I, and M = Li, Na, K, Rb), for example, occurs among others as a cube (**1**, T<sub>d</sub> symmetry), ladder (**2**), and ring (**3**, D<sub>4h</sub> symmetry).



Scheme 7.3. isomeric forms (T<sub>d</sub>, Ladder, and D<sub>4h</sub>) of the tetramer (XM)<sub>4</sub> clusters

(MX)<sub>4</sub> clusters of alkalimetals (M = Li, Na, K, Rb) tend to adopt a cubic T<sub>d</sub> conformation as the most stable, whereas group 11 transition state metals (M = Cu, Ag, Au) tend to prefer a ring D<sub>4h</sub> one. It must be mentioned that both groups of metal atoms present the ns<sup>1</sup> valence electronic configuration, with K: [Ar]4s<sup>1</sup> and Cu: [Ar]3d<sup>10</sup>4s<sup>1</sup>, for instance. However, these compounds with a similar valence configuration adopt quite different structures. Therefore, the comprehension of the reasons for such difference observed represents a challenge and was for us

the objective of this work. In the present work, we have undertaken a detailed investigation of alkalimetal ( $M = \text{Li, Na, K, and Rb}$ ) and group 11 transition metal ( $M = \text{Cu, Ag, and Au}$ )  $(\text{MX})_4$  tetramers with  $X = \text{H, F, Cl, Br, and I}$ , using a density functional theory method at the BP86/QZ4P level.

### 7.3.1 Alkalimetal halide and hydride tetramers $(\text{MX})_4$ ( $M = \text{Li, Na, K, and Rb}$ ; $X = \text{H, F, Cl, Br, and I}$ )

In all cases, the  $T_d$  geometry is more stable than the  $D_{4h}$ , with isomerization energies ( $\Delta E_{\text{iso}}$ ) values ranging from  $-2.6$  ( $\text{Na}_4\text{H}_4$ ) to  $-20.5$  ( $\text{Rb}_4\text{Cl}_4$ )  $\text{kcal}\cdot\text{mol}^{-1}$ . These  $\Delta E_{\text{iso}}$  increase when going from Li to Rb with the exception of  $\text{Na}_4\text{H}_4$  and also increase from F to Cl and then remains more or less constant for Br and I. In general, the  $M\text{-X}$  bond distances in the diatomic alkalimetal monomers increase for the same M with the increase of the atomic radii of X from F to Cl to Br and to I ( $X = \text{H}$  is an exception) and also for the same X when moving from Li to Rb.

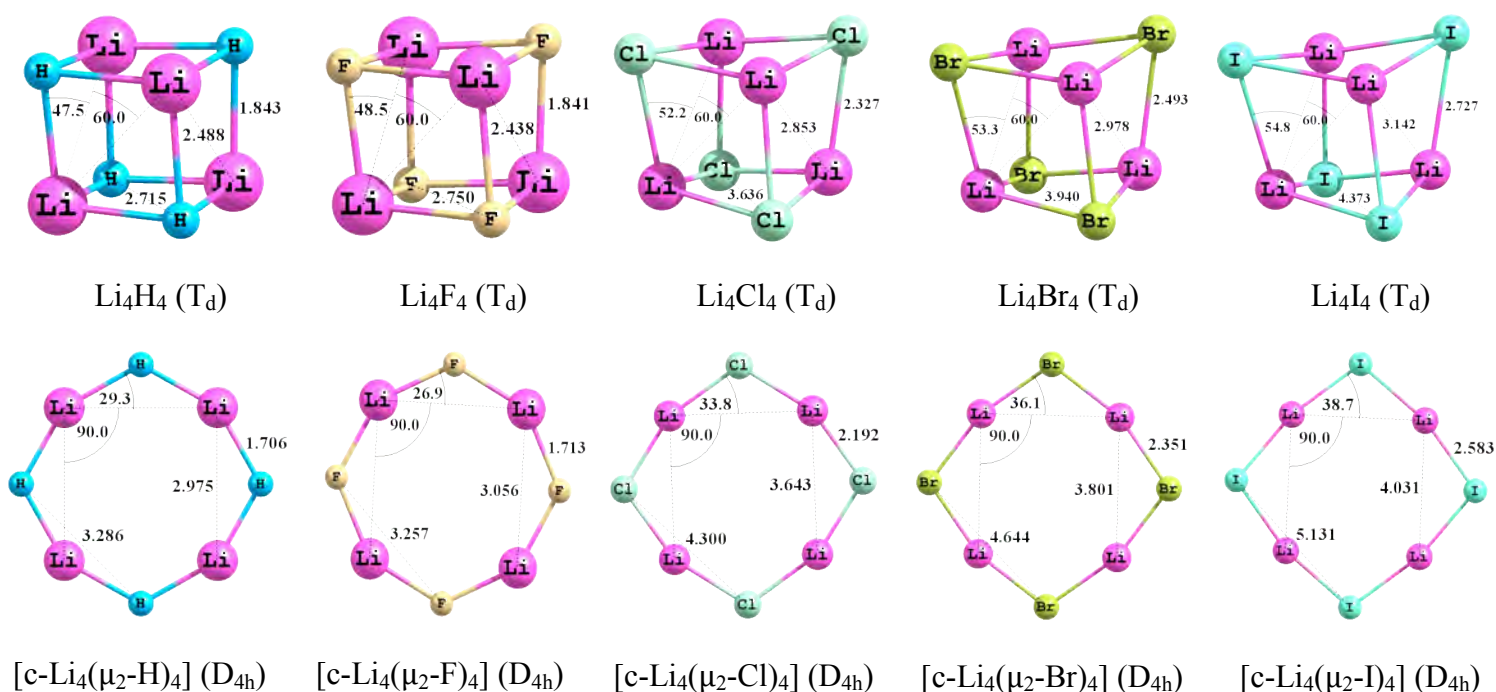


Figure 7.5. Structure of alkalimetal tetramers  $\text{M}_4\text{X}_4$  with  $X = \text{H, F, Cl, Br, I}$  and  $M = \text{Li}$  in both  $T_d$  and  $D_{4h}$  symmetries.

The computed BP86/QZ4P bond lengths are illustrated in Figure 7.5 for  $M = \text{Li}$ . Our results perfectly agree with earlier theoretical works,<sup>[495-497]</sup> as well as with experimental values (see the

supporting information in Chapter 5). Compared to the M–X monomer, tetramerization causes the M–X bond to expand approximately by 0.24 – 0.32 Å at  $T_d$  geometry, whereas at  $D_{4h}$  geometry the bond expands by 0.10 – 0.17 Å along X = H, F, Cl, Br, and I.

In order to identify the factors responsible for the higher stability of  $T_d$  geometries for such metal tetramers, we have undertaken an energy decomposition analysis (EDA). In particular, we have analyzed the stability of the alkalimetal halide and hydride tetramers from their bonding energy ( $\Delta E$ ) corresponding to the formation of  $T_d$  and  $D_{4h}$   $M_4X_4$  isomers from four MX monomers.

As we can see from the EDA result in Table 7.4, the  $T_d$  isomers are more stable than  $D_{4h}$  ones for all alkalimetal halide and hydride tetramers.  $\Delta E$  for the  $T_d$  isomers ranges from –94.3 ( $Rb_4H_4$ ) to –161.4 kcal·mol<sup>-1</sup> ( $Li_4F_4$ ). Among the different  $T_d$  isomers the most important stabilizing contribution corresponds to the electrostatic component ( $\Delta V_{elstat}$ ) that is more negative for species having monomer with larger dipole moments and short monomer-monomer distances. This is particularly the case of  $Li_4F_4$  that has the most stabilizing electrostatic term. Because the M–M and X–X distances in the  $T_d$  isomers are shorter, these structures have larger destabilizing Pauli repulsions ( $\Delta E_{Pauli}$ ) and deformation energies ( $\Delta E_{def}$ ), but also they have more stabilizing orbital interaction ( $\Delta E_{oi}$ ) contribution.

When compared to the  $D_{4h}$  isomer, the larger stabilization due to the  $\Delta V_{elstat}$  and  $\Delta E_{oi}$  terms in  $T_d$  is not compensated by the larger  $\Delta E_{Pauli}$  and  $\Delta E_{def}$  components, and the  $T_d$  form is the most stable. In many cases but not always the  $\Delta E_{oi} + \Delta E_{def}$  sum favors the  $D_{4h}$  isomer and because the Pauli repulsions always destabilize the  $T_d$  as compared the  $D_{4h}$  form, the decisive term is the electrostatic interaction that is much more stronger in the  $T_d$  structure.

Table 7.4. Energy decomposition analysis (in kcal.mol<sup>-1</sup>) of the tetramerization of M<sub>4</sub>X<sub>4</sub> systems with M = Li, Na, K and Rb.<sup>a</sup>

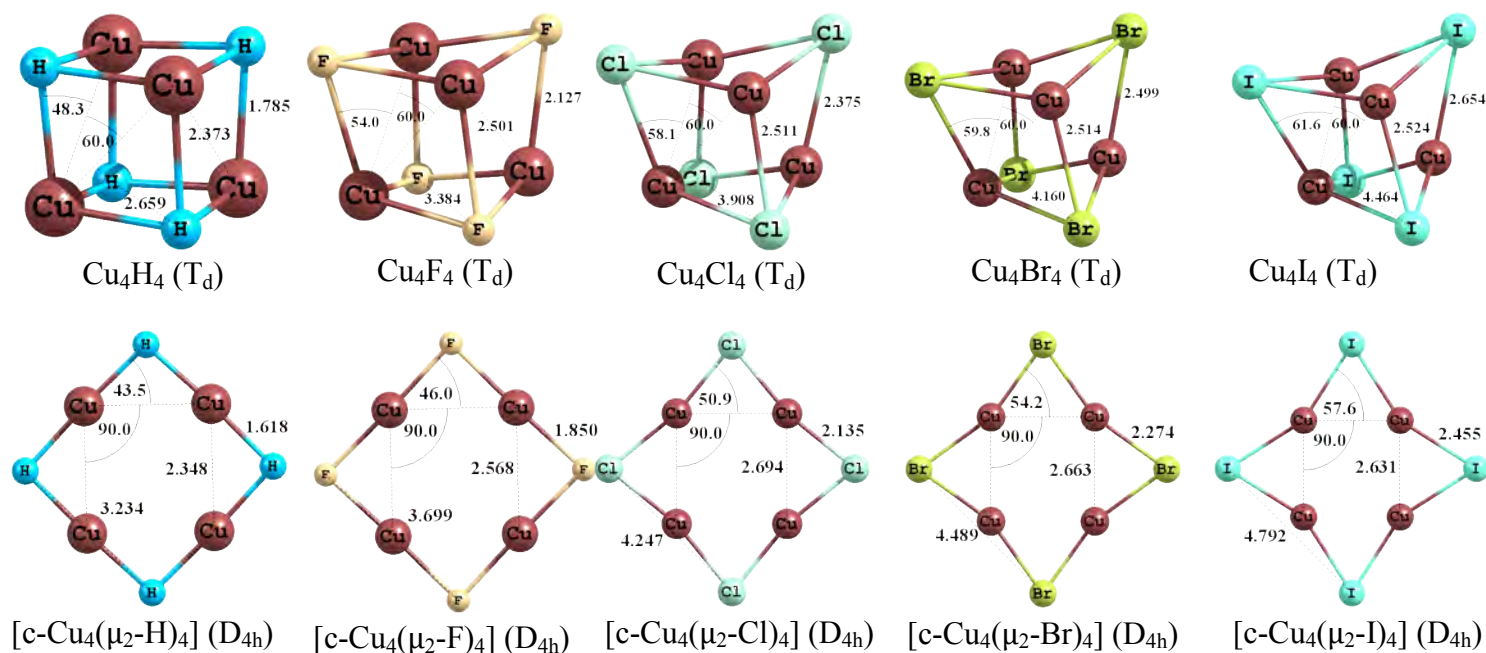
	Li <sub>4</sub> H <sub>4</sub>		Na <sub>4</sub> H <sub>4</sub>		K <sub>4</sub> H <sub>4</sub>		Rb <sub>4</sub> H <sub>4</sub>	
	T <sub>d</sub>	D <sub>4h</sub>	T <sub>d</sub>	D <sub>4h</sub>	T <sub>d</sub>	D <sub>4h</sub>	T <sub>d</sub>	D <sub>4h</sub>
ΔE <sub>Pauli</sub>	160.87	64.26	146.30	63.62	143.94	70.29	150.67	74.28
ΔE <sub>elstat</sub>	-227.33	-141.73	-192.83	-121.64	-202.22	-121.61	-201.82	-117.19
ΔE <sub>oi</sub>	-86.61	-56.14	-74.60	-48.23	-56.46	-43.09	-57.30	-43.80
ΔE <sub>int</sub>	-153.06	-133.61	-121.13	-106.25	-114.74	-94.40	-108.46	-86.71
ΔE <sub>def</sub>	12.40	2.64	16.56	4.32	14.28	5.32	14.16	5.84
ΔE	-140.66	-130.97	-104.57	-101.93	-100.46	-89.08	-94.30	-80.87
	Li <sub>4</sub> F <sub>4</sub>		Na <sub>4</sub> F <sub>4</sub>		K <sub>4</sub> F <sub>4</sub>		Rb <sub>4</sub> F <sub>4</sub>	
	T <sub>d</sub>	D <sub>4h</sub>	T <sub>d</sub>	D <sub>4h</sub>	T <sub>d</sub>	D <sub>4h</sub>	T <sub>d</sub>	D <sub>4h</sub>
ΔE <sub>Pauli</sub>	157.31	78.68	120.77	67.26	133.88	82.49	134.54	87.29
ΔE <sub>elstat</sub>	-279.09	-186.93	-258.31	-180.70	-236.02	-158.50	-224.85	-150.50
ΔE <sub>oi</sub>	-70.60	-56.21	-38.52	-34.68	-51.48	-45.55	-55.33	-49.45
ΔE <sub>int</sub>	-192.37	-164.46	-176.06	-148.12	-153.61	-121.55	-145.64	-112.66
ΔE <sub>def</sub>	31.00	10.08	18.36	5.88	25.60	12.56	27.24	13.92
ΔE	-161.37	-154.38	-157.70	-142.24	-128.01	-108.99	-118.40	-98.74
	Li <sub>4</sub> Cl <sub>4</sub>		Na <sub>4</sub> Cl <sub>4</sub>		K <sub>4</sub> Cl <sub>4</sub>		Rb <sub>4</sub> Cl <sub>4</sub>	
	T <sub>d</sub>	D <sub>4h</sub>	T <sub>d</sub>	D <sub>4h</sub>	T <sub>d</sub>	D <sub>4h</sub>	T <sub>d</sub>	D <sub>4h</sub>
ΔE <sub>Pauli</sub>	124.57	53.22	96.97	51.62	100.22	59.70	102.30	62.25
ΔE <sub>elstat</sub>	-200.83	-117.30	-195.43	-127.12	-186.96	-122.54	-182.66	-118.62
ΔE <sub>oi</sub>	-78.76	-61.41	-45.35	-40.46	-43.86	-38.82	-44.48	-39.25
ΔE <sub>int</sub>	-155.02	-125.49	-143.81	-115.96	-130.59	-101.67	-124.83	-95.63
ΔE <sub>def</sub>	23.16	7.96	16.48	5.60	16.76	7.72	17.04	8.36
ΔE	-131.86	-117.53	-127.33	-110.36	-113.83	-93.95	-107.79	-87.27
	Li <sub>4</sub> Br <sub>4</sub>		Na <sub>4</sub> Br <sub>4</sub>		K <sub>4</sub> Br <sub>4</sub>		Rb <sub>4</sub> Br <sub>4</sub>	
	T <sub>d</sub>	D <sub>4h</sub>	T <sub>d</sub>	D <sub>4h</sub>	T <sub>d</sub>	D <sub>4h</sub>	T <sub>d</sub>	D <sub>4h</sub>
ΔE <sub>Pauli</sub>	120.46	47.77	94.23	48.24	94.11	55.08	96.18	57.75
ΔE <sub>elstat</sub>	-183.48	-100.85	-179.12	-112.21	-173.31	-111.56	-170.08	-109.08
ΔE <sub>oi</sub>	-82.33	-62.76	-49.51	-42.86	-44.29	-38.76	-44.39	-38.63
ΔE <sub>int</sub>	-145.36	-115.85	-134.40	-106.82	-123.49	-95.23	-118.29	-89.94
ΔE <sub>def</sub>	21.48	7.36	15.88	5.40	15.24	6.80	15.24	7.28
ΔE	-123.88	-108.49	-118.52	-101.42	-108.25	-88.43	-103.05	-82.66
	Li <sub>4</sub> I <sub>4</sub>		Na <sub>4</sub> I <sub>4</sub>		K <sub>4</sub> I <sub>4</sub>		Rb <sub>4</sub> I <sub>4</sub>	
	T <sub>d</sub>	D <sub>4h</sub>	T <sub>d</sub>	D <sub>4h</sub>	T <sub>d</sub>	D <sub>4h</sub>	T <sub>d</sub>	D <sub>4h</sub>
ΔE <sub>Pauli</sub>	116.01	42.05	90.07	44.46	85.80	49.94	87.41	52.65
ΔE <sub>elstat</sub>	-161.69	-83.23	-157.66	-95.58	-155.20	-99.05	-153.23	-98.15
ΔE <sub>oi</sub>	-87.99	-64.25	-55.46	-45.54	-45.30	-38.58	-44.56	-37.78
ΔE <sub>int</sub>	-133.68	-105.44	-123.06	-96.65	-114.70	-87.70	-110.38	-83.28
ΔE <sub>def</sub>	19.12	6.72	15.12	5.32	13.60	6.08	13.52	6.40
ΔE	-114.56	-98.72	-107.94	-91.33	-101.10	-81.62	-96.86	-76.88

<sup>a</sup> ΔE = E(M<sub>4</sub>X<sub>4</sub>)-4E(MX).

### 7.3.2 Group 11 Transition metal tetramers (M = Cu, Ag, and Au; X = H, F, Cl, Br, and I)

In contrast to what is found for the alkali metal halide and hydride tetramers, it is observed how the  $D_{4h}$  or  $D_{2d}$  conformations are more stable than the  $T_d$  one. Another difference is that now that  $D_{2d}$  structures are present for all metal chlorides, bromides, and iodides. In fact, in these cases the structure with  $D_{2d}$  symmetry is lower in energy than the  $D_{4h}$  one, with a maximum difference of  $4.8 \text{ kcal mol}^{-1}$ .

For  $M = \text{Au}$ , the  $T_d$  conformation is not a minimum and the optimization process leads to a distorted cube of  $C_{3v}$  symmetry. The same happens for  $\text{Cu}_4\text{F}_4$  (see Figure 7.6) and  $\text{Ag}_4\text{H}_4$ . For this set of systems, the  $\Delta E_{\text{iso}}(T_d-D_{4h})$  values decrease ( $D_{4h}$  less favorable as compared to  $T_d$ ) when going down the halogen group (from F to I), as already observed with the alkali metal halide and hydride tetramers. The results for metal fluorides and chlorides obtained by Rabilloud et al.<sup>[498]</sup> agree with our results. The authors found that on  $(\text{MX})_4$  clusters ( $M = \text{Cu, Ag, Au; X} = \text{F, Cl, Br, I}$ ), all group 11 metal(I) halides adopt ring  $D_{4h}$  or out-of-plane distorted butterfly shape  $D_{2d}$  structures at the B3LYP level of theory, except for  $\text{Au}_4\text{Cl}_4$ , for which they found that the planar  $D_{4h}$  ring is more stable than the puckered  $D_{2d}$  form.



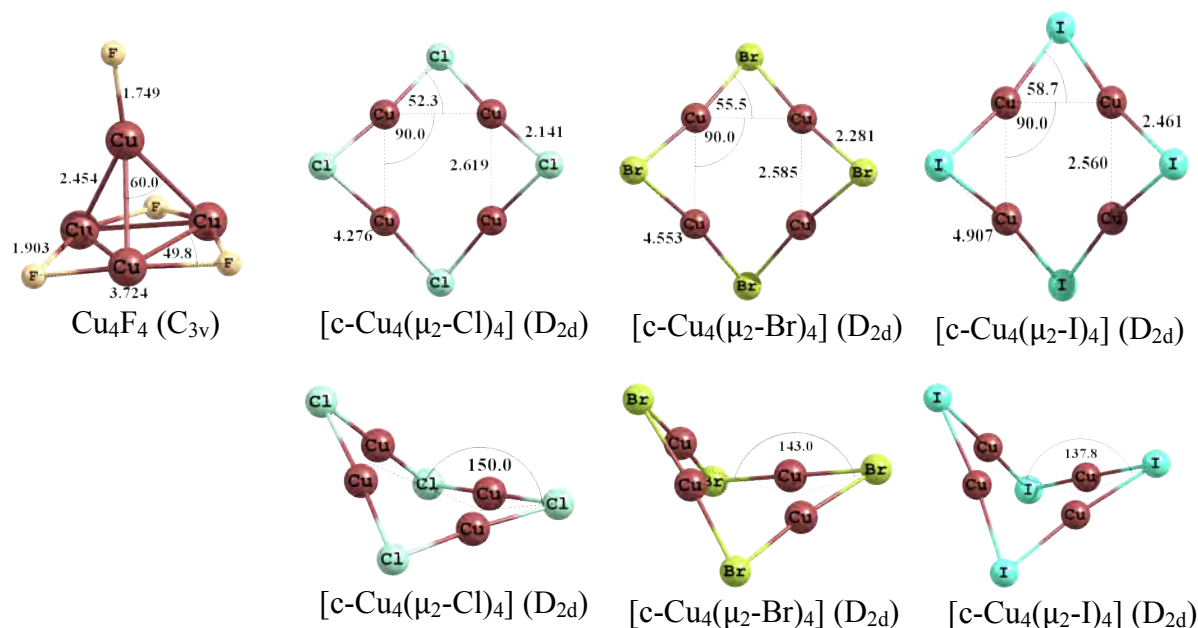


Figure 7.6. Structure of group 11 transition metal tetramers  $M_4X_4$  with  $X = H, F, Cl, Br,$  and  $I$  and  $M = Cu$ .

As can be seen all halide-bridged  $[c-Cu_4(\mu_2-X)_4]$  complexes with  $X = H$  and  $F$  contain a perfect square-planar  $Cu_4$  ring core structure, whereas for  $X = Cl, Br, I$  clusters, a “diamond-like” rhombic  $Cu_4$  ring structure of  $D_{2d}$  symmetry is preferred. The  $\angle MMMX$  dihedral angles are  $30.0^\circ, 37.0^\circ, 42.2^\circ$  for the chloro-, bromo-, and iodo-bridged copper clusters. As for alkali metal hydrides and halides,  $M-X$  bond distances are longer in the  $T_d$  cubic arrangement than in the  $D_{4h}$  planar structure.

The energy decomposition analysis of the tetramerization energy, shown in Table 7.5, is applied to understand the preference of the  $D_{4h}$  (or  $D_{2d}$ ) conformation over the  $T_d$  one with the group 11 metals. With the aim to have comparable EDA analyses, we have focused on the  $T_d$  conformation instead of the  $C_{3v}$ , even in those cases in which the former is not a minimum.

Table 7.5. Energy decomposition analysis (in kcal·mol<sup>-1</sup>) of the tetramerization of M<sub>4</sub>X<sub>4</sub> systems with M = Cu, Ag, and Au.<sup>a</sup>

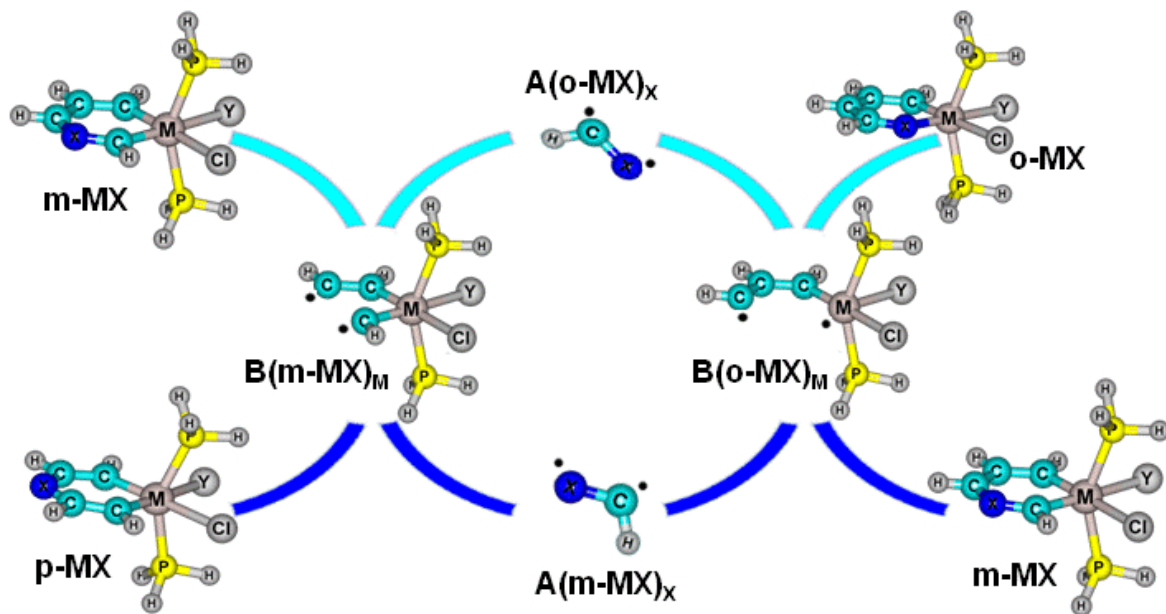
	Cu <sub>4</sub> H <sub>4</sub>			Ag <sub>4</sub> H <sub>4</sub>			Au <sub>4</sub> H <sub>4</sub>		
	T <sub>d</sub>	D <sub>4h</sub>	D <sub>2d</sub>	T <sub>d</sub>	D <sub>4h</sub>	D <sub>2d</sub>	T <sub>d</sub>	D <sub>4h</sub>	D <sub>2d</sub>
ΔE <sub>Pauli</sub>	786.95	341.49	-	642.07	331.28	-	738.74	454.84	-
ΔE <sub>elstat</sub>	-544.48	-318.22	-	-463.43	-309.99	-	-433.08	-359.10	-
ΔE <sub>oi</sub>	-397.31	-194.46	-	-291.33	-161.60	-	-386.81	-232.37	-
ΔE <sub>int</sub>	-154.83	-171.19	-	-112.69	-140.31	-	-81.16	-136.62	-
ΔE <sub>def</sub>	46.20	14.48	-	47.92	12.99	-	67.33	37.45	-
ΔE	-108.63	-156.71	-	-64.77	-127.32	-	-13.83	-99.17	-
	Cu <sub>4</sub> F <sub>4</sub>			Ag <sub>4</sub> F <sub>4</sub>			Au <sub>4</sub> F <sub>4</sub>		
	T <sub>d</sub>	D <sub>4h</sub>	D <sub>2d</sub>	T <sub>d</sub>	D <sub>4h</sub>	D <sub>2d</sub>	T <sub>d</sub>	D <sub>4h</sub>	D <sub>2d</sub>
ΔE <sub>Pauli</sub>	419.81	238.51	-	254.16	219.13	-	378.48	296.71	-
ΔE <sub>elstat</sub>	-380.06	-264.23	-	-265.88	-226.00	-	-303.08	-263.78	-
ΔE <sub>oi</sub>	-205.92	-163.60	-	-130.54	-132.52	-	-207.11	-188.87	-
ΔE <sub>int</sub>	-166.18	-189.32	-	-142.26	-139.39	-	-131.72	-155.95	-
ΔE <sub>def</sub>	74.74	9.84	-	44.88	5.20	-	95.10	10.20	-
ΔE	-91.44	-179.48	-	-97.38	-134.19	-	-36.62	-145.75	-
	Cu <sub>4</sub> Cl <sub>4</sub>			Ag <sub>4</sub> Cl <sub>4</sub>			Au <sub>4</sub> Cl <sub>4</sub>		
	T <sub>d</sub>	D <sub>4h</sub>	D <sub>2d</sub>	T <sub>d</sub>	D <sub>4h</sub>	D <sub>2d</sub>	T <sub>d</sub>	D <sub>4h</sub>	D <sub>2d</sub>
ΔE <sub>Pauli</sub>	577.11	282.63	289.05	370.11	256.35	263.72	525.36	354.51	356.69
ΔE <sub>elstat</sub>	-472.71	-275.74	-283.87	-330.60	-248.83	-255.50	-396.96	-300.13	-302.12
ΔE <sub>oi</sub>	-274.89	-188.17	-188.13	-177.82	-146.53	-148.04	-255.88	-218.09	-218.47
ΔE <sub>int</sub>	-170.50	-181.28	-182.95	-138.31	-139.02	-139.81	-127.48	-163.70	-163.89
ΔE <sub>def</sub>	45.47	5.12	5.80	35.09	2.20	2.56	71.15	4.64	4.80
ΔE	-125.03	-176.16	-177.15	-103.22	-136.82	-137.25	-56.33	-159.06	-159.09
	Cu <sub>4</sub> Cl <sub>4</sub>			Ag <sub>4</sub> Cl <sub>4</sub>			Au <sub>4</sub> Cl <sub>4</sub>		
	T <sub>d</sub>	D <sub>4h</sub>	D <sub>2d</sub>	T <sub>d</sub>	D <sub>4h</sub>	D <sub>2d</sub>	T <sub>d</sub>	D <sub>4h</sub>	D <sub>2d</sub>
ΔE <sub>Pauli</sub>	585.27	286.24	290.18	398.03	250.31	263.51	564.65	342.19	363.32
ΔE <sub>elstat</sub>	-476.88	-271.30	-279.73	-346.88	-242.16	-254.10	-427.48	-292.01	-310.06
ΔE <sub>oi</sub>	-280.77	-186.72	-185.60	-189.32	-142.32	-145.70	-266.70	-207.74	-212.99
ΔE <sub>int</sub>	-172.38	-171.79	-175.16	-138.17	-134.16	-136.30	-129.53	-157.55	-159.73
ΔE <sub>def</sub>	39.23	5.28	6.00	30.65	2.12	2.80	59.44	4.00	5.48
ΔE	-133.15	-166.51	-169.16	-107.52	-132.04	-133.50	-70.09	-153.55	-154.25
	Cu <sub>4</sub> I <sub>4</sub>			Ag <sub>4</sub> I <sub>4</sub>			Au <sub>4</sub> I <sub>4</sub>		
	T <sub>d</sub>	D <sub>4h</sub>	D <sub>2d</sub>	T <sub>d</sub>	D <sub>4h</sub>	D <sub>2d</sub>	T <sub>d</sub>	D <sub>4h</sub>	D <sub>2d</sub>
ΔE <sub>Pauli</sub>	624.19	305.71	307.09	447.03	247.74	275.20	641.94	350.62	387.47
ΔE <sub>elstat</sub>	-497.04	-275.94	-283.74	-375.05	-235.99	-259.20	-481.88	-296.24	-325.69
ΔE <sub>oi</sub>	-301.34	-192.52	-191.37	-209.95	-141.42	-149.30	-290.88	-208.00	-218.58
ΔE <sub>int</sub>	-174.19	-162.74	-168.03	-137.96	-129.68	-133.29	-130.82	-153.62	-156.79
ΔE <sub>def</sub>	31.68	5.48	6.00	25.77	1.88	2.76	46.66	3.57	5.89
ΔE	-142.51	-157.26	-162.03	-112.19	-127.80	-130.53	-84.16	-150.05	-150.90

<sup>a</sup> ΔE = E(M<sub>4</sub>X<sub>4</sub>)-4E(MX).

When compared to alkalimetals, the shorter bond lengths and the large number of electrons in group 11 transition metal tetramers results in a general increase of  $\Delta E_{\text{Pauli}}$ ,  $\Delta V_{\text{elstat}}$ , and  $\Delta E_{\text{oi}}$  components of the bonding energy. As in alkalimetals, the  $\Delta V_{\text{elstat}}$  and  $\Delta V_{\text{oi}}$  term are more stabilizing in the  $T_d$  form than in the  $D_{4h}$  structure. However, the higher stabilization of the  $\Delta V_{\text{elstat}}$  and  $\Delta E_{\text{oi}}$  contributions cannot compensate the much larger Pauli repulsions and deformation energies in the  $T_d$  form ( $\Delta E_{\text{Pauli}}$  for  $T_d$  is almost double to that of  $D_{4h}$ ) due to both short bond distances and the increased number of electrons (filled  $(n-1)d^{10}$  shell). Finally, for  $X = \text{Cl, Br and I}$ , for which the  $D_{2d}$  is slightly preferred to the  $D_{4h}$ , the EDA values allow to justify this fact from more favorable electrostatic interactions (about 8 kcal.mol<sup>-1</sup>) in the former, even though the latter presents a lower steric repulsion. So, at variance with previous studies that attributed the larger stabilization of the  $D_{2d}$  as compared to  $D_{4h}$  forms in some cases to better orbital interactions,<sup>[499-501]</sup> our results point out the key role of the more favorable electrostatic interactions in the  $D_{2d}$  isomer.

#### **7.4 An Analysis of the Relative Stabilities of Ortho, Meta, and Para $\text{MClY}(\text{XC}_4\text{H}_4)(\text{PH}_3)_2$ Heterometallabenzenes ( $\text{M} = \text{Ir, Rh; X} = \text{N, P; Y} = \text{Cl and M} = \text{Os, Ru; X} = \text{N, P; Y} = \text{CO}$ )**

In this work we have studied the relative stabilities of the ortho, meta, and para  $\text{MClY}(\text{XC}_4\text{H}_4)(\text{PH}_3)_2$  heterometallabenzenes ( $\text{M} = \text{Ir, Rh; X} = \text{N, P; Y} = \text{Cl and M} = \text{Os, Ru; X} = \text{N, P; Y} = \text{CO}$ ) with the objective to analyze the chemical bonding to unravel the reasons for the different isomer stabilities. To this end we have carried out an energy decomposition analysis for the formation of structural isomers (**o-MX** and **m-MX** or **m-MX** and **p-MX** with  $\text{M} = \text{Ir, Rh, Ru, Os; X} = \text{N, P}$ ) from triplet aza(phospha)ethenediyl ( $\text{A(o-MX)X}$  or  $\text{A(m-MX)X}$ ) and triplet metal ( $\text{B(o-MX)M}$  or  $\text{B(m-MX)M}$ ) fragments (see Scheme 7.4).



Scheme 7.4. Fragments considered in the EDA for the formation of the ortho, meta, and para isomers of  $MClY(XC_4H_4)(PH_3)_2$  complexes ( $M = Ir, Rh$ ,  $X = N, P$  and  $Y = Cl$  and  $M = Os, Ru$ ,  $X = N, P$  and  $Y = CO$ ).

**o-MX** and **m-MX** can be made from two identical aza(phospha)ethenediyl and metal fragments by just turning upside down the aza(phospha)ethenediyl. Then the different components of the bonding energy for the formation of the **o-MX** and **m-MX** complexes from the same fragments can be compared and the differences give a hint of the physical reasons for the relative stability differences. We have also compared the **m-MX** and **p-MX** heterometallabenzenes following the same approach making an EDA of the bonding energy for the formation of the **m-MX** and **p-MX** structural isomers from triplet aza(phospha)ethenediyl ( $A1(m-MX)_X$  or  $A1(p-MX)_X$ ) and triplet metal ( $B1(m-MX)_M$  or  $B1(p-MX)_M$ ) fragments (see Scheme 7.4).

In fact, to avoid the repetition, we restrict our discussion to irida and osmapyridines and phosphinines because for the rhodium and ruthenium pyridine and phosphinines the result are similar to those obtained for the equivalent iridium and osmium complexes. In this project, we use the nomenclature **o-IrN** to refer to the ortho-iridapyridine  $IrCl_2(NC_4H_4)(PH_3)_2$  species or **m-OsP** to denote the meta-osmaphosphinine  $OsCl(CO)(PC_4H_4)(PH_3)_2$  compound.

#### A. $MCl_2(XC_4H_4)(PH_3)_2$ complexes with $M = Ir, Rh$ and $X = N, P$

The results of relative energies obtained indicate that the meta isomers are the most stable for the **IrN** and **RhN** species by about 10 kcal/mol as compared to the ortho and para ones, while the

ortho species are the lowest-lying in energy for all metallaphosphinines studied by ca. 20 kcal/mol. Finally, the ortho and meta are almost isoenergetic for the **RuN** and **OsN** complexes. With the exception of the **o-IrN** and **o-IrP**, all heterometallabenzenes studied are planar or almost planar.

Table 7.6 contains the results of the analysis of the bonding for **o-IrN** from A(o-IrN)<sub>N</sub> and B(o-IrN)<sub>Ir</sub> fragments, **m-IrN** from A(m-IrN)<sub>N</sub> and B(m-IrN)<sub>Ir</sub> fragments, and two deformed **m-IrN** structures (**m-IrN<sub>a</sub>** and **m-IrN<sub>b</sub>**) obtained using A(o-IrN)<sub>N</sub> and B(o-IrN)<sub>Ir</sub> fragments. **m-IrN<sub>a</sub>** is **m-IrN** constructed from the frozen **o-IrN** fragments with C–N and C–Ir bond lengths equal to those of **o-IrN**. Therefore, **m-IrN<sub>a</sub>** is **o-IrN** with the N and C positions of the azaethendiyl fragment exchanged (the fragment turned-upside-down). **m-IrN<sub>b</sub>** is **m-IrN** constructed from the frozen **o-IrN** fragments with C–N and C–Ir bond lengths equal to those optimized in the **m-IrN** complex.

Table 7.6. Analysis of the bonding (in kcal/mol) between triplet azaethendiyl A(x-IrN)<sub>N</sub> and triplet IrCl<sub>2</sub>(PH<sub>3</sub>)<sub>2</sub>(C<sub>3</sub>H<sub>3</sub>) B(x-IrN)<sub>Ir</sub> fragments in **o-IrN**, **m-IrN**, and deformed **m-IrN** (**m-IrN<sub>a</sub>** and **m-IrN<sub>b</sub>**).<sup>a</sup>

	<b>o-IrN</b>		<b>m-IrN</b>		<b>m-IrN<sub>a</sub></b>		<b>m-IrN<sub>b</sub></b>	
	A(o-IrN) <sub>N</sub> + B(o-IrN) <sub>Ir</sub>		A(m-IrN) <sub>N</sub> + B(m-IrN) <sub>Ir</sub>		A(o-IrN) <sub>N</sub> + B(o-IrN) <sub>Ir</sub>		A(o-IrN) <sub>N</sub> + B(o-IrN) <sub>Ir</sub>	
ΔE <sub>Pauli</sub>	538.84		692.41 (153.57)		584.49 (45.65)		698.28 (159.44)	
ΔV <sub>elstat</sub>	-326.50		-402.69 (-76.19)		-350.66 (-24.16)		-400.97 (-74.47)	
ΔE <sub>oi</sub>	-429.96		-521.49 (-91.53)		-452.91 (-22.95)		-520.71 (-90.75)	
ΔE <sub>oi</sub> (σ)	<sup>-b</sup>		-459.83		<sup>-b</sup>		<sup>-b</sup>	
ΔE <sub>oi</sub> (π)	<sup>-b</sup>		-61.65		<sup>-b</sup>		<sup>-b</sup>	
ΔE <sub>int</sub>	-217.61		-231.76 (-14.15)		-219.08 (-1.47)		-223.40 (-5.79)	
ΔE <sub>def</sub>	47.98		53.17 (5.19)		47.98 (0.00)		47.98 (0.00)	
ΔE <sub>tot</sub> <sup>c</sup>	-169.63		-178.59 (-8.96)		-171.10 (-1.47)		-175.42 (-5.79)	
ΔE <sub>bondexact</sub> <sup>c</sup>	-162.53		-172.74 (-10.20)		-163.94 (-1.41)		-166.75 (-4.22)	
Correct.f <sup>c</sup>	<b>0.96</b>		<b>0.97</b>		<b>0.96</b>		<b>0.95</b>	

<sup>a</sup> Computed at the BP86/TZ2P level. See Scheme 1 for structures. A<sub>N</sub>/B<sub>Ir</sub>(o-IrN) and A<sub>N</sub>/B<sub>Ir</sub>(m-IrN) refer to A<sub>N</sub>/B<sub>Ir</sub> in the geometry it adopts in **o-IrN** and **m-IrN**, respectively; **m-IrN<sub>a</sub>** is **m-IrN** with frozen A<sub>N</sub>/B<sub>Ir</sub>(o-IrN) fragments but with connecting C–N and Ir–C bond distances as the corresponding C–C and Ir–N bond lengths in **o-IrN** (1.435 Å and 1.973 Å); **m-IrN<sub>b</sub>** is **m-IrN** with frozen A<sub>N</sub>/B<sub>Ir</sub>(o-IrN) fragments but with connecting C–N and Ir–C bond distances as the optimized bond lengths in **m-IrN** (1.348 Å and 1.971 Å).

<sup>b</sup> Non-planar species. The exact σ/π separation is not possible.

<sup>c</sup> ΔE<sub>bondexact</sub> is the exact bonding energy while ΔE<sub>tot</sub> is the sum of ΔE<sub>int</sub> and ΔE<sub>def</sub> and it is the bonding energy without taking into account the spin polarization effects in the fragment (see Theoretical Methods Section). Correct.f gives the ΔE<sub>bondexact</sub>/ΔE<sub>tot</sub> ratio and it is a measure of the error in the different energy components because of the lack of spin polarization effects in the fragments.

As can be seen in Table 7.6, 162.5 and 172.7 kcal/mol are released in the formation of **o-IrN** and **m-IrN** from triplet optimized azaethendiyl and IrCl<sub>2</sub>(C<sub>3</sub>H<sub>3</sub>)(PH<sub>3</sub>)<sub>2</sub> fragments, respectively, thus giving **m-IrN** as the most stable isomer by 10.2 kcal/mol. The higher stability of **m-IrN** cannot be ascribed to the deformation energy of the fragments (ΔE<sub>def</sub>) that is in fact somewhat more destabilizing for **m-IrN** by 5.2 kcal/mol. The main difference comes from the interaction energy

( $\Delta E_{\text{int}}$ ) that is 14.2 kcal/mol more stabilizing in **m-IrN**. The EDA results of the two  $\Delta E_{\text{int}}$  energies shows that the difference is not due to Pauli repulsions ( $\Delta E_{\text{Pauli}}$ ) that destabilize **m-IrN** with respect to **o-IrN** by as much as 153.6 kcal/mol, but to a combination of better electrostatic ( $\Delta V_{\text{elstat}}$ ) and orbital interaction ( $\Delta E_{\text{oi}}$ ) components. The higher  $\Delta E_{\text{Pauli}}$  and the more stabilizing  $\Delta V_{\text{elstat}}$  term in the **m-IrN** form is the result of the shorter bond length (1.348 Å) of the new C–N formed as compared to that of the new C–C bond (1.435 Å) generated in **o-IrN**.  $\Delta E_{\text{oi}}$  can be further decomposed into  $\sigma$  and  $\pi$  components ( $\Delta E_{\sigma}$  and  $\Delta E_{\pi}$ ), but only for the **m-IrN** because the **o-IrN** system is not planar.  $\Delta E_{\pi}$ , which measures the contribution of  $\pi$ -delocalization to the bonding energy, is significant in **m-IrN** (-61.7 kcal/mol), the percentage of  $\Delta E_{\text{oi}}$  stabilization due to the  $\pi$ -system (11.8%) is similar (somewhat smaller) to that found by Fernández and Frenking in a series of metallabenzenes.<sup>[502]</sup> This is the situation at the optimized geometries of **o-IrN** and **m-IrN**. When we move from **m-IrN** to **m-IrN<sub>a</sub>** (the **m-IrN** having the same geometry than the **o-IrN** species with the N and C atoms of the azaethendiyl fragment exchanged) we find that the bonding energy of the **m-IrN<sub>a</sub>** species matches that of the **o-IrN** complex as a result of the somewhat higher  $\Delta E_{\text{Pauli}}$  repulsion being compensated by a slightly more stabilizing  $\Delta V_{\text{elstat}}$  and  $\Delta E_{\text{oi}}$  terms. The higher  $\Delta E_{\text{Pauli}}$  in **m-IrN<sub>a</sub>** as compared to **o-IrN** is likely the result of larger Pauli repulsion for the C–N bond in comparison with the C–C bond. Partial relaxation of the **m-IrN<sub>a</sub>** to **m-IrN<sub>b</sub>** leads to a situation practically identical to that of **m-IrN**. When going from **m-IrN<sub>a</sub>** to **m-IrN<sub>b</sub>** there is an important increase of the Pauli repulsion term and a stabilization of the  $\Delta V_{\text{elstat}}$  and  $\Delta E_{\text{oi}}$  terms, as expected from the substantial C–N bond length reduction.

Following the same procedure we can compare the **m-IrN** and **p-IrN** isomers from the EDA of the bonding energy to form **m-IrN** and **p-IrN** from the two identical azaethendiyl  $A(x\text{-IrN})_N$  and the metal  $B(x\text{-IrN})_{\text{Ir}}$  fragments in their triplet states (see Scheme 7.4). Results in Table 7.7 show that 240.2 and 231.3 kcal/mol are released in the formation of **m-IrN** and **p-IrN** from triplet azaethendiyl and  $\text{IrCl}_2(\text{C}_3\text{H}_3)(\text{PH}_3)_2$  fragments. Thus, **m-IrN** is more stable than **p-IrN** by 8.9 kcal/mol. The bond lengths in the two fragments obtained from **m-IrN** and **p-IrN** complexes are quite similar and, consequently, the deformation energy of the fragments is almost the same for the two isomers. When comparing the geometries of the **m-IrN** and **p-IrN** complexes, one can see that the formed C–C and C–N bond distances differ by less than a hundredth of an Å. These similar bond lengths lead to comparable Pauli repulsion and orbital interaction terms.

Table 7.7. Analysis of the bonding (in kcal/mol) between triplet azaethenediyl A(x-IrN)<sub>N</sub> and triplet IrCl<sub>2</sub>(PH<sub>3</sub>)<sub>2</sub>(C<sub>3</sub>H<sub>3</sub>) B(x-IrN)<sub>Ir</sub> fragments in **m-IrN** and **p-IrN**, and deformed **p-IrN** (**p-IrN<sub>a</sub>** and **p-IrN<sub>b</sub>**).<sup>a</sup>

	<b>m-IrN</b>	<b>p-IrN</b>	<b>p-IrN<sub>a</sub></b>	<b>p-IrN<sub>b</sub></b>
	A1(m-IrN) <sub>N</sub> +B1(m-IrN) <sub>Ir</sub>	A(p-IrN) <sub>N</sub> + B(p-IrN) <sub>Ir</sub>	A1(m-IrN) <sub>N</sub> + B1(m-IrN) <sub>Ir</sub>	A1(m-IrN) <sub>N</sub> + B1(m-IrN) <sub>Ir</sub>
ΔE <sub>Pauli</sub>	792.53	789.37 (-3.16)	816.07 (23.54)	801.23 (8.70)
ΔV <sub>elstat</sub>	-420.13	-409.04 (11.09)	-416.51 (3.62)	-409.52 (10.61)
ΔE <sub>oi</sub>	-645.38	-644.17 (1.21)	-655.57 (-10.19)	-652.68 (-7.30)
ΔE <sub>oi</sub> (σ)	-551.91	-551.25 (0.66)	-557.64 (-5.73)	-559.05 (-7.14)
ΔE <sub>oi</sub> (π)	-93.47	-92.92 (0.55)	-97.92 (-4.45)	-93.62 (-0.15)
ΔE <sub>int</sub>	-272.98	-263.83 (9.15)	-256.01 (16.97)	-260.97 (12.01)
ΔE <sub>def</sub>	25.32	24.96 (-0.36)	25.32 (0.00)	25.32 (0.00)
ΔE <sub>tot</sub> <sup>b</sup>	-247.66	-238.87 (8.79)	-230.69 (16.97)	-235.65 (12.01)
ΔE <sub>bondexact</sub> <sup>b</sup>	-240.19	-231.32 (8.87)	-223.23 (16.96)	-229.01 (11.18)
Correct.f <sup>b</sup>	<b>0.97</b>	<b>0.97</b>	<b>0.97</b>	<b>0.97</b>

<sup>a</sup> Computed at BP86/TZ2P. See Scheme 1 for structures. A<sub>1N</sub>/B<sub>1Ir</sub>(m-IrN) and A<sub>N</sub>/B<sub>Ir</sub>(p-IrN) refer to A<sub>N</sub>/B<sub>Ir</sub> in the geometry it adopts in **m-IrN** and **p-IrN**, respectively; **p-IrN<sub>a</sub>** is **p-IrN** with frozen A<sub>1N</sub>/B<sub>1Ir</sub>(m-IrN) fragments but with connecting C–N and C–C bond distances as the corresponding C–C and C–N bond lengths in **m-IrN** (1.400 Å and 1.327 Å); **p-IrN<sub>b</sub>** is **p-IrN** with frozen A<sub>1N</sub>/B<sub>1Ir</sub>(m-IrN) fragments but with connecting C–N and C–C bond distances as the optimized bond lengths in **p-IrN** (1.342 Å and 1.395 Å).

<sup>b</sup> ΔE<sub>bondexact</sub> is the exact bonding energy while ΔE<sub>tot</sub> is the sum of ΔE<sub>int</sub> and ΔE<sub>def</sub> and it is the bonding energy without taking into account the spin polarization effects in the fragment (see Theoretical Methods Section). Correct.f gives the ΔE<sub>bondexact</sub>/ΔE<sub>tot</sub> ratio that is a measure of the error in the different energy components because of the lack of spin polarization effects in the fragments.

When comparing the EDA in **m-IrN** and **p-IrN** (Table 7.7), the main difference comes from the electrostatic interaction energy that is 11.1 kcal/mol more stabilizing in **m-IrN**. The ΔE<sub>oi</sub> term can be further decomposed into σ and π components (ΔE<sub>σ</sub> and ΔE<sub>π</sub>). Although the two components of ΔE<sub>oi</sub> favor the **m-IrN** isomer, differences between the σ- and the π-components of the two complexes are less than 1 kcal/mol. ΔE<sub>π</sub> in **m-IrN** and **p-IrN** complexes represents about 14.5% of the ΔE<sub>oi</sub> term. Interestingly, the values of ΔE<sub>π</sub> are significantly larger in **m-IrN** constructed from A1(m-IrN)<sub>N</sub> and B1(m-IrN)<sub>Ir</sub> fragments than in the same complex generated from A(m-IrN)<sub>N</sub> and B(m-IrN)<sub>Ir</sub> fragments (see Scheme 7.4). This ΔE<sub>π</sub> value is quite dependent on how the molecule is cut into fragments and, consequently, ΔE<sub>π</sub> values provide only a rough estimation of aromaticity in these compounds. Not unexpectedly, the more favorable ΔV<sub>elstat</sub> in m-IrN as compared to **p-IrN** is still present in the deformed **p-IrN<sub>a</sub>** and **p-IrN<sub>b</sub>** complexes.

On the other hand, it is interesting to discuss the effect in the relative stabilities of changing the N heteroatom by a P atom. We found that the ortho is the most stable isomer in all phosphametallabenzene studied in this work. The results of EDA of the bonding energy show that the main difference between **o-IrP** and **m-IrP** comes from the ΔE<sub>int</sub> term that is 21.6

kcal/mol more stabilizing in **o-IrP** (see Chapter 6). The lower  $\Delta E_{\text{int}}$  is not due to smaller Pauli repulsion but because of more stabilizing  $\Delta V_{\text{elstat}}$  and  $\Delta E_{\text{oi}}$  terms. In particular,  $\Delta E_{\text{oi}}$  is more favorable in **o-IrP** by as much as 65.8 kcal/mol. Moreover, the analysis of the bonding for **m-IrP**, **p-IrP**, and two deformed **p-IrP** structures (**p-IrP<sub>a</sub>** and **p-IrP<sub>b</sub>**) shows that the slightly higher stability of the **p-IrP** (compared with **m-IrP**) isomer comes from the somewhat more stabilizing  $\Delta V_{\text{elstat}}$  and  $\Delta E_{\text{oi}}$  terms that are not counterbalanced by the slightly larger Pauli repulsions. Interestingly the  $\Delta E_{\pi}$  component of the orbital interaction term is, first, almost the same for the **m-IrP** and **p-IrP** complexes (about 85 kcal/mol), and second, somewhat smaller than those of the **m-IrN** and **p-IrN** complexes (about 93 kcal/mol).

EDA trends observed in the iridium systems do not change when we move to rhodium for the  $\text{RhCl}_2(\text{XC}_4\text{H}_4)(\text{PH}_3)_2$  complexes with  $\text{X} = \text{N}, \text{P}$ . In all cases, however, the bonding energy is somewhat smaller in the rhodium complexes and this is in accordance with the fact that 5d metallabenzenes are more stable than their 4d analogues.<sup>[503-505]</sup>

## B. $\text{MCl}(\text{CO})(\text{XC}_4\text{H}_4)(\text{PH}_3)_2$ complexes with $\text{M} = \text{Os}, \text{Ru}$ ; $\text{X} = \text{N}, \text{P}$

BP86/TZ2P (B3LYP/cc-pVDZ-PP) relative energies indicate that the compound **o-OsN** is more stable than **m-OsN** isomer by only 0.8 kcal/mol (1.5 kcal/mol) and more stable than **p-OsN** by 5.9 kcal/mol (6.2 kcal/mol). The aromaticity of the singlet ground state of these three isomers is supported by the negative values of the NICS indicator of aromaticity and the positive value of the electronic delocalization multicenter index. As for **IrN** complexes, NICS(1)<sub>zz</sub> and MCI values point out that the aromaticity of the different **OsN** isomers is similar, the least stable **p-OsN** being somewhat more aromatic. The formation of **o-OsN** and **m-OsN** from triplet azaethendiyl and  $\text{OsCl}(\text{CO})(\text{C}_3\text{H}_3)(\text{PH}_3)_2$  fragments releases 174.9 and 174.1 kcal/mol, respectively. The **o-OsN** isomer is a little bit more stable by 0.8 kcal/mol. Also closing the metallacycle leads to significant better  $\pi$ -interactions in **m-OsN** than in **o-OsN**. The lower  $\Delta E_{\pi}$  term in **m-OsN** is an indication of somewhat higher aromaticity for this system and this is reflected by the MCI values, but not by the NICS(1)<sub>zz</sub> results. When we move from **m-OsN** to **m-OsN<sub>a</sub>** we find that the  $\Delta E_{\text{Pauli}}$  term decreases significantly as compared to **m-OsN** but also the stabilizing  $\Delta V_{\text{elstat}}$  and  $\Delta E_{\text{oi}}$  terms decrease in comparison to **m-OsN** and, as a whole, **m-OsN<sub>a</sub>** is 8.5 kcal/mol less stable than **o-OsN**. Partial relaxation of the **m-OsN<sub>a</sub>** to **m-OsN<sub>b</sub>**, the latter being a deformed **m-OsN** generated from  $\text{A}(\text{o-OsN})_{\text{N}}$  and  $\text{B}(\text{o-OsN})_{\text{Os}}$  fragments but with

connecting C–N and C–Os bond distances equal to the corresponding bond lengths in **m-OsN**, leads to a situation similar to that of **m-OsN**. On the other hand, EDA results show that 247.1 and 242.0 kcal/mol are released in the formation of **m-OsN** and **p-OsN** from triplet azaethendiyl and OsCl(CO)(C<sub>3</sub>H<sub>3</sub>)(PH<sub>3</sub>)<sub>2</sub> fragments, respectively. The  $\Delta E_{\sigma}$  and  $\Delta E_{\pi}$  components of  $\Delta E_{oi}$  favor the **p-OsN** isomer by about 5 kcal/mol. The larger  $\Delta E_{\pi}$  term in **p-OsN** concurs with its larger MCI and more negative NICS(1)<sub>zz</sub> values. The values of  $\Delta E_{\pi}$  are significantly larger in **m-OsN** constructed from A1(m-OsN)<sub>N</sub> and B1(m-OsN)<sub>Ir</sub> fragments than in the same complex generated from A(m-OsN)<sub>N</sub> and B(m-OsN)<sub>Ir</sub> fragments (see Scheme 7.4). Because the geometry of the deformed **p-OsN<sub>a</sub>** and **p-OsN<sub>b</sub>** complexes does not differ substantially from that of optimized **p-OsN**, EDA values for these deformed species are similar to those found for **p-OsN**.

As found in all phosphametallabenzene studied here, the ortho isomer is the most stable among the **OsP** isomers. The EDA results of **o-OsP** and **m-OsP** indicate that the reasons for the larger stability of **o-OsP** (16.8 kcal/mol) are the same as those described for **o-IrP**. Because a cancellation of the different terms, in this case one could attribute the energy difference almost fully to the  $\Delta E_{\pi}$  term. Once more, the larger  $\Delta E_{\pi}$  term (in absolute value) of **o-OsP** agrees with larger MCI and more negative NICS(1)<sub>zz</sub> values.

Finally, the EDA results for the **m-OsP** and **p-OsP** isomers show that they are almost isoenergetic (**p-OsP** is more stable by only 0.6 kcal/mol). The situation resembles that found for **m-IrP** and **p-IrP** isomers. EDA analysis shows that the slightly higher stability of the **p-OsP** isomer comes from the somewhat more stabilizing  $\Delta V_{elstat}$  and  $\Delta E_{oi}$  terms that are not compensated by the slightly larger Pauli repulsion. It is worth noting that the  $\Delta E_{\pi}$  component of the orbital interaction term in **m-OsP** and **p-OsP** is, first, somewhat more stabilizing for **m-OsP** than **p-OsP** (by 3.1 kcal/mol), and second, somewhat smaller than those of the **m-OsN** and **p-OsN** complexes (ca. 3-11 kcal/mol).

The EDA results for ruthenium show that ruthenapyridines and phosphonimines behave in the same way as their osmium analogues. This is not surprising if one takes into account that ruthenium and osmium belong to the same group in the periodic table (group 8) and have the same Pauling electronegativity (2.2). In all cases, however, the bonding energy is somewhat smaller in the ruthenium complexes and this is in accordance with the fact that *5d* metallabenzene are more stable than their *4d* analogues.<sup>[503-505]</sup>

## **Chapter 8: Conclusions**

---

The most important conclusions drawn from the studies of this thesis comparing the relative stabilities of different isomers are briefly summarized in this chapter.

---



### Project 1:

The isomerization energies of 1,2-/1,3-diazacyclobutadiene, pyrazole/imidazole, and pyridazine/pyrimidine are 10.6, 9.4, and 20.9 kcal/mol, respectively, at the BP86/TZ2P level of theory. In all cases the 1,3-isomer is more stable than the 1,2-counterpart.

Our results indicate that, in the three cases, **the higher stability** of the 1,3-isomers is **not due to lower Pauli repulsions** but because of the **more favorable  $\sigma$ -orbital** interactions involved in the formation of two C–N bonds in comparison with the generation of C–C and N–N bonds in the 1,2-isomers.

### Project 2:

The XYYX isomers appear to be in general more stable than  $X_2YY$  ( $X = \text{H, Li, Na, F, Cl, Br, I}$ ;  $Y = \text{O, S, Se, Te}$ ) because of the short, destabilizing X–X contact in the latter.

The X–Y bond weakens as the electronegativity difference decreases. For  $X = \text{Li and Na}$ , only one  $X_2Y_2$  equilibrium structure is obtained in which the alkali atoms adopt a bridging position between the Y atoms of the YY fragment. The character and length of the Y–Y bond can be tuned quite generally by the X–Y electronegativity difference.

If X is more electronegative (or electropositive) with respect to Y, the  $\pi^*$  orbital of the YY becomes effectively depopulated (or populated) in  $X_2YY$  and in XYYX and the Y–Y distance becomes shorter.

### Project 3:

In the case of the halide and hydride alkalimetal tetramers  $(MX)_4$ , the cubic isomer of  $T_d$  geometry is more stable than the ring structure with  $D_{4h}$  symmetry, whereas in the case of group 11 transition metal tetramers, the isomer with  $D_{4h}$  symmetry (or  $D_{2d}$  symmetry) is more stable than the  $T_d$  form.

The results obtained from energy decomposition analyses of the tetramerization energies show that in alkalimetal halide and hydride tetramers, the cubic geometry is the most stable because

the larger Pauli repulsion energies are compensated by the attractive electrostatic and orbital interaction terms. In the case of group 11 transition metal tetramers, the  $D_{4h}/D_{2d}$  geometry is more stable than the  $T_d$  one due to the reduction of electrostatic stabilization and the dominant effect of the Pauli repulsion.

#### **Project 4:**

The relative stabilities of the ortho, meta, and para  $M(Cl)Y(XC_4H_4)(PH_3)_2$  heterometallabenzenes ( $M = Ir, Rh; X = N, P; Y = Cl$  and  $M = Os, Ru; X = N, P; Y = CO$ ) indicate that the meta isomer is the most stable for the **IrN** and **RhN** complexes. The ortho is the most stable in all studied metallaphosphinines, and the ortho and meta are almost isoenergetic for **RuN** and **OsN** species.

EDA results for **IrN** and **RhN** species indicate that the meta isomer is more stable than the ortho because of the stronger  $Ir(Rh)-C$  than  $Ir(Rh)-N$  bonds, whereas the meta is more stable than the para because of better electrostatic interactions.

For the **OsN** and **RuN** families, EDA indicate the ortho and meta isomers are almost isoenergetic because the higher orbital interactions in the meta species is counterbalanced by larger Pauli repulsions.

For all metallaphosphinines, the ortho is the most stable due to the stronger  $M-P$  than  $C-C$  bonds as compared to  $M-C$  than  $C-P$  bonds and the para isomer is only marginally more stable than the meta one as expected since the bonds formed are of the same type.

The formal number of  $\pi$ -electrons in the heterometallabenzenes studied is controversial, the molecular orbitals indicate that they are  $10\pi$ -electron species. The values of the multicenter index of aromaticity and nucleus independent chemical shifts indicate that complexes studied have to be classified as aromatic or slightly aromatic.

## References

- (1) Frankland, E. *Phil. Trans. Roy. Soc.* **1852**, 142, 417.
- (2) Kekulé, F. A. *Ann. Chem.* **1857**, 104, 129.
- (3) Kolbe, A. W. H. *Ann. Chem.* **1857**, 101, 257.
- (4) Kekulé, A. *Annalen der Chemie und Pharmacie.* **1858**, 106 (2), 129.
- (5) Couper, A. S. *Compt. rend.* **1858**, 46, 1157.
- (6) Couper, A. S. *Ann. Chim. phys.* **1858**, 53, 469.
- (7) Butlerov, A. M. *Z. Chem. Pharm.* **1861**, 4, 549.
- (8) van't Hoff, J. H. *Arch. neerland. sci.* **1874**, 9, 445.
- (9) Bel, J. A. I. *Bull. soc. chim. France.* **1874**, 22, 337.
- (10) Werner, A. *Z. anorg. Chem.* **1893**, 3, 267.
- (11) Lewis, G. N. *J. Am. Chem. Soc.* **1916**, 38, 762.
- (12) Kossel, W. *Ann. Physik.* **1916**, 49, 229.
- (13) Langmuir, I. *J. Am. Chem. Soc.* **1919**, 41, 868.
- (14) Sidgwick, N. V. *Some Physical Properties of the covalen link in chemistry*, Cornell University Press **1933**, 42.
- (15) London, F. *Naturwissenschaften.* **1929**, 17, 525.
- (16) Pauling, L. *Cornell, Ithaca, NY* **1960**.
- (17) Coulson, C. A. *the valence. second edition. Oxford university press* **1961**.
- (18) Langmuir, I. *science.* **1921**, 54, 59.
- (19) Lowry, T. M. *Trans. Faraday. Soc.* **1923**, 18, 285.
- (20) Lowry, T. M. *J. Chem. Soc.* **1927**, 123, 822.
- (21) Sidgwick, N. V. *The Electronic Theory of Valency*, Clarendon Press, Oxford **1927**.
- (22) Born, M.; Oppenheimer, R. *Ann. Phys.* **1927**, 84, 457.
- (23) Hylleraas, E. A. *Z. Physik.* **1931**, 71, 739.
- (24) burrau, Ø. *Kgl. Danske Videnskab. Selskab.* **1927**, 7, 1.
- (25) Jaffé, G. *Z. Physik.* **1934**, 87, 535.
- (26) Pauling, L. *J. Am. Chem. Soc.* **1931**, 53, 3225.
- (27) Majorana, E. *Nuovo cimento.* **1931**, 8, 22.
- (28) Smith, A. L.; Johnston, H. L. *J. Am. Chem. Soc.* **1952**, 74, 4696.
- (29) Wheland, G. W. *Resonance in Organic Chemistry; Wiley, NY* **1955**.
- (30) Hückel, E. *Z. Phys.* **1931**, 70, 204.
- (31) Hückel, E. *Z. Phys.* **1931**, 72, 310.
- (32) Hückel, E. *Z. Phys.* **1932**, 76, 628.
- (33) Thomson, J. J. *Philos. Mag* **1912**, 24, 209.
- (34) Coulson, C. A. *Proc. Cambridge. Philos. Soc.* **1935**, 31, 244.
- (35) Pitzer, K. S. *J. Am. Chem. Soc.* **1945**, 67, 1126.
- (36) Duncan, J. L.; Harper, J. *Mol. Phys.* **1984**, 51, 371.
- (37) Pullman, A. *Prog. Org. Chem.* **1958**, 4, 31.
- (38) Shaik, S. S.; Hilberty, P. C.; Lefour, J.; Ohanessian, G. *J. Am. Chem. Soc.* **1987**, 109, 363.
- (39) Stanger, A.; Vollhardt, K. P. C. *J. Org. Chem.* **1988**, 53, 4889.
- (40) Copper, D. L.; Wright, S. C.; Gerratt, J.; Raimondi, M. *J. Chem. Soc. Perkin Trans* **1989**, 2, 255.
- (41) Jug, K.; Kóster, A. M. *J. Am. Chem. Soc.* **1990**, 112, 6772.
- (42) Aihara, J. *J. Bull. Chem. Soc.* **1990** 63, 1956.
- (43) Michael, B. S.; March, J. *"Advanced Organic Chemistry: Reactions, Mechanisms, and Structure." Sixth Edition*, 2007.
- (44) Ohring, M. *Eng. Mat. Sci.* **1995**, 2, 29.

- (45) Osuna, S.; Swart, M.; Baerends, E. J.; Bickelhaupt, F. M.; Solà, M. *Chem. Phys. Chem.* **2009**, *10*, 2955.
- (46) Ohring, M. *Engineering Materials Science. Academic Press. INC.* **1995**.
- (47) Pauling, L. *J. Am. Chem. Soc.* **1932**, *54*, 3570.
- (48) Mulliken, R. S. *J. Chem. Phys.* **1934**, *2*, 782.
- (49) Gordy, W. *Phys. Rev.* **1946**, *69*, 604.
- (50) Sanderson, R. T. *J. Chem. Educ.* **1952**, *29*, 539.
- (51) Allred, A. L.; Rochow, E. G. *J. Inorg. Nucl. Chem.* **1958**, *5*, 264.
- (52) Zhang, Y. *Inorg. Chem.* **1982**, *21*, 3886.
- (53) Portier, J.; Campet, G.; Etourneau, J.; B. Tanguy. *J. Alloys. Comp.* **1994**, *209*, 285.
- (54) Dyke, T.; Muentner, J. *J. Chem. Phys.* **1973**, *59*, 3125.
- (55) Lorentz, H. A. *The Theory of Electrons, Teubner, Leipzig* **1916**.
- (56) Pauli, W.; Jr. *Z. Physik.* **1927**, *41*, 81.
- (57) Seitz, F. *"the Modern Theory of Solids" McGraw-Hill Book Company, Inc., New York* **1958**.
- (58) Kittel, C. *"Introduction to Solid State Physics", John Wiley & Sons, Inc, New York* **1956**.
- (59) Ziman, J. M. *"Electrons and Phonons" Oxford University Press, New York* **1960**.
- (60) Vijh, A. K. *J. Phys. Chem. Solids.* **1969**, *30*, 1999.
- (61) Hooge, F. N. *Z. Phys. Chem.* **1960**, *24*, 275.
- (62) Scheiner, S. *Molecular Interactions. From van der Waals to Strongly Bond Complexes. Wiley, Chichester, UK* **1997**.
- (63) JM. Bowman, Z. B. *Molecular Clusters. Advances in Molecular Vibrations and Collision Dynamics, JAI Press, Stamford, CT* **1998**, *3*.
- (64) Arunan, E.; Desiraju, G. R.; Klein, R. A.; Sadlej, J.; Scheiner, S.; Alkorta, I.; Clary, D. C.; Crabtree, R. H.; Dannenberg, J. J.; Hobza, P.; Kjaergaard, H. G.; Legon, A. C.; Mennucci, B.; Nesbitt, D. J. *Pure Appl. Chem.* **2011**, *83*, 1637.
- (65) Tuck, D. G. *Prog. Inorg. Chem.* **1968**, *9*, 161.
- (66) Emsley, J. *Chem. Soc. Rev.* **1980**, *9*, 91.
- (67) Broene, H.; DeVries, T. *J. Am. Chem. Soc.* **1947**, *69*, 1844.
- (68) Baumann, E. W. *J. Inorg. Nucl. Chem.* **1969**, *31*, 3155.
- (69) Ellis, A. J. *J. Chem. Soc.* **1966**, 4300.
- (70) Kresge, A. J.; Chiang, Y. J. *Phys. Chem.* **1973**, *77*, 822.
- (71) J. D Dunitz, A. G. *Angew. Chem., Int. Ed* **2005**, *44*, 1766.
- (72) Bernstein, J.; Etter, M. C.; Leiserowitz, L. (eds H.-B. Bürgi and JD Dunitz), *Wiley-VCH Verlag GmbH, Weinheim, Germany.* **1994**, 431.
- (73) Alshateet, S. F.; Bishop, R.; Craig, D. C.; Scudder, M. L. *Cryst. Growth. Des.* **2004**, *4*, 837.
- (74) Bishop, R.; Marjo, C. E.; Scudder, M. L. *Mol. Cryst. Liq. Cryst.* **1998**, *313*, 75.
- (75) Bishop, R. *Synlett* **1999**, 1351.
- (76) Mazik, M.; Bläser, D.; Boese, R. *Tetrahedron.* **2001**, *57*, 5791.
- (77) Desiraju, G. R.; Steiner, T. *The Weak Hydrogen Bond in Structural Chemistry and Biology; Oxford University Press: Oxford* **1999**.
- (78) Madhavi, N. N. L.; Katz, A. K.; Carrell, H. L.; Nangia, A.; Desiraju, G. R. *Chem. Commun.* **1997**, 1953.
- (79) LeRoy, R. J.; *Can J. Phys.* **1974**, *55*, 246.
- (80) Liu, S.; Bacic, Z.; Moskowitz, J. W.; Schmidt, K. E. *J. Chem. Phys.* **1995**, *103*, 1829.
- (81) Boschke, L. E. *van der Waals Systems, Springer-Verlag, Berlin, Heidelberg* **1980**.
- (82) Parsegian, A. *van der Waals Forces, A Handbook for Biologists, Chemists, Engineers and Physicists, Cambridge University Press, Cambridge* **2005**.
- (83) Scholes, G. *Ann. Rev. Phys. Chem.* **1980**, *31*, 81.
- (84) Jeziorski, B.; Moszynski, R.; Szalewicz, K. *Chem. Rev.* **1994**, *94*, 1887.

- (85) Keesom, W. H. *Physikalische Zeit.* **1921**, 22, 129.
- (86) Debye, P. *Physikalische Zeit.* **1921**, 22, 302.
- (87) London, F. *Trans. Faraday. Soc.* **1937**, 33, 8.
- (88) Israelachvili, J. N. in : "*Intermolecular and Surface Forces*", Academic Press, London, second edition. **1991**.
- (89) Kleis, J.; Schröder, E. *J. Chem. Phys.* **2005**, 122, 164902.
- (90) L. A. Girifalco and M. Hodak *Phys. Rev. B* **2002**, 65, 125404.
- (91) Autumn, K.; al, e. *Proc. Natl. Acad. Sci. USA* **2002**, 99, 12252.
- (92) Brutschy, B.; Hobza, P. *Chem. Rev.* **2000**, 100, 3861.
- (93) Grimme, S.; Antony, J.; Ehrlich, S.; Krieg, H. *J. Chem. Phys.* **2010**, 132, 154104.
- (94) Grimme, S.; Ehrlich, S.; Goerigk, L. *J. Comput. Chem.* **2011**, 32, 1457.
- (95) Tjebbes, J. *Acta Chem. Scand.* **1962**, 16, 916.
- (96) Silva, G. d.; Moore, E. E.; Bozzelli, J. W. *J. Phys. Chem. A* **2006**, 110, 13979.
- (97) Bedford, A. F.; Edmondson, P. B.; Mortimer, C. T. *J. Chem. Soc.* **1962**, 2927.
- (98) Jiménez, P.; Roux, M. V.; Turrión, C.; Gomis, F. *J. Chem. Thermodyn.* **1987**, 19, 985.
- (99) Curutchet, C.; Poater, J.; Solà, M.; Elguero, J. *J. Phys. Chem. A* **2011**, 111, 8571.
- (100) Bird, C. W. *Tetrahedron.* **1996**, 52, 9945.
- (101) Bird, C. W. *Tetrahedron.* **1997**, 53, 3319.
- (102) Wang, Y.; Wu, J. I.-C.; Li, Q.; Schleyer, P. v. R. *Org. Lett.* **2010**, 12, 4824.
- (103) Lipkind, D.; Chickos, J. S. *J. Chem. Eng. Data.* **2010**, 55, 1628.
- (104) Hartley, G. S. *Nature.* **1937**, 140, 281.
- (105) Rau, H. In *Photochemistry and Photophysics*; CRC Press, I., Ed.: Boca Raton, FL **1990**, 2, 119.
- (106) IUPAC *Compendium of Chemical Terminology, 2nd ed. (the "Gold Book").* **1997**.
- (107) Nelson, D. J.; Brammer, C. N. *J. Chem. Educ.* **2011**, 88, 292.
- (108) Wang, Y.; Sessions, A. L.; Nielsen, R. J.; Ill, W. A. G. *Geochimica et Cosmochimica Acta.* **2013**, 107, 82.
- (109) Bhupinder, M.; Manju, M. *ORGANIC CHEMISTRY, Prentice-Hall of India Private Limited, New Delhi.* **2005**.
- (110) Bringmann, G.; Mortimer, A. J. P.; Keller, P. A.; Gresser, M. J.; Garner, J.; Breuning, M. *Angew. Chem. Int. Ed.* **2005**, 44, 5384.
- (111) Hill, D. J.; Mio, M. J.; Prince, R. B.; Hughes, h. S.; Moore, J. S. *Chem. Rev.* **2001**, 101, 3893.
- (112) Eichelbaum, M.; Gross, A. *Adv. Drug Res.* **1996**, 28, 2.
- (113) Schleyer, P. v. R. *Chem. Rev.* **2001**, 101, 1115.
- (114) Faraday, M. *Philos. Trans. Roy. London*, **1825**, 115, 440.
- (115) Mitscherlich, E. *Annalenpharm.* **1834**, 9(1), 39.
- (116) Kekulé, A. *Bull. Soc. Chim. Fr.* **1865**, 3, 98.
- (117) Kekulé, A. *Bull. Acad. R. Belg.* **1865**, 19, 501.
- (118) Kekule, A. *Ann. Chem. Pharm.* **1866**, 137, 129.
- (119) Kekule, A. *Ann. Chem.* **1872**, 162, 77.
- (120) Dewar, J. *Proc. R. Soc. Edinburgh.* **1867**, 1, 84.
- (121) Ladenburg, A. *Ber. Dtsch. Chem.* **1869**, 2, 140.
- (122) Ladenburg, A. *Ber. Dtsch. Chem.* **1872**, 5, 322.
- (123) Claus, A. *Theoretische Betrachtungen und deren Anwendung zur Systematik der organischen Chemie, Freiburg, germany* **1867**, 207.
- (124) Baeyer, A. *Chem. Ber.* **1886**, 19, 1797.
- (125) Baeyer, A. *Ann. Chem.* **1887**, 245, 103.
- (126) Baeyer, A. *Ann. Chem.* **1888**, 251, 257.
- (127) Baeyer, A. *Ann. Chem.* **1890**, 1, 256.

- (128) Baeyer, A. *Ann. Chem.* **1890**, 258, 145.  
 (129) Baeyer, A. *Ann. Chem.* **1892**, 266, 169.  
 (130) Baeyer, A. *Ann. Chem.* **1892**, 269, 145.  
 (131) Baeyer, A. *Ann. Chem.* **1893**, 276, 255.  
 (132) Armstrong, H. E. *J. Chem. Soc.* **1887**, 51, 258.  
 (133) Armstrong, H. E. *Philos. Mag.* **1887**, 23, 73.  
 (134) Finar, I. L. *Organic Chemistry, ELBS edition of sixth edition* **1985**.  
 (135) Armit, J. W.; Robinson, R. *J. Chem. Soc.* **1925**, 127, 1604.  
 (136) Heitler, W.; London, F. Z. *Phys.* **1927**, 44, 455.  
 (137) Pauling, L.; Wheland, G. W. *J. Chem. Phys.* **1933**, 1, 280.  
 (138) Pauling, L. *J. Chem. Phys.* **1936**, 4, 673.  
 (139) Hückel, E. *Trans. Faraday. Soc.* **1934**, 30, 40.  
 (140) PA Plattner, H. A. P. *Chim. Acta* **1937**, 20, 224.  
 (141) Anderson, A. G.; Nelson, J. A. *J. Am. Chem. Soc.* **1950**, 72, 3824.  
 (142) Robertson, J. M.; Shearer, H. M. M. *Nature.* **1956**, 177, 885.  
 (143) W. E. von Doering, L. H. K. *J. Am. Chem. Soc.* **1957**, 79, 352.  
 (144) Breslow, R.; Lockhart, J.; Small, A. J. *Am. Chem. Soc.* **1962**, 84, 2793.  
 (145) Heilbronner, E. *Tetrahedron. Lett.* **1964**, 29, 1923.  
 (146) Breslow, R. *Chem. Eng. News.* **1965**, 43, 90.  
 (147) Breslow, R. *Angew. Chem., Int. Ed. Engl* **1968**, 7, 565.  
 (148) Breslow, R.; Brown, J.; Gajewski, J. J. *J. Am. Chem. Soc.* **1967**, 89, 4383.  
 (149) Breslow, R. *Acc. Chem. Res.* **1973**, 6, 393.  
 (150) Allen, A. D.; Tidwell, T. T. *Chem. Rev.* **2001**, 101, 1333.  
 (151) Tsipis, C. A. *Coord. Chem. Rev.* **2005**, 249, 2740.  
 (152) Chen, Z.; Wannere, C. S.; Corminboeuf, C.; Puchta, R.; Schleyer, P. v. R. *Chem. Rev. (Washington, D.C.)* **2005**, 105, 3843.  
 (153) Schleyer, P. v. R.; Jiao, H. *Pure. Appl. Chem* **1996**, 68, 209.  
 (154) Boldyrev, A. I.; Wang, L. S. *Chem. Rev.* **2005**, 105, 3716.  
 (155) Glukhovstev, M. N.; Schleyer, P. V. R. *Chem. Phys. Lett.* **1992**, 198, 547.  
 (156) Suresh, H.; Koga, N. *J. Org. Chem.* **2002**, 67, 1965.  
 (157) George, P.; Trachtman, M.; Bock, C. W.; Brett, A. M. *J. Chem. Soc., Perkin Trans.* **1977**, 2, 1036.  
 (158) Proft, F. D.; Geerlings, P. *Chem. Rev.* **2001**, 101, 1451.  
 (159) Poater, J.; Fradera, X.; Duran, M.; Sola, M. *Chem. Eur.J.* **2003**, 9, 400.  
 (160) Poater, J.; Fradera, X.; Duran, M.; Sola, M. *Chem. Eur.J.* **2003**, 9, 1113.  
 (161) Lepetit, C.; Nielsen, M. B.; Diederich, F.; Chauvin, R. *Chem.-Eur. J.* **2003**, 9, 5056.  
 (162) Krygowski, T. M.; Cyrański, M. K. *Chem. Rev.* **2001**, 101, 1385.  
 (163) Krygowski, T. M. *J. Chem. Inf. Comput. Sci.* **1993**, 33, 70.  
 (164) Kruszewski, J.; Krygowski, T. M. *Tetrahedron Lett.* **1972**, 13, 3839.  
 (165) Amic, D.; Trinajstić, N. *Bull. Soc. Chim. Belg.* **1991**, 100, 527.  
 (166) Contreras, R.; Safont, V. S.; Perez, P.; Andres, J.; Moliner, V.; Tapia, O. *J. Mol. Struct. (THEOCHEM)*, **1998**, 426, 277.  
 (167) Dauben, H. J.; Wilson, J. D.; Laity, L. J. *J. Am. Chem. Soc.* **1968**, 90, 118.  
 (168) Hutter, D. H.; Flygare, W. H. *Top. Curr. Chem.* **1976**, 63, 89.  
 (169) Flygare, W. H. *Chem. Rev.* **1974**, 74, 653.  
 (170) Pople, J. A. *J. Chem. Phys.* **1956**, 24, 1111.  
 (171) Wannere, C. W.; Schleyer, P. V. R. *Org. Lett.* **2003**, 5, 605.  
 (172) Mitchell, R. H. *Chem. Rev.* **2001**, 101, 1301.  
 (173) Coriani, S.; Lazzeretti, P.; Malagoli, M.; Zanasi, R. *Theor. Chem. Acta.* **1994**, 89, 181.  
 (174) Fowler, P. W.; Steiner, E.; Zanasi, R.; Cadioli, B. *Mol. Phys.* **1999**, 96, 1099.

- (175) Steiner, E.; Fowler, P. W. *Chem. Commun.* **2001**, 21, 2220.
- (176) Steiner, E.; Fowler, P. W. *J. Phys. Chem. A.* **2001**, 105, 9553.
- (177) Steiner, E.; Fowler, P. W. *Phys. Chem. Chem. Phys.* **2004**, 2, 261.
- (178) Schleyer, P. v. R.; Maerker, C.; Dransfeld, A.; Jiao, H.; Hommes, N. J. R. v.-E. *J. Am. Chem. Soc.* **1996**, 118, 6317.
- (179) Schleyer, P. v. R.; Manoharan, M.; Wang, Z.-X.; Kiran, B.; Jiao, H.; Puchta, R.; Hommes, N. J. R. v. E. *Org. Lett.* **2001**, 3, 2465.
- (180) Schleyer, P. v. R.; Jiao, H.; Hommes, N. J. R. v. E.; Malkin, V. G.; Malkina, O. L. *J. Am. Chem. Soc.* **1997**, 119, 12669.
- (181) Jusélius, J.; Sundholm, D. *Phys. Chem. Chem. Phys.* **1999**, 1, 3429.
- (182) Gomes, J. A. N. F.; Mallion, R. B. *Chem. Rev. (Washington, D.C.)* **2001**, 101, 1349
- (183) Lazzaretti, P. *edited by J. W. Emsley, J. Feeney, and L. H. Sutcliffe (Elsevier, New York)* **2000**, 1.
- (184) Fleischer, U.; Kutzelnigg, W.; Lazzaretti, P.; Muéhlenkamp, V. *J. Am. Chem. Soc.* **1994**, 116, 5298.
- (185) Lazzaretti, P. *Phys. Chem. Chem. Phys.* **2004**, 6, 217.
- (186) Herges, R.; Geuenich, D. *J. Phys. Chem. A.* **2001**, 105, 3214.
- (187) Santos, J. C.; Tiznado, W.; Contreras, R.; Fuentealba, P. *J. Chem. Phys.* **2004**, 120, 1670
- (188) Santos, J. C.; Andres, J.; Aizman, A.; Fuentealba, P. *Chem. Theory. Comput.* **2005**, 1, 83.
- (189) Matito, E.; Duran, M.; Solà, M. *J. Chem. Phys.* **2005**, 122, 014109.
- (190) Bollini, C. G.; Giambiagi, M.; Giambiagi, M. S. d.; Figueiredo, A. P. d. *J. Math. Chem.* **2000**, 28, 71.
- (191) Bollini, C. G.; Giambiagi, M.; Giambiagi, M. S. D.; Figueiredo, A. P. D. *Struct.Chem.* **2001**, 12, 113.
- (192) Giambiagi, M.; Giambiagi, M. S. D.; Silva, C. D. D. S.; Figueiredo, A. P. D. *Phys. Chem. Chem. Phys.* **2000**, 2, 3381.
- (193) P. Bultinck, M. R., R. Ponec, B. van Gheluwe, R. Carbó-Dorca, P. Popelier *J. Phys. Chem. A* **2006**, 110, 7642.
- (194) Bultinck, P.; Mandado, M.; Mosquera, R. A. *J. Math. Chem.* **2008**, 43, 111.
- (195) Bultinck, P.; Ponec, R.; Damme, S. V. *J. Phys. Org. Chem.* **2005**, 18, 706
- (196) Ponec, R.; Bultinck, P.; Gallegos, A. *J. Phys. Chem. A.* **2005**, 109, 6606.
- (197) Bultinck, P.; Ponec, R.; Carbo-Dorca, R. *J. Comput. Chem.* **2007**, 28, 152.
- (198) Bultinck, P.; Fias, S.; Ponec, R. *Chem.Eur.J.* **2006**, 12, 8813.
- (199) Caramori, G. F.; Oliveira, K. T. d.; Galembeck, S. E.; Bultinck, P.; Constantino, M. G. *J. Org. Chem.* **2007**, 72, 76.
- (200) Mandado, M.; González-Moa, M. J.; Mosquera, R. A. *J. Comput. Chem.* **2007**, 28, 127.
- (201) Mandado, M.; González-Moa, M. J.; Mosquera, R. A. *J. Comput. Chem.* **2007**, 28, 1625.
- (202) Mandado, M.; Otero, N.; Mosquera, R. A. *Tetrahedron.* **2006**, 62, 12204.
- (203) Mandado, M.; González-Moa, M. J.; Mosquera, R. A. *Chem. Phys. Chem.* **2007**, 8, 696.
- (204) Mandado, M.; Bultinck, P.; González-Moa, M. J.; Mosquera, R. A. *Chem. Phys. Lett.* **2006**, 433, 5.
- (205) Cook, M. J.; Linda, P.; Katritzky, A. R. *Adv. Heterocycl. Chem.* **1974**, 17, 255.
- (206) Katritzky, A. R.; Karelson, M.; Malhotra, N. *Heterocycles.* **1991**, 32, 127.
- (207) Simkin, B. Y.; Minkin, V. I.; Glukhovtsev, M. N. *Adv. Heterocycl. Chem.* **1993**, 56, 303.
- (208) Raabe, G.; Michl, J. *The Chemistry of Organic Silicon Compounds, Ed. by S. Patai, Z. Rappoport, Wiley, New York* **1989**.
- (209) Balaban, A. T.; Oniciu, D. C.; Katritzky, A. R. *Chem. Rev.* **2004**, 104, 2777.
- (210) Katritzky, A. R.; Jug, K.; Oniciu, D. C. *Chem. Rev. (Washington, D.C.)* **2001**, 101, 1421.
- (211) Bordwell, F. G.; Drucker, G. E.; Fried, H. E. *J. Org. Chem.* **1981**, 46, 632.
- (212) Li, X.-W.; Pennington, W. T.; Robinson, G. H. *J. Am. Chem. Soc.* **1995**, 117, 7578.

- (213) Li, X.-W.; Xie, Y.; Schreiner, P. R.; Gripper, K. D.; Crittendon, R. C.; Campana, C. F.; III, H. F. S.; Robinson, G. H. *Organometallics*. **1996**, *15*, 3798.
- (214) Baudler, M.; Duster, D.; Ouzounis, D. Z. *Anorg. Allg. Chem.* **1987**, *544*, 87.
- (215) Malar, E. J. P. *J. Org. Chem.* **1992**, *57*, 3694.
- (216) Dransfeld, A.; Nyulaszi, L.; Schleyer, P. v. R. *Inorg. Chem.* **1998**, *37*, 4413.
- (217) Urnezis, E.; Brennessel, W. W.; Cramer, C. J.; Ellis, J. E.; Schleyer, P. v. R. *Science*. **2002**, *295*, 832.
- (218) Aihara, J. *J. Am. Chem. Soc.* **1978**, *100* 3339.
- (219) Aihara, J.; Hosoya, H. *Bull. Chem. Soc. Jpn.* **1988**, *61*, 2657.
- (220) Haddon, R. C.; Brus, L. E.; Raghavachari, K. *Chem. Phys. Lett.* **1986**, *125*, 459.
- (221) Bühl, M.; Hirsch, A. *Chem. Rev.* **2001**, *101*, 1153.
- (222) Chen, Z.; King, R. B. *Chem. Rev.* **2005**, *105*, 3613.
- (223) Lu, X.; Chen, Z. *Chem. Rev. (Washington, D.C.)* **2005**, *105*, 3643.
- (224) Winstein, S. *J. Am. Chem. Soc.* **1959**, *81*, 6524.
- (225) Winstein, S.; Sonnenberg, J.; deVries, L. *J. Am. Chem. Soc.* **1959**, *81*, 6523.
- (226) Williams, R. V. *Chem. Rev.* **2001**, *101*, 1185.
- (227) Gogonea, V.; Schleyer, P. v. R.; Schreiner, P. R. *Angew. Chem.* **1998**, *37*, 1945.
- (228) Jiao, H.; Schleyer, P. v. R. *J. Phys. Org. Chem.* **1998**, *11*, 655.
- (229) Li, X.; Kuznetsov, A. K.; Zhang, H. H.-F.; Boldyrev, A. I.; Wang, L. *Science*. **2001**, *291*, 859.
- (230) Fowler, P. W.; Havenith, R. W. A.; Steiner, E. *Chem. Phys. Lett.* **2001**, *342*, 85.
- (231) Fowler, P. W.; Havenith, R. W. A.; Steiner, E. *Chem. Phys. Lett.* **2002**, *359*, 530.
- (232) Havenith, R. W. A.; Fowler, P. W.; Steiner, E.; Shetty, S.; Kanhere, D. G.; Pal, S. *Phys. Chem. Chem. Phys.* **2004**, *6*, 285.
- (233) Havenith, R. W. A.; Fowler, P. W. *Phys. Chem. Chem. Phys.* **2006**, *8*, 3383.
- (234) Juselius, J.; Straka, M.; Sundholm, D. *J. Phys. Chem. A*. **2001**, *105*, 9939.
- (235) Lin, Y. C.; Jusélius, J.; Sundholm, D.; Gauss, J. *J. Chem. Phys.* **2005**, *122* 214308.
- (236) Chen, Z.; Corminboeuf, C.; Heine, T.; Bohman, J.; Schleyer, P. v. R. *J. Am. Chem. Soc.* **2003**, *125*, 13930.
- (237) Islas, R.; Heine, T.; Merino, G. *J. Chem. Theory. Comput.* **2007**, *3* 775.
- (238) Havenith, R. W. A.; Lenthe, J. H. V. *Chem. Phys. Lett.* **2004**, *385*, 198.
- (239) Zhan, C. G.; Zheng, F.; Dixon, D. A. *J. Am. Chem. Soc.* **2002**, *124*, 14795.
- (240) Kuznetsov, A. E.; Boldyrev, A. I. *Inorg. Chem.* **2002**, *41*, 532.
- (241) Chattaraj, P. K.; Roy, D. R.; Elango, M.; Subramanian, V. *J. Mol. Struct. (THEOCHEM)*, **2006**, *759* 109.
- (242) Power, P. P. *Struct. Bond.* **2002** *103* 58.
- (243) H. Tanaka, S. N., E. Janssens, R.E. Silverans, P. Lievens *J. Am. Chem. Soc.* **2003**, *125*, 2862.
- (244) Alexandrova, A. N.; Boldyrev, A. I.; Zhai, H.-J.; Wang, L. S. *J. Phys. Chem. A*. **2005** *109* 562.
- (245) Kong, Q.; Chen, M.; Dong, J.; Li, Z.; Fan, K.; Zhou, M. *J. Phys. Chem. A*. **2002** *106*, 11709.
- (246) Lein, M.; Frunzke, J.; Frenking, G. *Angew. Chem. Int. Ed* **2003**, *42*, 1303.
- (247) Kraus, F.; Hanauer, T.; Korber, N. *Inorg. Chem.* **2006**, *45* 1117
- (248) Hu, X.; Li, H.; Wang, C. *J. Phys. Chem. B*. **2006**, *110* 14046.
- (249) Mallajosyula, S. S.; Datta, A.; Pati, S. K. *J. Phys. Chem. B*. **2006**, *110* 20098
- (250) Datta, A.; Mallajosyula, S. S.; Pati, S. K. *Acc. Chem. Res.* **2007**, *40*(3) 213
- (251) Chattaraj, P. K.; Roy, D. R.; Elango, M.; Subramanian, V. *J. Phys. Chem. A*. **2005** *109* 9590.
- (252) Shetty, S.; Kanhere, D. G.; Pal, S. *J. Phys. Chem. A*. **2004**, *108*, 628.
- (253) Kuznetsov, A. E.; Boldyrev, A. I. *Chem. Phys. Lett.* **2004**, *388* 452
- (254) Kuznetsov, A. E.; Birch, K. A.; Boldyrev, A. I.; Li, X.; Zhai, H. J.; Wang, L. S. *Science*. **2003**, *300*, 622.
- (255) Mecero, J. M.; Ugalde, J. M. *J. Am. Chem. Soc.* **2004**, *126*, 3380.

- (256) Fowler, P. W.; Rogowska, A.; Soncini, A.; Lillington, M.; Olson, L. P. *J. Org. Chem.* **2006**, *71*, 6459.
- (257) Kuznetsov, A. E.; Boldyrev, A. I.; Li, X.; Wang, L. S. *J. Am. Chem. Soc.* **2001**, *123*, 8825.
- (258) Kuznetsov, A. E.; Boldyrev, A. I. *Struct. Chem.* **2002**, *13*, 141.
- (259) Zhai, H.-J.; Wang, L.-S.; Kuznetsov, A. E.; Boldyrev, A. I. *J. Phys. Chem.* **2002**, *106*, 5600.
- (260) Berzelius, J. J. *J. Chem. Phys.* **1812**, *6*, 119.
- (261) Kuznetsov, A. E.; Corbett, J. D.; Wang, L. S.; Boldyrev, A. I. *Angew. Chem. Int. Ed.* **2001**, *40*, 3369.
- (262) Li, X.; Zhang, H. F.; Wang, L. S.; Kuznetsov, A. E.; Cannon, N. A.; Boldyrev, A. I. *Angew. Chem. Int. Ed.* **2001**, *40*, 1867.
- (263) Chi, X. X.; Li, X. H.; Chen, X. J.; Yuang, Z. S. *J. Mol. Struct. (Theochem)*, **2004**, *677*, 21.
- (264) Kuznetsov, A. E.; Zhai, H. J.; Wang, L. S.; Boldyrev, A. I. *Inorg. Chem.* **2002**, *41*, 6062.
- (265) Xu, W. G.; Zhang, Y. C.; Xi, Q. *J. Mol. Struct. (TheoChem)* **2009**, *909(1-3)*, 129.
- (266) Xu, W. G.; Zhang, Y. C.; Lu, S. X.; Zhang, R. C. *J. Mol. Struct. (TheoChem)* **2009**, *900*, 44.
- (267) Höltzl, T.; Veldeman, N.; Veszpremi, T.; Lievens, P.; Nguyen, M. T. *Chem. Phys. Lett.* **2009**, *469*, 304.
- (268) Xu, W. G.; Zhang, R. C.; Lu, S. X.; Zhang, Y. C. *J. Mol. Struct. (TheoChem)* **2009**, *894*, 1.
- (269) Xu, W. G.; Zhang, R. C.; Lu, S. X.; Zhang, Y. C. *J. Mol. Struct. (TheoChem)* **2008**, *864*, 1.
- (270) Li, Z.; Zhao, C.; Chen, L. *J. Mol. Struct. (THEOCHEM)*. **2007**, *807*, 17.
- (271) Elliott, B. M.; Boldyrev, A. I. *J. Phys. Chem. A*, **2005**, *109*, 236.
- (272) Soto, L. A.; Tagle, R. R.; Pérez, R. A. *J. Phys. Chem. A*. **2009**, *113*, 671.
- (273) Lin, Y. C.; Sundholm, D.; J, J.; Cui, L. F.; Li, X.; Zhai, H. J.; Wang, L. S. *J. Phys. Chem. A*. **2006**, *110*, 4244.
- (274) Sobhy, M. A.; Reveles, J. U.; Gupta, U.; Khanna, S. N.; Castleman, A. W.; Jr. *J. Chem. Phys.* **2009**, *130*, 054304.
- (275) Lin, L.; Höltzl, T.; Gruene, P.; Claes, P.; Meijer, G.; Fielicke, A.; Lievens, P.; Nguyen, M. T. *Chem. Phys. Chem.* **2008**, *9*, 2471.
- (276) Chattaraj, P. K.; Giri, S. *J. Mol. Struct. (TheoChem)* **2008**, *865*, 53.
- (277) Chattaraj, P. K.; Roy, D. R.; Duley, S. *Chem. Phys. Lett.* **2008**, *460*, 382.
- (278) Khatua, S.; Roy, D. R.; Bultinck, P.; Bhattacharjee, M.; Chattaraj, P. K. *Phys. Chem. Chem. Phys.* **2008**, *10*, 2461.
- (279) Höltzl, T.; Janssens, E.; Veldeman, N.; Veszpremi, T.; Lievens, P.; Nguyen, M. T. *Chem. Phys. Chem.* **2008**, *9*, 833.
- (280) Duan, H.; Gong, Z.; Cheng, J.; Zhu, W.; Chen, K.; Jiang, H. *J. Phys. Chem. A*. **2006**, *110*, 12236.
- (281) Yu, H. *J. Mol. Struct. (TheoChem)* **2009**, *906*, 25.
- (282) Zhang, G. H.; Zhao, Y. F.; Wu, J. I.; Schleyer, P. v. R. *Inorg. Chem.* **2009**, *48*, 6773.
- (283) Tanaka, H.; Neukermans, S.; Janssens, E.; Silverans, R. E.; Lievens, P. *J. Am. Chem. Soc.* **2003**, *125*, 2862.
- (284) Wannere, C. S.; Corminboeuf, C.; Wang, Z. X.; Wodrich, M. D.; King, R. B.; Schleyer, P. v. R. *J. Am. Chem. Soc.* **2005**, *127*, 5701.
- (285) Chaitanya, S.; Corminboeuf, W. C.; Wang, Z. X.; Wodrich, M. D.; King, R. B.; Schleyer, P. v. R. *J. Am. Chem. Soc.* **2005**, *127*, 5701.
- (286) Corminboeuf, C.; Chaitanya, S.; Wannere, D.; Roy, D. R.; King, R. A.; Schleyer, P. v. R. *Inorg. Chem.* **2006**, *45*, 214.
- (287) Nigam, S.; Majumder, C.; Kulshreshtha, S. K. *J. Mol. Struct. (TheoChem)* **2005**, *755*, 187.
- (288) Nigam, S.; Majumder, C.; Kulshreshtha, S. K. *Comput. Lett.* **2005**, *1(4)*, 240.
- (289) Nigam, S.; Majumder, C.; Kulshreshtha, S. K. *J. Chem. Sci.* **2006**, *118*, 575.
- (290) Katritzky, A. R.; Barczynski, P.; Musumarra, G.; Pisano, D.; Szafran, M. *J. Am. Chem. Soc.* **1989**, *111*, 7.

- 146.
- (291) Pauling, L.; Sherman, J. J. *Chem. Phys.* **1933**, *1*, 606.
- (292) Kistiakowski, B.; Ruhoffm, J. R.; Smith, H. A.; Vaughan, W. E. *J. Am. Chem. Soc.* **1936**, *58*, 146.
- (293) Ehrenfest, P. *Physoca.* **1925**, *5*, 388.
- (294) Ehrenfest, P. *Z. Phys.* **1929**, *58*, 719.
- (295) Raman, C. V. *Nature.* **1929**, *123*, 945.
- (296) Raman, C. V. *Nature.* **1929**, *124*, 412.
- (297) Lonsdale, K. *Proc. R. Soc. London A.* **1937**, *159*, 149.
- (298) London, F. J. *Phys. Radium.* **1937**, *8*, 397.
- (299) Iijima, S. *Nature.* **1991**, *354*, 56.
- (300) Hameka, H. F. *Mol. Phys.* **1958**, *1*, 203.
- (301) McWeeny, R. *Phys. Rev.* **1962**, *126*, 1028.
- (302) Edwards, T. G.; McWeeny, R. *Chem. Phys. Lett.* **1971**, *10*, 283.
- (303) Ditchfield, R. J. *Chem. Phys.* **1972**, *56*, 5688.
- (304) Epstein, S. T. *J. Chem. Phys.* **1973**, *58*, 1592.
- (305) Mallion, R. B. *Mol. Phys.* **1973**, *25*, 1415.
- (306) Meyer, L. H.; Saika, A.; Gutowski, H. S. *J. Am. Chem. Soc.* **1953**, *75*, 4567.
- (307) Pople, J. A. *Mol. Phys.* **1958**, *1*, 175.
- (308) Dewar, M. J. S.; Gleicher, G. J. *J. Am. Chem. Soc.* **1965**, *87*, 685.
- (309) Dewar, M. J. S.; Gleicher, G. J. *J. Am. Chem. Soc.* **1965**, *87*, 692.
- (310) Dewar, M. J. S.; Gleicher, G. J. *J. Chem. Phys.* **1966**, *44*, 759.
- (311) Dewar, M. J. S.; Llano, C. d. *J. Am. Chem. Soc.* **1969**, *91*, 789.
- (312) Sondheimer, F.; Calder, I. C.; Elix, J. A.; Gaoni, Y.; Garratt, P. J.; Grohmann, K.; Maio, G. d.; Mayer, J.; Sargent, M. V.; Wolovsky, R. *Chem. Soc. Spec. Publ.* **1967**, *21*, 75.
- (313) Sondheimer, F. *Acc. Chem. Res.* **1972**, *5*, 81.
- (314) Julg, A.; François, P. *Theor. Chim. Acta.* **1967**, *7*, 249.
- (315) Dauben, H. J.; Jr.; Wilson, J. D.; Laity, J. L. *J. Am. Chem. Soc.* **1968**, *90*, 811.
- (316) Dauben, H. J.; Jr.; Wilson, J. D.; Laity, J. L. *J. Am. Chem. Soc.* **1969**, *91*, 1991.
- (317) Benson, R. C.; Flygare, W. H. *J. Am. Chem. Soc.* **1970**, *92*, 7523.
- (318) Benson, R. C.; Norris, C. L.; Flygare, W. H.; Beak, P. *J. Am. Chem. Soc.* **1971**, *93*, 5591.
- (319) Schmalz, T. G.; Norris, C. L.; Flygare, W. H. *J. Am. Chem. Soc.* **1973**, *95*, 7961.
- (320) Schmalz, T. G.; Gierke, T. D.; Beak, P.; Flygare, W. H. *Tetrahedron. Lett.* **1974**, *33* 2885.
- (321) Hess, B. A.; Jr.; Schaad, L. J. *J. Am. Chem. Soc.* **1971**, *93*, 305.
- (322) Hess, B. A.; Jr.; Schaad, L. J. *J. Am. Chem. Soc.* **1971**, *93*, 2413.
- (323) Hess, B. A.; Jr.; Schaad, L. J. *J. Org. Chem.* **1971**, *36*, 3418.
- (324) Hess, B. A.; Jr.; Schaad, L. J. *J. Am. Chem. Soc.* **1972**, *94*, 3068.
- (325) Hess, B. A.; Jr.; Schaad, L. J.; Holyoke, C. W. *Tetrahedron.* **1972**, *28*, 3657.
- (326) Hess, B. A.; Jr.; Schaad, L. J. *J. Am. Chem. Soc.* **1973**, *95*, 3907.
- (327) Clar, E. *The Aromatic Sextet*; Wiley: London **1972**.
- (328) Krygowski, T. M.; Cyranski, M. K. *Tetrahedron.* **1996**, *52* 10255.
- (329) Fringuelli, F.; Marino, G.; Taticchi, A.; Grandolini, G. *J. Chem. Soc., Perkin. Trans. 2.* **1974**, *2*, 332.
- (330) Gutman, I.; Milun, M.; Trinajstic, N. *Commun. Math. Comput. Chem.* **1975**, *1*, 171.
- (331) Gutman, I.; Milun, M.; Trinajstic, N. *J. Am. Chem. Soc.* **1977**, *99*, 1692.
- (332) Aihara, J. *J. Am. Chem. Soc.* **1976**, *98*, 2750.
- (333) Kutzelnigg, W. *Isr. J. Chem.* **1980**, *19*, 193.
- (334) Schindler, M.; Kutzelnigg, W. *J. Chem. Phys.* **1982**, *76*, 1919.
- (335) Schindler, M.; Kutzelnigg, W. *J. Am. Chem. Soc.* **1983**, *105*, 1360.
- (336) Kutzelnigg, W.; Fleischer, U.; Schindler, M. *Springer-Verlag: Berlin* **1990**, *23*, 165.
- (337) Lazzeretti, P.; Zanasi, R. *J. Chem. Phys.* **1981**, *75*, 5019.

- (338) Lazzeretti, P.; Zanasi, R. *Chem. Phys. Lett.* **1981**, *80*, 533.
- (339) Jug, K. J. *Org. Chem.* **1983**, *48*, 1344.
- (340) Pozharskii, A. F. *Khim. Geterotsikl. Soedin. (in Russian)* **1985**, 867.
- (341) Bird, C. W. *Tetrahedron.* **1985**, *41*, 1409.
- (342) Bird, C. W. *Tetrahedron.* **1986**, *42*, 89.
- (343) Bird, C. W. *Tetrahedron.* **1987**, *43*, 4725.
- (344) Bird, C. W. *Tetrahedron.* **1990**, *46*, 5697.
- (345) Bird, C. W. *Tetrahedron.* **1992**, *48*, 335.
- (346) Bird, C. W. *Tetrahedron.* **1992**, *48*, 1675.
- (347) Mizoguchi, N. *Chem. Phys. Lett.* **1987**, *134*, 371.
- (348) Zhou, Z.; Parr, R. G.; Garst, J. F. *Tetrahedron. Lett.* **1988**, *29*, 4843.
- (349) Zhou, Z.; Parr, R. G. *J. Am. Chem. Soc.* **1989**, *111*, 7371.
- (350) Zhou, Z.; Navangul, H. V. *J. Phys. Org. Chem.* **1990**, *3*, 784.
- (351) Zhou, Z. *J. Phys. Org. Chem.* **1995**, *8*, 103.
- (352) Paquette, L. A.; Bauer, W.; Sivik, M. R.; Bühl, M.; Feigel, M.; Schleyer, P. v. R. *J. Am. Chem. Soc.* **1990**, *112*, 8776.
- (353) Jiao, H.; Schleyer, P. v. R. *Angew. Chem., Int. Ed. Engl* **1993**, *32*, 1760.
- (354) Bühl, M.; Thiel, W.; Jiao, H.; Schleyer, P. v. R.; Saunders, M.; Anet, F. A. L. *J. Am. Chem. Soc.* **1994**, *116*, 6005.
- (355) Jiao, H.; Schleyer, P. v. R. *J. Am. Chem. Soc.* **1995**, *117*, 11529.
- (356) Schleyer, P. v. R.; Jiao, H.; Glukhovtsev, M. N.; Chandrasekhar, J.; Kraka, E. *J. Am. Chem. Soc.* **1994**, *116*, 10129.
- (357) Schleyer, P. v. R.; Freeman, P. K.; Jiao, H.; Goldfuss, B. *Angew. Chem., Int. Ed. Engl* **1995**, *34*, 337.
- (358) Sulzbach, H. M.; Schleyer, P. v. R.; Jiao, H.; Xie, Y.; Schaefer, H. F. *J. Am. Chem. Soc.* **1995**, *117*, 1369.
- (359) Jiao, H.; Schleyer, P. v. R. *Angew. Chem.* **1996**, *35*, 2383.
- (360) Schleyer, P. v. R.; Jiao, H.; Sulzbach, H. M.; Schaefer, H. F. *J. Am. Chem. Soc.* **1996**, *118*, 2093.
- (361) Goldfuss, B.; Schleyer, P. v. R.; Hampel, F. *Organometallics.* **1996**, *15*, 1755.
- (362) Jiao, H.; Schleyer, P. v. R. *J. Chem. Soc., Faraday Trans* **1994**, *90*, 1559.
- (363) Herges, R.; Jiao, H.; Schleyer, P. v. R. *Angew. Chem., Int. Ed. Engl* **1994**, *33*, 1376.
- (364) Jiao, H.; Schleyer, P. v. R. *Angew. Chem., Int. Ed. Engl* **1995**, *34*, 334.
- (365) Saunders, M.; Jiménez-Vázquez, H. A.; Cross, R. J.; Mroczkowski, S.; Freedberg, D. L.; Anet, F. A. L. *Nature.* **1994**, *367*, 256.
- (366) Saunders, M.; Cross, R. J.; Jiménez-Vázquez, H. A.; Shimshi, R.; Khong, A. *Science.* **1996**, *271*, 1693.
- (367) Saunders, M.; Jimenez-Vazquez, H. A.; Cross, R. J.; Billups, W. E.; Gesenberg, C.; Gonzalez, A.; Luo, W.; Haddon, R. C.; Diederich, F.; Herrmann, A. *J. Am. Chem. Soc.* **1995**, *117*, 9305.
- (368) Bühl, M. *Chem.-Eur. J.* **1998**, *4*, 734.
- (369) Krygowski, T. M.; Ciesielski, A.; Cyranski, M. *Chem. Pap.* **1995**, *49*, 128.
- (370) Steiner, E.; Fowler, P. W. *Int. J. Quantum. Chem.* **1996**, *60*, 609.
- (371) Bohmann, J. A.; Weinhold, F.; Farrar, T. C. *J. Chem. Phys.* **1997**, *107*, 1173.
- (372) Bean, G. P. *J. Org. Chem.* **1998**, *63*, 2497.
- (373) Sadlej-Sosnowska, N. *J. Org. Chem.* **2001**, *66*, 8737.
- (374) Balawender, R.; Komorowski, L.; Proft, F. D.; Geerlings, P. *J. Phys. Chem. A.* **1998**, *102*, 9912.
- (375) Chesnut, D. B. *Chem. Phys.* **1998**, *231*, 1.
- (376) Mo, Y.; Peyerimhoff, S. D. *J. Chem. Phys.* **1998**, *109*, 1687.
- (377) Mo, Y.; Zhang, Y.; Gao, J. *J. Am. Chem. Soc.* **1999**, *121*, 5737.

- (378) Mo, Y.; Song, L.; Wu, W.; Cao, Z.; Zhang, Q. *J. Theor. Comput. Chem.* **2002**, *1*, 137.
- (379) Jusélius, H.; Sundholm, D. *Phys. Chem. Chem. Phys.* **2000**, *2*, 2145.
- (380) Jusélius, J.; Sundholm, D. *J. Org. Chem.* **2000**, *65*, 5233.
- (381) Jusélius, J.; Sundholm, D. *Phys. Chem. Chem. Phys.* **2001**, *3*, 2433.
- (382) Berger, R. J. F.; Schmidt, M. A.; Jusélius, J.; Sundholm, D.; Sirsch, P.; Schmidbaur, H. *Z. Naturforsch. B.* **2001**, *56*, 979.
- (383) Jusélius, J.; Patzschke, M.; Sundholm, D. *THEOCHEM.* **2003**, *633*, 123.
- (384) Chesnut, D. B.; Bartolotti, L. *Chem. Phys.* **2000**, *253*, 1.
- (385) Fuster, F.; Sevin, A.; Silvi, B. *J. Phys. Chem. A.* **2000**, *104*, 852.
- (386) Silvi, B. *Phys. Chem. Phys. Chem.* **2004**, *6*, 256.
- (387) Patchkovskii, S.; Thiel, W. *J. Mol. Model.* **2000**, *6*, 67.
- (388) Schleyer, P. v. R.; Puhlhofer, F. *Org. Lett.* **2002**, *4*, 2873.
- (389) Sakai, S. *J. Phys. Chem. A.* **2002**, *106*, 10370.
- (390) Sakai, S. *J. Phys. Chem. A.* **2003**, *107*, 9422.
- (391) Matta, C. F.; Hernández-Trujillo, J. *J. Phys. Chem. A.* **2003**, *107*, 7496.
- (392) Corminboeuf, C.; Heine, T.; Weber, J. *Phys. Chem. Chem. Phys.* **2003**, *5*, 246.
- (393) Heine, T.; Schleyer, P. v. R.; Corminboeuf, C.; Seifert, G.; Reviakine, R.; Weber, J. *J. Phys. Chem. A.* **2003**, *107*, 6470.
- (394) Corminboeuf, C.; Heine, T.; Seifert, G.; Schleyer, P. v. R.; Weber, J. *Phys. Chem. Chem. Phys.* **2004**, *6*, 273.
- (395) Merino, G.; Heine, T.; Seifert, G. *Chem.-Eur. J.* **2004**, *10*, 4367.
- (396) Jusélius, J.; Sundholm, D.; Gauss, J. *J. Chem. Phys.* **2004**, *121*, 3952.
- (397) Johansson, M. P.; Jusélius, J.; Sundholm, D. *Angew. Chem.* **2005**, *44*, 1843.
- (398) Johansson, M. P.; Jusélius, J. *Lett. Org. Chem.* **2005**.
- (399) Cyrański, M.; Krygowski, T. *Chem. Rev.* **2005**, *105*, 3773
- (400) Aihara, J. *Chem. Phys. Lett.* **2002**, *365*, 34.
- (401) Glendening, E. D.; Badenhop, J. K.; Reed, A. E.; Carpenter, J. E.; Bohmann, J. A.; Morales, C. M.; Weinhold, F. *Theoretical Chemistry Institute, University of Wisconsin, Madison, WI* **2001**.
- (402) Fallah-Bagher-Shaidaei, H.; Wannere, C. S.; Corminboeuf, C.; Puchta, R.; Schleyer, P. *Org. Lett.* **2006**, *8*, 863.
- (403) Castro, A. C.; Osorio, E.; Jimenez-halla, J. O.; Matito, E.; Tiznado, W.; Merino, G. *J. Chem. Theory. Comput.* **2010**, *6* (9), 2701.
- (404) Matito, E.; Poater, J.; Duran, M.; Sola, M. *J. Mol. Struct. (Theochem)* **2005**, *727*, 165.
- (405) Poater, J.; Solà, M.; Viglione, R. G.; Zanasi, R. *J. Org. Chem.* **2004**, *69*, 7537.
- (406) Osuna, S.; Poater, J.; Bofill, J. M.; Alemany, P.; Solà, M. *Chem. Phys. Lett.* **2006**, *428*, 191.
- (407) Matito, E.; Feixas, F.; Sola, M. *J. Mol. Struct.* **2007**, *811*, 3.
- (408) Feixas, F.; Matito, E.; Poater, J.; Solà, M. *J. Phys. Chem. A.* **2007**, *111*, 4513.
- (409) Feixas, F.; Matito, E.; Poater, J.; Solà, M. *J. Comput. Chem.* **2008**, *29*, 1543.
- (410) Matito, E.; Salvador, P.; Duran, M.; Solà, M. *J. Phys. Chem. A.* **2006**, *110*, 5108.
- (411) Matito, E.; Solà, M.; Salvador, P.; Duran, M. *Faraday Discuss.* **2007**, *135*, 325.
- (412) Poater, J.; Duran, M.; Solà, M.; Silvi, B. *Chem. Rev.* **2005**, *105*, 3911.
- (413) Portella, G.; Poater, J.; Bofill, J. M.; Alemany, P.; Sola, M. *J. Org. Chem.* **2005**, *70*, 2509.
- (414) Poater, J.; Bofill, J.; Alemany, P.; Sola, M. *J. Phys. Chem. A.* **2005**, *109*, 10629.
- (415) Portella, G.; Poater, J.; Bofill, J. M.; Alemany, P.; Solà, M. *J. Org. Chem.* **2005**, *70*, 4560.
- (416) Güell, M.; Poater, J.; Luis, J. M.; MÓ, O.; Yáñez, M.; Solà, M. *Chem. Phys. Chem.* **2005**, *6*, 2552.
- (417) Huertas, O.; Poater, J.; Fuentes-Cabrera, M.; Orozco, M.; Solà, M.; Luque, F. J. *J. Phys. Chem. A.* **2006**, *110*, 12249.
- (418) Alonso, M.; Poater, J.; Solà, M. *Struct. Chem.* **2007**, *18*, 773.

- (419) Poater, J.; Bickelhaupt, F. M.; Solà, M. *J. Phys. Chem. A* **2007**, *111*, 5063.
- (420) Fulton, R. L. *J. Phys. Chem.* **1993**, *97*, 7516.
- (421) Bader, R. F. W.; Streitwieser, A.; Neuhaus, A.; Laidig, K. E.; Speers, P. *J. Am. Chem. Soc* **1996**, *118*, 4959.
- (422) Cioslowski, J.; Matito, E.; Solà, M. *J. Phys. Chem. A* **2007**, *111*, 6521.
- (423) Bultinck, P. *Faraday Discuss.* **2007**, *135*, 347.
- (424) Bultinck, P.; Rafat, M.; Ponec, R.; Gheluwe, B. v.; Carbó-Dorca, R.; Popelier, P. *J. Phys. Chem. A* **2006**, *110*, 7642.
- (425) Fias, S.; Damme, S. V.; Bultinck, P. *J. Comput. Chem.* **2010**, *31*, 2286.
- (426) Fias, S.; Fowler, P. W.; Cruz, J. L. D. d. I.; Hahn, U.; Bultinck, P. *J. Eur. Chem.* **2008**, *14*, 3093.
- (427) Roy, D.; Bultinck, P.; Subramanian, V.; Chattaraj, P. K. *J. Mol. Str. (THEOCHEM)* **2008**, *854* 35.
- (428) Kekulé, A. *Annalen der Chemie und Pharmacie*. **1857**, *104* (2), 129.
- (429) Mendeleïev, D. M. *J. Russ. Phys. Chem. Soc.* **1869**, *1*, 1.
- (430) Thomson, J. J. *Phil. Mag.* **1897**, *44*, 293.
- (431) Thomson, J. J. *The corpuscular Theory of Matter*. New York **1907**.
- (432) Rutherford *Phil. Mag.* **1911**, *21*, 669.
- (433) Bohr, N. *Phil. Mag. I.* **1913**, *26*, 1.
- (434) Bohr, N. *Phil. Mag. I.* **1913**, *26*, 857.
- (435) Heitler, W.; London, F. *Z. Physic.* **1928**, *44*, 579.
- (436) Pauling, L. *The Nature of Chemical Bond*, 3ed. Cornell University, Ithaca **1960**.
- (437) Mulliken, R. S. *J. Chem. Phys.* **1935**, *3*, 375.
- (438) Mayer, I. *Int. J. Quant. Chem.* **1983**, *23*, 341.
- (439) Pauli, W. *Z. Physic.* **1925**, *31*, 765.
- (440) Szabo, A.; Ostlund, N. S. *Quantum Chemistry*. McGraw-Hill Publishing Compagny, New York **1989**.
- (441) Levine, I. N. *Quantum Chemistry*. Prentice Hall **2000**.
- (442) Roothaan, C. C. J. *Rev. Mod. Phys.* **1951**, *23*, 69.
- (443) McWeeny, R.; Dierksen, G. *J. Chem. Phys.* **1968**, *49*, 4852
- (444) Pople, A.; Nesbet, R. K. *J. Chem. Phys.* **1954**, *22*, 571.
- (445) Dobson, J. F. *J. Chem. Phys.* **1991**, *94*, 4328.
- (446) Löwdin, P. O. *Adv. Chem. Phys.* **1959**, *2*, 207.
- (447) Sinanoglu, O. *Proc. N.A.S.* **1961**, *47*, 1217.
- (448) Hylleraas, E. A. *Z. Phys.* **1929**, *54*, 347.
- (449) James, H. M.; Coolidge, A. S. *J. Chem. Phys.* **1933**, *18*, 1561.
- (450) Pekeris, C. L. *Phys. Rev.* **1959**, *115*, 1216.
- (451) Koch, W.; Holthausen, M. C. *Chemist's Guide To Density Functional Theory*. Wiley VCH, Weinheim, **2000**.
- (452) Møller, C.; Plesset, M. S. *Phys. Rev.* **1934**, *46*, 618.
- (453) Head-Gordon, M.; Pople, J. A.; Frisch, M. J. *Chem. Phys. Lett.* **1988**, *153*, 503.
- (454) Bartlett, R. J.; Purvis, G. D. *Int. J. Quant. Chem.* **1978**, *14*, 516.
- (455) Purvis, G. D.; Bartlett, R. J. *J. Chem. Phys.* **1982**, *76*, 1910.
- (456) Scuseria, G. E.; Janssen, C. L.; Ill, H. F. S. *J. Chem. Phys.* **1988**, *88*, 7382.
- (457) Szalay, P. G.; Mueller, T.; Gidofalvi, G.; Lischka, H.; Shepard, R. *Chem. Rev.* **2012**, *112*, 108.
- (458) Szalay, P. G. *Configuration Interaction: Corrections for Size-Consistency*. P. vonRagué Schleyer, H. F. Schaefer, P. R. Schreiner, W. L. Jorgensen, W. Thiel, and R. C. Glen, Chchester, UK, 2005, John Wiley & Sons.
- (459) Pople, A.; Seeger, R.; Krishnan, R. *Int. J. Quant. Chem. Symp.* **1977**, *11*, 149.

- (460) Werner, H.; Knowles, P. J. *J. Chem. Phys.* **1988**, *89*, 5803.
- (461) Hinze, J.; Roothaan, C. C. J. *Progress. Theor. Physics. Supp.* **1967**, *40*, 37.
- (462) Shepard, R. *Adv. Chem. Phys.* **1987**, *69*, 63.
- (463) Roos, B. O. *Adv. Chem. Phys.* **1987**, *69*, 399.
- (464) Hohenberg, P.; Kohn, W. *Phys. Rev.* **1964**, 136.
- (465) Thomas, L. H. *Proc. Camb. Phil. Soc.* **1927**, *542*, 23.
- (466) Fermi, E. *Z. Phys.* **1928**, *48*, 73.
- (467) Weizsäcker, C. F. v. *Z. Phys.* **1935**, *96*, 431.
- (468) Kohn, W.; Sham, L. J. *Phys. Rev.* **1965**, *140*, 1133.
- (469) Slater, C. *Quantum Theory of Molecular and Solids: The Self-Consistent Field for Molecular and Solids*. McGraw-Hill, New York, **1974**, 4
- (470) Vosko, H.; Wilk, L.; Nusair, M. *Canadian J. Phys.* **1980**, *58*, 1200.
- (471) Becke, A. D. *Phys. Rev. A.* **1988**, *38*, 3098.
- (472) Gill, M. W. *Mol. Phys.* **1996**, *89*, 433.
- (473) Perdew, J. P.; Burke, K.; Ernzerhof, M. *Phys. Rev. Lett.* **1996**, *77*, 3865.
- (474) Perdew, J. P. *Phys. Rev. B.* **1986**, *33*, 8822.
- (475) Perdew, J. P.; Burke, K.; Wang, Y. *Phys. Rev. B.* **1996**, *84*, 16533.
- (476) Lee, C.; Yang, W.; Parr, R. G. *Phys. Rev. B.* **1988**, *37*, 785
- (477) Adamo, C.; Barone, V. *J. Chem. Phys.* **1999**, *110*, 6158.
- (478) Becke, A. D. *J. Chem. Phys.* **1993**, *98*, 5648.
- (479) Johnson, B. G.; Gill, P. M. W.; Pople, J. A. *J. Chem. Phys.* **1993**, *98*, 5612.
- (480) Kitaura, K.; Morokuma, K. *Int. J. Quantum. Chem.* **1976**, *10*, 325.
- (481) Morokuma, K. *Acc. Chem. Res.* **1977**, *10*, 294.
- (482) Bickelhaupt, F. M.; Baerends, E. J. *Lipkowitz, K. B., Boyd, D. B., Eds.; Wiley-VCH: New York* **2000**, *15*, 1.
- (483) Ziegler, T.; Rauk, A. *Theor. Chim. Acta.* **1977**, *46*, 1.
- (484) Ziegler, T.; Rauk, A. *Inorg. Chem.* **1979**, *18*, 1558.
- (485) Glukhovtsev, M. N.; Simkin, B. Y.; Minkin, V. I. *J. Struct. Chem.* **1987**, *28*, 483.
- (486) Nygaard, L.; Christen, D.; Nielsen, J. T.; Pedersen, E. J.; Snerling, O.; Vestergaard, E.; Sørensen, G. O. *J. Mol. Struct.* **1974**, *22*, 401.
- (487) Christen, D.; Griffiths, J. H.; Sheridan, J. Z. *Naturforsch. A.* **1982**, *36*, 1378.
- (488) Jorgensen, W. L.; McDonald, N. A. *J. Mol. Struct., THEOCHEM* **1998**, *424*, 145.
- (489) Craddock, S.; Liescheski, P. B.; Rankin, D. W. H.; Robertson, H. E. *J. Am. Chem. Soc.* **1988**, *110*, 2758.
- (490) Bickelhaupt, F. M.; Nibbering, N. M. M.; van Wezenbeek, E. M.; Baerends, E. J. *J. Phys. Chem.* **1992**, *96*, 4864.
- (491) Bickelhaupt, F. M.; Solà, M.; von RaguéSchleyer, P. J. *Comput. Chem.* **1995**, *16*, 465.
- (492) Zeng, Y.; Meng, L.; Li, X.; Zheng, S. *J. Phys. Chem. A* **2007**, *111*, 9093.
- (493) Jursic, B. S. *J. Comput. Chem.* **1996**, *17*, 835.
- (494) Allen, L. C. *J. Am. Chem. Soc.* **1989**, *111*, 9003.
- (495) Bickelhaupt, F. M.; Solà, M.; Guerra, C. F. *J. Chem. Theory Comput.* **2006**, *2*, 965.
- (496) Bickelhaupt, F. M.; Solà, M.; Guerra, C. F. *Faraday Discuss.* **2007**, *135*, 451.
- (497) Bickelhaupt, F. M.; Solà, M.; Guerra, C. F. *J. Comput. Chem.* **2007**, *28*, 238.
- (498) Rabilloud, F. *J. Comput. Chem.* **2012**, *33*, 2083.
- (499) Fokin, A. A.; Kiran, B.; Bremer, M.; Yang, X.; Jiao, H.; Schleyer, P. v. R.; Schreiner, P. R. *Chem. Eur. J.* **2000**, *6*, 1615.
- (500) Bremer, M.; Schleyer, P. v. R.; Fleischer, U. *J. Am. Chem. Soc.* **1989**, *111*, 1147.
- (501) McKee, W. C.; Wu, J. I.; Hofmann, M.; Berndt, A.; Schleyer, P. v. R. *Org. Lett.* **2012**, *14*, 5712.
- (502) Fernández, I.; Frenking, G. *Chem. Eur. J.* **2007**, *13*, 5873.

- (503) Landorf, C. W.; Haley, M. M. *Angew. Chem. Int. Ed.* **2006**, *45*, 3914.
- (504) Wright, L. J. *Dalton Trans.* **2006**, 1821.
- (505) Bleeke, J. R. *Chem. Rev.* **2001**, *101*, 1205.



---

## **Annex**

---



## A.1 Supplementary Information Chapter 3

### An Analysis of the Isomerization Energies of 1,2-/1,3-Diazacyclobutadiene, Pyrazole/Imidazole, and Pyridazine/Pyrimidine with the Turn-Upside-Down Approach

Majid El-Hamdi<sup>1</sup>, William Tiznado<sup>2</sup>, Jordi Poater<sup>\*,1</sup> and Miquel Solà<sup>\*,1</sup>

- 1: Institut de Química Computacional and Departament de Química, Universitat de Girona, Campus Montilivi, E-17071 Girona, Catalonia, Spain (Fax: +34-972-41 83 56. E-mail: jordi.poater@udg.edu and miquel.sola@udg.edu)
- 2: Departamento de Ciencias Químicas, Facultad de Ecología y Recursos Naturales, Universidad Andrés Bello, Avenida República 275, Piso 3, Santiago, Chile

**Figure S1.** Evolution of the  $\Delta E_{\text{Pauli}}$ ,  $\Delta V_{\text{elstat}}$ ,  $\Delta E_{\text{oi}}$  and  $\Delta E_{\text{bond}}$  for  $\text{CH}_3 \cdot \cdot \text{CH}_3$  (CC),  $\text{CH}_3 \cdot \cdot \text{NH}_2$  (CN) and  $\text{NH}_2 \cdot \cdot \text{NH}_2$  (NN) along the bond length distance (R) from 1.3 to 5.0 Å. Units in  $\text{kcal mol}^{-1}$ .

**Figure S2.** Evolution of the overlap between the fragment molecular orbitals with the unpaired electron, as well as the corresponding value of the Fock matrix, for  $\text{CH}_3 \cdot \cdot \text{CH}_3$  (CC),  $\text{CH}_3 \cdot \cdot \text{NH}_2$  (CN) and  $\text{NH}_2 \cdot \cdot \text{NH}_2$  (NN) along the bond length distance (R) from 1.3 to 5.0 Å. Units in  $\text{kcal mol}^{-1}$ .

Figure S1

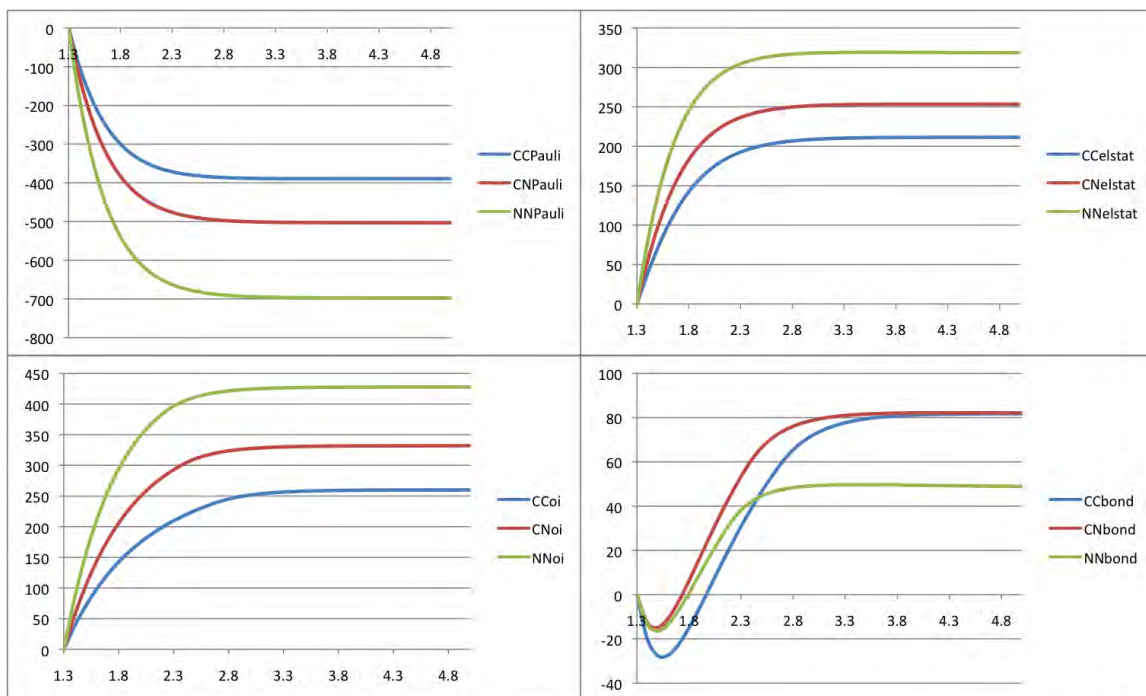
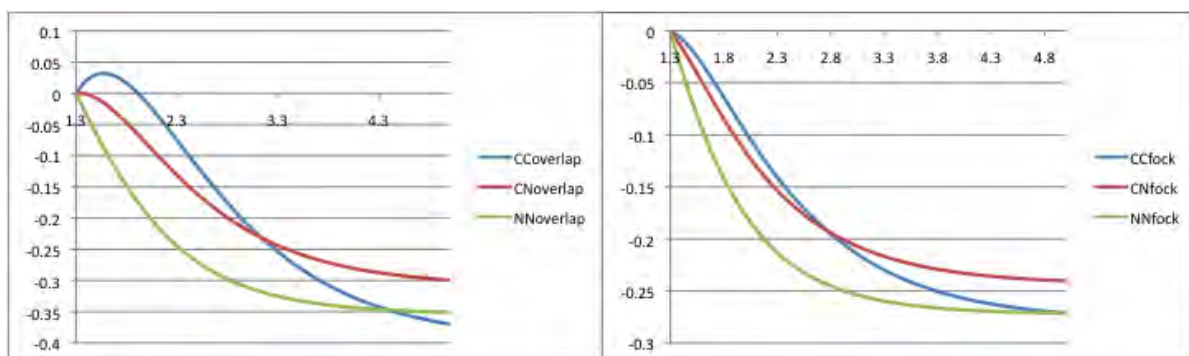


Figure S2



## A.2 Supplementary Information Chapter 4

### X<sub>2</sub>Y<sub>2</sub> Isomers: Tuning Structure and Relative Stability through Electronegativity Differences

(X = H, Li, Na, F, Cl, Br, I; Y = O, S, Se, Te)

Majid El-Hamdi,<sup>1</sup> Jordi Poater,<sup>1,\*</sup> F. Matthias Bickelhaupt<sup>2,\*</sup> and Miquel Solà<sup>1,\*</sup>

<sup>1</sup> *Institut de Química Computacional and Departament de Química, Universitat de Girona, Campus de Montilivi, 17071 Girona, Catalonia, Spain*

<sup>2</sup> *Department of Theoretical Chemistry and Amsterdam Center for Multiscale Modeling, VU University Amsterdam, De Boelelaan 1083, NL-1081 HV Amsterdam, The Netherlands, and Institute of Molecules and Materials, Radboud University Nijmegen, Heyendaalseweg 135, NL-6525 AJ Nijmegen, The Netherlands.*

**Table S2.** Experimental and calculated high level geometrical parameters of XSSX and X<sub>2</sub>SS isomers (bond lengths in Å and angles in degrees).

**Table S3.** Experimental and calculated high level geometrical parameters of XOOX and X<sub>2</sub>OO isomers (bond lengths in Å and angles in degrees).

**Table S4.** Energy decomposition analysis for XOOX and X<sub>2</sub>OO isomers (in kJmol<sup>-1</sup>).

**Table S5.** Geometrical parameters of XTeTeX and X<sub>2</sub>TeTe isomers (bond lengths in Å and angles in degrees), and isomerization relative energies (in kJ mol<sup>-1</sup>). Comparison with the inclusion of relativistic effects (ZORA) and dispersion corrections (Grimme-D<sub>3</sub>).

**Table S6.** Calculated Y-Y stretching frequencies (in cm<sup>-1</sup>) and the corresponding experimental IR frequencies, when available.

**Table S7.** Geometrical parameters of XSSX, X<sub>2</sub>SS, XOOX and X<sub>2</sub>OO isomers with X = CH<sub>3</sub> and CF<sub>3</sub> (bond lengths in Å and angles in degrees), Voronoi charges of X and Y atoms (in electrons), and isomerization relative energies (in kJ mol<sup>-1</sup>).

**Table S8.** Isomerization relative energies (in kJ mol<sup>-1</sup>) of XSSX and X<sub>2</sub>SS isomers, at the BP86/QZ4P, B3LYP/cc-pVQZ and CCSD(T)/cc-pVQZ levels.

**Figure S1.** Pauling electronegativity versus S-S bond length (in Å) plot for XSSX and X<sub>2</sub>SS series of compounds.

**Table S2.** Experimental and calculated high level geometrical parameters of XSSX and X<sub>2</sub>SS isomers (bond lengths in Å and angles in degrees).<sup>a</sup>

isomer	method	r <sub>S-S</sub>	r <sub>X-S</sub>	∠SSX	∠XSSX	Ref.
HSSH	BP86/QZ4P	2.071	1.358	98.7	90.8	this work
	MP2/6-311G++(2df,2p)	2.064	1.338	97.8	91.0	10
	QCISD/6-31++G(d,p)	2.086	1.334	98.3	90.9	70
	experimental (MW and IR)	2.0564(1)	1.3421(2)	97.88(5)	90.3(2)	71
H <sub>2</sub> SS	BP86/QZ4P	1.977	1.383	108.9	94.6/88.1 <sup>b</sup>	this work
	MP2/6-311G++(2df,2p)	1.979	1.355	108.3	89.6 <sup>b</sup>	10
FSSF	BP86/QZ4P	1.896	1.676	110.2	88.1	this work
	MP2/6-311G(2d,2p)	1.921	1.655	108.3	88.5	10
	CCSD(T)/aug-cc-pV(Q+d)Z	1.899	1.633	108.0	87.4	15
	experimental (MW)	1.888±0.01	1.635±0.01	108.3±0.5	87.9±1.5	72
F <sub>2</sub> SS	BP86/QZ4P	1.875	1.655	108.1	98.8/92.4 <sup>b</sup>	this work
	MP2/6-311G(2d,2p)	1.877	1.636	108.1	91.3 <sup>b</sup>	10
	experimental (MW)	1.860±0.015	1.598±0.012	107.5±1	92.5±1 <sup>b</sup>	72
ClSSCl	BP86/QZ4P	1.938	2.115	111.0	87.7	this work
	MP2/6-311G(2d,2p)	1.976	2.098	107.5	85.7	10
	CCSD(T)/aug-cc-pV(Q+d)Z	1.958	2.061	107.3	85.4	15
	experimental (ED)	1.97±0.03	2.07±0.01	107±2.5	82.5±12	74
Cl <sub>2</sub> SS	BP86/QZ4P	1.891	2.166	110.1	107.2/98.1 <sup>b</sup>	this work
	MP2/6-311G(2d,2p)	1.883	2.179	109.9	95.9 <sup>b</sup>	10
BrSSBr	BP86/QZ4P	1.940	2.289	111.5	87.6	this work
	CCSD(T)/aug-cc-pV(Q+d)Z	1.965	2.230	107.4	84.6	15
	CCSD(T)/CBS(D-Q)	1.959	2.223	107.4	84.5	73
	experimental (ED)	1.98±0.04	2.24±0.02	105±3	83.5±11	74
Br <sub>2</sub> SS	BP86/QZ4P	1.896	2.355	110.8	109.5/99.6 <sup>b</sup>	this work
	CCSD(T)/CBS(D-Q)	1.876	2.228	110.9	105.9	73
ISSI	BP86/QZ4P	1.961	2.497	111.8	86.6	this work
	B3LYP/6-311++G(2df)	2.004	2.417	108.4	85.3	16
I <sub>2</sub> SS	BP86/QZ4P	1.908	2.597	111.9	112.4/100.9 <sup>b</sup>	this work
	B3LYP/6-311++G(2df)	1.908	2.551	111.9	107.5	16
LiSSLi	BP86/QZ4P	2.204	2.225	60.3	117.9	this work
NaSSNa	BP86/QZ4P	2.230	2.572	64.3	135.7	this work

<sup>a</sup> Calculated r<sub>S-S</sub> for S<sub>2</sub> is 1.912 Å. <sup>b</sup> ∠XSSX angle for X<sub>2</sub>SS.

## New References

- (70) Gámez, J. A.; Serrano-Andrés, L.; Yáñez, M. *Phys. Chem. Chem. Phys.* **2009**, *12*, 1042.  
(71) Behrend, J.; Mittler, P.; Winnewisser, G.; Yamada, K. M. T. *J. Mol. Spectros.* **1991**, *150*, 99.  
(72) Kuczkowski, R. L. *J. Am. Chem. Soc.* **1964**, *86*, 3617.  
(73) Ornellas, F. R. *Chem. Phys.* **2008**, *344*, 95.  
(74) Hirota, E. *Bull. Chem. Soc. Jpn.* **1958**, *31*, 130.

**Table S3.** Experimental and calculated high level geometrical parameters of XOOX and X<sub>2</sub>OO isomers (bond lengths in Å and angles in degrees).<sup>a</sup>

isomer	method	r <sub>O-O</sub>	r <sub>X-O</sub>	∠OOX	∠XOOX	Ref.
HOOH	BP86/QZ4P	1.469	0.975	99.9	112.8	this work
	CCSD/TZ2P	1.442	0.961	100.5	111.2	<sup>75</sup>
	Experimental (IR)	1.475±0.004	0.950±0.005	94.8±2.0	119.8±2.0	<sup>75,76</sup>
H <sub>2</sub> OO	BP86/QZ4P	1.536	0.978	100.6	109.2/106.5 <sup>b</sup>	this work
	CCSD/TZ2P	1.534	0.964	106.7	106.7 <sup>b</sup>	<sup>75</sup>
FOOF	BP86/QZ4P	1.200	1.608	111.2	89.3	this work
	HF/6-31G(d)	1.311	1.367	105.8	84.1	<sup>77</sup>
	MP2/6-31G(d)	1.291	1.496	106.9	85.8	<sup>77</sup>
	B3LYP/6-311G(3df)	1.238	1.503	108.6	87.0	<sup>77</sup>
	experimental (MW)	1.217±0.003	1.575±0.003	109.5±0.5	87.5±0.5	<sup>77</sup>
F <sub>2</sub> OO	BP86/QZ4P	1.175	1.683	110.4	108.9/99.4 <sup>b</sup>	this work
ClOOCl	BP86/QZ4P	1.282	1.881	113.9	85.3	this work
	HF/cc-pVTZ	1.356	1.658	110.3	89.4	<sup>78</sup>
	MP2/cc-pCVQZ	1.414	1.698	108.9	81.8	<sup>78</sup>
	experimental	1.4259(21)	1.7044(4)	110.07(1)	81.03(1)	<sup>79,80</sup>
Cl <sub>2</sub> OO	BP86/QZ4P	1.208	2.100	114.6	117.0/101.6 <sup>b</sup>	this work
BrOOBr	BP86/QZ4P	1.283	2.034	115.0	84.2	this work
	MP2/6-311+G(2d)	1.406	1.886	111.4	84.7	<sup>81</sup>
	B3LYP/6-311++G(3df,3d)	1.335	1.922	113.3	85.6	<sup>82</sup>
Br <sub>2</sub> OO	BP86/QZ4P	1.219	2.245	115.9	119.0/101.6 <sup>b</sup>	this work
IOOI	BP86/QZ4P	1.334	2.149	115.2	79.9	this work
	MP2/ECPnMWBpol1	1.393	2.086	118.8	86.9	<sup>83</sup>
I <sub>2</sub> OO	BP86/QZ4P	1.235	2.446	118.5	119.3/98.6 <sup>b</sup>	this work
LiOOLi	BP86/QZ4P	1.585	1.734	62.8	-179.7	this work
NaOONa	BP86/QZ4P	1.601	2.092	67.5	-179.9	this work

<sup>a</sup> Calculated r<sub>O-O</sub> for O<sub>2</sub> is 1.221 Å. <sup>b</sup> ∠XOX angle for X<sub>2</sub>OO.

## New References

- (75) Meredith, C.; Hamilton, T. P.; Schaefer, H. F. *J. Phys. Chem.* **1992**, *96*, 9250.  
(76) Redington, R. L.; Olson, W. B.; Cross, P. C. *J. Chem. Phys.* **1962**, *36*, 1311.  
(77) (a) Jackson, R. H. *J. Chem. Soc.* **1962**, 4585; (b) Lucchese, R. R.; Schaefer III, H. F.; Rodwell, W. R.; Radom, L. *J. Chem. Phys.* **1978**, *68*, 2507.  
(78) Christen, D.; Mack, H. G.; Muller, H. *J. Mol. Struct.* **1999**, *509*, 137.  
(79) Birk, M.; Friedl, R. R.; Cohen, E. A.; Pickett, H. M.; Sander, S. P. *J. Chem. Phys.* **1989**, *91*, 6588.  
(80) Müller, H. S. P.; Willner, H. *Ber. Bunsenges. Phys. Chem.* **1992**, *96*, 427.  
(81) Papayannis, D.; Kosmas, A. M.; Melissas, V. S. *Chem. Phys.* **1999**, *243*, 249.  
(82) Guha, S.; Joseph, S. *J. Phys. Chem. A* **1997**, *101*, 5347.  
(83) Papayannis, D. K.; Melissas, V. S.; Kosmas, A. M. *Chem. Phys. Lett.* **2001**, *349*, 299.

**Table S4.** Energy decomposition analysis terms for XOOX and X<sub>2</sub>OO isomers (in kJ mol<sup>-1</sup>).

isomer	$\Delta E_{Pauli}$	$\Delta V_{elstat}$	$\Delta E_{oi}$	$\Delta E_{int}$	$\Delta E_{prep}$	$\Delta E$
HOOH	2132.3	-738.8	-2121.2	-727.8	122.8	-605.0
H <sub>2</sub> OO	2073.7	-740.4	-1916.7	-583.4	174.8	-408.6
FOOF	1183.0	-429.8	-1066.6	-313.4	1.5	-311.9
F <sub>2</sub> OO	879.9	-324.5	-824.8	-269.4	7.8	-261.6
CLOOCl	1308.0	-524.5	-979.7	-196.2	11.1	-185.1
Cl <sub>2</sub> OO	608.6	-250.1	-470.7	-112.2	0.5	-111.6
BrOOBr	1083.9	-458.3	-786.2	-160.6	11.2	-149.4
Br <sub>2</sub> OO	525.3	-226.6	-376.0	-77.3	0.0	-77.3
IOOI	1211.7	-533.7	-837.3	-159.3	33.5	-125.8
I <sub>2</sub> OO	456.1	-204.4	-298.7	-47.0	0.7	-46.3
LiOOLi/Li <sub>2</sub> OO	941.2	-499.8	-1195.9	-754.4	213.8	-540.6
NaOONa/Na <sub>2</sub> OO	657.2	-370.5	-801.7	-514.9	226.4	-288.6

**Table S5.** Geometrical parameters of XTeTeX and X<sub>2</sub>TeTe isomers (bond lengths in Å and angles in degrees), and isomerization relative energies (in KJ mol<sup>-1</sup>). Comparison with the inclusion of relativistic effects (ZORA) and dispersion corrections (Grimme-D<sub>3</sub>).

X	r <sub>Y-Y</sub>	r <sub>X-Y</sub>	∠YYX	∠XYYX	r <sub>Y-Y</sub>	r <sub>X-Y</sub>	∠YYX	∠XYYX	ΔE <sub>rel</sub>
	X <sub>2</sub> TeTe				XTeTeX				
<b>Manuscript Values</b>									
F	2.558	1.935	105.1	92.5	2.599	1.957	104.1	89.1	9.6
Cl	2.575	2.426	107.3	100.7	2.634	2.404	106.1	88.8	-25.9
Br	2.580	2.605	107.8	103.4	2.640	2.567	106.8	88.7	-30.5
I	2.591	2.850	108.8	106.6	2.659	2.782	107.5	88.3	-39.3
H	2.651	1.712	105.7	90.2	2.737	1.684	96.1	90.3	-85.4
Li	2.881	2.609	56.4	107.9	2.881	2.609	56.4	107.9	-
Na	2.909	2.943	60.3	117.5	2.909	2.943	60.3	117.5	-
<b>ZORA Relativistic Effects</b>									
F	2.547	1.949	105.6	94.2	2.589	1.968	104.7	89.4	5.2
Cl	2.564	2.438	107.8	102.8	2.623	2.410	106.7	89.1	-26.7
Br	2.571	2.608	108.3	105.5	2.629	2.568	107.4	89.0	-29.9
I	2.582	2.843	109.2	108.6	2.646	2.777	108.2	88.8	-36.8
H	2.649	1.710	105.5	89.8	2.733	1.680	95.9	90.0	-88.4
Li	2.879	2.596	56.3	107.0	2.879	2.596	56.3	106.9	-
Na	2.909	2.930	60.2	115.5	2.909	2.929	60.2	115.7	-
<b>Grimme-D<sub>3</sub> Dispersion Correction</b>									
F	2.556	1.935	104.7	92.4	2.597	1.957	103.5	89.1	11.0
Cl	2.572	2.423	106.7	100.1	2.631	2.402	105.2	88.6	-23.9
Br	2.577	2.599	107.2	102.1	2.637	2.564	105.5	88.1	-27.7
I	2.587	2.840	108.0	104.2	2.656	2.777	105.6	87.0	-35.9
H	2.650	1.710	105.4	89.8	2.736	1.683	95.6	90.5	-85.3
Li	2.893	2.672	57.2	106.5	2.893	2.672	57.2	106.5	-
Na	2.917	3.007	61.0	115.2	2.917	3.007	61.0	115.2	-

**Table S6.** Calculated Y-Y stretching frequencies (in  $\text{cm}^{-1}$ ) and the corresponding experimental IR frequencies, when available.

X	X <sub>2</sub> SS	XSSX
F	729	614 <sup>a</sup>
Cl	687	565 <sup>b</sup>
Br	679	565 <sup>c</sup>
I	660	539
H	800	494 <sup>d</sup>
Li	396	-
Na	402	-

<sup>a</sup> Experimental IR frequency is  $614.6 \text{ cm}^{-1}$ , from Spectrochim. Acta 26A 1986, 1375

<sup>b</sup> Experimental IR frequency is  $540 \text{ cm}^{-1}$ , from J. Chem. Phys. 1971, 55, 2715.

<sup>c</sup> Experimental IR frequency is  $534 \text{ cm}^{-1}$ , from J. Chem. Phys. 1971, 55, 2715.

<sup>d</sup> Experimental IR frequency is  $509 \text{ cm}^{-1}$ , from J. Chem. Phys. 1968, 49, 3465.

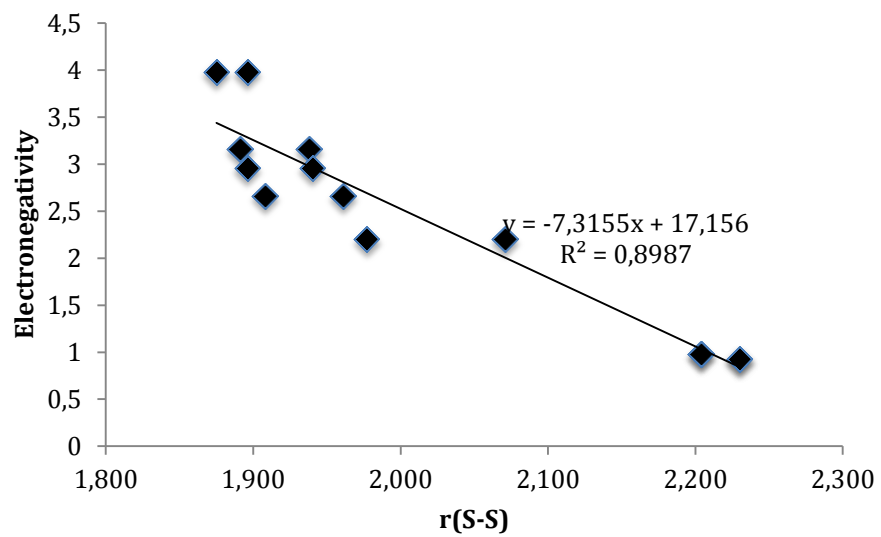
**Table S7.** Geometrical parameters of XSSX, X<sub>2</sub>SS, XOOX and X<sub>2</sub>OO isomers with X = CH<sub>3</sub> and CF<sub>3</sub> (bond lengths in Å and angles in degrees), Voronoi charges of X and Y atoms (in electrons), and isomerization relative energies (in KJ mol<sup>-1</sup>).

X	r <sub>Y-Y</sub>	r <sub>X-Y</sub>	∠YYX	∠XYXX	Q(X)	Q(Y <sub>1</sub> )	Q(Y <sub>2</sub> )	r <sub>Y-Y</sub>	r <sub>X-Y</sub>	∠YYX	∠XYXX	Q(X)	ΔE <sub>rel</sub>
	X <sub>2</sub> SS							XSSX					
CH <sub>3</sub>	1.978	1.829	107.3	103.6	0.088	-0.363	0.185	2.050	1.828	104.5	88.1	0.061	-55.4
CF <sub>3</sub>	1.936	1.953	108.9	102.7	0.035	-0.230	0.156	2.038	1.856	103.4	95.6	0.003	-106.2
	X <sub>2</sub> OO							XOOX					
CH <sub>3</sub>	1.477	1.460	107.1	121.0	0.172	-0.419	0.076	1.492	1.415	104.5	179.9	0.100	-180.7
CF <sub>3</sub>	1.462	1.517	107.6	127.2	0.190	-0.391	0.012	1.472	1.399	106.4	128.3	0.073	-275.9

**Table S8.** Isomerization relative energies (in KJ mol<sup>-1</sup>) of XSSX and X<sub>2</sub>SS isomers, at the BP86/QZ4P, B3LYP/cc-pVQZ and CCSD(T)/cc-pVQZ levels.

X	$\Delta E_{\text{rel}}$		
	BP86/QZ4P	B3LYP/cc-pVQZ	CCSD(T)/cc-pVQZ
<u>X<sub>2</sub>SS / XSSX</u>			
F	1.3	-2.7	7.4
Cl	-41.0	-53.2	-54.2
Br	-43.1	-55.8	-57.7
H	-100.4	-112.9	-117.1

**Figure S1.** Pauling electronegativity versus S-S bond length (in Å) plot for XSSX and X<sub>2</sub>SS series of compounds.





### A.3 Supplementary Information Chapter 5

#### A Comparison between Alkalimetal and Group 11 Transition Metal Halide and Hydride Tetramers: Molecular Structure and Bonding

Majid El-Hamdi,<sup>1</sup> Miquel Solà,<sup>1\*</sup> Gernot Frenking<sup>2\*</sup> and Jordi Poater<sup>1\*</sup>

<sup>1</sup> *Institut de Química Computacional i Catàlisi (IQCC) and Departament de Química, Universitat de Girona, Campus de Montilivi, E-17071 Girona, Catalonia, Spain*

<sup>2</sup> *Fachbereich Chemie, Philipps-Universität Marburg, Hans-Meerwein-Strasse, D-35039 Marburg, Germany*

**Table S2.** Structural parameters (in Å) of the isomers  $\text{Li}_4\text{X}_4$  ( $T_d$ ),  $[\text{Li}_4(\mu_2\text{-X})_4]$  ( $D_{4h}$ ) and  $\text{XLi}$  monomers.

**Table S3.** Structural parameters (in Å) of the isomers  $\text{Na}_4\text{X}_4$  ( $T_d$ ),  $[\text{Na}_4(\mu_2\text{-X})_4]$  ( $D_{4h}$ ) and  $\text{XNa}$  monomers.

**Table S4.** Structural parameters (in Å) of the isomers  $\text{K}_4\text{X}_4$  ( $T_d$ ),  $[\text{K}_4(\mu_2\text{-X})_4]$  ( $D_{4h}$ ) and  $\text{XK}$  monomers.

**Table S5.** Structural parameters (in Å) of the isomers  $\text{Rb}_4\text{X}_4$  ( $T_d$ ),  $[\text{Rb}_4(\mu_2\text{-X})_4]$  ( $D_{4h}$ ) and  $\text{XRb}$  monomers.

**Table S6:** Structural parameters (in Å) of the isomers  $\text{Cu}_4\text{X}_4$  ( $T_d$ ),  $[\text{Cu}_4(\mu_2\text{-X})_4]$  ( $D_{4h}$ ,  $D_{2d}$ ) and  $\text{XCu}$  monomers.

**Table S7:** Structural parameters (in Å) of the isomers  $\text{Ag}_4\text{X}_4$  ( $T_d$ ),  $[\text{Ag}_4(\mu_2\text{-X})_4]$  ( $D_{4h}$ ,  $D_{2d}$ ) and  $\text{XAg}$  monomers.

**Table S8:** Structural parameters (in Å) of the isomers  $\text{Au}_4\text{X}_4$  ( $T_d$ ),  $[\text{Au}_4(\mu_2\text{-X})_4]$  ( $D_{4h}$ ,  $D_{2d}$ ) and  $\text{XAu}$  monomers.

**Table S9.** Voronoi deformation density (VDD) charges of the alkalimetals and group 11 transition metals of all monomers studied. For symmetry reasons, the charge of the halogen is  $q_X = -q_M$ .

**Table S10.** Voronoi deformation density (VDD) charges of the alkalimetals and group 11 transition metals in the optimized systems. For symmetry reasons, the charge of the halogen is  $q_X = -q_M$ .

**Table S11.** Voronoi deformation density (VDD) charges of the alkalimetals and group 11 transition metals in fragments used in the EDA analysis. For symmetry reasons, the charge of the halogen is  $q_X = -q_M$ .

**Table S12.** Energy decomposition analysis (in  $\text{kcal}\cdot\text{mol}^{-1}$ ) of the tetramerization of  $\text{M}_4\text{X}_4$  systems with  $\text{M} = \text{Cu}$ ,  $\text{Ag}$ , and  $\text{Au}$ , which adopt a  $C_{3v}$  conformation.

**Table S2: Structural parameters (in Å) of the isomers  $\text{Li}_4\text{X}_4$  ( $T_d$ ),  $[\text{Li}_4(\mu_2\text{-X})_4]$  ( $D_{4h}$ ), and  $\text{LiX}$  monomers**

System	Method	X-M	M-M	X-X	ref
LiH	BP86/QZ4P	1.603	-	-	This work 506-507
	Exp.	1.5949	-	-	
$\text{Li}_4\text{H}_4$ ( $T_d$ )	BP86/QZ4P	1.843	2.488	2.715	This work 508
	BP86/TZ2P	1.879	2.525	2.777	
$[\text{c-Li}_4(\mu_2\text{-H})_4]$ ( $D_{4h}$ )	BP86/QZ4P	1.706	2.975	3.286	This work
LiF	BP86/QZ4P	1.576	-	-	This work 509
	BP86/TZ2P	1.615	-	-	
	Exp: microwave	1.56389	-	-	
$\text{Li}_4\text{F}_4$ ( $T_d$ )	BP86/QZ4P	1.841	2.438	2.750	This work 509
	BP86/TZ2P	1.859	2.483	2.761	
$[\text{c-Li}_4(\mu_2\text{-F})_4]$ ( $D_{4h}$ )	BP86/QZ4P	1.713	3.056	3.257	This work
LiCl	BP86/QZ4P	2.032	-	-	This work 511
	BP86/TZ2P	2.077	-	-	
	exptl: microwave	2.02067(6)	-	-	
$\text{Li}_4\text{Cl}_4$ ( $T_d$ )	BP86/QZ4P	2.327	2.853	3.636	This work 511
	BP86/TZ2P	2.369	2.922	3.690	
$[\text{c-Li}_4(\mu_2\text{-Cl})_4]$ ( $D_{4h}$ )	BP86/QZ4P	2.192	3.643	4.300	This work
LiBr	BP86/QZ4P	2.183	-	-	This work
$\text{Li}_4\text{Br}_4$ ( $T_d$ )	BP86/QZ4P	2.493	2.978	3.940	This work
$[\text{c-Li}_4(\mu_2\text{-Br})_4]$ ( $D_{4h}$ )	BP86/QZ4P	2.351	3.801	4.644	This work
LiI	BP86/QZ4P	2.405	-	-	This work
$\text{Li}_4\text{I}_4$ ( $T_d$ )	BP86/QZ4P	2.727	3.142	4.373	This work
$[\text{c-Li}_4(\mu_2\text{-I})_4]$ ( $D_{4h}$ )	BP86/QZ4P	2.583	4.031	5.131	This work

**Table S3: Structural parameters (in Å) of the isomers Na<sub>4</sub>X<sub>4</sub> (T<sub>d</sub>), [Na<sub>4</sub>(μ<sub>2</sub>-X)<sub>4</sub>] (D<sub>4h</sub>), and NaX monomer**

System	Method	X-M	M-M	X-X	ref
NaH	BP86/QZ4P	1.895	-	-	This work 508 513-514
	BP86/TZ2P	1.935	-	-	
	Exp.	1.8874	-	-	
Na <sub>4</sub> H <sub>4</sub> (T <sub>d</sub> )	BP86/QZ4P	2.225	3.074	3.216	This work 508
	BP86/TZ2P	2.300	3.155	3.345	
[c-Na <sub>4</sub> (μ <sub>2</sub> -H) <sub>4</sub> ] (D <sub>4h</sub> )	BP86/QZ4P	2.049	3.643	3.902	This work
NaF	BP86/QZ4P	1.949	-	-	This work 515 516
	Exp: microwave	1.92595	-	-	
	Exp: electron diffraction	1.917(2)	-	-	
Na <sub>4</sub> F <sub>4</sub> (T <sub>d</sub> )	BP86/QZ4P	2.188	3.019	3.166	This work 509
	BP86/TZ2P	2.241	3.095	3.241	
[c-Na <sub>4</sub> (μ <sub>2</sub> -F) <sub>4</sub> ] (D <sub>4h</sub> )	BP86/QZ4P	2.074	3.759	3.897	This work
NaCl	BP86/QZ4P	2.381	-	-	This work 517-518 519 519 519
	exptl: microwave	2.3606(1)	-	-	
	exptl: microwave	2.3609	-	-	
	exptl: electron diffraction	2.359(8)	-	-	
	exptl: electron diffraction	2.388(8)	-	-	
Na <sub>4</sub> Cl <sub>4</sub> (T <sub>d</sub> )	BP86/QZ4P	2.666	3.460	4.036	This work 511
	BP86/TZ2P	2.727	3.545	4.123	
[c-Na <sub>4</sub> (μ <sub>2</sub> -Cl) <sub>4</sub> ] (D <sub>4h</sub> )	BP86/QZ4P	2.535	4.372	4.906	This work
NaBr	BP86/QZ4P	2.524	-	-	This work
Na <sub>4</sub> Br <sub>4</sub> (T <sub>d</sub> )	BP86/QZ4P	2.825	3.585	4.336	This work
[c-Na <sub>4</sub> (μ <sub>2</sub> -Br) <sub>4</sub> ] (D <sub>4h</sub> )	BP86/QZ4P	2.687	4.529	5.248	This work
NaI	BP86/QZ4P	2.735	-	-	This work
Na <sub>4</sub> I <sub>4</sub> (T <sub>d</sub> )	BP86/QZ4P	3.056	3.759	4.767	This work
[c-Na <sub>4</sub> (μ <sub>2</sub> -I) <sub>4</sub> ] (D <sub>4h</sub> )	BP86/QZ4P	2.912	4.762	5.737	This work

**Table S4: Structural parameters (in Å) of the isomers  $K_4X_4$  ( $T_d$ ),  $[K_4(\mu_2-X)_4]$  ( $D_{4h}$ ), and  $KX$  monomers**

System	Method	X-M	M-M	X-X	ref
KH	BP86/QZ4P	2.232	-	-	This work
	BP86/TZ2P	2.310	-	-	<sup>508</sup>
	Exp.	2.240	-	-	513-514
$K_4H_4$ ( $T_d$ )	BP86/QZ4P	2.592	3.736	3.592	This work
	BP86/TZ2P	2.656	3.783	3.729	<sup>508</sup>
$[c-K_4(\mu_2-H)_4]$ ( $D_{4h}$ )	BP86/QZ4P	2.437	4.546	4.458	This work
KF	BP86/QZ4P	2.163	-	-	This work
	BP86/TZ2P	2.296	-	-	<sup>509</sup>
	Exp: microwave	2.17144	-	-	520
	Exp: electron diffraction	2.161(4)	-	-	516
$K_4F_4$ ( $T_d$ )	BP86/QZ4P	2.485	3.590	3.434	This work
	BP86/TZ2P	2.548	3.664	3.540	<sup>509</sup>
$[c-K_4(\mu_2-F)_4]$ ( $D_{4h}$ )	BP86/QZ4P	2.373	4.464	4.297	This work
KCl	BP86/QZ4P	2.666	-	-	This work
	BP86/TZ2P	2.769	-	-	<sup>511</sup>
	exptl: microwave	2.6666(1)	-	-	518,521
	exptl: microwave	2.6668	-	-	519
	exptl: electron diffraction	2.669(8)	-	-	519
	exptl: electron diffraction	2.703(8)	-	-	519
$K_4Cl_4$ ( $T_d$ )	BP86/QZ4P	2.991	4.103	4.349	This work
	BP86/TZ2P	3.046	4.167	4.439	<sup>511</sup>
$[c-K_4(\mu_2-Cl)_4]$ ( $D_{4h}$ )	BP86/QZ4P	2.873	5.204	5.402	This work
KBr	BP86/QZ4P	2.824			This work
$K_4Br_4$ ( $T_d$ )	BP86/QZ4P	3.156	4.254	4.656	This work
$[c-K_4(\mu_2-Br)_4]$ ( $D_{4h}$ )	BP86/QZ4P	3.033	5.412	5.764	This work
KI	BP86/QZ4P	3.056			This work
$K_4I_4$ ( $T_d$ )	BP86/QZ4P	3.398	4.464	5.103	This work
$[c-K_4(\mu_2-I)_4]$ ( $D_{4h}$ )	BP86/QZ4P	3.270	5.706	6.295	This work

**Table S5: Structural parameters (in Å) of the isomers  $\text{Rb}_4\text{X}_4$  ( $T_d$ ),  $[\text{Rb}_4(\mu_2\text{-X})_4]$  ( $D_{4h}$ ), and  $\text{RbX}$  monomers**

System	Method	X-M	M-M	X-X	ref
RbH	BP86/QZ4P	2.356	-	-	This work
	BP86/TZ2P	2.405	-	-	<sup>508</sup>
	Exp.	2.367	-	-	513-514
$\text{Rb}_4\text{H}_4$ ( $T_d$ )	BP86/QZ4P	2.732	4.001	3.716	This work
	BP86/TZ2P	2.774	3.939	3.907	<sup>508</sup>
$[\text{c-Rb}_4(\mu_2\text{-H})_4]$ ( $D_{4h}$ )	BP86/QZ4P	2.583	4.900	4.621	This work
RbF	BP86/QZ4P	2.267	-	-	This work
	BP86/TZ2P	2.397	-	-	<sup>509</sup>
	Exp: microwave	2.26554	-	-	522
	Exp: electron diffraction	2.268(8)	-	-	516
$\text{Rb}_4\text{F}_4$ ( $T_d$ )	BP86/QZ4P	2.612	3.847	3.528	This work
	BP86/TZ2P	2.650	3.820	3.673	<sup>509</sup>
$[\text{c-Rb}_4(\mu_2\text{-F})_4]$ ( $D_{4h}$ )	BP86/QZ4P	2.497	4.768	4.422	This work
RbCl	BP86/QZ4P	2.790	-	-	This work
	BP86/TZ2P	2.878	-	-	<sup>511</sup>
	exptl: microwave	2.78670(6)	-	-	523
	exptl: microwave	2.7869	-	-	519
	exptl: electron diffraction	2.784(4)	-	-	519
	exptl: electron diffraction	2.817(4)	-	-	519
$\text{Rb}_4\text{Cl}_4$ ( $T_d$ )	BP86/QZ4P	3.131	4.374	4.479	This work
	BP86/TZ2P	3.163	4.336	4.603	<sup>511</sup>
$[\text{c-Rb}_4(\mu_2\text{-Cl})_4]$ ( $D_{4h}$ )	BP86/QZ4P	3.014	5.552	5.588	This work
RbBr	BP86/QZ4P	2.951	-	-	This work
$\text{Rb}_4\text{Br}_4$ ( $T_d$ )	BP86/QZ4P	3.296	4.527	4.789	This work
$[\text{c-Rb}_4(\mu_2\text{-Br})_4]$ ( $D_{4h}$ )	BP86/QZ4P	3.176	5.770	5.959	This work
RbI	BP86/QZ4P	3.188	-	-	This work
$\text{Rb}_4\text{I}_4$ ( $T_d$ )	BP86/QZ4P	3.541	4.747	5.244	This work
$[\text{c-Rb}_4(\mu_2\text{-I})_4]$ ( $D_{4h}$ )	BP86/QZ4P	3.417	6.087	6.502	This work

**Table S6: Structural parameters (in Å) of the isomers  $\text{Cu}_4\text{X}_4$  ( $\text{T}_d$ ),  $[\text{Cu}_4(\mu_2\text{-X})_4]$  ( $\text{D}_{4h}$ ,  $\text{D}_{2d}$ ), and  $\text{CuX}$  monomers**

System	method	X-M	M-M	X-X	ref
CuH	BP86/QZ4P	1.452	-	-	This work
$\text{Cu}_4\text{H}_4$ $\text{T}_d$	BP86/QZ4P	1.785	2.373	2.659	This work
$[\text{c-Cu}_4(\mu_2\text{-H})_4]$ $\text{D}_{4h}$	BP86/QZ4P	1.618	2.348	3.234	This work
	BP86/cc-pVDZ-PP/Ucc pVDZ(E)	1.624	2.344	-	<sup>524</sup>
CuF	BP86/QZ4P	1.739	-	-	This work
$\text{Cu}_4\text{F}_4$ $\text{T}_d$	BP86/QZ4P	2.127	2.501	3.384	This work
$[\text{c-Cu}_4(\mu_2\text{-F})_4]$ $\text{D}_{4h}$	BP86/QZ4P	1.850	2.568	3.699	This work
	BP86/cc-pVDZ-PP/Ucc pVDZ(E)	1.860	2.570	-	<sup>524</sup>
CuCl	BP86/QZ4P	2.041	-	-	This work
$\text{Cu}_4\text{Cl}_4$ $\text{T}_d$	BP86/QZ4P	2.375	2.511	3.908	This work
$[\text{c-Cu}_4(\mu_2\text{-Cl})_4]$ $\text{D}_{4h}$	BP86/QZ4P	2.135	2.694	4.247	This work
$[\text{c-Cu}_4(\mu_2\text{-Cl})_4]$ $\text{D}_{2d}$	BP86/QZ4P	2.141	2.619	4.276	This work
	BP86/cc-pVDZ-PP/Ucc pVDZ(E)	2.168	2.565	-	<sup>524</sup>
CuBr	BP86/QZ4P	2.172	-	-	This work
$\text{Cu}_4\text{Br}_4$ $\text{T}_d$	BP86/QZ4P	2.499	2.514	4.160	This work
$[\text{c-Cu}_4(\mu_2\text{-Br})_4]$ $\text{D}_{4h}$	BP86/QZ4P	2.274	2.663	4.489	This work
$[\text{c-Cu}_4(\mu_2\text{-Br})_4]$ $\text{D}_{2d}$	BP86/QZ4P	2.281	2.585	4.553	This work
CuI	BP86/QZ4P	2.342	-	-	This work
$\text{Cu}_4\text{I}_4$ $\text{T}_d$	BP86/QZ4P	2.654	2.524	4.464	This work
$[\text{c-Cu}_4(\mu_2\text{-I})_4]$ $\text{D}_{4h}$	BP86/QZ4P	2.455	2.631	4.792	This work

**Table S7: Structural parameters (in Å) of the isomers  $\text{Ag}_4\text{X}_4$  ( $\text{T}_d$ ),  $[\text{Ag}_4(\mu_2\text{-X})_4]$  ( $\text{D}_{4h}$ ,  $\text{D}_{2d}$ ), and  $\text{AgX}$  monomers**

System	method	X-M	M-M	X-X	ref
AgH	BP86/QZ4P	1.612			This work
$\text{Ag}_4\text{H}_4 \text{ T}_d$	BP86/QZ4P	2.004	2.762	2.902	This work
$[\text{c-Ag}_4(\mu_2\text{-H})_4] \text{ D}_{4h}$	BP86/QZ4P	1.790	2.710	3.571	This work <sup>524</sup>
	BP86/cc-pVDZ-PP/Ucc -pVDZ(E)	1.789	2.713	-	
AgF	BP86/QZ4P	1.991			This work
$\text{Ag}_4\text{F}_4 \text{ T}_d$	BP86/QZ4P	2.338	3.157	3.443	This work
$[\text{c-Ag}_4(\mu_2\text{-F})_4] \text{ D}_{4h}$	BP86/QZ4P	2.089	2.983	4.179	This work <sup>524</sup>
	BP86/cc-pVDZ-PP/Ucc -pVDZ(E)	2.088	3.010	-	
AgCl	BP86/QZ4P	2.289			This work
$\text{Ag}_4\text{Cl}_4 \text{ T}_d$	BP86/QZ4P	2.632	2.983	4.245	This work
$[\text{c-Ag}_4(\mu_2\text{-Cl})_4] \text{ D}_{4h}$	BP86/QZ4P	2.361	3.174	4.717	This work
$[\text{c-Ag}_4(\mu_2\text{-Cl})_4] \text{ D}_{2d}$	BP86/QZ4P	2.368	3.058	4.734	This work <sup>524</sup>
	BP86/cc-pVDZ-PP/Ucc -pVDZ(E)	2.379	3.105	-	
AgBr	BP86/QZ4P	2.409			This work
$\text{Ag}_4\text{Br}_4 \text{ T}_d$	BP86/QZ4P	2.743	2.963	4.490	This work
$[\text{c-Ag}_4(\mu_2\text{-Br})_4] \text{ D}_{4h}$	BP86/QZ4P	2.485	3.234	4.955	This work
$[\text{c-Ag}_4(\mu_2\text{-Br})_4] \text{ D}_{2d}$	BP86/QZ4P	2.496	3.026	4.991	This work <sup>524</sup>
	BP86/cc-pVDZ-PP/Ucc -pVDZ(E)	2.506	3.025	-	
AgI	BP86/QZ4P	2.568			This work
$\text{Ag}_4\text{I}_4 \text{ T}_d$	BP86/QZ4P	2.888	2.957	4.789	This work
$[\text{c-Ag}_4(\mu_2\text{-I})_4] \text{ D}_{4h}$	BP86/QZ4P	2.643	3.476	5.274	This work
$[\text{c-Ag}_4(\mu_2\text{-I})_4] \text{ D}_{2d}$	BP86/QZ4P	2.660	3.019	5.317	This work <sup>524</sup>
	BP86/cc-pVDZ-PP/Ucc -pVDZ(E)	2.675	3.014	-	

**Table S8: Structural parameters (in Å) of the isomers Au<sub>4</sub>X<sub>4</sub> (T<sub>d</sub>), Au<sub>4</sub>(μ<sub>2</sub>-X)<sub>4</sub> (D<sub>4h</sub>, D<sub>2d</sub>), and AuX monomers**

System	method	X-M	M-M	X-X	ref
AuH	BP86/QZ4P	1.538	-	-	This work
Au <sub>4</sub> H <sub>4</sub> T <sub>d</sub>	BP86/QZ4P	1.907	2.976	2.343	This work
[c-Au <sub>4</sub> (μ <sub>2</sub> -H) <sub>4</sub> ] D <sub>4h</sub>	BP86/QZ4P	1.788	2.672	3.571	This work
	BP86/cc-pVDZ-PP/Ucc -pVDZ(E)	1.792	2.689	-	<sup>524</sup>
AuF	BP86/QZ4P	1.941	-	-	This work
Au <sub>4</sub> F <sub>4</sub> T <sub>d</sub>	BP86/QZ4P	2.456	2.832	3.936	This work
[c-Au <sub>4</sub> (μ <sub>2</sub> -F) <sub>4</sub> ] D <sub>4h</sub>	BP86/QZ4P	2.064	2.944	4.128	This work
	BP86/cc-pVDZ-PP/Ucc -pVDZ(E)	2.083	2.992	-	<sup>524</sup>
AuCl	BP86/QZ4P	2.225	-	-	This work
Au <sub>4</sub> Cl <sub>4</sub> T <sub>d</sub>	BP86/QZ4P	2.689	2.865	4.417	This work
[c-Au <sub>4</sub> (μ <sub>2</sub> -Cl) <sub>4</sub> ] D <sub>4h</sub>	BP86/QZ4P	2.315	3.249	4.630	This work
[c-Au <sub>4</sub> (μ <sub>2</sub> -Cl) <sub>4</sub> ] D <sub>2d</sub>	BP86/QZ4P	2.316	3.220	4.633	This work
	BP86/cc-pVDZ-PP/Ucc -pVDZ(E)	2.346	3.181	-	<sup>524</sup>
AuBr	BP86/QZ4P	2.352	-	-	This work
Au <sub>4</sub> Br <sub>4</sub> T <sub>d</sub>	BP86/QZ4P	2.786	2.874	4.612	This work
[c-Au <sub>4</sub> (μ <sub>2</sub> -Br) <sub>4</sub> ] D <sub>4h</sub>	BP86/QZ4P	2.440	3.378	4.878	This work
[c-Au <sub>4</sub> (μ <sub>2</sub> -Br) <sub>4</sub> ] D <sub>2d</sub>	BP86/QZ4P	2.456	3.085	4.910	This work
	BP86/cc-pVDZ-PP/Ucc -pVDZ(E)	2.472	3.132	-	<sup>524</sup>
AuI	BP86/QZ4P	2.510	-	-	This work
Au <sub>4</sub> I <sub>4</sub> T <sub>d</sub>	BP86/QZ4P	2.899	2.904	4.829	This work
[c-Au <sub>4</sub> (μ <sub>2</sub> -I) <sub>4</sub> ] D <sub>4h</sub>	BP86/QZ4P	2.597	3.659	5.193	This work
[c-Au <sub>4</sub> (μ <sub>2</sub> -I) <sub>4</sub> ] D <sub>2d</sub>	BP86/QZ4P	2.624	3.034	5.244	This work
	BP86/cc-pVDZ-PP/Ucc -pVDZ(E)	2.649	3.044	-	<sup>524</sup>

**Table S9.** Voronoi deformation density (VDD) charges of the alkalimetals and group 11 transition metals of all monomers studied. For symmetry reasons, the charge of the halogen is  $q_X = -q_M$ .

$X \downarrow \backslash M \rightarrow$	Li	Na	K	Rb	Cu	Ag	Au
H	0.456	0.446	0.513	0.509	0.196	0.201	0.080
F	0.506	0.605	0.568	0.552	0.364	0.413	0.272
Cl	0.464	0.575	0.613	0.619	0.298	0.358	0.406
Br	0.435	0.546	0.605	0.616	0.255	0.316	0.369
I	0.402	0.508	0.589	0.598	0.197	0.257	0.314

**Table S10.** Voronoi deformation density (VDD) charges of the alkalimetals and group 11 transition metals in the optimized systems. For symmetry reasons, the charge of the halogen is  $q_X = -q_M$ .

$X \downarrow \backslash M \rightarrow$	Li		Na		K		Rb	
	$T_d$	$D_{4h}$	$T_d$	$D_{4h}$	$T_d$	$D_{4h}$	$T_d$	$D_{4h}$
H	0.282	0.323	0.364	0.381	0.389	0.409	0.386	0.405
F	0.304	0.341	0.415	0.447	0.401	0.419	0.392	0.406
Cl	0.247	0.308	0.389	0.443	0.417	0.472	0.425	0.480
Br	0.221	0.285	0.369	0.426	0.411	0.475	0.425	0.488
I	0.182	0.246	0.336	0.394	0.400	0.470	0.421	0.494

$X \downarrow \backslash M \rightarrow$	Cu			Ag			Au		
	$T_d$	$D_{4h}$	$D_{2d}$	$T_d$	$D_{4h}$	$D_{2d}$	$T_d$	$D_{4h}$	$D_{2d}$
H	0.239	0.221		0.239	0.214		0.143	0.156	
F	0.296	0.244		0.346	0.279		0.317	0.172	
Cl	0.200	0.172	0.172	0.269	0.221	0.222	0.209	0.120	0.121
Br	0.149	0.126	0.126	0.218	0.178	0.180	0.150	0.074	0.082
I	0.086	0.069	0.068	0.152	0.122	0.123	0.071	0.012	0.029

**Table S11.** Voronoi deformation density (VDD) charges of the alkalimetals and group 11 transition metals in fragments used in the EDA analysis. For symmetry reasons, the charge of the halogen is  $q_X = -q_M$ .

$X \downarrow \setminus M \rightarrow$	Li		Na		K		Rb	
	$T_d$	$D_{4h}$	$T_d$	$D_{4h}$	$T_d$	$D_{4h}$	$T_d$	$D_{4h}$
H	0.455	0.455	0.454	0.450	0.531	0.525	0.535	0.516
F	0.555	0.531	0.632	0.620	0.646	0.626	0.642	0.608
Cl	0.525	0.497	0.616	0.594	0.661	0.645	0.671	0.645
Br	0.499	0.473	0.588	0.572	0.646	0.629	0.665	0.648
I	0.464	0.435	0.556	0.533	0.635	0.613	0.648	0.637

$X \downarrow \setminus M \rightarrow$	Cu			Ag			Au		
	$T_d$	$D_{4h}$	$D_{2d}$	$T_d$	$D_{4h}$	$D_{2d}$	$T_d$	$D_{4h}$	$D_{2d}$
H	0.194	0.194		0.220	0.210		0.084	0.082	
F	0.448	0.392		0.487	0.440		0.388	0.311	
Cl	0.350	0.313	0.314	0.410	0.370	0.372	0.276	0.228	0.228
Br	0.302	0.270	0.271	0.362	0.328	0.329	0.217	0.181	0.183
I	0.234	0.211	0.212	0.294	0.266	0.268	0.138	0.117	0.118

**Table S12.** Energy decomposition analysis (in kcal·mol<sup>-1</sup>) of the tetramerization of M<sub>4</sub>X<sub>4</sub> systems with M = Cu, Ag, and Au, which adopt a C<sub>3v</sub> conformation.<sup>a</sup>

	<b>Cu<sub>4</sub>F<sub>4</sub></b>	<b>Ag<sub>4</sub>H<sub>4</sub></b>	<b>Au<sub>4</sub>H<sub>4</sub></b>	<b>Au<sub>4</sub>F<sub>4</sub></b>	<b>Au<sub>4</sub>Cl<sub>4</sub></b>	<b>Au<sub>4</sub>Br<sub>4</sub></b>	<b>Au<sub>4</sub>I<sub>4</sub></b>
$\Delta E_{\text{Pauli}}$	279.77	328.53	403.66	340.82	385.91	380.10	387.75
$\Delta E_{\text{elstat}}$	-255.75	-282.20	-266.28	-277.86	-310.60	-308.60	-313.71
$\Delta E_{\text{oi}}$	-184.87	-145.74	-212.38	-202.39	-217.79	-213.44	-214.50
$\Delta E_{\text{int}}$	-160.84	-99.42	-74.99	-139.43	-142.48	-141.94	-140.45
$\Delta E_{\text{def}}$	14.61	15.55	20.71	20.25	10.32	8.41	6.72
$\Delta E$	-146.23	-83.87	-54.28	-119.18	-132.16	-133.53	-133.73

<sup>a</sup>  $\Delta E = E(\text{M}_4\text{X}_4) - 4E(\text{MX})$ .

## A.4 Supplementary Information Chapter 6

An Analysis of the Relative Stabilities of Ortho, Meta, and Para  
MClY(XC<sub>4</sub>H<sub>4</sub>)(PH<sub>3</sub>)<sub>2</sub> Heterometallabenzenes (M = Ir, Rh; X = N, P; Y = Cl and M  
= Os, Ru; X = N, P; Y = CO)

Majid El-Hamdi<sup>1,2</sup>, Ouissam El Bakouri El Farri<sup>1</sup>, Pedro Salvador<sup>1</sup>, Ben Ali  
Abdelouahid<sup>2</sup>, Mohamed Soussi El Begrani<sup>2</sup>, Jordi Poater<sup>\*,1</sup> and Miquel Solà<sup>\*,1</sup>

1: Institut de Química Computacional and Departament de Química, Universitat de Girona,  
Campus Montilivi, E-17071 Girona, Catalonia, Spain (Fax: +34-972-41 83 56. E-mail:  
[jordi.poater@udg.edu](mailto:jordi.poater@udg.edu) and [miquel.sola@udg.edu](mailto:miquel.sola@udg.edu))

2: Département de Chimie, Faculté des Sciences, Université Abdelmalek Essaâdi, M'Hannech II  
B.P.2121, C.P. 93002 Tétouan, Morocco

**Tables S2; S3; S4; S5; S6; S7; S8; S9 ; S10 ; S11:** EDA results of: o-OsP, m-OsP, m-OsP<sub>a</sub>, m-OsP<sub>b</sub>, m-OsP, p-OsP, p-OsP<sub>a</sub>, m-OsP<sub>b</sub>, o-RuN, m-RuN, m-RuN1, p-RuN, m-RuN<sub>a</sub>, m-RuN<sub>b</sub>, p-RuN<sub>a</sub>, p-RuN<sub>b</sub>, o-RuP, m-RuP, m-RuP1, p-RuP, m-RuP<sub>a</sub>, m-RuP<sub>b</sub>, p-RuP<sub>a</sub>, p-RuP<sub>b</sub>; o-OsN, m-OsN, m-OsN1, p-OsN, m-OsN<sub>a</sub>, m-OsN<sub>b</sub>, p-OsN<sub>a</sub>, p-OsN<sub>b</sub>, o-OsP, m-OsP, m-OsP1, p-OsP, m-OsP<sub>a</sub>, m-OsP<sub>b</sub>, p-OsP<sub>a</sub>, p-OsP<sub>b</sub>

**Table S12:** Voronoi charges (electrons) of fragments (see Figure 1): A(o-MX)<sub>X</sub>, A(m-MX)<sub>X</sub>, A1(m-MX)<sub>X</sub>, A(p-MX)<sub>X</sub>; B(o-MX)<sub>M</sub>, B(m-MX)<sub>M</sub>, B1(m-MX)<sub>M</sub>, B(p-MX)<sub>M</sub> fragments (with M= Ir, Rh, Ru, Os; X= N, P; Y=Cl or CO) used in the studies of energy decomposition analysis (EDA).

**Table S13:** Energies of the optimized singlet and the triplet states of ortho, meta, and para M(Cl)Y(XC<sub>4</sub>H<sub>4</sub>)(PH<sub>3</sub>)<sub>2</sub> heterometallabenzenes (M = Rh, Ir; X = N, P; Y = Cl and M = Ru, Os; X = N, P; Y = CO).

**Table S14.** Contribution of the atomic orbitals of the metal to the π-molecular orbitals of the system (in %).

**Figure S1:** Optimized molecular geometries obtained using the ChemCraft software.

**Figure S2:** Plot of the valence π orbitals of the ring of meta-osmapyridine compound.

**Table S2.** Analysis of the bonding (in kcal/mol) between triplet Phosphaethenyl  $A(x\text{-OsP})_p$  and triplet  $\text{OsCl}(\text{CO})(\text{PH}_3)_2(\text{C}_3\text{H}_3)$   $B(x\text{-OsP})_{\text{Os}}$  fragments in **o-OsP**, **m-OsP**, and deformed m-OsP (**m-OsP<sub>a</sub>** and **m-OsP<sub>b</sub>**).<sup>a</sup> In parenthesis the differences with respect to the values for the **o-OsP** system.

	<b>o-OsP</b>		<b>m-OsP</b>		<b>m-OsP<sub>a</sub></b>		<b>m-OsP<sub>b</sub></b>	
	A(o-OsP) <sub>p</sub> + B(o-OsP) <sub>Os</sub>		A(m-OsP) <sub>p</sub> + B(m-OsP) <sub>Os</sub>		A(o-OsP) <sub>p</sub> + B(o-OsP) <sub>Os</sub>		A(o-OsP) <sub>p</sub> + B(o-OsP) <sub>Os</sub>	
$\Delta E_{\text{Pauli}}$	513.78		436.80 (-76.98)		753.53 (239.75)		440.95 (-72.83)	
$\Delta V_{\text{elstat}}$	-334.70		-298.21 (36.49)		-421.55 (-86.85)		-299.61 (35.09)	
$\Delta E_{\text{oi}}$	-398.62		-341.50 (57.12)		-451.75 (-53.13)		-342.88 (55.74)	
$\Delta E_{\text{oi}}(\sigma)$	-348.35		-305.70 (42.65)		-372.39 (-24.04)		-305.40 (42.95)	
$\Delta E_{\text{oi}}(\pi)$	-50.27		-35.80 (14.47)		-79.37 (-29.10)		-37.48 (12.79)	
$\Delta E_{\text{int}}$	-219.53		-202.91 (16.62)		-119.77 (99.76)		-201.54 (17.99)	
$\Delta E_{\text{def}}$	48.46		44.95 (-3.51)		48.46 (0.00)		48.46 (0.00)	
$\Delta E_{\text{tot}}^{\text{b}}$	-171.07		-157.96 (13.11)		-71.31 (99.76)		-153.08 (17.99)	
$\Delta E_{\text{bondexact}}^{\text{b}}$	-163.14		-146.35 (16.79)		-63.28 (99.86)		-145.32 (17.82)	
Correct.f <sup>b</sup>	<b>0.95</b>		<b>0.93</b>		<b>0.89<sup>d</sup></b>		<b>0.95</b>	

<sup>a</sup> Computed at BP86/TZ2P. See Scheme 1 for structures.  $A_p/B_{\text{Os}}(\text{o-OsP})$  and  $A_p/B_{\text{Os}}(\text{m-OsP})$  refer to  $A_p/B_{\text{Os}}$  in the geometry it adopts in **o-OsP** and **m-OsP**, respectively; **m-OsP<sub>a</sub>** is **m-OsP** with frozen  $A_p/B_{\text{Os}}(\text{o-OsP})$  fragments but with connecting C-P and Os-C bond distances as the corresponding C-C and Os-P bond lengths in **o-OsP** (1.409 Å and 2.430 Å); **m-OsP<sub>b</sub>** is **m-OsP** with frozen  $A_p/B_{\text{Os}}(\text{o-OsP})$  fragments but with connecting C-P and Os-C bond distances as the optimized bond lengths in **m-OsP** (1.787 Å and 2.095 Å).

<sup>b</sup>  $\Delta E_{\text{bondexact}}$  is the exact bonding energy while  $\Delta E_{\text{tot}}$  is the sum of  $\Delta E_{\text{int}}$  and  $\Delta E_{\text{def}}$  and it is the bonding energy without taking into account the spin polarization effects in the fragment (see Theoretical Methods Section). Correct.f gives the  $\Delta E_{\text{bondexact}}/\Delta E_{\text{tot}}$  ratio that is a measure of the error in the different energy components because of the lack of spin polarization effects in the fragments.

<sup>d</sup> Low Correct.f factor due to constrained geometry that leads to low  $\Delta E_{\text{tot}}$  and  $\Delta E_{\text{bondexact}}$  values.

**Table S3.** Analysis of the bonding (in kcal/mol) between triplet phosphoethenyl A(x-OsP)<sub>p</sub> and triplet OsCl(CO)(PH<sub>3</sub>)<sub>2</sub>(C<sub>3</sub>H<sub>3</sub>) B(x-OsP)<sub>Os</sub> fragments in **m-OsP**, **p-OsP**, and Deformed **p-OsP** (**p-OsP<sub>a</sub>** and **p-OsP<sub>b</sub>**).<sup>a</sup> In parenthesis the differences with respect to the values for the **m-OsP** system.

	<b>m-OsP</b>		<b>p-OsP</b>		<b>p-OsP<sub>a</sub></b>		<b>p-OsP<sub>b</sub></b>	
	A1(m-OsP) <sub>p</sub> + B1(m-OsP) <sub>Os</sub>		A(p-OsP) <sub>p</sub> + B(p-OsP) <sub>Os</sub>		A1(m-OsP) <sub>p</sub> + B1(m-OsP) <sub>Os</sub>		A1(m-OsP) <sub>N</sub> +B1(m-OsP) <sub>Os</sub>	
$\Delta E_{\text{Pauli}}$	653.43		671.38 (17.95)		863.05 (209.62)		667.60 (14.17)	
$\Delta V_{\text{elstat}}$	-382.55		-389.52 (-6.97)		-447.74 (-65.19)		-387.24 (-4.69)	
$\Delta E_{\text{oi}}$	-534.09		-543.16 (-9.07)		-550.11 (-16.02)		-543.86 (-9.77)	
$\Delta E_{\text{oi}}(\sigma)$	-433.11		-445.27 (-12.16)		-442.04 (-8.93)		-444.47 (-11.36)	
$\Delta E_{\text{oi}}(\pi)$	-100.99		-97.89 (3.10)		-108.07 (-7.08)		-99.40 (1.59)	
$\Delta E_{\text{int}}$	-263.21		-261.30 (1.91)		-134.80 (128.41)		-263.50 (-0.29)	
$\Delta E_{\text{def}}$	35.65		33.22 (-2.43)		35.65 (0.00)		35.65 (0.00)	
$\Delta E_{\text{tot}}^{\text{b}}$	-227.56		-228.08 (-0.52)		-99.15 (128.41)		-227.85 (-0.29)	
$\Delta E_{\text{bondexact}}^{\text{b}}$	-219.35		-219.97 (-0.61)		-90.93 (128.42)		-219.68 (-0.33)	
Correct.f <sup>b</sup>	<b>0.96</b>		<b>0.96</b>		<b>0.92</b>		<b>0.96</b>	

<sup>a</sup> Computed at BP86/TZ2P. See Scheme 1 for structures. A<sub>1p</sub>/B<sub>1Os</sub>(m-OsP) and A<sub>p</sub>/B<sub>Os</sub>(p-OsP) refer to A<sub>p</sub>/B<sub>Os</sub> in the geometry it adopts in **m-OsP** and **p-OsP**, respectively; **p-OsP<sub>a</sub>** is **p-OsP** with frozen A<sub>1p</sub>/B<sub>1Os</sub>(m-OsP) fragments but with connecting C-P and C-C bond distances as the corresponding C-C and C-P bond lengths in **m-OsP** (1.380 Å and 1.713 Å); **p-OsP<sub>b</sub>** is **p-OsP** with frozen A<sub>1p</sub>/B<sub>1Os</sub>(m-OsP) fragments but with connecting C-P and C-C bond distances as the optimized bond lengths in **p-OsP** (1.730 Å and 1.372 Å).

<sup>b</sup>  $\Delta E_{\text{bondexact}}$  is the exact bonding energy while  $\Delta E_{\text{tot}}$  is the sum of  $\Delta E_{\text{int}}$  and  $\Delta E_{\text{def}}$  and it is the bonding energy without taking into account the spin polarization effects in the fragment (see Theoretical Methods Section). Correct.f gives the  $\Delta E_{\text{bondexact}}/\Delta E_{\text{tot}}$  ratio that is a measure of the error in the different energy components because of the lack of spin polarization effects in the fragments.

**Table S4.** Analysis of the Bonding (in kcal/mol) between Triplet Azaethenediyl ( $A_N$ ) and Triplet  $Rh(Cl)_2(PH_3)_2(C_3H_3)$  ( $B_{Rh}$ ) Fragments in **o-RhN**, **m-RhN**, and Deformed **m-RhN** (**m-RhN<sub>a</sub>** and **m-RhN<sub>b</sub>**).<sup>a</sup>

	<b>o-RhN</b>	<b>m-RhN</b>	<b>m-RhN<sub>a</sub></b>	<b>m-RhN<sub>b</sub></b>
	$A(o-RhN)_N + B(o-RhN)_{Rh}$	$A(m-RhN)_N + B(m-RhN)_{Rh}$	$A(o-RhN)_N + B(o-RhN)_{Rh}$	$A(o-RhN)_N + B(o-RhN)_{Rh}$
$\Delta E_{Pauli}$	478.82	636.99 (158.17)	518.62 (39.80)	632.69 (153.87)
$\Delta V_{elstat}$	-294.05	-363.52 (-69.47)	-307.71 (-13.66)	-362.55 (-68.50)
$\Delta E_{oi}$	-393.68	-492.83 (-99.15)	-421.76 (-28.08)	-485.76 (-92.08)
$\Delta E_{oi}(\sigma)$	-350.36	-434.52 (-84.16)	-380.18 (-29.82)	-431.34 (-80.98)
$\Delta E_{oi}(\pi)$	-43.32	-58.31 (-14.99)	-41.57 (1.75)	-54.42 (-11.10)
$\Delta E_{int}$	-208.91	-219.36 (-10.45)	-210.85 (-1.94)	-215.63 (-6.72)
$\Delta E_{def}$	40.01	47.46 (7.45)	40.01 (0.00)	40.01 (0.00)
$\Delta E_{tot}^b$	-168.90	-171.90 (-3.00)	-170.84 (-1.94)	-175.62 (-6.72)
$\Delta E_{bondexact}^b$	-161.88	-171.55 (-9.67)	-163.80 (-1.91)	-168.60 (-6.71)
Correct.f <sup>b</sup>	<b>0.96</b>	<b>1.00</b>	<b>0.96</b>	<b>0.96</b>

<sup>a</sup> Computed at BP86/TZ2P. See Scheme 1 for structures.  $A_N/B_{Rh}(o-RhN)$  and  $A_N/B_{Rh}(m-RhN)$  refer to  $A_N/B_{Rh}$  in the geometry it adopts in **o-RhN** and **m-RhN**, respectively; **m-RhN<sub>a</sub>** is **m-RhN** with frozen  $A_N/B_{Rh}(o-RhN)$  fragments but with connecting C–N and Rh–C bond distances as the corresponding C–C and Rh–N bond lengths in **o-RhN** (1.439 Å and 1.989 Å); **m-RhN<sub>b</sub>** is **m-RhN** with frozen  $A_N/B_{Rh}(o-RhN)$  fragments but with connecting C–N and Rh–C bond distances as the optimized bond lengths in **m-RhN** (1.351 Å and 1.958 Å).

<sup>b</sup>  $\Delta E_{bondexact}$  is the exact bonding energy while  $\Delta E_{tot}$  is the sum of  $\Delta E_{int}$  and  $\Delta E_{def}$  and it is the bonding energy without taking into account the spin polarization effects in the fragment (see Theoretical Methods Section). Correct.f gives the  $\Delta E_{bondexact}/\Delta E_{tot}$  ratio that is a measure of the error in the different energy components because of the lack of spin polarization effects in the fragments.

**Table S5.** Analysis of the Bonding (in kcal/mol) between Triplet Azaethenediyl ( $A_N$ ) and Triplet  $Rh(Cl)_2(PH_3)_2(C_3H_3)$  ( $B_{Rh}$ ) Fragments in **m-RhN**, **p-RhN**, and Deformed **p-RhN** (**p-RhN<sub>a</sub>** and **p-RhN<sub>b</sub>**).<sup>a</sup>

	<b>m-RhN</b>	<b>p-RhN</b>	<b>p-RhN<sub>a</sub></b>	<b>p-RhN<sub>b</sub></b>
	$A1(m-RhN)_N+B1(m-RhN)_{Rh}$	$A(p-RhN)_N+B(p-RhN)_{Rh}$	$A1(m-RhN)_N+B1(m-RhN)_{Rh}$	$A1(m-RhN)_N+B1(m-RhN)_{Rh}$
$\Delta E_{Pauli}$	790.91	779.31 (-11.60)	810.24 (19.33)	782.68 (-8.23)
$\Delta V_{elstat}$	-414.64	-400.75 (13.89)	-409.40 (5.24)	-401.53 (13.11)
$\Delta E_{oi}$	-654.13	-646.00 (8.13)	-659.96 (-5.83)	-648.58 (5.55)
$\Delta E_{oi}(\sigma)$	-558.32	-552.73 (5.59)	-560.35 (-2.03)	-554.51 (3.81)
$\Delta E_{oi}(\pi)$	-95.81	-93.27 (2.54)	-99.61 (-3.80)	-94.07 (1.74)
$\Delta E_{int}$	-277.85	-267.43 (10.42)	-259.12 (18.73)	-267.43 (10.42)
$\Delta E_{def}$	36.87	36.66 (-0.21)	36.87 (0.00)	36.87 (0.00)
$\Delta E_{tot}^b$	-240.98	-230.77 (10.21)	-222.25 (18.73)	-230.56 (10.42)
$\Delta E_{bondexac}^b$	-233.06	-222.75 (10.31)	-214.33 (18.73)	-222.20 (10.86)
Correct.f <sup>b</sup>	<b>0.97</b>	<b>0.97</b>	<b>0.96</b>	<b>0.96</b>

<sup>a</sup> Computed at BP86/TZ2P. See Scheme 1 for structures.  $A1_N/B1_{Rh}(m-RhN)$  and  $A_N/B_{Rh}(p-RhN)$  refer to  $A_N/B_{Rh}$  in the geometry it adopts in **m-RhN** and **p-RhN**, respectively; **p-RhN<sub>a</sub>** is **p-RhN** with frozen  $A1_N/B1_{Rh}(m-RhN)$  fragments but with connecting C–N and C–C bond distances as the corresponding C–C and C–N bond lengths in m-RhN (1.402 Å and 1.318 Å); **p-RhN<sub>b</sub>** is **p-RhN** with frozen  $A1_N/B1_{Rh}(m-RhN)$  fragments but with connecting C–N and C–C bond distances as the optimized bond lengths in **p-RhN** (1.345 Å and 1.393 Å).

<sup>b</sup>  $\Delta E_{bondexac}$  is the exact bonding energy while  $\Delta E_{tot}$  is the sum of  $\Delta E_{int}$  and  $\Delta E_{def}$  and it is the bonding energy without taking into account the spin polarization effects in the fragment (see Theoretical Methods Section). Correct.f gives the  $\Delta E_{bondexac}/\Delta E_{tot}$  ratio that is a measure of the error in the different energy components because of the lack of spin polarization effects in the fragments.

**Table S6.** Analysis of the Bonding (in kcal/mol) between Triplet Azaethenediyl (A)<sub>p</sub> and Triplet Rh(Cl)<sub>2</sub>(PH<sub>3</sub>)<sub>2</sub>(C<sub>3</sub>H<sub>3</sub>) (B)<sub>Rh</sub> Fragments in **o-RhP**, **m-RhP**, and Deformed **m-RhP** (**m-RhP<sub>a</sub>** and **m-RhP<sub>b</sub>**).<sup>a</sup>

	<b>o-RhP</b>	<b>m-RhP</b>	<b>m-RhP<sub>a</sub></b>	<b>m-RhP<sub>b</sub></b>
	A(o-RhP) <sub>p</sub> + B(o-RhP) <sub>Rh</sub>	A(m-RhP) <sub>p</sub> + B(m-RhP) <sub>Rh</sub>	A(o-RhP) <sub>p</sub> + B(o-RhP) <sub>Rh</sub>	A(o-RhP) <sub>p</sub> + B(o-RhP) <sub>Rh</sub>
ΔE <sub>Pauli</sub>	558.42	472.87 (-85.55)	830.51 (272.09)	473.62 (-84.80)
ΔV <sub>elstat</sub>	-348.38	-308.54 (39.84)	-454.66 (-106.28)	-307.84 (40.54)
ΔE <sub>oi</sub>	-424.51	-354.69 (69.82)	-476.90 (-52.39)	-356.69 (67.82)
ΔE <sub>oi</sub> (σ)	- <sup>b</sup>	-306.91	- <sup>b</sup>	- <sup>b</sup>
ΔE <sub>oi</sub> (π)	- <sup>b</sup>	-47.79	- <sup>b</sup>	- <sup>n</sup>
ΔE <sub>int</sub>	-214.48	-190.37 (24.11)	-101.04 (113.44)	-190.91 (23.57)
ΔE <sub>def</sub>	43.83	43.80 (-0.03)	43.83 (0.00)	43.83 (0.00)
ΔE <sub>tot</sub> <sup>c</sup>	-170.65	-146.57 (24.08)	-57.21 (113.44)	-147.08 (23.57)
ΔE <sub>bondexact</sub> <sup>c</sup>	-163.48	-140.33 (23.14)	-49.99 (113.49)	-139.93 (23.55)
Correct.f <sup>c</sup>	<b>0.96</b>	<b>0.96</b>	<b>0.87<sup>d</sup></b>	<b>0.95</b>

<sup>a</sup> Computed at BP86/TZ2P. See Scheme 1 for structures. A<sub>p</sub>/B<sub>Rh</sub>(o-RhP) and A<sub>p</sub>/B<sub>Rh</sub>(m-RhP) refer to A<sub>p</sub>/B<sub>Rh</sub> in the geometry it adopts in **o-RhP** and **m-RhP**, respectively; **m-RhP<sub>a</sub>** is **m-RhP** with frozen A<sub>p</sub>/B<sub>Rh</sub>(o-RhP) fragments but with connecting C–P and Rh–C bond distances as the corresponding C–C and Rh–P bond lengths in **o-RhP** (1.398 Å and 2.251 Å); **m-RhP<sub>b</sub>** is **m-RhP** with frozen A<sub>p</sub>/B<sub>Rh</sub>(o-RhP) fragments but with connecting C–P and Rh–C bond distances as the optimized bond lengths in **m-RhP** (1.770 Å and 1.960 Å).

<sup>b</sup> Non-planar species. The exact σ/π separation is not possible.

<sup>c</sup> ΔE<sub>bondexact</sub> is the exact bonding energy while ΔE<sub>tot</sub> is the sum of ΔE<sub>int</sub> and ΔE<sub>def</sub> and it is the bonding energy without taking into account the spin polarization effects in the fragment (see Theoretical Methods Section). Correct.f gives the ΔE<sub>bondexact</sub>/ΔE<sub>tot</sub> ratio and it is a measure of the error in the different energy components because of the lack of spin polarization effects in the fragments.

<sup>d</sup> Low Correct.f factor due to constrained geometry that leads to low ΔE<sub>tot</sub> and ΔE<sub>bondexact</sub> values.

**Table S7.** Analysis of the Bonding (in kcal/mol) between Triplet Azaethenediyl Fragment (A)<sub>p</sub> and Triplet Rh(Cl)<sub>2</sub>(PH<sub>3</sub>)<sub>2</sub>(C<sub>3</sub>H<sub>3</sub>) (B)<sub>Rh</sub> in **m-RhP**, **p-RhP**, and Deformed **p-RhP** (**p-RhP<sub>a</sub>** and **p-RhP<sub>b</sub>**)<sup>a</sup>

Rh	<b>m-RhP</b>		<b>p-RhP</b>		<b>p-RhP<sub>a</sub></b>		<b>p-RhP<sub>b</sub></b>	
	A1(m-RhP) <sub>p+</sub>	B1(m-RhP) <sub>R</sub>	A(p-RhP) <sub>p+</sub>	B(p-RhP) <sub>Rh</sub>	A1(m-RhP) <sub>p+</sub>	B1(m-RhP) <sub>Rh</sub>	A1(m-RhP) <sub>p+</sub>	B1(m-RhP) <sub>Rh</sub>
$\Delta E_{\text{Pauli}}$	631.27		656.81 (25.54)		835.60 (204.33)		654.67 (23.40)	
$\Delta V_{\text{elstat}}$	-360.55		-369.59 (-9.04)		-424.95 (-64.40)		-368.12 (-7.57)	
$\Delta E_{\text{oi}}$	-518.43		-534.64 (-16.21)		-534.93 (-16.50)		-536.25 (-17.82)	
$\Delta E_{\text{oi}}(\sigma)$	-431.14		-448.49 (-17.35)		-439.75 (-8.61)		-448.01 (-16.87)	
$\Delta E_{\text{oi}}(\pi)$	-87.29		-86.14 (1.15)		-95.18 (-7.89)		-88.24 (-0.95)	
$\Delta E_{\text{int}}$	-247.70		-247.42 (0.28)		-124.28 (123.42)		-249.70 (-2.00)	
$\Delta E_{\text{def}}$	38.57		35.73 (-2.84)		38.57 (0.00)		38.57 (0.00)	
$\Delta E_{\text{tot}}^{\text{b}}$	-209.13		-211.69 (-2.56)		-85.71 (123.42)		-211.13 (-2.00)	
$\Delta E_{\text{bondexact}}^{\text{b}}$	-201.84		-204.43 (-2.59)		-78.41 (123.43)		-203.96 (-2.12)	
Correct.f <sup>b</sup>	<b>0.97</b>		<b>0.97</b>		<b>0.91</b>		<b>0.97</b>	

<sup>a</sup> Computed at BP86/TZ2P. See Scheme 1 for structures. A<sub>1p</sub>/B<sub>1Rh</sub>(m-RhP) and A<sub>p</sub>/B<sub>Rh</sub>(p-RhP) refer to A<sub>p</sub>/B<sub>Rh</sub> in the geometry it adopts in **m-RhP** and **p-RhP**, respectively; **p-RhP<sub>a</sub>** is **p-RhP** with frozen A<sub>1p</sub>/B<sub>1Rh</sub>(m-RhP) fragments but with connecting C–P and C–C bond distances as the corresponding C–C and C–P bond lengths in **m-RhP** (1.396 Å and 1.730 Å); **p-RhP<sub>b</sub>** is **p-RhP** with frozen A<sub>1p</sub>/B<sub>1Rh</sub>(m-RhP) fragments but with connecting C–P and C–C bond distances as the optimized bond lengths in **p-RhP** (1.750 Å and 1.383 Å).

<sup>b</sup>  $\Delta E_{\text{bondexact}}$  is the exact bonding energy while  $\Delta E_{\text{tot}}$  is the sum of  $\Delta E_{\text{int}}$  and  $\Delta E_{\text{def}}$  and it is the bonding energy without taking into account the spin polarization effects in the fragment (see Theoretical Methods Section). Correct.f gives the  $\Delta E_{\text{bondexact}}/\Delta E_{\text{tot}}$  ratio that is a measure of the error in the different energy components because of the lack of spin polarization effects in the fragments.

**Table S8.** Analysis of the Bonding (in kcal/mol) between Triplet Azaethenediyl Fragment ( $A_N$ ) and Triplet  $Ru(Cl)(CO)(PH_3)_2(C_3H_3)$  ( $B_{Ru}$ ) in **o-RuN**, **m-RuN**, and Deformed **m-RuN** (**m-RuN<sub>a</sub>** and **m-RuN<sub>b</sub>**)<sup>a</sup>

Ru	<b>o-RuN</b>		<b>m-RuN</b>		<b>m-RuN<sub>a</sub></b>		<b>m-RuN<sub>b</sub></b>	
	A(o-RuN) <sub>N</sub> + B(o-RuN) <sub>Ru</sub>	A(m-RuN) <sub>N</sub> + B(m-RuN) <sub>Ru</sub>	A(o-RuN) <sub>N</sub> + B(o-RuN) <sub>Ru</sub>	A(m-RuN) <sub>N</sub> + B(m-RuN) <sub>Ru</sub>	A(o-RuN) <sub>N</sub> + B(o-RuN) <sub>Ru</sub>	A(m-RuN) <sub>N</sub> + B(m-RuN) <sub>Ru</sub>	A(o-RuN) <sub>N</sub> + B(o-RuN) <sub>Ru</sub>	A(m-RuN) <sub>N</sub> + B(m-RuN) <sub>Ru</sub>
$\Delta E_{\text{Pauli}}$	442.79	564.25 (121.46)	480.54 (37.75)	563.57 (120.78)				
$\Delta V_{\text{elstat}}$	-280.85	-327.34 (-46.49)	-290.49 (-9.64)	-326.22 (-45.37)				
$\Delta E_{\text{oi}}$	-381.89	-457.70 (-75.81)	-401.88 (-19.99)	-452.29 (-70.40)				
$\Delta E_{\text{oi}}(\sigma)$	-345.99	-411.20 (-65.21)	-366.77 (-20.78)	-408.63 (-62.64)				
$\Delta E_{\text{oi}}(\pi)$	-35.90	-46.50 (-10.60)	-35.11 (0.79)	-43.67 (-7.77)				
$\Delta E_{\text{int}}$	-219.96	-220.78 (-0.82)	-211.83 (8.13)	-214.94 (5.02)				
$\Delta E_{\text{def}}$	39.50	40.70 (1.20)	39.50 (0.00)	39.50 (0.00)				
$\Delta E_{\text{tot}}^b$	-180.46	-180.08 (0.38)	-172.33 (8.13)	-175.44 (5.02)				
$\Delta E_{\text{bondexact}}^b$	-172.02	-172.03 (-0.02)	-163.88 (8.14)	-166.98 (5.04)				
Correct.f <sup>b</sup>	<b>0.95</b>	<b>0.96</b>	<b>0.95</b>	<b>0.95</b>				

<sup>a</sup>Computed at BP86/TZ2P. See Scheme 1 for structures.  $A_N/B_{Ru}(\text{o-RuN})$  and  $A_N/B_{Ru}(\text{m-RuN})$  refer to  $A_N/B_{Ru}$  in the geometry it adopts in **o-RuN** and **m-RuN**, respectively; **m-RuN<sub>a</sub>** is **m-RuN** with frozen  $A_N/B_{Ru}(\text{o-RuN})$  fragments but with connecting C–N and Ru–C bond distances as the corresponding C–C and Ru–N bond lengths in **o-RuN** (1.447 Å and 2.059 Å); **m-RuN<sub>b</sub>** is **m-RuN** with frozen  $A_N/B_{Ru}(\text{o-RuN})$  fragments but with connecting C–N and Ru–C bond distances as the optimized bond lengths in **m-RuN** (1.364 Å and 2.070 Å).

<sup>b</sup>  $\Delta E_{\text{bondexact}}$  is the exact bonding energy while  $\Delta E_{\text{tot}}$  is the sum of  $\Delta E_{\text{int}}$  and  $\Delta E_{\text{def}}$  and it is the bonding energy without taking into account the spin polarization effects in the fragment (see Theoretical Methods Section). Correct.f gives the  $\Delta E_{\text{bondexact}}/\Delta E_{\text{tot}}$  ratio that is a measure of the error in the different energy components because of the lack of spin polarization effects in the fragments.

**Table S9.** Analysis of the Bonding (in kcal/mol) between Triplet Azaethenediyl Fragment (A)<sub>N</sub> and Triplet Ru(Cl)(CO)(PH<sub>3</sub>)<sub>2</sub>(C<sub>3</sub>H<sub>3</sub>) (B)<sub>Ru</sub> in **m-RuN**, **p-RuN**, and Deformed **p-RuN** (**p-RuN<sub>a</sub>** and **p-RuN<sub>b</sub>**)<sup>a</sup>

Ru	<b>m-RuN</b>		<b>p-RuN</b>		<b>p-RuN<sub>a</sub></b>		<b>p-RuN<sub>b</sub></b>	
	A1(m-RuN) <sub>N</sub> + B1(m-RuN) <sub>Ru</sub>		A(p-RuN) <sub>N</sub> + B(p-RuN) <sub>Ru</sub>		A1(m-RuN) <sub>N</sub> + B1(m-RuN) <sub>Ru</sub>		A1(m-RuN) <sub>N</sub> +B1(m-RuN) <sub>Ru</sub>	
ΔE <sub>Pauli</sub>	798.59		803.60 (5.01)		815.36 (16.77)		817.29 (18.70)	
ΔV <sub>elstat</sub>	-423.94		-417.35 (6.59)		-419.09 (4.85)		-420.75 (3.19)	
ΔE <sub>oi</sub>	-664.13		-670.03 (-5.90)		-670.63 (-6.50)		-674.93 (-10.80)	
ΔE <sub>oi</sub> (σ)	-559.63		-562.05 (-2.42)		-560.33 (-0.70)		-566.21 (-6.58)	
ΔE <sub>oi</sub> (π)	-104.51		-107.98 (-3.47)		-110.30 (-5.79)		-108.71 (-4.20)	
ΔE <sub>int</sub>	-289.49		-283.78 (5.71)		-274.36 (15.13)		-278.39 (11.10)	
ΔE <sub>def</sub>	37.80		38.43 (0.63)		37.80 (0.00)		37.80 (0.00)	
ΔE <sub>tot</sub> <sup>b</sup>	-251.69		-245.35 (6.34)		-236.56 (15.13)		-240.59 (11.10)	
ΔE <sub>bondexact</sub> <sup>b</sup>	-243.01		-236.56 (6.45)		-227.89 (15.12)		-232.74 (10.27)	
Correct.f <sup>b</sup>	<b>0.97</b>		<b>0.96</b>		<b>0.96</b>		<b>0.97</b>	

<sup>a</sup>Computed at BP86/TZ2P. See Scheme 1 for structures. A<sub>N</sub>/B<sub>Ru</sub>(m-RuN) and A<sub>N</sub>/B<sub>Ru</sub>(p-RuN) refer to A<sub>N</sub>/B<sub>Ru</sub> in the geometry it adopts in **m-RuN** and **p-RuN**, respectively; **p-RuN<sub>a</sub>** is **p-RuN** with frozen A<sub>N</sub>/B<sub>Ru</sub>(m-RuN) fragments but with connecting C–N and C–C bond distances as the corresponding C–C and C–N bond lengths in **m-RuN** (1.390 Å and 1.316 Å); **p-RuN<sub>b</sub>** is **p-RuN** with frozen A<sub>N</sub>/B<sub>Ru</sub>(m-RuN) fragments but with connecting C–N and C–C bond distances as the optimized bond lengths in **p-RuN** (1.328 Å and 1.378 Å).

<sup>b</sup> ΔE<sub>bondexact</sub> is the exact bonding energy while ΔE<sub>tot</sub> is the sum of ΔE<sub>int</sub> and ΔE<sub>def</sub> and it is the bonding energy without taking into account the spin polarization effects in the fragment (see Theoretical Methods Section). Correct.f gives the ΔE<sub>bondexact</sub>/ΔE<sub>tot</sub> ratio that is a measure of the error in the different energy components because of the lack of spin polarization effects in the fragments.

**Table S10.** Analysis of the Bonding (in kcal/mol) between Triplet Azaethenediyl Fragment (A)<sub>p</sub> and Triplet Ru(Cl)(CO)(PH<sub>3</sub>)<sub>2</sub>(C<sub>3</sub>H<sub>3</sub>) (B)<sub>Ru</sub> in **o-RuP**, **m-RuP**, and Deformed **m-RuP** (**m-RuP<sub>a</sub>** and **m-RuP<sub>b</sub>**)<sup>a</sup>

Ru	<b>o-RuP</b>	<b>m-RuP</b>	<b>m-RuP<sub>a</sub></b>	<b>m-RuP<sub>b</sub></b>
	A(o-RuP) <sub>p</sub> + B(o-RuP) <sub>Ru</sub>	A(m-RuP) <sub>p</sub> + B(m-RuN) <sub>Ru</sub>	A(o-RuP) <sub>p</sub> + B(o-RuP) <sub>Ru</sub>	A(o-RuP) <sub>p</sub> + B(o-RuP) <sub>Ru</sub>
ΔE <sub>Pauli</sub>	496.00	415.05 (-80.95)	768.32 (272.32)	418.20 (-77.80)
ΔV <sub>elstat</sub>	-317.69	-278.54 (39.15)	-419.32 (-101.63)	-279.34 (38.35)
ΔE <sub>oi</sub>	-391.14	-330.64 (60.50)	-447.43 (-56.29)	-332.17 (58.97)
ΔE <sub>oi</sub> (σ)	-340.06	-294.89 (45.17)	-365.31 (-25.25)	-294.62 (45.44)
ΔE <sub>oi</sub> (π)	-51.08	-35.75 (15.33)	-82.13 (-31.05)	-37.55 (13.53)
ΔE <sub>int</sub>	-212.83	-194.12 (18.71)	-98.43 (114.40)	-193.31 (19.52)
ΔE <sub>def</sub>	43.06	38.87 (-4.19)	43.06 (0.00)	43.06 (0.00)
ΔE <sub>tot</sub> <sup>b</sup>	-169.77	-155.25 (14.52)	-55.37 (114.40)	-150.25 (19.52)
ΔE <sub>bondexact</sub> <sup>b</sup>	-162.03	-143.46 (18.57)	-47.61 (114.42)	-142.55 (19.48)
Correct.f <sup>b</sup>	<b>0.95</b>	<b>0.92</b>	<b>0.86<sup>c</sup></b>	<b>0.95</b>

<sup>a</sup>Computed at BP86/TZ2P. See Scheme 1 for structures. A<sub>p</sub>/B<sub>Ru</sub>(o-RuP) and A<sub>p</sub>/B<sub>Ru</sub>(m-RuP) refer to A<sub>p</sub>/B<sub>Ru</sub> in the geometry it adopts in **o-RuP** and **m-RuP**, respectively; **m-RuP<sub>a</sub>** is **m-RuP** with frozen A<sub>p</sub>/B<sub>Ru</sub>(o-RuP) fragments but with connecting C-P and Ru-C bond distances as the corresponding C-C and Ru-P bond lengths in **o-RuP** (1.408 Å and 2.407 Å); **m-RuP<sub>b</sub>** is **m-RuP** with frozen A<sub>p</sub>/B<sub>Ru</sub>(o-RuP) fragments but with connecting C-P and Ru-C bond distances as the optimized bond lengths in **m-RuP** (1.787 Å and 2.075 Å)

<sup>b</sup> ΔE<sub>bondexact</sub> is the exact bonding energy while ΔE<sub>tot</sub> is the sum of ΔE<sub>int</sub> and ΔE<sub>def</sub> and it is the bonding energy without taking into account the spin polarization effects in the fragment (see Theoretical Methods Section). Correct.f gives the ΔE<sub>bondexact</sub>/ΔE<sub>tot</sub> ratio that is a measure of the error in the different energy components because of the lack of spin polarization effects in the fragments.

<sup>c</sup> Low Correct.f factor due to constrained geometry that leads to low ΔE<sub>tot</sub> and ΔE<sub>bondexact</sub> values.

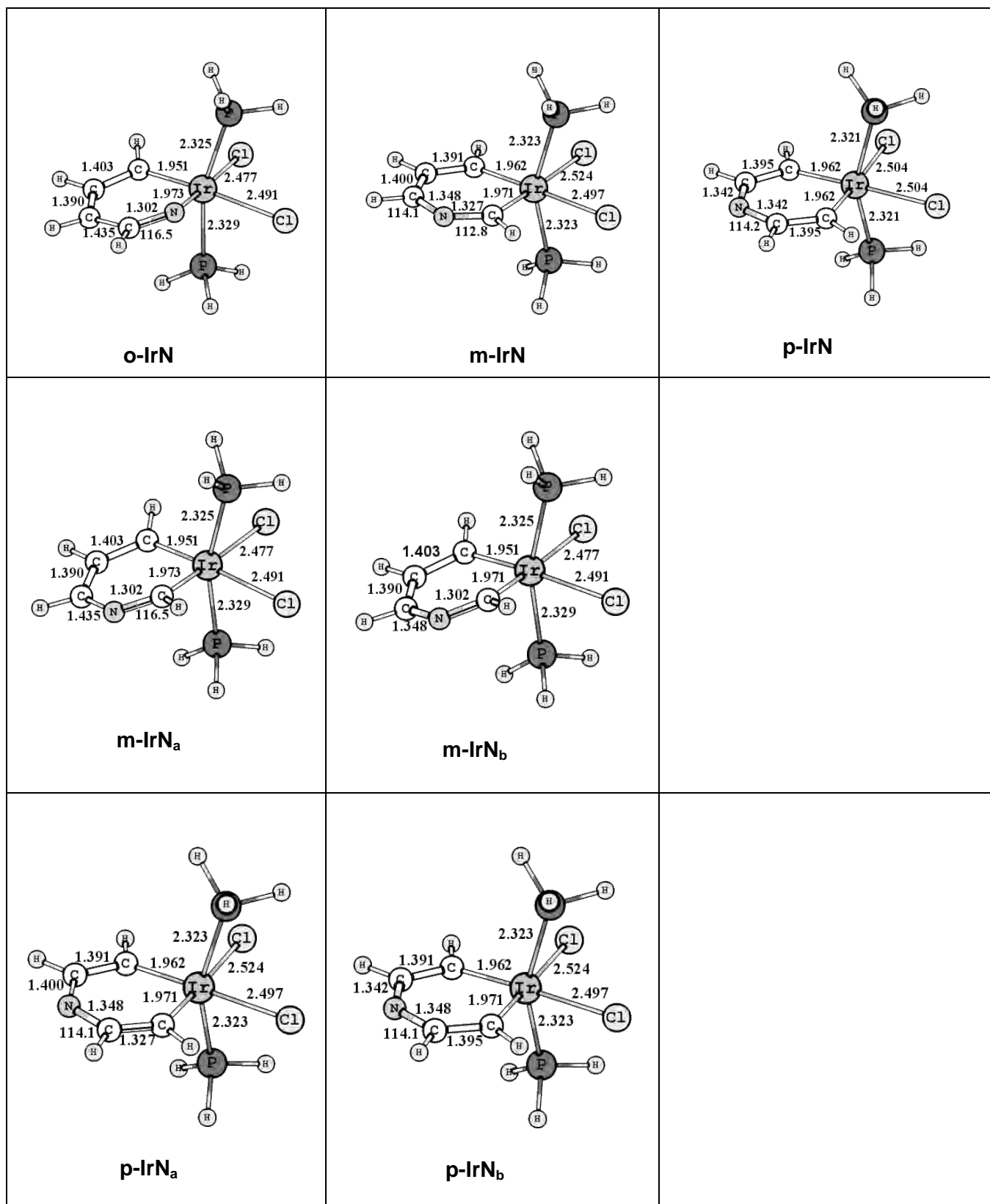
**Table S11.** Analysis of the Bonding (in kcal/mol) between Triplet Azaethenediyl Fragment (A)<sub>p</sub> and Triplet Ru(Cl)(CO)(PH<sub>3</sub>)<sub>2</sub>(C<sub>3</sub>H<sub>3</sub>) (B)<sub>Os</sub> in **m-RuP**, **p-RuP**, and Deformed **p-RuP** (**p-RuP<sub>a</sub>** and **p-RuP<sub>b</sub>**)

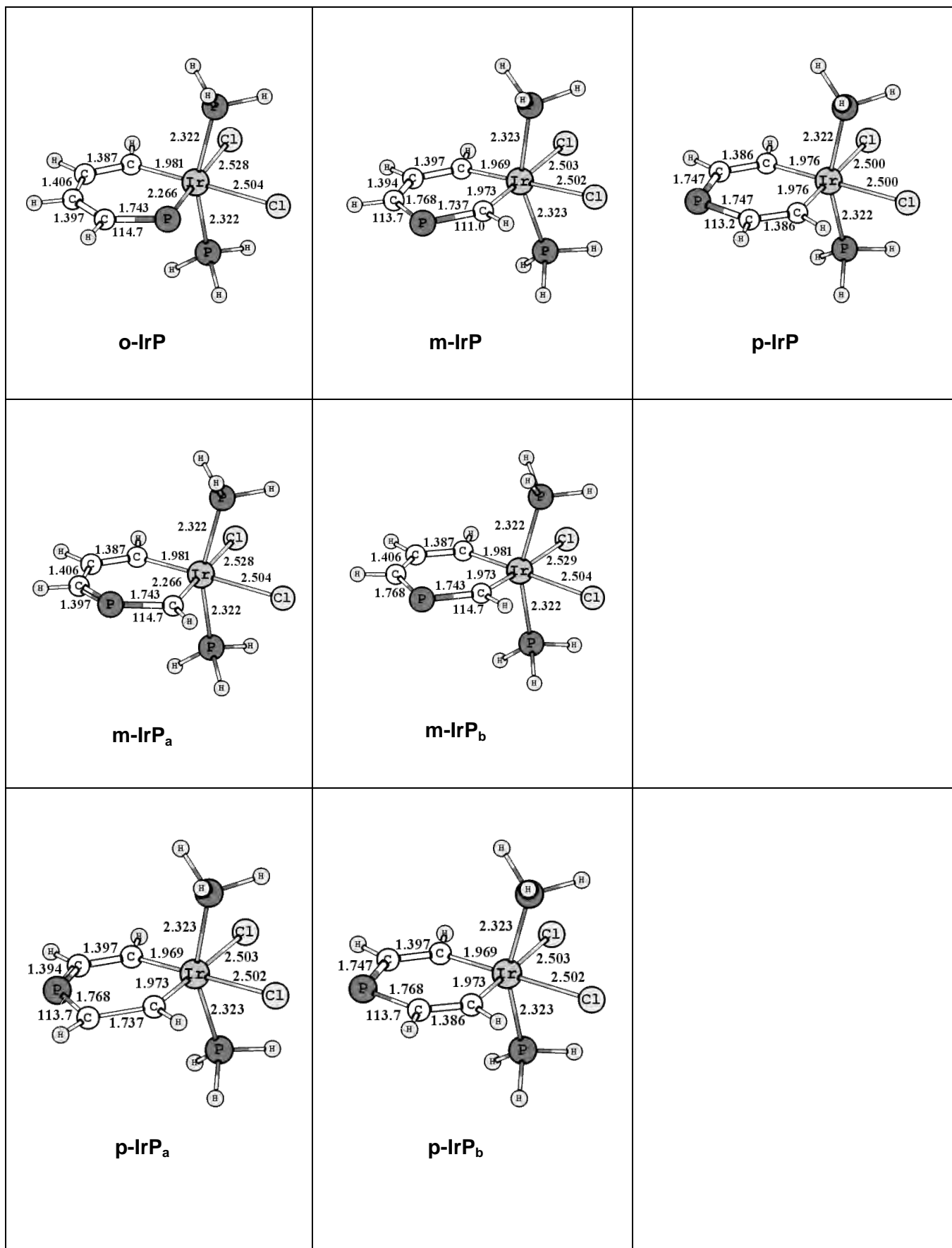
Ru	<b>m-RuP</b>	<b>p-RuP</b>	<b>p-RuP<sub>a</sub></b>	<b>p-RuP<sub>b</sub></b>
	A1(m-RuP) <sub>p</sub> + B1(m-RuP) <sub>Ru</sub>	A(p-RuP) <sub>p</sub> + B(p-RuP) <sub>Ru</sub>	A1(m-RuP) <sub>p</sub> + B1(m-RuP) <sub>Ru</sub>	A1(m-RuP) <sub>N</sub> +B1(m-RuP) <sub>Ru</sub>
$\Delta E_{\text{Pauli}}$	652.19	670.36 (18.17)	859.21 (207.02)	667.64 (15.45)
$\Delta V_{\text{elstat}}$	-378.89	-385.19 (-6.30)	-443.02 (-64.13)	-383.45 (-4.56)
$\Delta E_{\text{oi}}$	-535.69	-545.63 (-9.94)	-552.49 (-16.80)	-547.30 (-11.61)
$\Delta E_{\text{oi}}(\sigma)$	-435.52	-448.91 (-13.39)	-445.75 (-10.23)	-448.71 (-13.19)
$\Delta E_{\text{oi}}(\pi)$	-100.17	-96.72 (3.45)	-106.75 (-6.58)	-98.59 (1.58)
$\Delta E_{\text{int}}$	-262.40	-260.46 (1.94)	-136.30 (126.10)	-263.11 (-0.71)
$\Delta E_{\text{def}}$	39.88	36.89 (-2.98)	39.88 (0.00)	39.88 (0.00)
$\Delta E_{\text{tot}}^{\text{b}}$	-222.52	-223.57 (-1.04)	-96.42 (126.10)	-223.23 (-0.71)
$\Delta E_{\text{bondexact}}^{\text{b}}$	-214.44	-215.61 (-1.16)	-88.34 (126.10)	-215.05 (-0.61)
Correct.f <sup>b</sup>	<b>0.96</b>	<b>0.96</b>	<b>0.92</b>	<b>0.96</b>

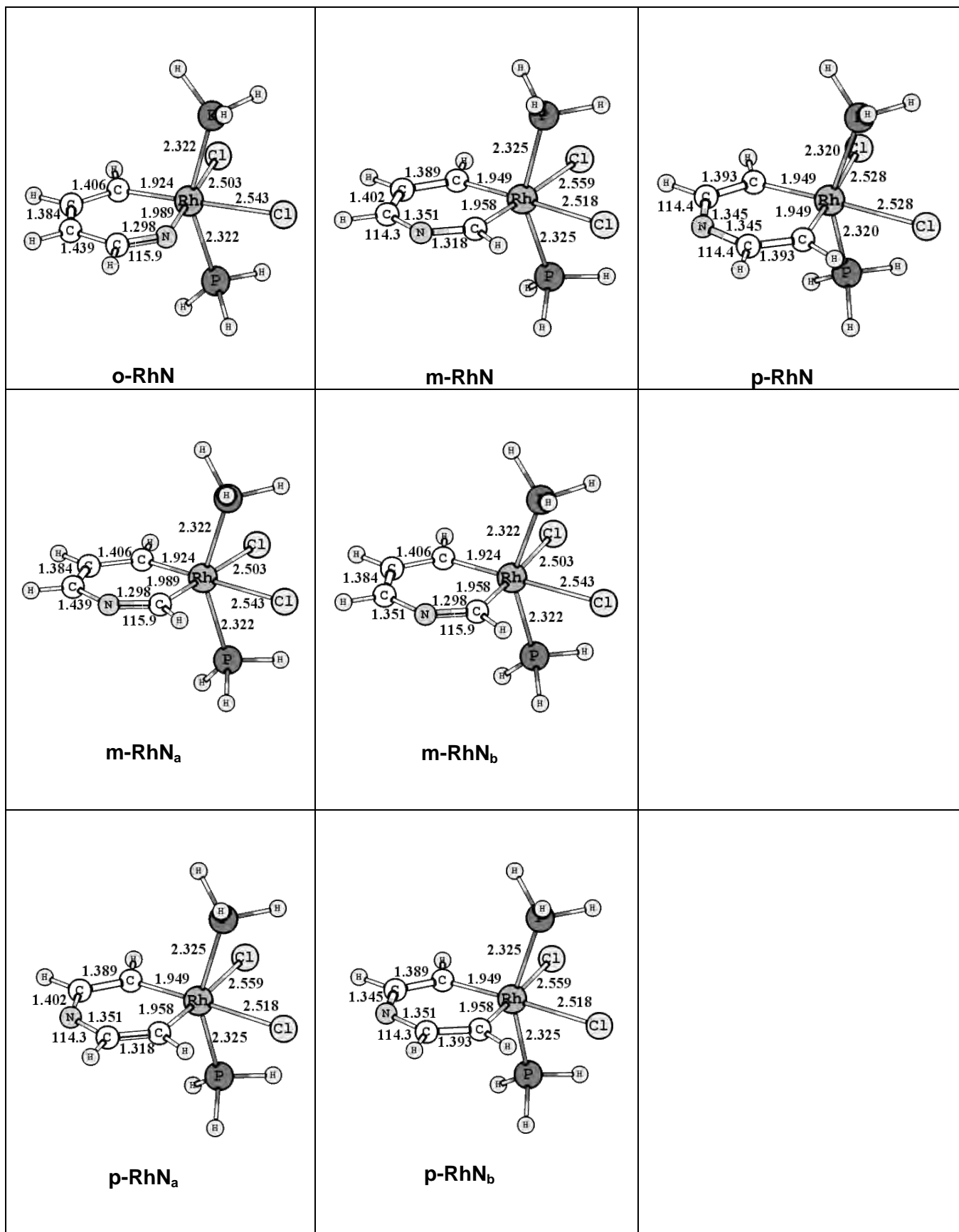
<sup>a</sup>Computed at BP86/TZ2P. See Scheme 1 for structures. A1<sub>p</sub>/B1<sub>Ru</sub>(m-RuP) and A<sub>p</sub>/B<sub>Ru</sub>(p-RuP) refer to A<sub>p</sub>/B<sub>Ru</sub> in the geometry it adopts in **m-RuP** and **p-RuP**, respectively; **p-RuP<sub>a</sub>** is **p-RuP** with frozen A1<sub>p</sub>/B1<sub>Ru</sub>(m-RuP) fragments but with connecting C–P and C–C bond distances as the corresponding C–C and C–P bond lengths in **m-RuP** (1.383 Å and 1.713 Å); **p-RuP<sub>b</sub>** is **p-RuP** with frozen A1<sub>p</sub>/B1<sub>Ru</sub>(m-RuP) fragments but with connecting C–P and C–C bond distances as the optimized bond lengths in **p-RuP** (1.735 Å and 1.373 Å).

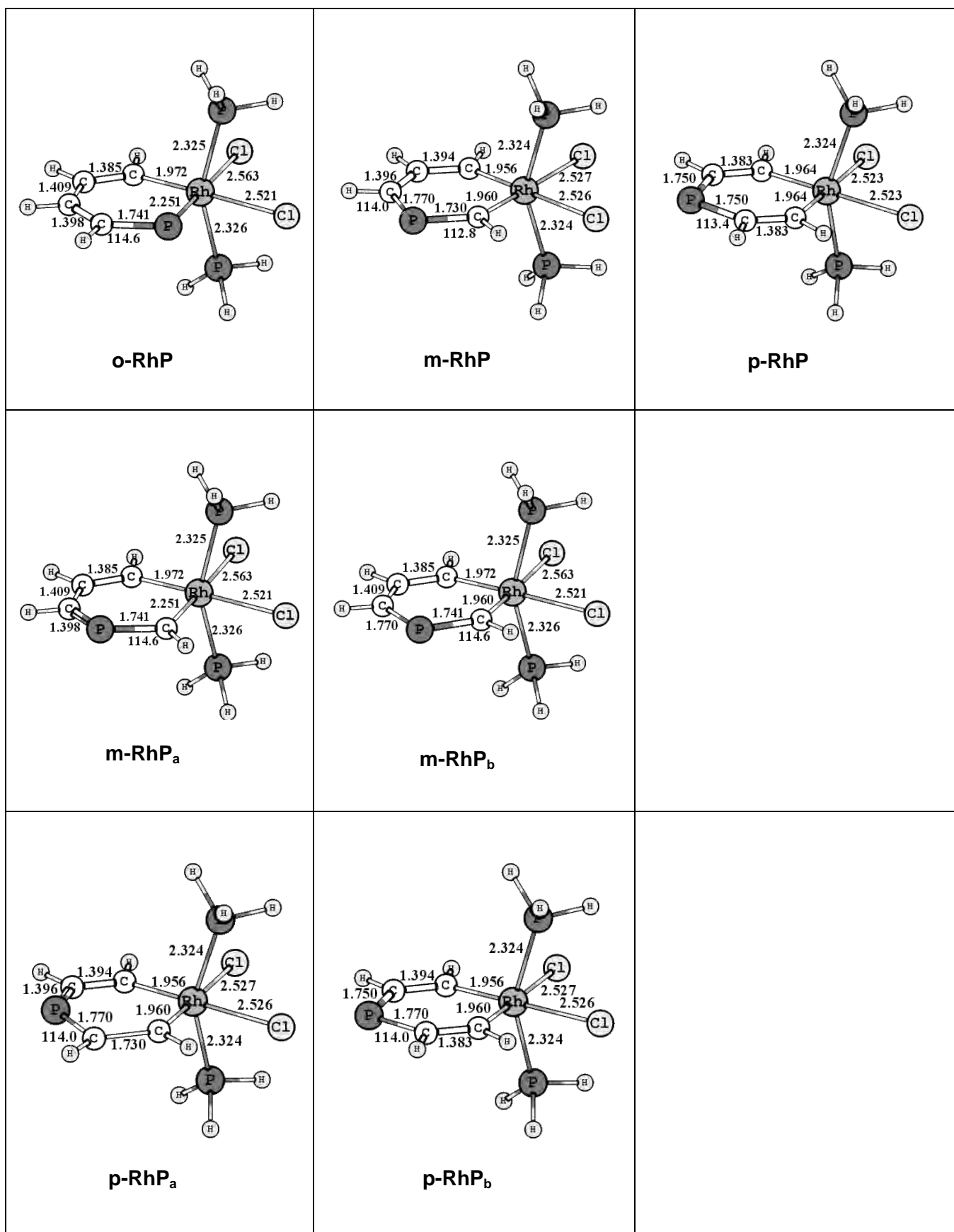
<sup>b</sup>  $\Delta E_{\text{bondexact}}$  is the exact bonding energy while  $\Delta E_{\text{tot}}$  is the sum of  $\Delta E_{\text{int}}$  and  $\Delta E_{\text{def}}$  and it is the bonding energy without taking into account the spin polarization effects in the fragment (see Theoretical Methods Section). Correct.f gives the  $\Delta E_{\text{bondexact}}/\Delta E_{\text{tot}}$  ratio that is a measure of the error in the different energy components because of the lack of spin polarization effects in the fragments.

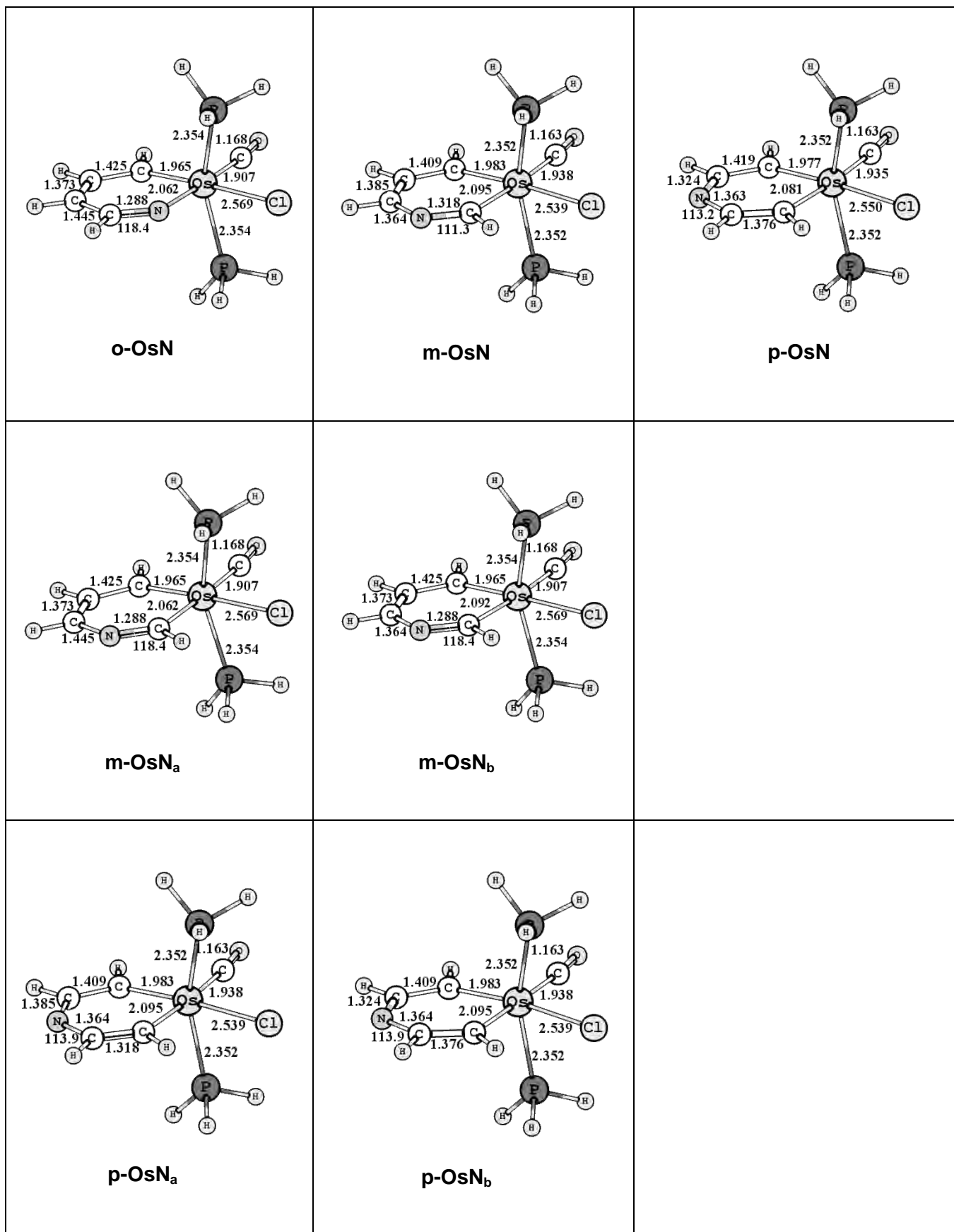
**Figure S1:** Molecular structures of all heterometallobenzenes studied in this work. Bond distances in Å and angles in degrees.

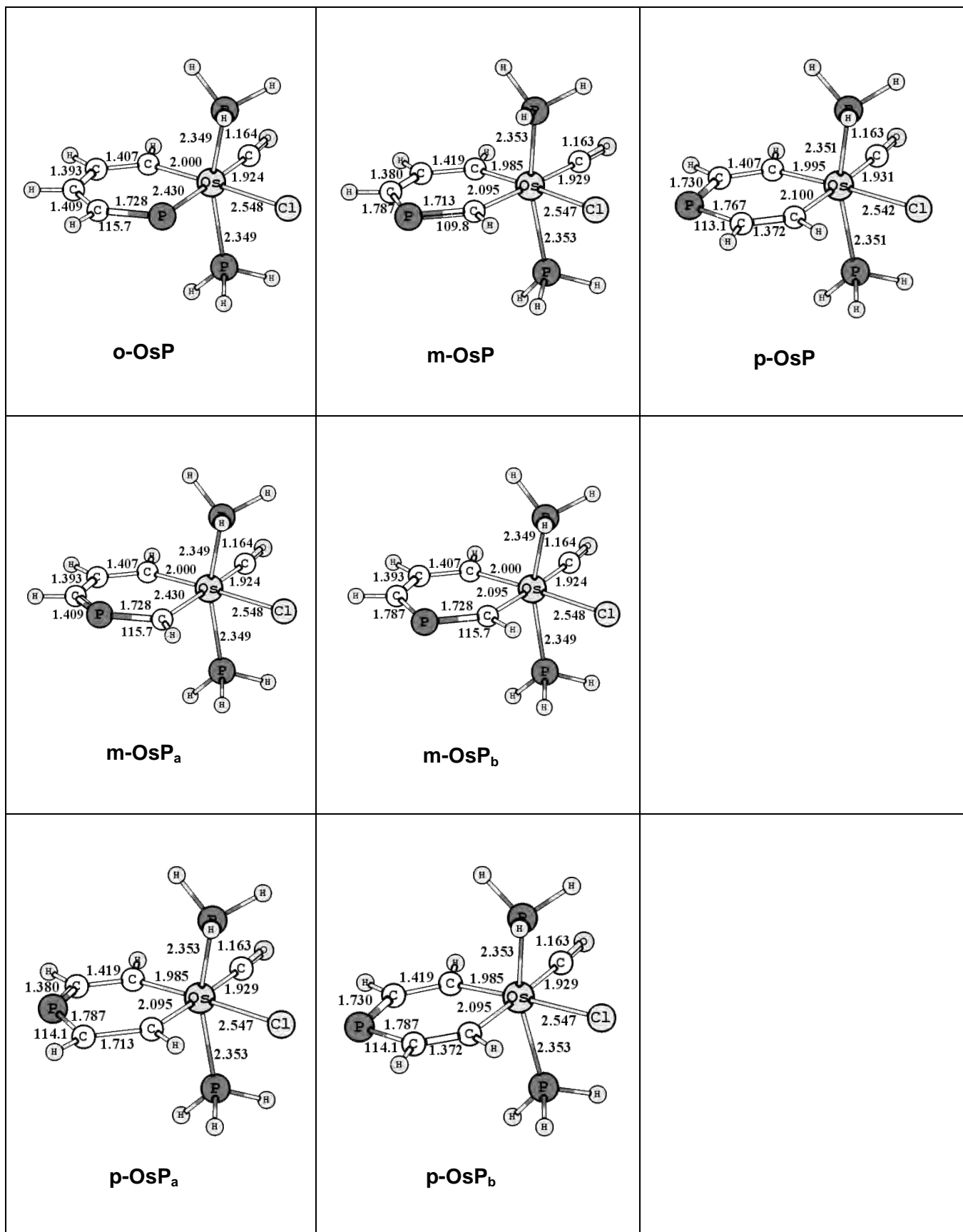


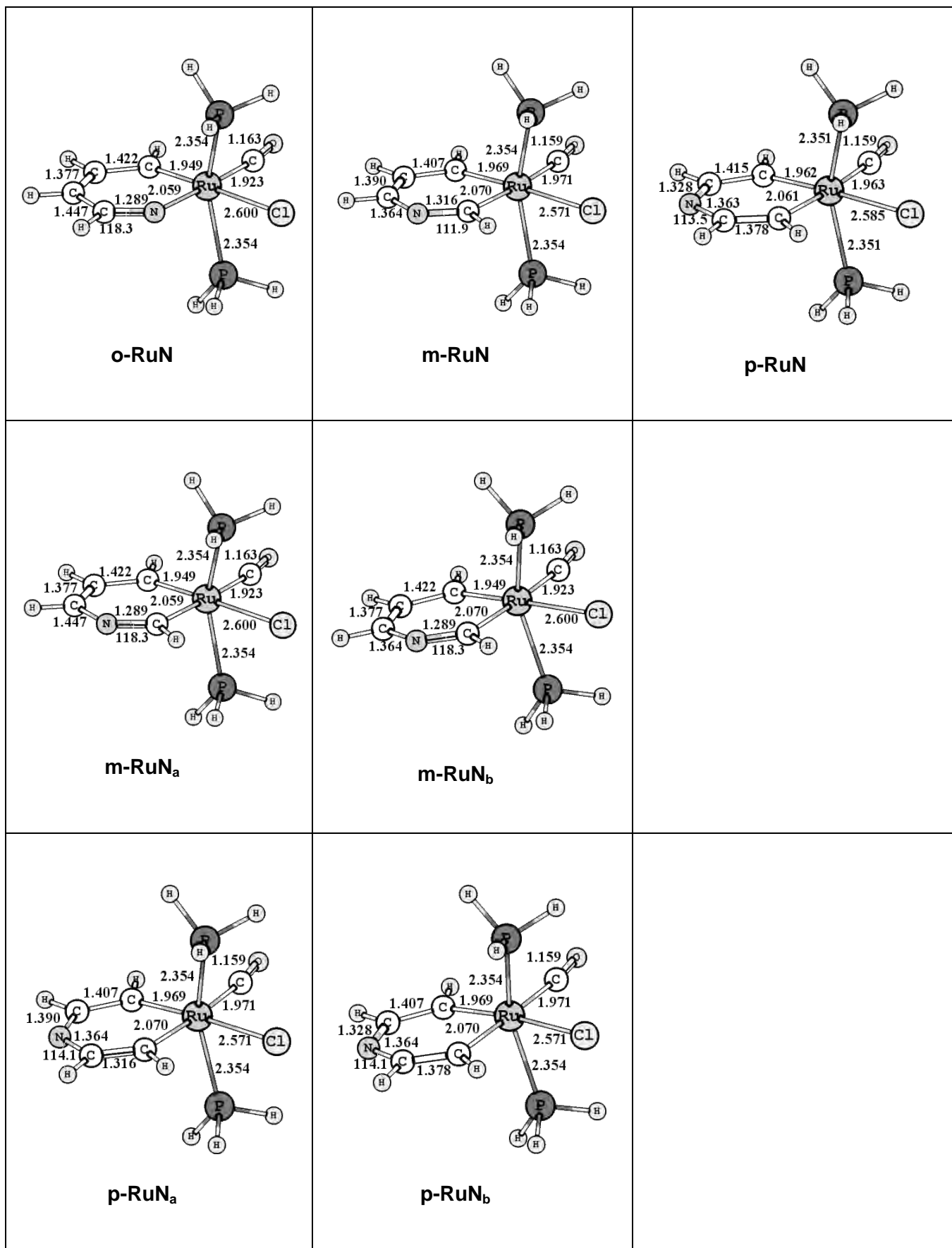














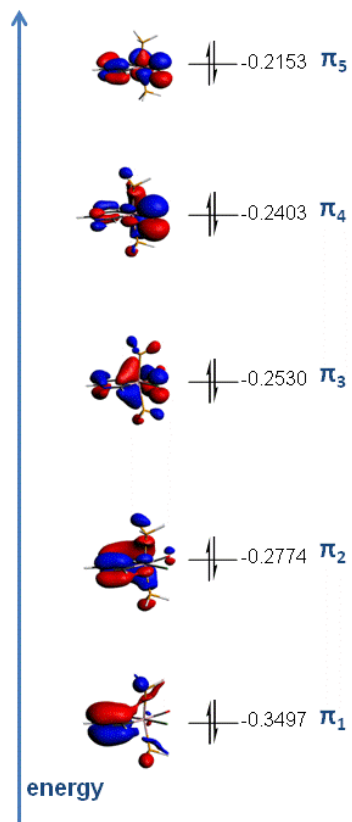


**Figure S2.** Plot of the valence  $\pi$  orbitals of the ring of meta-osmapyridine compound.



